



University of  
**Nottingham**  
UK | CHINA | MALAYSIA



BRITISH  
PHARMACOLOGICAL  
SOCIETY

# Universal sensors for identifying use-dependent intracellular allosteric modulators of G protein coupled receptors

James Pietro Farmer MSc Hons

Thesis submitted to the University of Nottingham for the degree of Doctor of  
Philosophy

January 2024

School of Life Sciences

School of Pharmacy

University of Nottingham

Nottingham

UK

***Declaration of Own Work***

This thesis is entirely the candidate's own work. The experiments described in this thesis were performed by the author between October 2020 and August 2023 in the Cell Signalling Research Group at the Centre of Membrane Proteins and Receptors, University of Nottingham, UK. No part of this material has been submitted previously for a degree or any other qualification at any University.

## Abstract

G protein-coupled receptors (GPCRs) represent the largest family of cell surface receptors targeted by therapeutics. Their diverse signalling capabilities lead to involvement in a wide range of physiological and disease responses. The vast majority of molecules currently available to target GPCRs are designed to act at the binding site (the orthosteric site) for endogenous ligands, either promoting receptor signalling as agonists, or inhibiting as antagonists. However, a continuing challenge within GPCR drug discovery is to develop compounds with sufficient selectivity across closely related targets, and more nuanced mechanisms of action than classical agonism or antagonism. Ultimately these may offer both improved therapeutic efficacy, and better minimise the occurrence of on- and off-target side effects.

This challenge has given rise to rapidly advancing understanding of alternative allosteric mechanisms for GPCRs, in which molecules bind in a separate location from the orthosteric ligand to influence receptor activity. One such class are the intracellular allosteric modulators that bind at the receptor-G protein interface, thereby inhibiting effector coupling and acting as non-competitive antagonists. These types of molecules have been identified for a few GPCR family members currently (e.g. chemokine receptors), and offer advantages in tackling receptors with large orthosteric binding sites, and in emergent properties such as use dependence. Currently broader development and understanding of intracellular allosteric modulators is hindered by a lack of suitable, high-throughput, screening methods, with the majority identified via bespoke receptor functional studies. There is a need for the development of a more universally applicable screening platform for the rapid identification of intracellular allosteric modulators at the GPCR superfamily.

This thesis describes the development of a novel approach for screening ligands able to bind the GPCR intracellular binding site, employing G protein derived peptidomimetics. These are 11 – 24 amino acid peptides derived from the C-terminal tail of G protein alpha-subunits

previously identified to display G protein selective inhibition of effector signalling, with the potential to also act as positive modulators of agonist binding. This G protein-based selectivity is hypothesised to provide these peptidomimetics with the ability to couple to multiple GPCRs, thereby making them putative tools in developing more universally applicable probes for the GPCR intracellular binding site.

Initially, a range of these peptides were characterised, varying in length and amino acid sequence, based on their ability to alter orthosteric agonist binding at the Gs coupled  $\beta_2$ -adrenoceptor and Gi coupled Neuropeptide Y1 receptor. This was achieved by the development of TR-FRET binding assays to determine orthosteric agonist affinity via competition analysis, in the absence and presence of G $\alpha$  C terminal peptide. Peptides were evaluated based on their ability to positively modulate agonist affinity, on the hypothesis that their binding promotes the receptor active conformation.

Selected peptides with the greatest modulatory capacity were then engineered to contain a tetramethyl rhodamine fluorophore at their N terminus and evaluated for GPCR binding directly using NanoBRET technology. NanoBRET binding studies confirmed that fluorescent G $\alpha$  C peptides bound to the  $\beta_2$ -adrenoceptor and Y1 receptor in an orthosteric agonist dependent binding mechanism, preferentially coupling to the GPCR active conformation. These studies (for example for the Gs receptor tracer TMR-G $\alpha$ s19cha18) demonstrated both the use of these probes as tracers in competition binding studies to identify competitive unlabelled ligands binding at the intracellular modulator site, and also as activation sensors for the receptors to rank the potency and efficacy of orthosteric agonists. Further, proof of concept data indicated that TMR-G $\alpha$ s19cha18 is a probe that can be used with advanced bioimaging techniques in conjunction with solubilised receptor lipid particles, including fluorescence correlation spectroscopy (FCS), to provide information about both binding and stoichiometry of the bound peptide-receptor complexes. These studies provided future directions for further development of labelled G protein peptidomimetic tracers to be used in FCS analysis systems.

Finally, TMR-G $\alpha$ s19cha18 was employed in a small-scale screening assay to identify novel intracellular modulators of the Gs prostaglandin EP<sub>2</sub> receptor. Utilising NanoBRET competition assays and the TMR-G $\alpha$ s19cha18 probe, unlabelled small-molecule modulators were screened, allowing accurate derivation of their binding affinity at the EP<sub>2</sub> receptor intracellular site and subsequent evaluation of ligand structure activity relationships. CD006 was identified as a novel small molecule inhibitor of the EP<sub>2</sub> receptor, validated through employment of NanoBiT complementation assay to evaluate CD006's functional effect on receptor- $\beta$ -arrestin2 recruitment by PGE<sub>2</sub>.

Together, the data presented in this thesis identify G protein C-terminus mimetic peptides to be effective tools for the development of novel, broadly applicable, tracers for GPCR intracellular allosteric binding sites.

## **Publications arising:**

### ***Papers:***

Farmer, J. P., Mistry, S. N., Laughton, C. A., & Holliday, N. D. (2022). Development of fluorescent peptide G protein-coupled receptor activation biosensors for NanoBRET characterization of intracellular allosteric modulators. *The FASEB Journal*, 36(11), e22576.  
<https://doi.org/10.1096/FJ.202201024R>

Casella, B. M., Farmer, J. P., Nesheva, D. N., Williams, H. E. L., Charlton, S. J., Holliday, N. D., Laughton, C. A., & Mistry, S. N. (2023). Design, Synthesis, and Application of Fluorescent Ligands Targeting the Intracellular Allosteric Binding Site of the CXC Chemokine Receptor 2. *Journal of Medicinal Chemistry*.  
<https://doi.org/10.1021/ACS.JMEDCHEM.3C00849>

### ***Conference proceedings:***

James P Farmer, Shailesh N Mistry, Charles A Laughton, Nicholas D Holliday.(2022) A fluorescent G protein mimetic peptide probe for high-throughput characterization of intracellular allosteric modulator binding and GPCR activation. (Poster presentation at Keystone: GPCRs: An Odyssey from Structure, Signaling and Regulation to Therapeutics, Snowbird, Utah, USA)

James P Farmer, Shailesh N Mistry, Charles A Laughton, Nicholas D Holliday.(2022) A fluorescent G protein mimetic peptide probe for high-throughput characterization of intracellular allosteric modulator binding and GPCR activation. (Poster presentation: Pharmacology 2022, Liverpool, UK)

James P Farmer, Constance Dalton, Shailesh N Mistry, Charles A Laughton, Nicholas D Holliday.(2023) A fluorescent G protein mimetic peptide probe for high-throughput characterisation of EP<sub>2</sub> intracellular allosteric modulator binding and GPCR activation. (Poster presentation: 11<sup>th</sup> Adrenoceptor symposium [WCP satellite], Glasgow, UK)

James P Farmer, Constance Dalton, Shailesh N Mistry, Charles A Laughton, Nicholas D Holliday.(2023) A fluorescent G protein mimetic peptide probe for high-throughput characterisation of intracellular allosteric modulator binding and GPCR activation. (Oral communication [prize winner] Life Sciences PGR Conference, Nottingham, UK)

## Acknowledgments

“ I much regret that want of space prevents my having the satisfaction of acknowledging the generous assistance which I have received from very many” – Charles Darwin, *On the Origins of Species*

Much like Darwin on his renowned voyage on HMS *Beagle*, the journey which has culminated in this thesis has not been possible without the support of so many. I would first like to thank my incredible PhD supervisors Nicholas Holliday, Shailesh Mistry and Charles Laughton. Charlie, although we didn't have the opportunity to work together as much as planned, your input (especially when preparing for publication) was invaluable. I am particularly grateful for your kindness and generosity to a pharmacologist stuck in the headlights of oncoming chemistry during my time in the BDI, always making me feel like an integral part of the BDI family. Shailesh, your abiding enthusiasm and patience (with a pharmacologist playing chemist) is unmatched. Your inclusiveness and determination encourages the very best from your students and has given me the opportunity to learn much more than I could have hoped for amongst such admirable scientists. Lastly, Nick, it remains a privilege and honour to have had your steadfast leadership these past five years. Your faith in an overenthusiastic undergraduate and unwavering support has shaped me into the (still overenthusiastic) scientist I am today. You have pushed and inspired me through this turbulent journey, whether it be the highs of the first binding data or the lows of interpreting FCS data. You have encouraged me to present, network and engage with the wider scientific community and enabled my development at every opportunity and I will be forever grateful.

Secondly, it has been a joy to be a part of the Cell Signalling family. I have been welcomed since my first day as an undergraduate and the shared sense of humour and passion for science has been infectious and made for a unique environment to grow as a scientist. There are too many people to thank, but I would like to specially thank Laura Humphrys for introducing me to this

wonderful group and giving me the best possible start; Marleen for being the secret hero keeping everything running as it should; Tim, Joelle and all the SLIM team for guiding me through the complex world of microscopy (getting dangerously close to physics) and all the PIs for always being willing to give up their time, either to discuss findings or the latest quirks with the most recent University IT update. During my PhD I have made life-long friends, particularly Bianca Maria Casella, Desislava Nesheva, Clare Harwood, Hannah Lockington, Kelvin Cheung, Noemi Karsai, George Coney, Marieke Van Daele, Dehan Comez, Simon Platt, Owen Underwood, Lydia Ogorzinski and many more. Your friendship has been a constant delight; you are all fantastic scientists, and I can't wait to see what the future holds for you all. A particular mention should go to Nikki, your friendship, guidance, laughter and ability to put up with incessant classical music has kept me on the straight and narrow.

I must also thank the fantastic team at the British Pharmacological Society, without whom this research would not have been possible. I sincerely thank everyone involved with the Society and the AJ Clark Scholarship. Rachel Lambert-Forsyth and the entire team at the Schild Plot have been instrumental in providing opportunities, both as part of the studentship and the early career advisory group. Additionally, I would like to thank the Researcher Academy and Biochemical Society for awarding me travel grants to travel internationally to present my PhD findings.

I would also like to take the opportunity to acknowledge the teachers who had faith and guided me to pursue a love of science and biology. Particularly Laura Roberts, Paul Lott and Ian Harvey for always entertaining my need to know more.

Finally, all this would not have been possible without the support of my family. To my parents, you have provided me with more than anyone could dream of, ensuring I had the best possible teachers and encouraging me throughout my education. You have always been there when I have needed a confidence boost and even when I am on my own battling a particularly difficult experiment, your encouragement has kept me going. All my achievements I owe to you. I must also thank my sister, Emma, who I can

always rely on to make me laugh after a hard day. Lastly, I would like to thank Alice. I cannot imagine the last three years without your enduring support and encouragement.

## Abbreviations

$\beta$ -AR -  $\beta$  Adrenoceptor

ATCM - Allosteric ternary complex model

BRET - Bioluminescence Resonance Energy Transfer

B<sub>max</sub> – Maximal binding response

BSA - Bovine Serum Albumin

cAMP - Adenosine-3',5' cyclic monophosphate

CHA – Cyclohexyl alanine

CHO - Chinese Hamster Ovary

COPD - Chronic obstructive pulmonary disease

CRC - Concentration response curve

Cryo-EM - Cryogenic-electron microscopy

Cy5 – Cyanine5

DAG – Diacylglycerol

DDM - n-dodecyl- $\beta$ -D-maltopyranoside

DIBMA - di-isobutylene maleic acid

DMEM - Dulbecco's modified Eagle's medium

DMSO - Dimethyl Sulphoxide

DNA – Deoxyribonucleic acid

ECL - Extracellular Loop

EDTA - Ethylenediaminetetraacetic acid

ERK 1/2 - Extracellular Regulated Kinase 1/2

FBS - Foetal Bovine Serum

FCS – Fluorescence correlation spectroscopy

Fl-propranolol - BODIPY-FL-PEG8-(S)-Propranolol

FRET - Förster (or Fluorescence) Resonance Energy Transfer

GDP - Guanosine 5'-diphosphate

GPCR - G Protein Coupled Receptor

Gpp(NH)p - 5'-Guanylyl imidodiphosphate

GRK - G protein-coupled receptor kinase

GTP - Guanosine 5'-triphosphate

H33342 - Hoechst 33342 nuclear stain

HEK - Human Embryonic Kidney

HEPES - 4-(2-hydroxyethyl)-1-piperazineethanesulfonic acid

ICL - Intracellular Loop

IP3 - Inositol trisphosphate

mRNA – Messenger ribonucleic acid

NAM - Negative allosteric modulator

Nb - Nanobodies

Neo - Neomycin

NPY – Neuropeptide Y

NSB - Non-Specific Binding

PAM - Positive allosteric modulator

PBS - Phosphate Buffered Saline

PCH – Photon counting histogram

PCR - Polymerase Chain Reaction

PIP<sub>2</sub> - Phosphatidylinositol 4,5-bisphosphate

PKA - Protein Kinase A

PKC - Protein Kinase C

PYY – Peptide YY

RLU - Raw Luminescence Units

$R_{\max}$  - Relative Maximal Response

Tb - Terbium

TCM - Ternary complex model

TM - Transmembrane Domain

TMR/TAMRA – Tetramethyl rhodamine

TR-FRET - Time-Resolved FRET

Zeo - Zeocin

# Contents

Abstract .....	3
Publications arising: .....	6
Acknowledgments.....	8
Abbreviations .....	11
Contents .....	14
1. Introduction.....	2
1.1. On the subject of receptors. ....	2
1.2. G protein coupled receptors.....	7
1.2.1. Relating structure to function of GPCRs .....	10
1.2.2. Advances in exploration of G protein structure and function, in relation to the activation mechanism of GPCRs .....	14
1.2.3. The GPCR-G protein interaction and the high affinity state. ....	14
1.2.4. Pharmacological models of receptor binding and activation - GPCR conformational dynamics upon ligand binding .....	16
1.2.5. The ternary complex model.....	17
1.2.6. Pharmacological processes to quantify and explore receptor pharmacology .....	20
1.3. The advancement in intracellular allosteric modulator pharmacology .....	35
1.3.1. Unlocking the potential of intracellular allosteric modulators ...	35
1.3.2. Recent advancement in intracellular allosteric modulator drug discovery .....	38
1.4. G protein peptidomimetics .....	41
1.4.1. Exploring the GPCR-G protein interaction using G protein mimetics peptides.....	41

1.4.2.	Recent advancement in G $\alpha$ peptides and their potential role in Cryo-EM.....	45
2.	Thesis Aims .....	48
3.	Materials and Methods .....	51
3.1.	Materials .....	51
3.2.	Development of receptor constructs for cellular and membrane-based assays .....	52
3.2.1.	$\beta_2$ -AR constructs:.....	55
3.2.2.	NPY Y1 receptor constructs: .....	59
3.2.3.	Prostanoid EP <sub>2</sub> receptor constructs:.....	60
3.3.	Cell culture.....	60
3.3.1.	Cell line maintenance and passaging.....	60
3.3.2.	Cell line stable transfection by lipofectamine 3000 .....	63
3.3.3.	Procedure for cell freezing.....	63
3.3.4.	Derivation of SNAP-tagged receptor expression .....	64
3.4.	G $\alpha$ C-terminal peptides.....	65
3.5.	Membrane preparation and Terbium labelling of SNAP tagged receptors.....	65
3.6.	Time resolved Förster (or Fluorescence) Resonance Energy Transfer (TR-FRET) and Bioluminescence Resonance Energy Transfer (BRET) Assays: .....	67
3.6.1.	Direct measurement of fluorescent tracer binding recruitment measured by TR-FRET and BRET .....	67
3.6.2.	Characterisation of unlabelled ligand binding through fluorescent ligand competition.....	69
3.7.	Data analysis .....	69
4.	Identification of G $\alpha$ C-terminus peptides able to promote the GPCR high affinity state for orthosteric agonist binding.....	74
4.1.	Chapter introduction .....	74

4.2.	Introduction to employed techniques and receptors within this chapter. ....	74
4.2.1.	Time-resolved Förster Resonance Energy Transfer (FRET) assays for GPCR ligand binding. ....	74
4.2.2.	Targeting the $\beta_2$ -Adrenoceptor. ....	79
4.2.3.	Targeting the Neuropeptide Y Y1 receptor. ....	84
4.3.	Chapter aims: .....	86
4.4.	Methods .....	86
4.4.1.	Cell line generation and membrane preparation .....	86
4.4.2.	TR-FRET assessment to derive BODIPY-FL-PEG8-(S)-Propranolol affinity at the $\beta_2$ -adrenoceptor. ....	86
4.4.3.	TR-FRET assessment to determine allosteric behaviour of unlabelled $G\alpha_s$ C-terminal peptides. ....	88
4.5.	Results .....	90
4.5.1.	Validation of the HEK SNAP- $\beta_2$ -AR cell line and Fl-propranolol for use in TR-FRET ligand binding assays. ....	90
4.5.2.	Measuring the allosteric effects of $G\alpha_s$ C-terminus peptides on ligand binding at the $\beta_2$ -Adrenoceptor. ....	95
4.5.3.	Characterisation of $G_i$ derived peptide allosteric actions on NPY Y1 receptor ligand binding.....	107
4.6.	Discussion.....	109
4.6.1.	Initial validation of employing TR-FRET techniques for measuring ligand binding .....	110
4.6.2.	Using TR-FRET binding to determine the allosteric effects of G protein mimetic peptides. ....	112
5.	A click-chemistry approach to facilitating peptide-fluorophore coupling for the generation of fluorescent $G\alpha$ C-terminus peptides. ....	119
5.1.	Introduction.....	119

5.1.1.	Click chemistry and the advancement of fluorescent ligand technology and development.....	119
5.2.	Application of CuAAC for the generation of varied fluorescent <i>Gas19cha18</i> peptide tracers.....	121
5.2.1.	General methods .....	121
5.2.2.	Experimental procedures .....	123
5.2.3.	Results .....	124
5.2.4.	Discussion.....	130
6.	Development of fluorescent $G\alpha$ -C terminal peptides as GPCR binding and signalling biosensors through intracellular NanoBRET. ....	135
6.1.	Chapter introduction: .....	135
6.2.	Introduction.....	135
6.2.1.	NanoBRET as a method of detecting receptor-ligand interactions. ....	135
6.2.2.	Current methods for characterisation of intracellular allosteric modulator binding .....	138
6.2.3.	Background to additional alternative candidate $G_i$ coupled receptors used in this study. ....	139
6.3.	Chapter aims: .....	145
6.4.	Methods .....	145
6.4.1.	Cell line generation and validation .....	145
6.4.2.	Bioluminescence resonance energy transfer (NanoBRET) assays to monitor fluorescent G protein peptide recruitment. ....	146
6.5.	Results .....	149
6.5.1.	Establishing a NanoBRET binding assay to directly monitor TMR- <i>Gas19cha18</i> recruitment to the $\beta_2$ -Adrenoceptor in HEK293 cell membranes. ....	149

6.5.2.	Establishing a NanoBRET assay to directly monitor TMR-Gαi19cha18 recruitment to the Y1 receptor.....	169
6.5.3.	Characterisation of TMR-Gαi19cha18 binding at alternate GiPCRs.....	176
6.6.	Chapter discussion.....	179
7.	Employing Fluorescence Correlation Spectroscopy (FCS) to determine TMR-Gαs19cha18 stoichiometric binding relationships and GPCR low-affinity conformation binding.....	185
7.1.	Chapter introduction.....	185
7.2.	Introduction.....	186
7.2.1.	Fluorescence correlation spectroscopy as an approach to measure receptor-ligand interactions.....	186
7.2.2.	Current methods for the solubilization of cell surface receptors.....	188
7.2.3.	Chapter aims:.....	191
7.3.	Methods.....	191
7.3.1.	Characterisation of the effect of Bovine Serum Albumin (BSA) on measured TMR-peptide concentration in solution-based FCS.....	191
7.3.2.	Solubilization of ssβ <sub>2</sub> -AR-tsNluc receptors for use in FCS-based binding experiments.....	192
7.3.3.	Characterisation of TMR-Gαs19cha18 binding to DIBMA or DDM solubilized β <sub>2</sub> -Adrenoceptors by FCS.....	193
7.3.4.	General FCS acquisition setup.....	193
7.3.5.	NanoBRET binding assay for the characterisation of DDM and DIBMA solubilized receptors.....	194
7.3.6.	FCS data analysis.....	195
7.4.	Results and Discussion.....	198
7.4.1.	Characterisation of TMR-Gαs19cha18 in solution within Fluorescence correlation spectroscopy.....	198

7.4.2.	Application of FCS-based techniques to determine fluorescent ligand-receptor binding. ....	203
7.4.3.	PCH analysis of TMR- probe species in the absence and presence of $\beta_2$ -AR DIBMA particles. ....	209
7.4.4.	TMR- $G\alpha_s$ probe binding to DDM solubilised receptors can also be detected by FCS.....	211
7.4.5.	DIBMA and DDM purified $\beta_2$ -AR do not show agonist-dependent TMR- $G\alpha_s$ binding in NanoBRET binding studies. ....	216
7.4.6.	Concluding remarks.....	218
8.	Identification of novel intracellular modulators of the prostaglandin EP <sub>2</sub> receptor. ....	221
8.1.	Chapter introduction:.....	221
8.2.	Introduction.....	221
8.2.1.	Prostaglandin receptors and the role of EP <sub>2</sub> in disease.....	221
8.3.	Chapter aims:.....	224
8.4.	Materials and Methods .....	225
8.4.1.	Materials .....	225
8.4.2.	NanoBRET binding studies to monitor TMR- $G\alpha_s$ binding at the EP <sub>2</sub> receptor.....	225
8.4.3.	NanoBiT complementation assays to determine functional antagonism by candidate modulators.....	227
8.5.	Results and Discussion .....	228
8.5.1.	Validation of TMR- $G\alpha_s$ as an intracellular probe for small-molecule screening at the prostaglandin EP <sub>2</sub> receptor .....	228
8.5.2.	Employing TMR- $G\alpha_s$ in the screening of novel EP <sub>2</sub> receptor intracellular allosteric modulators.....	233
8.5.3.	Evaluation of CD006 efficacy in whole cell functional responses using NanoBiT complementation.....	237
9.	General Discussion .....	244

9.1.	Thesis Discussion .....	244
9.2.	Final Conclusions .....	255
10.	Bibliography .....	257

# **Chapter 1**

## Introduction

# 1. Introduction

## 1.1. On the subject of receptors.

The turn of the 20<sup>th</sup> century saw the birth of arguably the most revolutionary concept in modern medicinal biology, receptor theory. In 1905 J.N. Langley, and arguably his contemporary P. Ehrlich, both postulated there existed a chemical substance which mediated drug action of physiological stimuli and explained the variability and selectivity of drugs upon different tissues, which Langley first described as the “receptive substance”(Hill, 2006; Maehle et al., 2002). This paved the way for Hill and Langmuir to propose a relationship between drug action and receptor occupancy in 1909, which began the era of quantitative pharmacology(Hill, 1909). Hill’s equation envisaged receptors as chemical entities for the first time and described drug action based on the relative concentrations of ligand and receptor and an equilibrium dissociation constant ( $K_D$ ) defining ligand affinity. However, it was not until 1926 when this theory was first utilised experimentally by Professor Alfred Joseph Clark to describe the concentration response curve(Clark, 1926). Clark’s proposed theory assumed functional response was directly related to the proportion of occupied receptors(Clark, 1933). Clark’s pioneering work allowed for the era of quantitative pharmacology to flourish, identifying methods for the characterisation of agonist and antagonist properties from functional responses in isolated tissue, exemplified by the work of Gaddum, Schild (see section 1.2.6.2) and Stephenson. Building on from Clark’s initial hypotheses, Stephenson postulated agonist effect was due not only to defined affinity (occupancy), but also agonist efficacy. This provided the first mathematical explanation of the idea of a disconnect between agonist affinity and agonist efficacy, allowing for the conceptualisation of full versus partial agonism and the existence of receptor reserve(Stephenson, 1956). Despite these findings however, receptor theory divided the scientific community until

1948 when R. Ahlquist first defined the  $\alpha$  and  $\beta$  adrenergic responses to adrenaline, noradrenaline and isoprenaline at various tissues(Ahlquist, 1948).

Today we have a plethora of receptor and protein families, thanks to advancements in cellular and molecular pharmacology assays and genome sequencing. Subsequently, early-stage therapeutic validation has shifted away from identifying broad physiological responses to defining specific receptor functions and designing receptor targeted compounds to bring about specific physiological change. Of these receptors, G protein coupled receptors (GPCRs) are the largest superfamily of membrane-bound receptors in the human genome with over 800 singular full-length receptors encoded. GPCRs remain the most therapeutically targeted receptor family, with over 27% of the global market share of therapeutic drugs(Hauser et al., 2017). This domination of the pharmacological market is primarily due to their diverse signalling characteristics and their subsequent role in numerous physiological processes across all aspects of human physiology. Despite the large number of identified GPCRs, only around 100 have been employed by therapeutics, of which only 40-50 target class A GPCRs(Alexander et al., 2011). This small proportion of receptors relative to the multitude of available therapeutics targeting GPCRs (over 400 in 2017(Hauser et al., 2017)) highlights the flexibility of responses available through GPCR exploitation, and leaves open the possibility for alternative therapeutic modalities to exploit this family further.

Of the therapeutics available, the majority function as orthosteric ligands, binding at the same site as the endogenous ligand, and produce either inhibition or activation of GPCR signalling. This form of modulation has proven effective at treating a host of diseases, however, it is not without its disadvantages, including the problem of low receptor selectivity (due to high homology within receptor subtypes, such as muscarinic or adrenoceptor families) and

thus producing off-target side effects(Andersson et al., 2011; D. Yang et al., 2021a).

Functional characterisation of receptor ligands through effects on signalling leads to the following broad groups: orthosteric agonists, orthosteric antagonists, and allosteric ligands. Orthosteric agonists primarily function through mimicking of the endogenous ligand binding properties, allowing for binding within the orthosteric binding pocket and activation of the receptor once bound (their intrinsic efficacy). Therapeutic agonists classically promote the same response to that seen with the endogenous ligand responses (Figure 1.1). However, agonists can vary in intrinsic efficacy relative to the endogenous or other reference agonists, for example a lower efficacy agonist can be revealed as partial agonism, in which its maximum response in an assay is lower than that for the reference ligand(Bosier and Hermans, 2007). Furthermore, several recent studies have suggested that some ligands function as biased agonists, in which the balance of effects through different downstream pathways (e.g. G protein,  $\beta$ -arrestin) differs from the reference agonist. Structural explanations for biased agonism describe the ability of these ligands to select between different functionally distinct receptor conformations, though other explanations (e.g., different ligand binding kinetics affecting spatiotemporal signalling) are also possible(Herenbrink et al., 2016; Piekielna-Ciesielska et al., 2018; Reiter et al., 2012; Sengmany et al., 2017; Sivertsen et al., 2013; Stott et al., 2016).

Antagonists inhibit receptor signalling and are further subcategorised based on their ability to be overcome through increased concentrations of agonist and their mode of action (Figure 1.1). Surmountable antagonism is the most classical example of antagonism, whereby antagonism arises from competitive reversible interactions at the orthosteric binding site, thus allowing complete reversal of inhibition upon addition of higher concentrations of agonist. In contrast, non-surmountable effects (reduction in the

agonist maximum response, regardless of its concentration) can be derived from non-equilibrium conditions (e.g. the antagonist is slowly dissociating or irreversibly bound), or through ligands exhibiting allosteric non-competitive behaviour (Hulme and Trevethick, 2010; Sykes and Charlton, 2018).

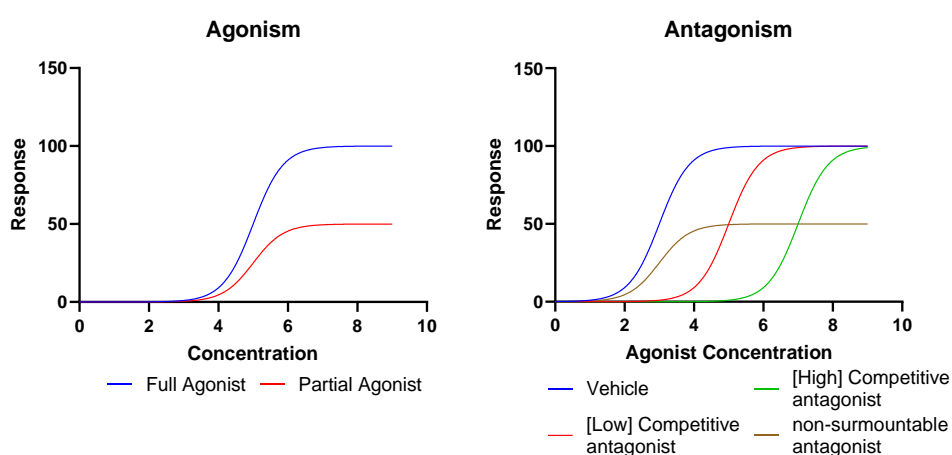


**Figure 1.1. Example data depicting the classical responses attributed to different classes of therapeutic ligands.**

Allosteric ligands exhibit a wide variety of behaviours less easily defined than classical agonists and antagonists, however, broadly encompass compounds which bind at sites independent from the orthosteric binding site (usually affording them greater capacity for target selectivity between closely related receptors). Traditionally, allosteric ligands are said to modify the effects of orthosteric agonist cooperatively, such as endocrine or neurotransmitter signalling. Positive allosteric modulators (PAMs) increase agonist affinity and/or efficacy, thereby increasing activity, by promoting agonist-favoured receptor conformations and may or may not have their own efficacy as receptor agonists (agoPAMs). Conversely, negative allosteric modulators (NAMs) or “non-competitive antagonists” decrease the effects of agonists either by reducing the affinity for agonist ligands or by reducing the ability of receptors to

signal via secondary messengers (either by steric hindrance or unfavourable conformational stabilisation). Additionally, allosteric modulator binding has the potential to be dependent on receptor conformation. For example, modulator binding may be increased at the active conformation, in this instance “uncompetitive” mechanisms may be observed whereby the inhibitory effect of the modulator is enhanced by the presence and binding of the orthosteric agonist. This in particular is a potentially useful mechanism for the design of more selective compounds which display a “use-dependence” (effects of the modulator will be greater in physiological systems and receptors with a high degree of native stimulation), thereby having the greatest therapeutic effect at localised sites of receptor activation (Åström and Persson, 1961; Chen et al., 1992). An example of this benefit can be seen with the drug Memantine, a low affinity, voltage-dependent, uncompetitive antagonist of glutamatergic NMDA receptors. Used to reduce the cognitive decline in Alzheimer's disease, Memantine is used to reduce the effects of excitotoxicity at glutaminergic neurones. Its ability to target the high proportion of over-active NMDA channels at the site of hyperexcitation, while having limited effects on physiological levels of glutamate signalling, allows Memantine to display reduced side-effect profiles to more classical competitive inhibitors (Cacabelos et al., 1999; Chen et al., 1992). True allosteric modulators, without their own pharmacological activity, also provide the additional benefit of being reliant on the binding of endogenous orthosteric ligands to observe an effect. In many instances the maximal size of this effect on orthosteric agonist pharmacology (either affinity, or efficacy or both) is limited by the extent of co-operativity between the orthosteric and allosteric ligands. This can generate a “ceiling” to the maximum response of the allosteric modulator, which can be advantageous in reducing the risk of on-target side-effects and overdose (Casadó-Anguera and Casadó, 2022; May, 2003; Oswald et al., 2016a; Sachpatzidis et al., 2003).

## 1.2. G protein coupled receptors

The GPCR superfamily can be separated into classes dependent on their evolutionary homology and specific receptor families: Classes A (Rhodopsin family), B (secretin family), C (metabotropic glutamate family), D (Fungal only), E (Cyclic AMP family [from *D. discoideum*]) and F (Frizzled/Smoothed family). Over 700 GPCRs belong to the Class A family, the majority of which are olfactory receptors and 241 are non-olfactory receptors, and therefore Class A GPCRs are most commonly targeted by therapeutics (Kroeze, 2003).

GPCRs mediate their cellular responses through the employment of at least two distinct signalling cascades, the G-protein and  $\beta$ -arrestin pathways (although more recent studies suggest additional signalling protein interactions exist for certain GPCR families (Happ et al., 2022)). G-protein signalling can be separated into four main classes depending on the specific G-protein employed by the receptor, which classically differ through employment of variable  $\alpha$  subunits, in combination with  $\beta$  and  $\gamma$  subunits. All classes of G-proteins function in a GTPase cycle and therefore rely on the exchange of GDP to GTP within the  $G\alpha$  subunit to facilitate activation, followed by GTP hydrolysis to terminate  $G\alpha$  protein signalling. Agonist binding and the subsequent change in receptor conformation to an “active state” results in G-protein GDP-GTP exchange, uncoupling from the receptor and separation of the three subunits into two functional units, membrane bound  $G\alpha$ -GTP and the  $G\beta\gamma$  dimer, which both signal in various downstream pathways (Syrovatkina et al., 2016).

G-protein classes are defined by the specific  $G\alpha$  subunit employed:  $G\alpha_{i/o}$ ,  $G\alpha_s$ ,  $G\alpha_{q/11}$  or  $G\alpha_{12/13}$ . These classes can be further separated into isoforms, with qualitatively similar signalling mechanisms.  $G\alpha_{i/o}$  is the largest class made up of  $G\alpha_{i1}$ ,  $G\alpha_{i2}$ ,  $G\alpha_{i3}$ ,  $G\alpha_o$ ,  $G\alpha_t$ ,  $G\alpha_g$

and  $G\alpha_z$  (Schiöth and Lagerström, 2008). Both  $G\alpha_{i/o}$  and  $G\alpha_s$  are involved with regulation of cyclic adenosine monophosphate (cAMP) production through adenylyl cyclases and the subsequent control of cAMP sensitive binding proteins, such as protein kinase A.  $G\alpha_s$  primarily stimulates adenylyl cyclases and promotes cAMP mediated signalling. Increased cellular cAMP activates protein kinase A (PKA) by binding to the regulatory PKA domains of the inactive tetramer, freeing the catalytic PKA domains to act on downstream targets (Taylor et al., 2012). Such targets include modulating the activity of key intracellular signalling molecules in the mitogen-activated protein (MAP) kinase cascade pathway (Goldsmith and Dhanasekaran, 2007), driving changes in gene transcription and ERK signalling. Additionally, cAMP also signals through exchange proteins directly regulated by cAMP (EPACs) which bind cAMP and are associated with cellular functions including hormone secretion and formation of cell junctions (Cheng et al., 2008).

Activated PKA also acts to regulate L-type  $Ca^{2+}$  voltage channels in cardiac muscle for  $\beta_1$ -adrenoceptor ( $\beta_1$ -AR) mediated contraction (Budde et al., 2002), and activate myosin light chain phosphatase for  $\beta_2$ -adrenoceptor ( $\beta_2$ -AR) mediated smooth muscle relaxation (Aslam et al., 2010). In contrast,  $G\alpha_{i/o}$  subunits inhibit the function of certain isoforms of adenylyl cyclases (AC1, 5 & 6) (Sadana and Dessauer, 2009), reducing intracellular cAMP and limiting further downstream signalling, such as PKA driven processes.  $G\alpha_{i/o}$  signalling also drives ERK activation and subsequent gene transcription (as a result of inhibiting PKA driven crosstalk with the Ras-Raf-MAPK cascade usually associated with tyrosine kinase signalling (Goldsmith and Dhanasekaran, 2007)).

Unlike these cAMP associated counterparts,  $G\alpha_{q/11}$  is primarily involved in driving release of intracellular calcium.  $G\alpha_{q/11}$  subunits activate phospholipase C $\beta$  which in turn facilitates the conversion of phosphatidylinositol 4,5-bisphosphate (PIP<sub>2</sub>) into inositol

trisphosphate (IP<sub>3</sub>) and diacylglycerol (DAG). IP<sub>3</sub> is then able to release calcium stored in the endoplasmic reticulum, increasing intracellular calcium, and DAG promotes activation of protein kinase C and further downstream signalling (Syrovatkina et al., 2016). Both G $\alpha_i$  and G $\alpha_s$  have also been shown to play a role in calcium mobilisation, primarily through employment of the G $\beta\gamma$  subunit which has been shown to regulate adenylyl cyclases, K<sup>+</sup> channels and Ca<sup>2+</sup> channels via the  $\beta$ -isoforms of phospholipase C (Khan et al., 2013).

The  $\beta$ -arrestin signalling pathway is primarily involved in GPCR inactivation and receptor internalisation, although arrestin independent internalisation has been shown to occur (Bhatnagar et al., 2001; Gray et al., 2003; Lee et al., 1998). In total, there are four main isoforms of arrestin, Arrestins-1 to 4. Despite these various isoforms, Arrestin-2&3 ( $\beta$ -arrestin-1/2) are the primary forms involved in classical signalling and are denoted as “non-visual” due to their ubiquitous expression compared with the “visual” arrestins almost exclusively found within photoreceptive cells (Shukla and Dwivedi-Agnihotri, 2020).

$\beta$ -arrestin signalling is promoted upon receptor activation, and subsequent GPCR C-terminal and / or intracellular loop phosphorylation by G protein-coupled receptor kinases (GRKs) recruited by the free membrane G $\beta\gamma$  subunit (Lefkowitz and Shenoy, 2005).  $\beta$ -arrestin recruitment facilitates receptor inactivation through several pathways.  $\beta$ -arrestin binding itself provides steric inhibition of G-protein binding thus preventing further G-protein signalling, and promotes clathrin mediated receptor internalisation and receptor degradation through binding of E3 ubiquitin ligases (Shenoy and Lefkowitz, 2011). Additionally, arrestins can promote the activation of proteins involved in degradation of G-protein mediated secondary messengers, such as diacylglycerol kinases for the degradation of DAG and phosphodiesterases (PDEs) for the localised degradation of cAMP (Baillie et al., 2007; Houslay et al.,

2017). These reduce the downstream effects of G-protein pathways upon  $\beta$ -arrestin activation(Reiter et al., 2012). In addition to this inhibitory role,  $\beta$ -arrestin signalling has been shown to scaffold proteins involved in ERK pathway signalling and gene expression, and potentially drive receptor compartmentalisation post internalisation, suggesting  $\beta$ -arrestins play a larger role in cellular control than just GPCR inactivation(Thomsen et al., 2016; Zhao et al., 2004). Indeed, it is the dual functionality of  $\beta$ -arrestins that has driven research into therapeutics with a preferred effect on the signalling of certain secondary messengers, termed biased signalling (see section 1.1). Additionally, recent advancements in our understanding of arrestin structure and function have highlighted possible routes for therapeutic exploitation. The identification of GPCR phosphorylation patterns which drive particular arrestin functional activities, termed “phosphorylation barcoding”, and recent structural information, suggest the possibility of multiple arrestin conformations driving particular functions(Cao et al., 2022; Kawakami et al., 2022; Nobles et al., 2011). These new concepts have opened the door for a wider appreciation of arrestin-mediated responses in early drug discovery. Together, such diverse GPCR mediated signalling pathways allow for GPCRs and G-proteins to play a vital role across a plethora of physiological responses and, as such, are perfectly positioned for pharmacological exploitation.

### *1.2.1. Relating structure to function of GPCRs*

GPCRs all display a degree of structural homology, consisting of an extracellular N-terminus, seven  $\alpha$ -helical transmembrane domains (from which they get their alternative name seven transmembrane receptors [7TM]), three extracellular loops, three intracellular loops and an intracellular C-terminus, which is often linked to the plasma membrane via palmitate to produce a fourth intracellular loop in

certain families. This bundled  $\alpha$ -helical structure allows for multiple binding pockets within and around the receptor, allowing access for smaller compounds with the potential to alter receptor conformation and function(Alexander et al., 2011).

The orthosteric binding site for endogenous and small molecule ligands is generally found within the upper half of the 7TM bundle, accessed via the extracellular surface, and relies on interactions with multiple transmembrane helices to facilitate orthosteric ligand binding (Figure 1.2).The classical example of this relationship can be seen with the binding mechanisms of ligands to the  $\beta_2$ -AR. When binding its endogenous catecholamine ligands (e.g., adrenaline, noradrenaline), a subset of particular residues within the upper region of the 7TM bundle facilitate ligand binding and receptor activation. Initial mutagenesis studies by Strader and Dixon identified an aspartic acid residue (D113<sup>3,32</sup>) on TM3 was essential for ligand binding through the formation of an ionic bridge between its carboxyl group and the amine group of catecholamine ligands. Similarly, mutation of serine residues S204 and S207 in helix 5 results in a reduction in agonist efficacy due to a loss of hydrogen bonding with their respective hydroxy side chains, while loss of F290 further limits agonist binding through its ability to stabilize the interaction of the aromatic catechol-containing ring with the receptor(Rasmussen et al., 1999; Rosenbaum et al., 2007; Strader et al., 1989, 1987).

Further diversity of the GPCR orthosteric ligand binding pocket can be achieved through the incorporation of interactions with the extracellular loops and N-terminus for larger ligands. This is exemplified in the case of peptide ligands (e.g., chemokines) which, due to their greater size and structural variability, allow for much greater and diverse binding modalities(Wacker et al., 2010; Yang et al., 2018; Zerbe et al., 2021). Chemokines in particular display a two-step binding method, forming initial interactions with the receptor N terminus, facilitating, through conformational change of

the extracellular regions, further binding with the ECL and 7TM regions(Liu et al., 2022).

In the case of the class A receptors, various ligands bind to similar binding sites within the helical bundle, however, structural variations among the extracellular loops, variations in pocket size and physiochemical properties, results in diverse ligand recognition(Katritch et al., 2013). Despite this diversity, Class A receptor activation mechanics remain relatively conserved throughout the various ligand sub-families. Within the structures are evolutionary conserved motifs termed “micro-switches” such as CWxP, PIF, Na<sup>+</sup> binding pocket, NPxxY, and DRY regions, which link the orthosteric binding pocket to the G protein-coupling region and promote G protein activation via allosteric interactions(Rasmussen et al., 2011; Zhou et al., 2019). As discussed previously relating to the  $\beta_2$ -AR, agonist binding promotes co-ordinated reorganisation of the rotameric switch of W<sup>6.48</sup> (using the Ballesteros/Weinstein numbering system(Ballesteros and Weinstein, 1995)) within the CWxP motif, disruption of the NPxxY motif interactions with TM1 and 2 inner ends, TM3 DRY motif network with TM6 and intracellular loop residues, and PIF and Na<sup>+</sup> pocket structural rearrangements. Together these result in a structural rearrangement that involves rotation and movement of the inner ends of key transmembrane helices relative to each other, particularly of an outward displacement of the cytoplasmic end of TM6, the classical sign of receptor activation. Rearrangement of the Na<sup>+</sup> site also facilitates the inward movement of TM7 towards TM3 which, combined with the rotation of Y<sup>7.53</sup> in the NPxxY motif, allows for significant packing together of TM7-TM3. This packing alters the function of the DRY region found at the base of TM7, which forms a salt bridge interaction between D/E<sup>3.49</sup> and R<sup>3.50</sup>. R<sup>3.50</sup> also forms an additional salt bridge (the “ionic lock”) with E<sup>6.30</sup> stabilising the connection between TM3 and ICL2/TM6 in the inactive state,

however, this interaction is lost upon ligand binding and R<sup>3.50</sup> is freed to interact with alternative residues and facilitate stronger G protein binding (D. Yang et al., 2021b). Additionally, binding of G $\alpha$  subunits through interactions with rearranged TM3, 5 and 6 and the intracellular loops, aids in the elimination of this interaction and promotes formation of the active state, leading to the allosteric cooperativity between agonist and G protein binding to the receptor, discussed below.

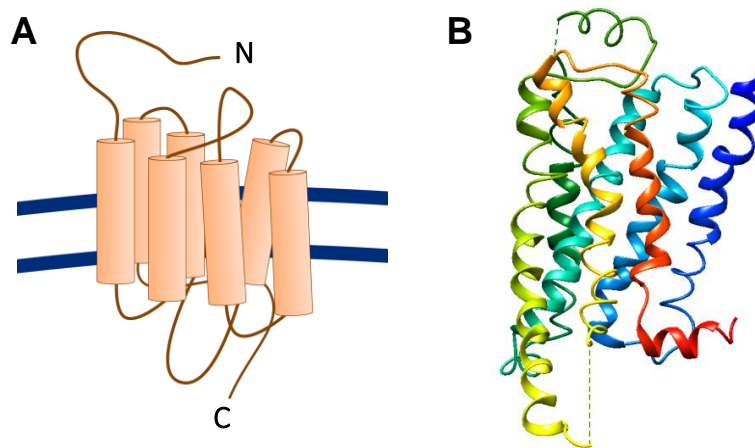


**Figure 1.2. Structure of a classical class A GPCR.** (A) Representation of Class A GPCR structure embedded in the plasma membrane. (B) Cryo-EM derived structure of the class A  $\beta_2$ -adrenoceptor (verified through numerous x-ray crystallography and cryo-EM structures) indicating N terminus in blue and C terminus in red (PDB: 7DHI)(Yang et al., 2020). (Intracellular loop 3 is excluded due to high positional variability as a result of structural flexibility, and is often deleted or replaced in the protein to aid crystallisation)

### *1.2.2. Advances in exploration of G protein structure and function, in relation to the activation mechanism of GPCRs*

In recent years, GPCR drug discovery has benefitted from increasing availability of crystal and cryoEM structures to provide a more rational basis for drug design. Previously, the ability to obtain GPCR crystal structures has been hindered by difficulties in receptor extraction, crystal formation for X-ray crystallography and large variability in receptor conformations. The recent development and advancement of Fab fragment, nanobody, mini-G-protein, stabilising mutations (e.g., STAR technology), and the increasing resolution of cryo-EM technologies, has driven the exponential increase in available GPCR structures in the last decade. Such technologies have allowed for stabilisation and visualisation of receptors in multiple conformational states while bound to effectors and ligands. This revolution in structural technology is perfectly demonstrated by how studies such as the visualisation of the active  $\beta_2$ -adrenoceptor in complex with  $G\alpha_s$  solved in 2011, which allowed visualisation of the integral interactions required for receptor activation incorporating effector binding and thus broadening our understanding of GPCR dynamics (Rasmussen et al., 2011), to become almost routine.

### *1.2.3. The GPCR-G protein interaction and the high affinity state.*

G protein  $\alpha$  subunits form the primary interactions between heterotrimeric G proteins and receptors. Structurally,  $\alpha$  subunits consist of a GTP-binding domain, helical insertion domain and protruding C terminal tail. The GTP-binding domain shares a large portion of structural homology with Ras-like, small, GTPases and contains both switch 1 and switch 2 regions, which change conformation depending on the nature of the bound nucleotide. The helical insertion domain is found within the GTP-binding region before switch 1 and hinders the nucleotide dissociation from the

GTP-binding site. The C terminal region predominantly forms an alpha helical structure, termed the  $\alpha 5$  helix, which is one of the main regions involved in GPCR binding and selectivity for particular  $G\alpha$  subunits (Cherfils and Chabre, 2003).

The improved understanding of GPCR activation and crystallisation, in combination with previous mutagenesis studies and recent molecular dynamic simulations, allows for the identification of essential sites of interaction between GPCRs and G proteins (Hilger et al., 2018; Maeda et al., 2019; Mafi et al., 2023; Rasmussen et al., 2011; Toyoda et al., 2023; Weis and Kobilka, 2008). These structures have shed light on the mechanism behind the observed ability for G protein binding to promote increased agonist affinity for GPCRs, and vice versa, therefore promoting a receptor “high-affinity state”. Ultimately the allosteric stabilisation of this ternary complex is the basis of agonist action at GPCRs. Co-crystallised GPCR-G protein structures indicate the helical C-terminal region of the different  $G\alpha$  subunits is essential for its selective recognition and activation by receptors (Flock et al., 2017; Mafi et al., 2023). The  $\alpha 5$  helix docks within a cavity between TM3 and TM5 facilitating the outward movement of TM5-TM6, thereby generating a conformation towards the classical active conformation, and aiding in breaking of the ionic lock (Mafi et al., 2023). Additionally, the  $\alpha 5$ -helix limits the reformation of the ionic lock between TM3 and ICL2/TM6, maintaining the outward shift indicative of orthosteric ligand binding and receptor activation. This interaction is primarily through non-polar interactions within the pocket, with the final four amino acids of the  $\alpha 5$  helix being essential for coupling, as identified through mutagenesis and chimeric messenger studies (Gilchrist et al., 2002; Hamm et al., 1988; Rens-Domiano and Hamm, 1995; Thaker et al., 2014). In the case of  $G\alpha_s$ , the final amino acids YELL form a reverse turn motif which allows for the last two leucine residues to form a contact point with TM6 and aid in the outward displacement of this region

in receptor activation. Similarly, the tyrosine (Y) residue strongly interacts with the conserved arginine (R) residue in TM3 and aids in locking the two proteins together (Mannes et al., 2021). In the case of  $G\alpha_i$  binding, the binding pocket of  $G\alpha_i$  selective receptors is narrower, requiring  $G\alpha_i$  to form much closer hydrophobic interactions within the binding pocket (for class A GPCRs). This may aid in explaining the greater  $G\alpha_i$  promiscuity displayed by classically defined  $G\alpha_s$  coupled receptors (e.g.,  $\beta_2$ -Adrenoceptors), than  $G\alpha_i$  coupled receptors (Edward Zhou et al., 2019).

#### 1.2.4. *Pharmacological models of receptor binding and activation - GPCR conformational dynamics upon ligand binding*

Receptors, such as GPCRs can be most simply described as molecular switches which exist in a dynamic equilibrium between an unbound, bound and activated states:



*Unbound Inactive Active*

How well drugs bind to a site of the receptor ( $D + R \rightleftharpoons DR$ ) is known as the “affinity”, whilst the ability of the drug, once bound, to activate the receptor ( $DR \rightleftharpoons DR^*$ ) is known as the intrinsic efficacy. Both elements, alongside characteristics of the signalling system, then relate to the potency and maximal response of agonist concentration responses curves determined by the activated receptor engaging secondary messenger effector proteins, including G proteins and arrestin signalling (Stott et al., 2016).

Based on the law of mass action, the affinity of a ligand can be defined by the forward and reverse rates of binding  $D+R \rightarrow DR/ D+R \leftarrow DR$ , which are each proportional to the participant

concentrations. The constants relating concentration to these rates are respectively, the ligand association ( $k_{on}$ ) and dissociation rate constants ( $k_{off}$ ). At dynamic equilibrium association and dissociation rates are equal, such that the concentrations in the binding event (D, R and DR) no longer change.  $K_D$  ( $k_{off}/k_{on}$ ) is defined at this point as the equilibrium dissociation constant.  $K_D$  has been a staple measurement of ligand-receptor interaction since its first coinage by Hill in 1909. Hill reported that ligand affinity,  $K_D$  relates to receptor proportional occupancy ( $\alpha$ ) and ligand concentration in the Hill-Langmuir equation (Hill, 1909):

Equation 1.

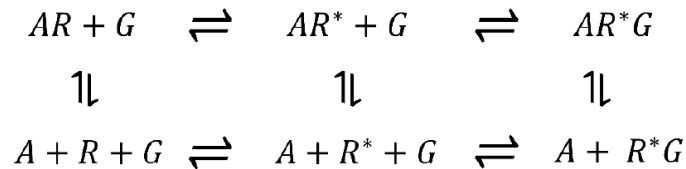
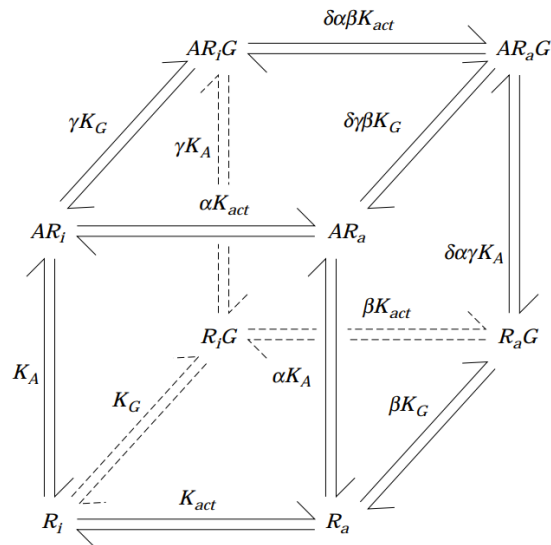
$$\alpha = \frac{[D]}{[D] + K_D}$$

Through this,  $K_D$  can further be defined as the concentration of ligand [D] required to occupy 50% of receptors at equilibrium (when  $K_D = [D]$ ,  $\alpha=0.5$ ). However, although this relationship provides a basic description of GPCR function/dynamics, it remains incomplete due to the lack of incorporation of effector proteins. The need to account for the role of such effectors resulted in the “ternary complex model” (De Lean et al., 1980).

#### 1.2.5. *The ternary complex model*

As shown in both the GPCR activation pathway and the interactions with native G proteins (see section 1.2.1&1.2.3), the relationship between the inactive “DR” complex and the active “DR\*” relies on complex conformational changes as a result of both ligand and secondary messenger binding. As such, it is suggested that agonist bound GPCRs stabilise effector binding allosterically, while effector binding equally enhances the binding affinity of orthosteric

agonists, generating distinct low- and high-affinity states (in reference to the orthosteric agonist)(Warne et al., 2019). This three-way interaction is described by the “ternary complex model” (Figure 1.3A), originally described by De Lean in 1980(De Lean et al., 1980).

**A****B****C**

**Figure 1.3. Evolution of the Ternary Complex model** (A) The original ternary complex model derived from the two-state model and incorporated G protein binding, where G protein binding promotes the stabilisation of the ARG complex(De Lean et al., 1980). (B) The extended ternary complex model incorporated constitutively active receptors ( $R^*$ ), where a receptor can adopt the active conformation in the absence of an agonist (Costa and Herz, 1989; Samama et al., 1993) (C) The cubic ternary complex model proposes the receptor exists in eight different forms, either bound to a ligand (A) and/or a G protein (G) and existing in an active ( $R_a$ ) or inactive ( $R_i$ ) state(Weiss et al., 1996).

However, this initial hypothesis was first expanded upon to incorporate the identification of receptor constitutive activity (creating the “extended ternary complex model”), before again being expanded to include the thermodynamic interactions between G protein and GPCR in the absence of agonist to create the “cubic ternary complex model” (Figure 1.3B&C).

The intricacy of the cubic model, although the most complete description of the agonist-receptor-effect interaction, renders it unlikely to be of use in any practical application. Similarly, despite the growing complexity of the ternary complex model, the cubic model also remains incomplete in describing the complex interactions at play between GPCR, ligand and effector, especially in the context of ligand bias.

#### *1.2.6. Pharmacological processes to quantify and explore receptor pharmacology*

##### 1.2.6.1. Derivation of agonist functional parameters and their relation to ligand affinity and efficacy.

Development of novel therapeutics has changed dramatically since the first synthetic therapeutic, chloral hydrate, was developed in 1869. However, despite rapid advancement in scientific knowledge and opportunity, the main question asked of any new drug has not changed, what does it do? This forms the bases of all functional experiments used to examine and identify novel therapeutics.

Within the realms of GPCR pharmacology, there are two main aims within experimental setups: measurement of ligand binding parameters (e.g.,  $K_D$ ,  $B_{max}$ ) and measurement of receptor functional responses ( $EC_{50}/IC_{50}$ ,  $R_{max}$ , co-operativity factors)(Hill, 2006). Advancement in radioligand/fluorescent ligand binding studies has provided accessibility to ligand affinity data, however, the measurement of ligand efficacy remains challenging(Soave et al., 2020a; Stott et al., 2016). At the forefront of this problem is the

conditional nature of functional assays, whereby their output is both a result of ligand intrinsic efficacy, affinity and system dependent factors (such as cell type, receptor expression levels, accessory proteins and point in the signalling cascade). As such, what is usually described as ligand efficacy is a combination of both intrinsic and system dependent efficacy describing the ability of a ligand to promote downstream signalling (Stott et al., 2016). Of the various methods of quantifying ligand parameters, the concentration-response curve is the most widely used for the derivation of ligand maximal responses ( $R_{\max}$ ) and potency ( $EC_{50}$ ). These parameters are a mainstay in modern pharmacology, however, despite providing a method of comparing ligands in a single experiment (at chosen endpoints) their high system dependence makes them poor candidates for derivation of comparable affinity and efficacy values. In particular, the application of over expressing cell systems (e.g., Hek 293/CHO transfected lines), or functional readouts with high amplification in the signalling pathway, resulting in  $R_{\max}$  being achieved with only a fraction of total receptor occupancy, resulting in the presence of “spare receptors” commonly known as receptor reserve. In particular, this can result in agonists of quite different intrinsic efficacy producing the same  $R_{\max}$  (though through different proportional receptor occupancies), thereby overestimating efficacy because of the lack of observed partial agonism.

Subsequently, the need to quantify functional data and derive parameters that represent pharmacological properties of GPCR agonists in a comparable way, led to the development of various empirical operational models. The most well-known of these is the Black and Leff operational model of agonism (Black and Leff, 1983). The Black and Leff model has become prominent within pharmacology due in part to its ability to employ sets of concentration response curve (CRC) data. The maximal response of the system must also be estimated in the fit ( $E_{\max}$ ) requiring the

operational model to be fit globally to multiple data sets, rather than to individual experimental data sets. Their model provides an estimate of ligand efficacy through a transducer ratio in the form of “ $\tau$ ”. Black and Leff put forward a model which described agonist ligand action as a function of the system maximal response ( $E_{max}$ ), agonist dissociation constant ( $K_A$  or  $K_D$ ), agonist concentration ( $[A]$ ) and efficacy ( $\tau$ ):

Equation 2.

$$E = \frac{E_{max}\tau[A]}{K_A + [A](1 + \tau)}$$

This is derived from the ligand occupancy Hill equation ( $K_D$  is represented as  $K_A$  in equation 2), that is, receptors and ligands follow the laws of mass action, and that the concentration of agonist occupied receptors  $[AR]$  is dependent on ligand concentration, number of receptors and ligand affinity. The relationship between  $[AR]$  and the system response was then modelled as a hyperbolic curve, leading to the definition of  $K_E$  concentration of agonist-receptor complexes that produce a half-maximal response. In equation 2,  $\tau$  is a parameter based on the total receptor concentration ( $R_T$ ) and  $K_E$  ):

Equation 3.

$$\tau = \frac{R_T}{K_E}$$

This therefore still makes  $\tau$  a combined parameter for ligand and systemic effects, since  $R_T$  is a property of the system (receptor number), and the coupling efficiency  $K_E$  depends both on ligand intrinsic efficacy and system effects. As a consequence,  $\tau$  (or the transduction coefficient  $\tau / K_A$ ) is often expressed relative to a reference agonist to allow normalisation and ranking of agonists

across assays, for example in considering ligand bias (Stott et al., 2016). Furthermore, the exploration of different ligands within the same assay system and subsequent normalisation of response data to remove system dependent components further strengthens the validity of  $\tau$  as an estimation of intrinsic efficacy.

One weakness of operational models is their assumption that all data collected is at experimental equilibrium. For example, Klein Herenbrink et al (Herenbrink et al., 2016) have demonstrated that functional measurements of agonist dissociation constants and  $\tau$  using the operational model vary drastically depending on the timepoint of collection. This can arise because agonists with slow binding kinetics ( $k_{off}$ ) take longer to reach binding equilibrium, affecting functional potency and maximal response at earlier (non-equilibrium) timepoints. With recent development of techniques applicable for measuring responses regularly over time, real-time functional response assays have allowed for the development of analyses to model functional kinetic data by Hoare *et al* (Hoare, 2018; Hoare et al., 2020). These models use the concepts of the Black and Leff model as a basis to determine kinetically derived measures of affinity ( $K_D$ ) and efficacy through direct measurement of functional response over time. By facilitating analysis of complete kinetic profiles of cellular responses, it is possible to obtain a much broader understanding of cellular processes resulting from ligand/therapeutic intervention. These models and their application are considered in more detail in chapter 6.

#### 1.2.6.2. Functional derivation of antagonist affinity.

Mathematical scrutiny of functional responses allowed easy analysis of agonist action; however, these initial methods of defining ligand action provide little aid in the characterisation of antagonists. Studies carried out by Clark and Gaddum established a pattern of rightward shifts in agonist responses with the addition of

a competitive reversible antagonist(Clark, 1937). Gaddum based his equation on assuming equilibrium and that an equivalent functional response could be generated by the same (although unknown) level of proportional receptor occupancy ( $\rho_A$ ) by the agonist ( $[A]$ ). Equations 4 and 5 show the expressions for  $\rho_A$ ,  $\rho_{A'}$  in the absence and presence of the antagonist  $[B]$ , where  $K_A$  is the equilibrium dissociation constant of the agonist and  $K_B$  is the equilibrium dissociation constant of the antagonist (Gaddum, 1937):

Equation 4.

$$\rho_A = \frac{[A]/K_A}{\frac{[A]}{K_A} + 1}$$

Equation 5.

$$\rho_{A'} = \frac{[A']/K_A}{\frac{[A']}{K_A} + \frac{[B]}{K_B} + 1}$$

By equating  $\rho_A$  and  $\rho_{A'}$ , the Gaddum equation defining the antagonist affinity  $K_B$  on the basis of the concentration ratio (CR,  $[A']/[A]$ ) and the known antagonist concentration  $[B]$  is derived. This elegant simplification is known as a null method as properties of the agonist (e.g. affinity and efficacy) determining the position of the control curve are not required – it is the magnitude of the curve shift in the presence of the antagonist, expressed as CR that is important.

Equation 6.

$$K_B = \frac{[B]}{CR - 1}$$

Later, Schild expanded upon this equation to allow its use with functional response data, in which curve shifts are collected in response to multiple concentrations of antagonist(Schild, 1947). Equation 7 demonstrates the relationship underpinning Schild analysis, in which a plot of  $\log [CR-1]$  against  $\log [B]$  should be

linear, with an x intercept providing the estimate of antagonist affinity as  $\log [K_B]$  or  $-pK_B$ . These estimates historically are also often referred to as  $pA_2$  values, since the antagonist concentration at its  $K_D$  estimate produces a two-fold change as the concentration ratio. Schild plots can be used to check that conditions are satisfied for an appropriate  $K_D$  estimate, since they should be linear with unit slope if measurements are made at binding equilibrium (non-surmountable antagonism can result from non-competitive or slow / irreversible effects) and the antagonist is competitive and reversible at the agonist binding site.

Equation 7.

$$pK_B = \log(CR - 1) - \log [B]$$

#### 1.2.6.3. Kinetic aspects of drug action.

The characterisation methods described thus far rely on the assumption of experimental equilibrium, however, within the last decade there has been growing appreciation for the role of ligand binding kinetics and non-equilibrium conditions within pharmacological profiling.

Since the employment of traceable ligands (e.g., fluorescent/radio-ligands) to characterise ligand binding kinetics, it has become apparent that binding kinetics (especially ligand dissociation rate) have a strong influence on drug action. The inherent longer residence time of a ligand due to a slow off rate ( $k_{off}$ ) has been linked to an increased duration of action in *in vivo* studies (Vauquelin and Van Liefde, 2006). Similarly in the case of antagonist with long dissociation times, this prolonged residency provides ligands with a displayed non-surmountable mode of action at early time points and in systems with highly variable agonist environments (Dijon et al., 2021). An example of this is found within the immune system and the release of localised chemokines or cytokines. Within this dynamic environment, the addition of a

high residency time chemokine receptor antagonist would act as an insurmountable antagonist regardless of the high endogenous agonist local concentration (which would ordinarily outcompete rapidly dissociating ligands)(Casella et al., 2023).

Similarly, ligand association rate influences therapeutic capacity for rebinding. Within environments able to facilitate ligand rebinding more easily (i.e., local reservoirs with reduced capacity for drug exchange with the bulk fluid subject to clearance (e.g. plasma), and a high target protein concentration) the addition of a fast association rate ligand results in high levels of rebinding, effectively producing a perceived increase in localised therapeutic concentration(Sykes et al., 2017). From a clinical perspective this results in an increase in therapeutic duration of action and increases the occurrence of on- and off-target adverse reactions.

#### 1.2.6.4. The Allosteric ternary complex model

The presented methods by Black and Leff/Schild and Gaddum provide a way of characterising orthosteric ligands using functional data, however, these have limited utility to define key parameters for allosteric modulators using functional data. An expansion on the classical ternary complex model by Leach *et al* 2007 allowed for further estimation on the effects of allosteric interaction on receptor interactions(Changeux and Christopoulos, 2016; Leach et al., 2007). This allosteric ternary complex model (ATCM) provides description of allosteric interactions in terms of equilibrium dissociation constants for the free receptor,  $K_A$  and  $K_B$  for orthosteric and allosteric ligands/effectors, respectively, and the subsequent allosteric effect that each exerts on affinity (governed by the cooperativity factor “ $\alpha$ ”). Values of  $\alpha > 1$  imply positive cooperativity, values of  $\alpha < 1$  but  $> 0$  denote negative cooperativity, and  $\alpha$  values equal to 1 indicate neutral cooperativity. However, this

model is limited by its inability to account for allosteric effects on efficacy. Consequently, an expansion to the ATCM was derived to account for modification of agonist efficacy through combination of the ATCM with an operational model of orthosteric agonism and allowing the allosteric ligand to possess efficacy, resulting in the incorporation of an additional parameter,  $\beta$  – as shown in equation 8.

Equation 8.

$$E = \frac{E_m(\tau_A[A](K_B + \alpha\beta[B]) + \tau_B[B]K_A)^n}{([A]K_B + K_AK_B + K_A[B] + \alpha[A][B])^n + (\tau_A[A](K_B + \alpha\beta[B]) + \tau_B[B]K_A)^n}$$

Values of  $\beta < 1$  denote an allosteric attenuation in signalling, values of  $\beta = 1$  indicate no change in the signalling capacity of the receptor when bound to both ligands and values of  $\beta > 1$  denote an increased capacity of the receptor to signal when bound to both orthosteric and allosteric agonist. Within the subsequent model, the parameters  $\tau_A$  and  $\tau_B$  denote the capacity of orthosteric and allosteric ligands, respectively, to exhibit agonism and incorporate the intrinsic efficacy of each ligand, the total density of receptors and the efficiency of stimulus–response coupling. The terms  $E_m$  and  $n$  denote the maximal possible system response and the slope factor of the transducer function that links occupancy to response, respectively. This model, therefore, allows estimation of allosteric interactions through exploitation of  $\alpha$  and  $\beta$  functions, which have the capacity to change with ligands/receptors chosen, but remain constant between assay systems. In practice the allosteric operational model can be challenging to fit to experimental data due to the number of parameters that need to be estimated for the orthosteric and allosteric ligands, and the system, requiring global fitting across several data sets (e.g. using different modulators as well as differing concentrations) and / or the use of independent

estimates, e.g. for ligand affinities, to simplify the constraints. Occasionally, simplification can be achieved by representing overall allosteric ligand co-operativity as the combined parameter  $\alpha\beta$  (Kenakin and Christopoulos, 2013; Leach et al., 2007; Thal et al., 2018).

#### 1.2.6.5. Practical characterisation of GPCR functional responses, using complementation and BRET / FRET assays

Regarding GPCRs there are a plethora of functional responses and techniques available for monitoring ligand activity, at both a cellular level and phenotypic level. The dual signalling nature of GPCRs provides multiple opportunities to measure cellular responses at various stages of the signalling pathway, from G protein/arrestin coupling to downstream changes of ion levels, protein phosphorylation/activation, receptor regulation and trafficking, and functional phenotypic readouts such as proliferation, secretion and contraction / relaxation (Anton et al., 2022a; Dixon et al., 2016; Garbison et al., 2004). Equally common amongst studies is the use of changing cellular cAMP concentrations as a measure of  $G_{s/i}$  coupled receptor activity, or the detection of accumulating intracellular calcium, usually through the use of fluorescent calcium sensitive dyes or biosensors (Cullum et al., 2023). These responses represent the primary consequences of receptor activation and subsequent G protein activation as previously discussed. However, beyond the seen downstream consequences of receptor activation, these techniques give little information about the relative recruitment of effectors by the receptors itself and risk miss-characterisation of partial agonists (particularly in over expressing systems). Initially described in 2016, recent advancement in split luciferase bioassays utilising a nanoluciferase (NanoLuc, Promega, Wisconsin, USA), split into

two large and small fragments (termed LgBiT and SmBiT respectively) which independently display negligible luciferase activity, but upon reversible complementation, regain enzymatic function, allows for much easier visualisation and measurement of direct protein-protein interactions in real time in the presence of substrate (compared to previous irreversible approaches) (Dixon et al., 2016). This assay, termed “NanoBiT complementation”, is unlike more classical functional assays as it does not measure the downstream cellular response but instead measures the recruitment of chosen effectors to receptors directly. By fusion of the NanoLuc fragments onto the two proteins of interest, the detection of protein interactions is possible by the reconstitution of the nanoluciferase fragments into a functional luciferase, which is only achieved when the fragments (and subsequently the proteins of interest) are close to each other. In comparison to other protein-protein interaction approaches based on resonance energy transfer (RET, e.g. NanoBRET), the distance constraints and reversibility to detect the signal may be similar, but complementation offers a simpler luminescence based readout compared to the ratiometric measurements required for RET donor / acceptor interaction. The SmBiT tag (18 amino acids) is also much smaller than RET partner proteins, allowing its incorporation in proteins where larger tags might disrupt function, and for example in genome modified native receptor genes using CRISPR (Dijon et al., 2021; Dixon et al., 2016; Soave et al., 2020d; White et al., 2020a, 2017).

#### 1.2.6.6. Recent advancement in GPCR conformational biosensors

In line with the aims of NanoBiT complementation, conformational biosensors represent an emerging strategy to interrogate ligand efficacy at the receptor level. Development of these sensors blurs the line between classical functional assays and binding assays, relying on binding of labelled transducers, nanobodies and/or resonance energy transfer techniques to detect receptor

conformational change. Such sensors have widened our understanding receptor states beyond those proposed by the various models (as described previously), highlighting the many alternative conformations stabilised by different agonists, both full and partial, and the conformational equilibrium bound receptors occupy. These include conformations which differentially activate particular signalling pathways (biased ligands) or those stabilised by the binding of an allosteric ligand, altering the activity/affinity of orthosteric ligands (such as promoting the high affinity state)(J Olsen et al., 2022).

Initial sensors designed to detect particular receptor conformations employed nanobody technology. Nanobodies (Nb) are single-domain antibodies that provide high selectivity and affinity for particular 3D target receptor conformations. The relatively large protein structure of Nbs allows for a high degree of modification (e.g., addition of fluorophores or affinity tags) without having a detrimental effect on Nb affinity or conformation (Soave et al., 2020d). Their high degree of receptor selectivity and ability to stabilise particular receptor conformations has particularly driven their use within the field of GPCR crystallography and cryogenic-electron microscopy (cryo-EM), fuelling an increase in available GPCR structures(Robertson et al., 2022).

Transducer-based sensors have also been developed, employing fluorescently labelled versions of proteins known to interact with GPCRs (e.g., GRKs, G proteins, miniG proteins and arrestins)(Wan et al., 2018). These sensors allow the possibility of measuring distinct receptor states (when used in parallel) and facilitate characterisation of the activation of multiple distinct signalling pathways by the same receptor. MiniG proteins are a key example of such sensors, miniG proteins are synthetic G protein mimetics which consist of the Ras-like GTPase domain of the G $\alpha$  subunit with a truncated N terminus, removing the G $\beta\gamma$  interface and the membrane anchoring groups, and deletion of the alpha helical

domain (Carpenter et al., 2016). Removal of the membrane anchors allows the mini G $\alpha$  protein to localise to the cytosol under basal conditions and be recruited to the membrane upon GPCR activation (Wan et al., 2018). Several mutations facilitate thermostabilisation of the protein for expression and purification, including a mutation in the  $\alpha 5$  helix of the mini G $\alpha$  protein C terminal to uncouple nucleotide release upon mini G $\alpha$ s protein-GPCR binding (Carpenter et al., 2016). Mutations in the mini G $\alpha$ s protein gene sequence allow for variations of peptide expression and alteration of the GPCR interface and allow receptor specific binding and representing other G $\alpha$  protein families: G $\alpha i/o$ , G $\alpha q/11$  and G $\alpha 12/13$ (Carpenter et al., 2016).

Further to this technique, the employment of tethered transducer proteins (e.g., SPASM sensors – tethered G protein alpha subunits) is providing insight into small changes in receptor conformation(Gupte et al., 2017; Kim et al., 2021). The advancement within these transducer systems has also allowed for the advancement of GPCR crystallography in the study of GPCR-effector interactions, in particular the increase in structures highlighting the interactions between GPCRs and G proteins.

#### 1.2.6.7. Fluorescence based approaches to derive ligand binding parameters.

Classically, the use of radiolabelled ligands has been a staple method for the characterisation of receptor-ligand binding since first use by Paton and Rang in 1965, however, more recent advancements within fluorescence-based approaches are becoming more popular(Paton and Rang, 1965). In particular, the use of resonance energy transfer provides advantages over radioligand binding assays by allowing continuous homogeneous measurements to be taken over a given time-period in real time, avoiding

separation of bound ligand from free for quantification (e.g. by filtration).

Initially described by Theodor Förster in 1948, Förster (or Fluorescence) Resonance Energy Transfer (FRET) is a technique which utilises the transfer of non-radiative energy from one fluorescent molecule (fluorophore or fluorescent protein) to another, resulting in the subsequent release of detectable photons from the receiving molecule (Förster, 1948). Traditionally carried out between two fluorophores, each fluorophore must have a distinct excitation and emission wavelength profile with a small degree of overlap between the “donor” emission and “acceptor” excitation wavelengths, allowing for excitation of the acceptor fluorophore by the donor emission (Comeo et al., 2020; Degorce et al., 2009; Halls, 2019; Hoffmann et al., 2005; Soave et al., 2020b; Sykes et al., 2017). The efficacy of energy transfer can be affected by a number of factors which provide FRET advantages within assay setups. Most important is the role of proximity between donor and acceptor fluorophores, with FRET occurring at peak efficacy within 1-10nm. In the context of studying ligand-receptor or protein-protein interactions, this distance is most likely to occur during protein interaction, allowing detection of binding within a homogeneous system in real time (Sykes and Charlton, 2018).

A similar principle is applied within Bioluminescence Resonance Energy Transfer assays (BRET). BRET again relies on the transfer of light energy from a donor to acceptor for the measurement of protein interactions (Angers et al., 2000; Pflieger and Eidne, 2006). Where BRET differs from FRET is through the generation of the donor emission. Unlike FRET, BRET makes use of bioluminescence generated by luciferase enzymes (upon substrate addition), rather than fluorophore laser driven excitation, to provide the excitation necessary from stimulation of nearby fluorophores. This removes the need for receptor/protein labelling with expensive reagents such as Terbium (e.g. in TR-FRET) and simpler detection

with platereader based systems, since the donor emission is controlled with addition of a substrate, rather than fluorescence excitation (Pfleger and Eidne, 2006; Stoddart et al., 2016, 2015; White et al., 2020a).

As mentioned, the primary benefit (beyond safety advantages) of using these fluorescence-based approaches is the ability to measure binding in real time over a chosen time-period within a single assay well. This contrasts with previous radioligand binding approaches which were used primarily to measure equilibrium “endpoint” readings due to greater complexity in carrying out kinetic experimentation using single timepoints per well. The ability to measure ligand interactions from non-equilibrium timepoints to equilibrium has opened novel methods for quantifying ligand affinity and efficacy kinetically and given insight into how non-equilibrium conditions affects drug action. The ability to characterise ligands through their kinetic profile is essential, however, understanding of collected data (and subsequent derivation of meaningful parameters) can be challenging. Mathematical models aim to address this by allowing for derivation of standard ligand affinity values ( $k_{on}/k_{off}$ ,  $K_D$ ) through global fitting of experimental kinetic data. A key methodology for utilising binding data to understand the kinetics of competing compounds was designed by Motulsky and Mahan in 1984 (Motulsky and Mahan, 1984). Their method explored the relationships between labelled ligand (radioligand in the original study) and unlabelled ligand binding within competitive association experiments. Through this competition analysis they aimed to describe pharmacological parameters of the unlabelled ligand at non-equilibrium conditions in relation to the labelled ligand’s association and dissociation rates, and the concentration used. This model generates competition association curves to multiple unlabelled compounds with varied association and dissociation rate constants according to:

Equation 9.

$$Y = Q \cdot \left( \frac{k_4 \cdot DIFF}{K_F \cdot K_S} + \frac{k_4 - F_F}{K_F} \cdot e^{(-K_F \cdot X)} - \frac{k_4 - K_S}{K_S} \cdot e^{(-K_S \cdot X)} \right)$$

Where:

Equation 10.

$$K_A = k_1[L] + k_2$$

Equation 11.

$$K_B = k_3[I] + k_4$$

Equation 12.

$$S = \sqrt{((K_A - K_B)^2 + 4 \cdot k_1 \cdot k_3 \cdot [L] \cdot [I] \cdot 10^{-18})}$$

Equation 13.

$$K_F = 0.5 \cdot (K_A + K_B + S)$$

Equation 14.

$$K_S = 0.5 \cdot (K_A + K_B - S)$$

Equation 15.

$$DIFF = K_F - K_S$$

Equation 16.

$$Q = \frac{B_{max} \cdot k_1 \cdot [L] \cdot 10^{-9}}{DIFF}$$

where X = time (minutes), Y = Specific binding,  $k_1 = k_{on}$  tracer (molar<sup>-1</sup> minute<sup>-1</sup>),  $k_2 = k_{off}$  tracer (minute<sup>-1</sup>), [L] = tracer ligand concentration (nM) and [I] = unlabelled ligand concentration (nM). Fixing these values to those obtained from tracer binding experiments carried out on the same day allowed derivation of

unlabelled ligand association ( $k_3$ ) and dissociation ( $k_4$ ) rate constants and  $B_{\max}$  = system maximal specific binding at equilibrium.

More recent development of fluorescent homogeneous technology as allowed for an increase in the appreciation of ligand kinetic parameters. This has driven an increase in the available techniques for measuring ligand kinetic parameters, particularly in the context of orthosteric ligands, however the role of allosteric ligand kinetics remains underexplored.

### 1.3. The advancement in intracellular allosteric modulator pharmacology

#### 1.3.1. *Unlocking the potential of intracellular allosteric modulators*

An emerging technique designed to counteract the issues resulting from poor therapeutic selectivity is the use of intracellular allosteric antagonists. Intracellular allosteric modulators provide a novel approach for selectively targeting GPCR signalling by direct steric inhibition of effector (e.g., G protein/arrestin) binding (Mohanty et al., 2023; Ortiz Zacarías et al., 2018). The G protein binding pocket between TM3 and TM5 discussed in section 1.2.3 provides an allosteric binding site accessible to such cell permeable small molecule therapeutics. These have the potential to not only antagonise receptor function, but also harbour greater selectivity for distinct receptor conformations, for example active versus inactive states (Figure 1.4). Potentially this would allow different modalities of the allosteric antagonist to emerge, such as a use-dependent, uncompetitive, mode of action (Jiang et al., 2020).

To date, the exploration of use-dependent ligands has been limited within the field of GPCR drug discovery, however the benefit of these ligands has been extensively utilised within ion channel and

enzyme therapeutics (as discussed in section 1.1)(Boulton et al., 2018; Cacabelos et al., 1999). The benefit of these ligands is they provide reduced on- and off-target side effects due to their preference for the active conformation, thereby increasing their potency considerably at sites of high receptor activity such as sites of inflammation. Despite the benefits displayed by such ligands, the development of GPCR uncompetitive ligands has been hindered by the limited conformational change within the orthosteric binding pocket upon receptor activation. Enzyme and ion channel targeted uncompetitive ligands are able to exploit highly dynamic protein conformational changes to carry out their function, however, the region of GPCR conformational change is spread more evenly across the receptor transmembrane structure. However, the largest conformational shift occurs to facilitate release of activated G proteins at the intracellular site which provides a putative mechanism for the development of GPCR targeted use-dependent ligands(Latorraca et al., 2017; Liu et al., 2017a; Xu et al., 2023). Despite the more universal binding mechanisms employed by the native G protein alpha subunits, the helical bundle structure of GPCRs allows for multiple smaller putative small molecule binding regions within this intracellular pocket which displays high sequence diversity across receptor families compared to the orthosteric binding site(Flock et al., 2017). This holds the potential for the development of increasingly selective therapies with potential uncompetitive, use-dependent, modes of action. Such compounds, employed alone or in combination with other therapeutics, would provide a new angle for tackling the problem of on- and off-target side effects within GPCR therapeutics.

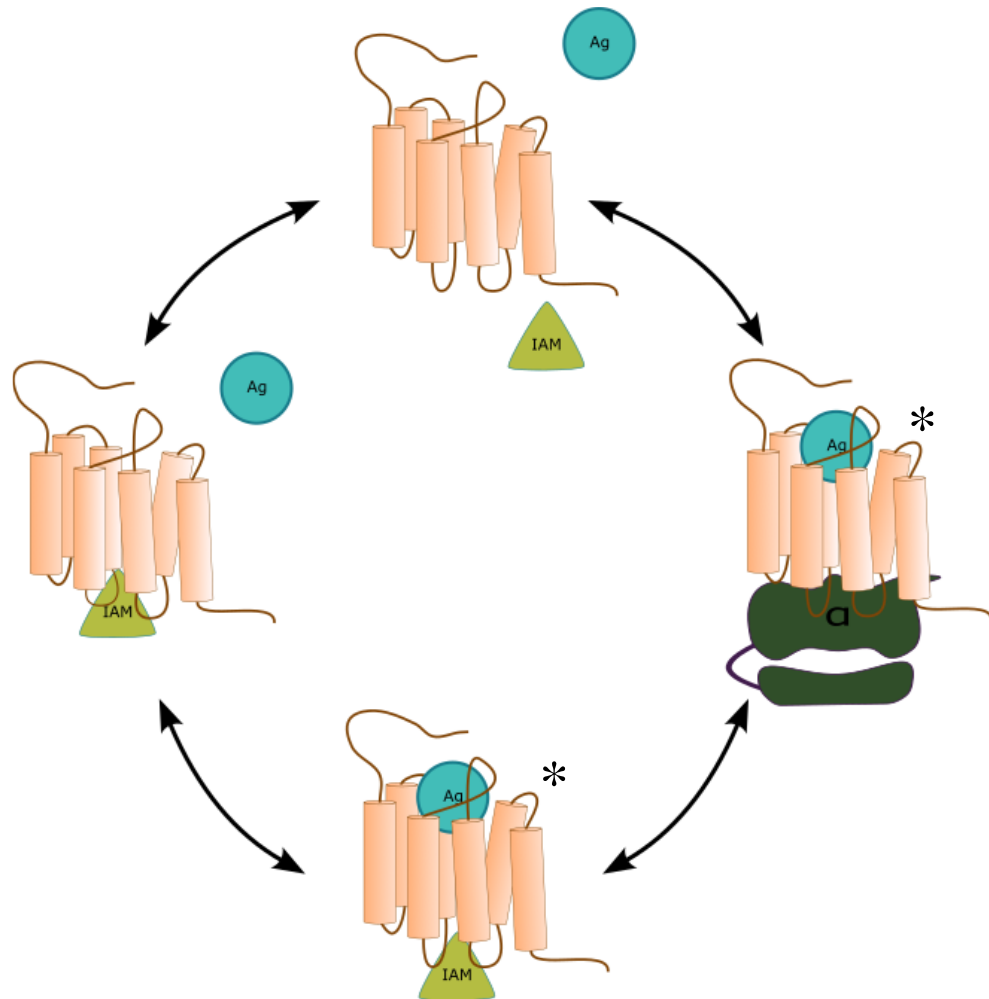


**Figure 1.4. Representation of intracellular allosteric modulator function.** Binding of the intracellular modulator occurs within the same region as the native secondary messengers (e.g., G proteins), thereby inhibiting downstream signalling. \*Indicates active receptor complex.

To date there has been limited success in the identification and development of novel small molecule compounds able to exploit the intracellular binding pocket, with a key limitation being the difficulty of identifying compounds which preferentially bind this region in a high throughput manner. Current techniques designed to identify and characterise these compounds are very receptor specific and rely on determining effects on functional responses brought about by these compounds or the effects these compounds have on agonist binding. However, without carrying out these assays in combination with mutagenesis studies of the chosen receptor it is increasingly difficult to identify the exact mode of action and binding site of these compounds. More recently, the employment of cryo-EM technology has facilitated increased identification and understanding of intracellular allosteric ligand-receptor interactions (Jiang et al., 2020; Liu et al., 2017a), however, this remains a highly complex and low-throughput method for characterisation of novel ligands and therefore limits the rate of drug discovery in this area. Additionally, ligands identified in this manner are not necessarily successful when transferred into biological systems, likely due to cryo-EM's need for exceptionally high ligand concentrations and employment of a purified receptor system resulting in interactions incompatible within native environments (Andrews et al., 2008; Huber et al., 2022; Liu et al., 2017a; Oswald et al., 2016b).

### *1.3.2. Recent advancement in intracellular allosteric modulator drug discovery*

Among the small number of compounds identified which bind to this region, the greatest success has come from targeting the chemokine receptor families, especially CXCR and CCR families. CCR4 was the first of these receptors to be targeted by such compounds and Andrews *et al*, through a combination of

mutagenesis studies, radioligand binding assays and functional assays, identified two compounds able to antagonise CCR4 signalling with selectivity over CCR5 being dependent on the structure of the intracellular C terminus. By showing that these compounds required intracellular access and preferential binding to receptors with CCR4 C termini, they were able to devise a putative intracellular binding model for compounds which bound to this region of CCR4, and to a lesser degree CCR5 (Andrews *et al.*, 2008). Similarly, radioligand binding studies by Zweemer *et al* and Walter *et al* employing a number of CCR2 and CCR9 targeted ligands, respectively, identified CCR2-RA-[R] and CCX282-B, allosteric modulators of CCR2/CCR9 signalling. Further mutagenesis studies identified their respective binding sites to be located at the intracellular site of the receptor (Walters *et al.*, 2010; Zheng *et al.*, 2016; Zweemer *et al.*, 2014, 2013).

Following on from these initial findings, Nicholls *et al* were able to identify compounds with similar binding properties at CXCR1 and CXCR2 (Nicholls *et al.*, 2008). In addition to similar mutagenesis and functional assays, they were able to show that antagonist binding within this intracellular region had a negative effect on endogenous ligand binding, in this case CXCL8. This relationship suggested highly negatively co-operative mode of allosteric antagonism when targeting this site, whereby, the binding of the antagonist and orthosteric agonist is mutually exclusive and has the appearance of an effective competitive binding model despite these ligands having independent binding sites. This hypothesis was further strengthened by the inclusion of receptor modelling of CXCR2 and the identification of a potential intracellular hydrophobic cavity which, combined with mutagenesis and compound structural relationships, is a putative binding site for these compounds.

The identification of this intracellular site and compounds able to bind this region led to the development of further compounds

targeting CXCR1 and 2 with greater selectivity and efficacy at this binding site, as well as greater characterisation of pre-existing compounds. Navarixin is one such compound. Originally discovered in 2006, navarixin was shown to inhibit chemotaxis of polymorphonuclear cells, such as macrophages, a response known to be attributed to CXCR1/2 activation (Dwyer et al., 2006; Gonsiorek et al., 2007a). The inclusion of a chiral centre results in two (R and S) enantiomers which display large variation in affinity for both CXCR1 and CXCR2 (Casella et al., 2023; Lu et al., 2018). This variability, and subsequent variability in selectivity for CXCR2 over CXCR1, indicates the importance of this chiral centre in producing selective binding and highlights the selective potential provided of this intracellular binding site in future compound development. Additionally, recent fluorescent-navarixin binding data has furthered the potential role this binding region can play through characterisation of various CXCR2 intracellular ligands displaying large variability in their binding kinetics, and therefore a high degree of selectivity and functional potential (Casella et al., 2023).

More recently, this intracellular site has been identified and exploited at the prostaglandin receptor EP<sub>2</sub> (discussed in section 8.2.1) and  $\beta_2$ -adrenoceptor, indicating the presence of a conserved allosteric binding site potentially present across a range of GPCRs (Jiang et al., 2020; Liu et al., 2017b). These compounds are the first examples of a more general potential to design IAMs acting at Gs, as well as Gi coupled receptors, and beyond the specific chemokine receptor family.

The  $\beta_2$ -adrenoceptor ligand “compound-15” was identified in 2017 through employment of X-ray crystallography and subsequent radioligand binding assays to determine IAM mediated changes to agonist affinity. Compound 15 was found to bind within the G protein binding site, displaying a preference for binding the inactive receptor conformation. This resulted in compound-15 having the

capacity to decrease orthosteric agonist affinity, potentially having a dual role in inhibiting signalling through both steric hindrance of effector coupling, and reduction in agonist binding. However, compound-15 was only shown to have significant therapeutic potential at high concentration (<30 $\mu$ M). The combination of a low modulatory potency with additional complications, including the potential for protein binding, ligand degradation and reduced target access, means compound-15 is unlikely to have a clinically relevant effect. Additionally, the methods employed to facilitate X-ray crystallography require a high degree of receptor modification in order to stabilise the protein conformation. As such, mutations are introduced, a number of which are within the compound-15 binding site, thereby providing limited translational data regarding the native endogenous receptors.

#### 1.4. G protein peptidomimetics

##### *1.4.1. Exploring the GPCR-G protein interaction using G protein mimetics peptides*

An alternative approach to targeting receptor-G protein effector allosteric sites has been highlighted by the investigation of G $\alpha$ C-terminal peptides (Gilchrist et al., 2002). These peptides are derived from the final amino acids found at the C-terminal end of the G $\alpha$ 5 helix, however the exact length of the peptides used to date varies. The initial concept of G $\alpha$ C-terminal peptides was born from the identification of key residues in G-proteins, primarily residing in the C-terminus, which facilitate GPCR-G $\alpha$  subunit binding and G-protein selectivity as discussed above in section 1.2.1, 1.2.2 & 1.2.3 (Hirsch et al., 1991; Miller et al., 1988). G-peptides were first employed during these initial studies as tools for identifying the interacting residues between G-proteins and GPCRs. Previous research had already broadly implicated the C-terminus of G $\alpha$ -proteins with GPCR binding and therefore Hamm *et al* pioneered

these peptides and utilised the final 17 amino acids of  $G\alpha_t$ , as a  $G\alpha$  peptide, to show that this region of the G-protein was able to bind to and inhibit signalling from the rhodopsin receptor (Hamm et al., 1988). Furthermore, the team also pioneered and demonstrated the use of synthetically designed  $G\alpha$  peptides as tools for understanding GPCR-effector interactions.

Mutagenesis studies from Conklin *et al* (Conklin et al., 1993) built upon these early findings and provided early evidence for the role of the  $G\alpha_5$  helix C-terminus in G-protein recruitment. This study involved the manipulation of  $G\alpha_q$  and subsequent switching of preferred GPCR effector subtype through modification of the  $G\alpha_5$  C-terminal region of G-proteins. In this study the  $\alpha_2$ -adrenoceptor, Adenosine 1 receptor and Dopamine 2 receptor were employed due to their selectivity for  $G\alpha_i$  coupling. It was hypothesised that varied, incremental, alterations of the final 23 amino acids of the  $G\alpha_q$  subunit to match corresponding residues found in the  $G\alpha_i$   $\alpha_5$  helix would result in varied activation of the  $G\alpha_q$  PLC pathway upon receptor activation through chimeric  $G\alpha_{q/i}$  recruitment. Initial experiments gave positive results for  $G\alpha_q$  mediated responses with varied degrees of PLC activation, predominantly dependent on the number of  $G\alpha_i$  amino acids incorporated. Further analysis indicated that chimeras containing the final 3-13  $G\alpha_i$  amino acids produced the most PLC activation indicating their prominent role in GPCR-G-protein interactions and strengthening previous findings regarding the role of G-protein C-termini.

Alongside these observations came the proposal that overexpression of C-terminal peptides as minigenes may provide a form of inhibition through competition with native G-proteins for GPCR binding. Initial testing of this hypothesis by Palm *et al* and Rasenick *et al* gave evidence supporting this hypothesis, showing that expression of  $G\alpha_s$  peptides of varying lengths produced varying levels of selective G-protein inhibition or signalling modification (Palm et al., 1990; Rasenick et al., 1994). Furthermore,

these initial studies provided hypotheses and evidence for identifying the role of G $\alpha$  peptide binding in promoting the active state of GPCRs, thus increasing agonist affinity. Rasenick *et al* emphasised the potential for this phenomenon through identification of G $\alpha_s$  peptides able to increase agonist affinity at  $\beta$ -adrenoceptors. The study made use of C6 cell membranes and saponin treated cells (promoting cell permeability) to study the effects of synthetic, site-specific, peptides from G $\alpha_s$  corresponding to amino acids 15-29, 354-372, and 384-394 and G $\alpha_i$  (8-22, 315-324, and 345-455). Firstly, the peptide's ability to bind, and therefore inhibit signalling from, the  $\beta$ -adrenoceptors was assessed through measurement of cAMP levels upon stimulation with isoprenaline. In permeable cells, incorporation of G $\alpha_s$  peptides 354-372 and 384-394 produced a large reduction in isoprenaline driven cAMP levels compared to untreated, G $\alpha_i$  and G $\alpha_s$ -15-29 treated cells. Having indicated their selective binding capability these peptides were then used in cell-based competition assays measuring binding affinities of cold isoproterenol through competition with <sup>125</sup>I-pindolol (IPIN). These assays showed that G $\alpha_s$  384-394 and 354-372 peptides were able to increase isoproterenol affinity, indicating promotion of the active receptor conformation. Carrying this forward these peptides were tested for a concentration dependent relationship with isoproterenol-IPIN competition (using fixed concentrations of both ligands). This identified peptide 384-394 was able to cause an increase in isoproterenol potency with increased peptide concentration, thus again indicating an increase in active state receptors.

Rasenick *et al* further showed that peptide-G-protein competition did indeed occur through the addition of Gpp(NH)p into isoproterenol competition studies. Gpp(NH)p acts as an alternative to GDP/GTP in G-protein activation, allowing binding within the RAS domain but inhibiting hydrolysis. This causes permanent uncoupling of the G-protein from receptors which displays as a

reduction in agonist affinity through promotion of the inactive state. The addition of Gpp(NH)p into the previous competition assays, using a fixed concentration of peptide 384-394, showed that even in the presence of the peptide there was a proportional decrease in agonist affinity upon Gpp(NH)p addition, indicating that the 100  $\mu$ M concentration of peptide still allowed for native G-protein binding. However, this native binding was negated through increased concentration of peptide 384-394, indicated by Gpp(NH)p having no effect on agonist affinity in these assays. The combination of these results indicated that peptide 384-394 displayed a competitive, surmountable antagonistic relationship with native G-proteins.

Studies by Gilchrist *et al* enhanced these concepts through characterization of  $G\alpha_i$  peptides and their inability to promote the active conformation of the receptor (Gilchrist et al., 1998). Gilchrist *et al* began by characterising the effects of multiple  $G\alpha$  C-terminal peptides, consisting of the final 11 amino acid residues of various  $G\alpha$  subtypes, on the Adenosine A1 receptor. A1 preferentially functions through the use of  $G\alpha_i$  and it was hypothesised that  $G\alpha_i$  peptides and  $G\alpha_t$  peptides, which share a large proportion of sequence homology, would selectively inhibit A1 signalling. Using membranes from an A1 expressing CHO-K1 cell line, the effects of peptides derived from  $G\alpha_i$ , o, s, t and six synthetic t variants were determined through use of radioligand binding assays and competition assays, measuring the receptor affinity for N6-cyclohexyl-adenosine (CHAd) or N6-R-phenylisopropyladenosine (R-PIA, A1 agonist) with and without the presence of  $G\alpha$  peptides. These assays showed that  $G\alpha_i$  and  $G\alpha_o$  inhibited CHAd specific binding in a concentration specific manner. Conversely to previous  $G\alpha_s$  peptide data, these initial observations suggested that  $G\alpha_{i/o}$  peptides could still compete with heterotrimeric G proteins for interactions with A1 but did not promote the active state of the receptor.

In addition to the primary research outcomes presented, both Rasenick's and Gilchrist's publications indicate that not all the C-terminal  $\alpha 5$  helix is needed to produce a G protein selective peptide. In both cases only the final 11 amino acids were used and were still able to cause selective functional inhibition of G protein signalling.

#### *1.4.2. Recent advancement in $G\alpha$ peptides and their potential role in Cryo-EM*

More recently the subject of G protein mimetics, particularly regarding  $\alpha 5$  derived peptide length, has been further explored by Mannes et al through radioligand binding studies at the  $\beta_2$ -adrenoceptor (Mannes et al., 2021). Here the affinity of unlabelled agonist isoproterenol was determined through competition with [ $^3\text{H}$ ]-dihydroalprenolol in the presence of  $G\alpha_s$  peptides of varying sequence length, structural alterations, or sequence modifications. In agreement with previously published findings, Mannes found that these peptides promote the active conformation, however in contradiction to previous publications, the 11 amino acid peptide did not have any effect on agonist affinity. To further explore these findings the team developed alternative peptides derived from the  $G\alpha_s$  C terminus incorporating peptide elongations (11-25 amino acid chains), non-native amino acids, N/C-terminal modifications, and cross-linking "molecular staples" for stabilisation of the peptide structure. Through subsequent radioligand binding assays they were able to derive the effects of these modifications on the relative modulatory effects elicited by the peptides, through modulation of isoproterenol affinity. These results indicate that the integrity of the secondary structure, and subsequent structural homology to native protein alpha subunits, is integral for the binding and function of the peptides in promoting the receptor active state (Mannes et al., 2021). Furthermore, of the 17 peptides explored, those which facilitated the greatest increase in agonist affinity (thereby

promoting the greatest number of high-affinity receptor states) incorporated a cyclohexylalanine residue within the C-terminal region. This modification (in place of leucine residues in the -2 position) appears to act by increasing the hydrophobicity of this peptide region and suggests, as has previously been shown, that the final amino acids of the  $\alpha 5$  helix play an essential role in promoting receptor interactions.

## **Chapter 2.**

### Thesis Aims

## 2. Thesis Aims

The ability to bind to the intracellular binding pocket of GPCRs provides G protein based peptidomimetics similar characteristics to the previously developed mini-G protein technology and the use of GPCR conformationally selective nanobodies. As such, there are a plethora of established roles in which these peptidomimetics can be utilised, ranging from stabilisation of GPCR states for structural studies to understanding and exploiting receptor-effector interactions. The initial development of mini-G proteins and nanobody techniques was for the identification of novel GPCR structures within particular conformations. Subsequently, these tools were designed to have high binding affinity and long residency times to produce an irreversible mechanism of binding and allow for stabilisation of active receptor conformation. Where these peptides differ functionally from these more established forms of characterising the intracellular binding site is primarily in their putative lower affinity. Furthermore, observed competition between  $G\alpha$  peptidomimetics and native G proteins highlights their potential use in competition-based screening assays for identifying new intracellular modulators, including small molecules. A low affinity and shorter residency time would provide G protein peptidomimetics the unique ability to provide fast kinetic profiles of both orthosteric and allosteric ligand interaction. Additionally, their G protein origin potentially allows for screening without having to rely on selective receptor-tracer interactions, opening the possibility of wider target screening where fluorescent/radiolabelled tracers are limited.

This thesis aims to explore a range of G protein derived peptidomimetics for multiple G protein classes and determine their utility in a range of pharmacologically relevant techniques, including their use as more universally applicable fluorescent tracers for the characterisation of GPCR ligand interactions.

In Chapter 4, the allosteric efficacies of various  $G\alpha_s$  and  $G\alpha_i$  derived peptides are determined through changes in agonist affinities, measured using fluorescence resonance energy transfer techniques. Peptides consisting of 11-24 amino acids are employed to identify the role of peptide primary and secondary structure on their ability to modulate signalling at the  $\beta_2$ -Adrenoceptor and Neuropeptide Y1 receptor.

Chapter 5 explores the use of click-chemistry techniques in the development of alternative  $G\alpha_s$  derived peptide tracers.

Chapter 6 employs fluorescently tagged peptides to further explore the binding of G protein peptidomimetics directly. Use of BRET technology allowed for identification of the use-dependent nature of peptide binding as well as their role as tracers in intracellular competition assays and as orthosteric agonist driven active-state biosensors.

Chapter 7 aims to characterise the use of fluorescently labelled peptides in fluorescence correlation spectroscopy techniques. Binding of tracer peptides to  $\beta_2$ -Adrenoceptors is explored to determine acute peptide binding events and future utility in microscopy-based techniques (e.g., the identification of receptor dimerization).

Chapter 8 describes the use of a novel peptidomimetic tracer within a small scale, medium-throughput screen of novel small molecule intracellular allosteric modulators of the prostaglandin EP<sub>2</sub>.

# **Chapter 3.**

## **General Materials and Methods**

## 3. Materials and Methods

### 3.1. Materials

Gα C-terminus peptides and HiBiT peptide were purchased from Genscript Biosciences Ltd (New Jersey, USA), generated by solid-phase peptide synthesis with <98% purity. Stocks were stored as solid or in solution (double distilled H<sub>2</sub>O or DMSO) at a 10mM concentration in individual 2 μl aliquots at -20°C. All additional compounds (manufacturer as stated in specified chapters) were stored in solution using either double distilled H<sub>2</sub>O or DMSO at concentrations of 10mM-200μM in individual aliquots at -20°C prior to use. All mammalian expression vectors and lipofectamine/lipofectamine 3000 reagents were purchased from Invitrogen (Paisley, UK). All cell culture reagents and additional buffer reagents were obtained from Sigma Aldrich (UK). Human Embryonic Kidney 293T (HEK293T, ATCC CRL-3216, Invitrogen) cells were selected as a commonly used model cell line used to express recombinant proteins of interest<sup>1</sup>. HEK293T cells are engineered to express the simian virus 40 (SV40) large T antigen (DuBridgde et al., 2023). This enhances high efficiency transfection of expression vectors, such as pcDNA3.1, where the antibiotic resistance gene is controlled by an SV40 promoter (Fox et al., 2015). Mammalian expression selection antibiotics zeocin and Geneticin were provided by Thermo Fisher Scientific and Invitrogen. The SmBiT and LgBiT sequences for the NanoBiT assay constructs, and Nanoluciferase substrate furimazine were obtained from Promega corporation (Madison, US). Compounds for EP<sub>2</sub> competition screening were synthesised and purified by Constance Dalton and Shailesh Mistry (University of Nottingham) and stored at a 10mM concentration in DMSO as individual 2 μl aliquots at -20°C.

### 3.2. Development of receptor constructs for cellular and membrane-based assays

Gene expression vectors are employed to encode proteins of interest for transfection and expression within mammalian and prokaryotic cell cultures (Makrides, 1999). These also facilitate modification of the expressed proteins to aid in biological exploration, including conjugating to a peptide tag or mutating key amino acids. A number of expression vectors have been developed to suit different expression systems. These share common features to ensure suitable transcription (generation of mRNA from DNA for protein translation) efficiency, propagation in prokaryotic cells and selection in mammalian cells. In all cases, expression vectors contain promoters and enhancers to facilitate the initiation of transcription, such as the human cytomegalovirus (CMV) promoter to enhance protein transcription in mammalian cell lines. Vectors also contain a polyadenylation tail to protect mRNA from degradation, for which a SV40 poly(A) sequence was used (Hoff et al., 1993). Expression protein cDNA inserts typically contain a Kozak consensus sequence to improve the efficiency of protein translation (Kozak, 1987).

Within this thesis, receptor constructs were placed within pcDNA3.1(+)-neo vectors (Figure 3.1). This vector contains the human cytomegalovirus immediate-early (CMV) promoter to achieve high expression of the inserted cDNA within mammalian cell lines, and a bovine growth hormone (bGH) polyadenylation site for effective termination of transcription. Inclusion of neomycin (neo) and ampicillin resistance genes allows for efficient selection of transfected colonies in both mammalian and *E.coli* systems. In all cases, constructs were generated by restriction digestion of previously generated receptor constructs, and re-ligation of desired fragments into target plasmids.

Restriction digestion is the process of cutting DNA into smaller fragments via endonuclease enzymes. Specific endonucleases recognise particular sequences within DNA strands and cut the phospholipid backbone either symmetrically (generating “blunt ends”) or asymmetrically (generating “sticky ends”). All endonucleases employed within this thesis resulted in the formation of sticky ends for easy reconstitution of DNA fragments and re-ligation (reforming of the phospholipid backbone integrity) within new vectors. Where indicated, receptor templates utilised were modified to include an N-terminal SNAP-tag sequence for the benzyl guanine mediated conjugation of fluorophores (Keppler et al., 2004).

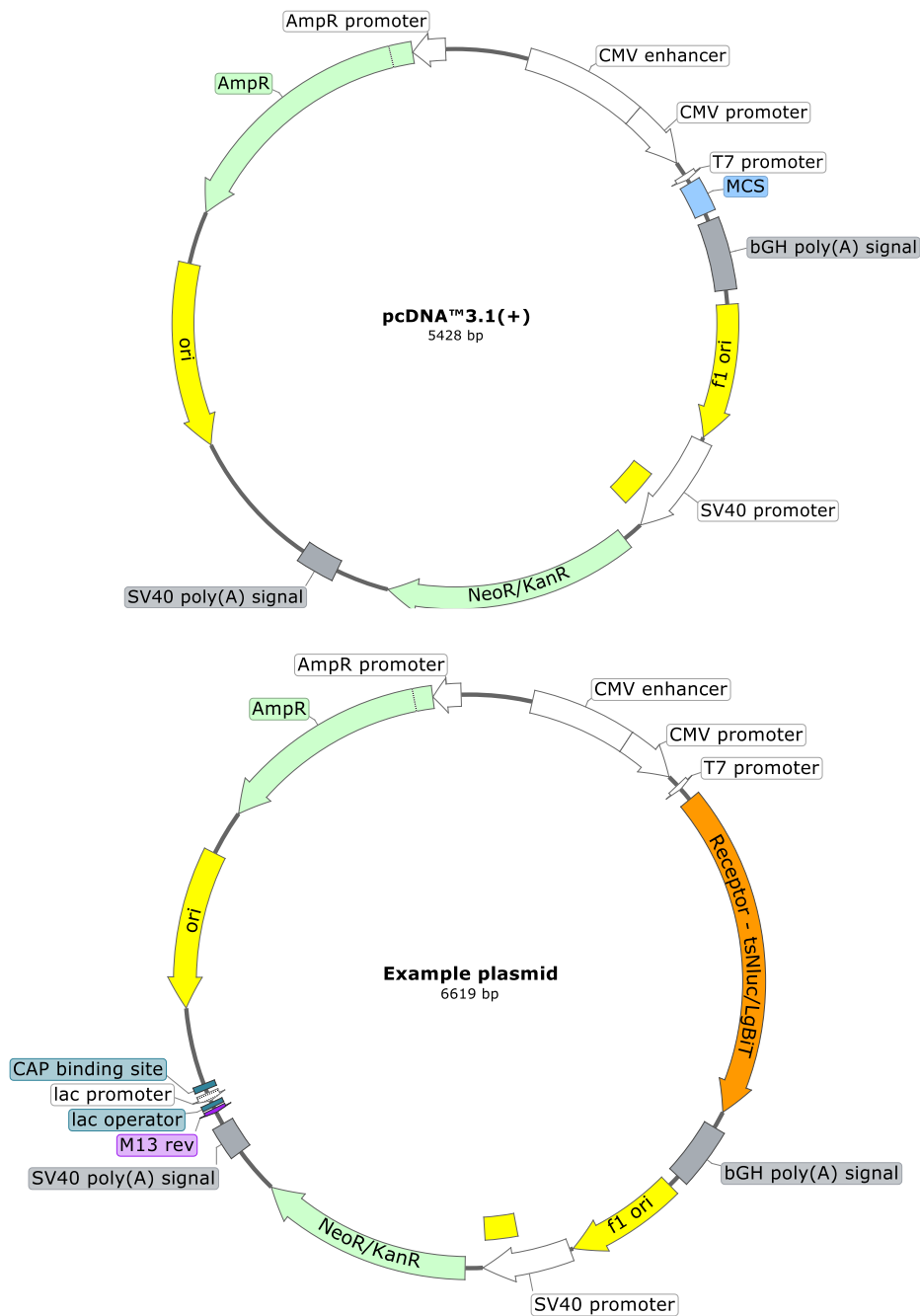


**Figure 3.1. Plasmid maps.** (Top) p3.1 vector plasmid indicating functional regions of DNA sequence used for the expression and replication of the plasmid in both bacteria and mammalian systems. (Bottom) p3.1 vector with example receptor/thermostable(ts)Nluc/LgBiT fragments inserted within the multiple cloning site (MCS). Other regions shown include antibiotic resistance genes (NeoR/KanR/AmpR), various bacterial and mammalian enhancer/promoter regions for RNA polymerase binding and bacterial and mammalian replication origin sites (ori) for DNA polymerase binding.

### 3.2.1. $\beta_2$ -AR constructs:

p3.1neo(+)-SNAP- $\beta_2$ -AR (GenBank: BC073856.1) was provided by Dr Nicholas Holliday. Modified  $\beta_2$ -AR construct p3.1neo(+)-SNAP- $\beta_2$ -AR-tsNluc (Figure 3.1) was made from previously generated plasmid vectors p3.1neo(+)-SNAP- $\beta_2$ -AR-LgBiT (generated by Dr Nicola Dijon, University of Nottingham) and p3.1neo(+)-thermostable Nanoluciferase (tsNluc, GeneArt Gene synthesis, Invitrogen; designed by Dr Nicola Dijon). The thermostable nanoluciferase includes point mutations to improve nanoluciferase stability, as described in Hoare et al (2023, submitted for publication) and by Promega (Dixon et al., 2016).

To perform restriction digests, 2 $\mu$ L 10 x Digestion buffer Green (New England Biolabs, containing gel loading dye) was added to 2 $\mu$ g p3.1neo(+)-tsNluc plasmid, and 2 $\mu$ L 10x digestion buffer was added to 2 $\mu$ g p3.1neo(+)-SNAP- $\beta_2$ -AR-LgBiT. Double distilled H<sub>2</sub>O was added to a final assay buffer volume of 20  $\mu$ l. cDNA vectors underwent digestion with 1U XhoI and XbaRI (New England Biolabs) for 2 hours at 37°C prior to enzyme inactivation at 72°C for 20 minutes. This digestion excised the LgBiT and tsNluc fragments from each vector.

Gel electrophoresis was used to isolate 522bp tsNluc insert fragments from digestion reaction mixture containing p3.1neo(+)-tsNluc. Gel electrophoresis is the separation of DNA fragments by size using a 1% agarose gel and applying an electrical field to move negatively charged DNA towards the positive electrode (Aaij and Borst, 1972). The agarose gel percentage adjusts the separation of shorter and longer DNA fragments based on the speed of their migration. To do this, 40mL TBE buffer (89mM Tris base, 89mM boric acid, 2mM EDTA, pH: 7.6) was added to 400mg agarose solid and microwaved for 1 minute to allow for full solubilisation of agarose. Once cooled to room temperature, 0.125 $\mu$ LmL<sup>-1</sup> ethidium bromide (to visualise the DNA under UV illumination) was added

prior to addition of resulting 1% agarose gel to the mould. Once solidified, the gel was transferred to electrophoresis gel tank containing 500mL TBE buffer. 6 $\mu$ L 1kb DNA ladder (New England Biolabs) was added to outer wells and digestion reaction sample (20 $\mu$ L) was loaded into adjacent well. The gel was run for 40 minutes using 80V, 100A electrical output to allow sufficient DNA separation. The gel was then removed and imaged by ultra-violet light prior to collection of the fragment aligning to the 500bp region of reference ladder. tsNluc fragment was obtained from gel using Sigma-Aldrich Gel purification kit. tsNluc containing gel fragment was immersed in 3 volumes of gel solubilisation solution (300  $\mu$ l / 100 mg gel) and heated at 52°C until dissolved. A silica filter “GenElute” binding column was prepared using high salt column prep solution applied by centrifugation (14000rpm, 1 minute). Solubilised gel fragment was treated with 1x volume of gel fragment (~100 $\mu$ L) isopropanol, then loaded into the column and spun at 14000rpm for 1 minute to bind the DNA fragment into silica. Membrane was then washed with manufacturers wash solution supplemented with ethanol by centrifugation (14000rpm, 2.5 minute) to remove excess salts. DNA was then collected from membrane by application of 40 $\mu$ L ddH<sub>2</sub>O and centrifugation (14000rpm, 1 minute).

Digested SNAP- $\beta_2$ -AR- vector fragment sticky ends were dephosphorylated, to prevent relegation, by treatment with Fast Alkaline Phosphatase (FastAP) enzyme. 1 $\mu$ L FastAP buffer and 1U FastAP enzyme (New England Biolabs) were added to the digestion reaction mixture and incubated at 37°C for 30 minutes prior to inactivation as before.

pcDNA3.1 SNAP- $\beta_2$ -AR- vector fragments were then purified using PCR clean-up kit (Sigma-Aldrich, Pool, UK) again utilising silica binding columns. The SNAP- $\beta_2$ -AR- reaction mixture was diluted with 5 volumes of binding buffer, and loaded into

preprepared silica column by centrifugation (14000rpm, 1 minute). Membrane was then washed as before, and DNA fragment was eluted using 50µL ddH<sub>2</sub>O by centrifugation (14000rpm, 1 minute).

Generated fragments were then joined by DNA ligation. Ligation reactions were performed at a specific molar ratio of insert:vector DNA optimised according to the 3:1 molar end ratio, with a total vector DNA amount of 50ng per reaction. The enzyme T4 DNA ligase (New England Biolabs) was used to form p3.1neo(+)-SNAP-β<sub>2</sub>-AR-tsNluc by addition of tsNluc and p3.1neo(+)-SNAP-β<sub>2</sub>-AR fragments to 1µL ligation buffer + 1U T4 ligase (New England Biolabs) [making up volume to 10µL with ddH<sub>2</sub>O]. Ligation mixture was then incubated for 16 hours at 16°C prior to inactivation as before.

Resulting constructs were used to transform competent bacterial cells (TOP10F', Invitrogen) by heat shock. 2.5µL Ligation sample was incubated with 25µL TOP10F' chemically competent cells for 30 minutes before rapid heating to 42°C for 30 seconds to promote uptake of environmental DNA constructs. Sterile LB (Lurio Bertoni) Broth (20 g/L) was then added to the suspension and both positive and negative controls (+/- ligation DNA) were incubated at 37°C for one hour in a shaking plate. Suspensions were then plated onto separate agar plates (LB Agar 35mg/ml) containing 75µg/mL Ampicillin or 30 µg/ml Kanamycin as required and incubated overnight at 37°C. Four of the resulting colonies were picked using a 200µL sterile pipette tips, which were expelled into universals containing 5mL LB broth supplemented with 100µg mL<sup>-1</sup> ampicillin. Negative controls of bacterial transformations were conducted as described, using ligation reactions without the addition of insert DNA. Miniprep cultures were then grown for 16 hours in a shaking incubator at 37°C prior to cell lysis and DNA acquisition (miniprep kit, Sigma-Aldrich, Pool, UK).

DNA extraction was performed according to the manufacturer's instructions using a Sigma Aldrich miniprep kit. 1.5mL miniprep colony sample suspension was transferred to 1.5mL Eppendorf tubes and separating by centrifugation (4000rpm, 5 minutes – repeated twice to amass larger cell pellets). The resulting cell pellets were then resuspended in resuspension buffer supplemented with RNase as per kit instructions. Samples were treated with Alkaline lysis buffer (NaOH/ sodium dodecyl sulphate [SDS]), ensuring effective mixing, for five minutes. This mixture of strong alkali and detergent disrupts bacterial cell membranes and allows the alkali to contact and denature unwanted proteins and genomic (but not plasmid) DNA. Post incubation the sample is treated with a neutralisation solution of potassium acetate to prevent further denaturation of DNA and precipitation of the SDS detergent. Resulting suspensions were then spun (14000rpm, 10 minutes) to separate lysate from cell material and detergent and supernatant was transferred to reprepared (100µL column prep solution, 12,000rpm, 30sec) silica filtration columns for DNA extraction. DNA was collected as previously described, eluting in 100µL ddH<sub>2</sub>O. Samples were screened by Sanger sequencing (courtesy of University of Nottingham deep sequencing department) to identify colonies containing p3.1neo(+)-SNAP-β<sub>2</sub>-AR-tsNluc plasmids.

Successfully transformed colonies were then amplified and DNA extracted using the Qiagen Maxiprep kit (Qiagen, Germany), performed as manufacturer's guidance. Colonies were amplified in 120mL LB Broth overnight before collection of bacteria by centrifugation (6000g, 15 minutes). Pellet was then dried and resuspended in RNase supplemented resuspension buffer before addition of lysis buffer. Cell lysis was allowed to occur for 5 minutes before addition of neutralisation buffer and transfer of mixture into a filtration column. Lysate was allowed to separate within the column for 15 minutes prior to filtration into a pre-prepared QIAGEN-tip silica filtration column. Column was allowed

to drain by gravity for 15 minutes before double washing and draining with manufacturers wash solution supplemented with ethanol. Once fully drained, the QIAGEN-tip was transferred to a collection tube and filled with manufacturers elution buffer and allowed to drain by gravity. Collected elute was then treated with 0.7x volume isopropanol and spun at 4000rpm for one hour. Resulting DNA pellet was resuspended in 300 $\mu$ L Tris-EDTA buffer (TE, 10mM Tris-Cl, 1mM EDTA, pH 8.0) and transferred to a 1.5mL Eppendorf tube. 30 $\mu$ L NaOAC and 660 $\mu$ L 100% ethanol were added to precipitate the DNA prior to centrifugation (14000rpm, 10 minutes). Supernatant was discarded and replaced with 200 $\mu$ L 70% ethanol without resuspending the DNA pellet. After an additional spin (14000rpm, 5 minutes) the pellet was left to half dry before resuspension in 300 $\mu$ L TE. DNA concentration was determined by measuring sample absorbance with a Nanodrop, measuring light absorption at 260nm. Furthermore, the ratio of absorbances at 260nm, 230nm and 280nm (260/230 or 260/280) provides insight on sample purity. Due to RNA also having high absorbance at 260nm and the amino acids in proteins (in particular those with aromatic side chains) absorbing strongly at 280nm, a 260/280 ratio of 1.8 is considered optimal, with ratios of 1.7-1.9 accepted as being relatively free of contamination. A ratio of less than 1.7 indicates high protein contamination whereas a ratio of greater than 1.9 indicates high RNA contamination. Similarly, organic compounds(e.g., trizols, phenols), likely forming part of a solvent or buffer, absorb at 230nm and again this allows for determination of sample purity.

### 3.2.2. *NPY Y1 receptor constructs:*

P3.1neo(+)-SNAP-ratY1-tsNluc and P3.1neo(+)-SNAP-ratY1-LgBiT were generated using previously generated p3.1zeo(+)-SNAP-ratY1 (provided by Dr Nicholas Holliday, GenBank: z11504), p3.1neo(+)-tsNluc and p3.1neo(+)-SNAP- $\beta_2$ -AR-LgBiT cDNA vectors. Exchange of the tsNluc and LgBiT fragments was

performed using excision and relegation with Not1 and XbaR1. LgBiT insert and SNAP-ratY1 vector fragments were isolated as previously described above and P3.1neo(+)-SNAP-ratY1-tsNluc or P3.1neo(+)-SNAP-ratY1-LgBiT constructs were obtained using T4 DNA ligation and TOP10F' transformation and mini/maxiprep as before.

### 3.2.3. *Prostanoid EP<sub>2</sub> receptor constructs:*

P3.1neo(+)-EP<sub>2</sub>-tsNluc was generated using previously generated p3.1neo(+)-human EP<sub>2</sub> -LgBiT (provided by Dr Nicola Dijon, GenBank: NM00956.4) and p3.1neo(+)-SNAP-β<sub>2</sub>-AR-tsNluc cDNA vectors. In this instance, the receptor cDNA was transferred between vectors, with the EP<sub>2</sub> insert DNA isolated by HindIII and Xho1 digestion. This insert was ligated into Hind III / Xho I digested p3.1neo tsNluc as previously described, followed by transformation and mini/maxiprep.

## 3.3. Cell culture

### 3.3.1. *Cell line maintenance and passaging*

The cell lines primarily used for the generation of membrane suspensions and NanoBiT complementation assays were mixed population HEK293 cell lines stably expressing cDNA of above constructs. Cell lines utilised in NanoBiT complementation assays were dual transfected lines containing receptor constructs as indicated above as well as expressing SmBiT114-β-arrestin-2, a modified version of β-arrestin-2 with the nanoluciferase SmBiT114 fragment fused to the N terminus, through the transfection of p3.1(+)-zeo-SmBiT114-βarrestin2 (courtesy of Dr Nicholas Holliday and Nichola Dijon). All cell lines were maintained in Dulbecco's modified Eagle's medium (DMEM) supplemented with glucose (4.5g/L) and L-glutamine (4.5g/L), and with 10% foetal bovine serum (FBS) (Life Technologies, Paisley, U.K.) in a humidified

atmosphere of 5% CO<sub>2</sub> at 37°C. Medium was supplemented with the appropriate maintenance concentration of relevant antibiotic where needed. For neomycin resistance lines, 0.8mg/mL geneticin was used to maintain selection and for NanoBiT lines 200µg/mL zeocin was included. Cells were passaged at 80% confluency into T25-T175 flasks and all maintenance was carried out in sterile conditions. Cell splitting was carried out by first removal of maintenance DMEM/10%FBS and cells were washed with sterile phosphate buffered saline (PBS). PBS was aspirated and either 0.5/1/3 mL of sterile trypsin solution was added to the T25/75/175 flask, respectively, and incubated for 5 minutes at 37°C. Flasks were physically agitated by knocking the side of the flask and, using 10 mL DMEM/10%FBS, cells were washed off the flask and collected in a 30 mL sterile universal tube. To remove trypsin and pellet cells, the universal was centrifuged (1000 g, 5 minutes) and the pellet resuspended in 5 mL of DMEM/10%FBS. Cells were split according to required ratio or a sample was counted for seeding plates.

**Table 3.1. Cell lines**

Cell Line	Transfected constructs	Origin
Hek-ss $\beta_2$ AR	p3.1neo(+)-SNAP- $\beta_2$ -AR [Terbium labelled for TR-FRET assays]	Courtesy of Dr Nicholas Holliday, University of Nottingham
Hek-ss $\beta_2$ AR-tsNluc	p3.1neo(+)-SNAP- $\beta_2$ -AR-tsNluc	Generated during project, University of Nottingham
Hek-ss $\beta_1$ AR-LgBiT	p3.1neo(+)-SNAP- $\beta_1$ -AR-LgBiT	Courtesy of Dr Nicola Dijon, University of Nottingham
Hek-ssY1	p3.1zeo(+)-SNAP-ratY1 [Terbium labelled for TR-FRET assays]	Courtesy of Dr Nicholas Holliday, University of Nottingham
Hek-Y1-tsNluc	p3.1neo(+)-ratY1-tsNluc	Generated during project
Hek-EP <sub>2</sub> -LgBiT/SmBiT- $\beta$ -arrestin2	p3.1neo(+)-EP <sub>2</sub> -LgBiT/ p3.1zeo(+)-SmBiT114- $\beta$ -arrestin-2	Courtesy of Dr Nicola Dijon, University of Nottingham
Hek-EP <sub>2</sub> -tsNluc	p3.1neo(+)-EP <sub>2</sub> -tsNluc	Generated during project
Hek-EP <sub>4</sub> -tsNluc	p3.1neo(+)-EP <sub>4</sub> -tsNluc	Courtesy of Dr Nicola Dijon, University of Nottingham
Hek-ssCXCR2-tsNluc	p3.1neo(+)-SNAP-CXCR2-tsNluc	Courtesy of Dr Desislava Nesheva, University of Nottingham
Hek ssA <sub>2</sub> A-tsNluc	p3.1neo(+)-SNAP-A <sub>2</sub> AR-Nluc	Courtesy of Dr Mark Soave, University of Nottingham
Hek-MOR-LgBiT	p3.1neo(+)-MOR-LgBiT	Courtesy of Dr Nicola Dijon, University of Nottingham
Hek-mGluR2-tsNluc	p3.1neo(+)-mGluR2-tsNluc	Courtesy of Professor Dmitry Veprintsev, University of Nottingham

“ss” indicates the presence of signal sequence and SNAP labelling.

### 3.3.2. *Cell line stable transfection by lipofectamine 3000*

All cell lines were transfected using Lipofectamine 3000 reagent (Invitrogen, Thermofisher, Loughborough, UK). Lipofectamine mediates nucleic acid transfer across cell membranes by the formation of liposomes with a positively charged surface (aided by co-lipid p3000), encasing the DNA of interest. These liposomes can then fuse with the negatively charged plasma membrane of cells and, due to co-lipid mediated fusion of the liposome with the cell membrane, transfer the nucleic acid cargo molecules into the cytoplasm.

For transfection of a T25 flask of adherent HEK293T cells, two 25mL tubes were prepared, each with 250 $\mu$ L Opti-MEM (Thermofisher, Loughborough, UK) media. 5 $\mu$ g cDNA and 10 $\mu$ L p3000 reagent was added to the first tube and 7.5 $\mu$ L lipofectamine was added to the other tube. Both tube solutions were then combined and gently mixed prior to incubation at room temperature for 5 minutes. During incubation, 60% confluent (T25) HEK293 wild-type cells were removed from the incubator, DMEM removed and washed with Opti-MEM (Thermofisher). Media was replaced with 1.2mL Opti-MEM. 450 $\mu$ L Opti-MEM was added to DNA suspension before all 1mL of DNA-lipofectamine suspension was added to the cells. Cells were incubated overnight at 37°C, in 5% CO<sub>2</sub>, before splitting 1:2 into a fresh T25 flask containing DMEM and allowed to grow for a further 24 hours before addition of required antibiotic. Cells were allowed to select for one week prior to expansion into 2x T75 flasks for maintenance as described previously. All Cell lines employed are listed in table 2.1.

### 3.3.3. *Procedure for cell freezing*

One flask was used to generate frozen cell line stores [with a low passage] for future use. Cells were allowed to grow to 90% confluency in T75 flasks before centrifugation and splitting into 3mL freezing media (FBS supplemented with 10% DMSO) and

suspension separation into 3x cryovials. Vials were placed in room temperature freezing container (Mr Frosty, Nalgene, Thermofisher, Loughborough, UK). The freezing container contained isopropyl alcohol to ensure cooling of cells by 1°C/min in -80°C freezer conditions, thus preventing protein degradation. The freezing container was placed in -80°C freezer for 24 hours, before transferring cryovials to liquid nitrogen stores.

#### *3.3.4. Derivation of SNAP-tagged receptor expression*

Cells transfected with receptor constructs incorporating the SNAPtag fusion protein were screened for receptor expression by SNAP labelling. Cells were seeded onto 8 wells of a poly-D-Lysine coated, clear bottom, 96 well black plate (Greiner, Cat: 655090) at 30,000 cells/well and allowed to grow overnight at 37°C, 5% CO<sub>2</sub>. Cells were then SNAP labelled by first removing growth media and replacing media with 0.1µM SNAP-surface AF488 (NEB Biolabs) in DMEM/10%FBS. Cells were incubated with labelling media for 30 minutes at 37°C, 5% CO<sub>2</sub> before washing with phosphate buffered saline solution (PBS). Cells were then fixed by replacing PBS with 3% paraformaldehyde (PFA) solution and incubating at room temperature (in the dark) for 10 minutes. PFA was removed from cells and cells were washed twice in PBS to ensure complete removal of PFA from wells before labelling with 2 µg/mL Hoechst 33342 nuclear stain (H33342) in PBS, incubating at room temperature for 15 minutes in the dark. After staining, H33342 solution was removed and replaced with 100µL PBS and plate was wrapped in foil and stored at 4°C until required for imaging. An IX Micro Widefield Plate reader was used to image labelled cells, imaging four sites per well with a 20x extra long working distance objective, using FITC and DAPI excitation / emission filters for imaging SNAP-surface AF488 (receptors) and H33342 (nuclei) labels respectively.

### 3.4. Gα C-terminal peptides

All peptides were ordered from Genscript Biosciences Ltd, generated by solid-phase peptide synthesis with >98% purity. Sequences and modifications are shown in Table 2.2.

**Table 2.2. Gα C-terminus peptides employed across project**

<b>Name</b>	<b>Sequence (N-C terminus left to right)</b>
<b>Gas11</b>	QRMHLRQYELL
<b>Gas24</b>	NIRRVFNDC RDII QRMHLRQYELL
<b>Gas19</b>	FNDC RDII QRMHLRQYELL
<b>Gas19cha18</b>	FNDC RDII QRMHLRQYE{CHA}L
<b>Pra-Gas19cha18</b>	Propargylglycine- <b>Gas19cha18</b>
<b>PalmGas19cha18</b>	Palmitoyl- <b>Gas19cha18</b>
<b>Gai24</b>	NVQFVFDAV TDVI IKNNLKDCGLF
<b>Gai19</b>	FDAV TDVI IKNNLKDCGLF
<b>Gai19cha18</b>	FDAV TDVI IKNNLKDCG{CHA}F
<b>TMR-Gas19cha18</b>	Tetramethylrhodamine-Gas19cha18
<b>TMR-Gai19cha18</b>	Tetramethylrhodamine-Gai19cha18

“CHA” indicates the inclusion of the non-native amino acid cyclohexyl alanine.

### 3.5. Membrane preparation and Terbium labelling of SNAP tagged receptors.

For membrane-based assays, cells were grown in four poly-D-lysine coated T175 flasks to 90% confluency. Terbium (Tb) labelling was optionally performed where membrane preparations were to be used in TR-FRET assays. Cell culture medium was removed from T175cm<sup>2</sup> flasks containing confluent adherent Hek-ssβ<sub>2</sub>-AR/ssY1 and replaced with 10mL of Tag-lite labelling medium (LABMED, Perkin Elmer, Bagnols-sur-Ce'ze, France) containing 100nM SNAP-Lumi4-Tb (Cisbio Bioassays). Cells were incubated in labelling medium for one hour at 37°C under 5% CO<sub>2</sub>.

Labelling medium was removed and retained for repeat use (up to 5 times) and cells were washed twice with PBS before harvesting.

For all membrane preparations, cells were then harvested by addition of 10mL fresh PBS and removal of cells from flask walls by scraping. Cell suspensions were then collected into 25mL universals and spun to obtain a cell pellet (2000rpm, 10 minutes). Supernatant was removed thoroughly, and cell pellets were frozen at -20°C until required for membrane preparation.

Cell pellets were thawed on ice to prevent receptor degradation. 20mL of wash buffer (10mM HEPES, 10mM EDTA, pH: 7.4) was added to the pellet before homogenised using an electrical homogeniser, Ultra-Turrax (Ika-Werk GmbH & Co. KG, Staufen, Germany) (position 4, 8 short bursts), and subsequently centrifuged at 48 000g at 4 °C. Supernatant was discarded and the pellet was resuspended in 20mL wash buffer and centrifuged again as above. The final pellet was resuspended in cold 10 mM HEPES with 0.1 mM EDTA (pH 7.4). Protein concentration was determined using the bicinchoninic acid assay kit (Sigma-Aldrich, Pool, UK) using bovine serum albumin (BSA) as standard, and aliquots were maintained at -80 °C until required. The bicinchoninic acid assay exploits the change in light absorption brought about by the interaction of copper(II) ions with protein alpha helical structures to measure protein content, comparing a known standard (BSA) with test sample absorption. 160µL 1M copper(II) sulphate solution was added to 8mL bicinchoninic acid to form a green solution. Serial dilutions of BSA in ddH<sub>2</sub>O ranging from 1000mg/mL – 0mg/mL [decreasing in steps of 200mg/mL] were generated and plated in 96 well, clear bottom plates (Greiner) [25µL/well in triplicate]. Membrane test sample was diluted 1/10 with a final volume of 100µL and added in triplicate to plate (25µL/well). Once all samples were plated, 200µL bicinchoninic acid-copper sulphate solution was added to each well using a multichannel pipette to ensure addition at equal times. Plate was incubated for 30 minutes

at 37°C before reading on a PHERAstar FS plate reader, measuring optical density (OD) per well. Control data was then plotted against protein concentration and assessed using simple linear regression. Sample data was then incorporated into the resulting linear equation to determine membrane protein content in µg/mL. Membrane samples were then aliquoted to give individual tubes suitable for addition of 1 µg/well membrane to half a 384-well plate and stored at -80°C.

### 3.6. Time resolved Förster (or Fluorescence) Resonance Energy Transfer (TR-FRET) and Bioluminescence Resonance Energy Transfer (BRET) Assays:

Experimental methods for these assays are described in detail in the relevant chapters, including assay conditions, concentrations and timepoints. A brief general overview is provided in this section for reference.

#### 3.6.1. *Direct measurement of fluorescent tracer binding recruitment measured by TR-FRET and BRET*

Characterisation of fluorescent ligand binding affinity employed both saturation endpoint and/or association kinetic approaches as described in data analysis (section 3.7). The fluorescent probe of interest was diluted in assay buffer (composition as stated within relevant chapter) to eight decreasing concentrations. The appropriate concentration of ligand was then incubated with Hek293 cell membranes containing the receptor construct of interest, with additional 10µM purified HiBiT [seq: VSGWRLFKKIS] when using LgBiT-fused receptors as indicated) and either vehicle or a saturating concentration of non-specific binding (NSB) compound as stated in relevant chapters. In the case of binding assays utilizing NanoBRET technology, luciferase

substrate furimazine (Promega, Wisconsin, USA) was added to either the assay plate or pre-mixed with membrane suspension (for kinetic assays) and incubated with membranes for 5 minutes prior to online plate injection and acquisition of binding data. Final concentrations of ligands were multiplied by 3x for TR-FRET assays (final volume, 30 $\mu$ L), 4x for vehicle only BRET assays (final volume, 40 $\mu$ L) or 5x for BRET assays (final volume, 50 $\mu$ L) incorporating additional agonist concentrations, to account for experimental dilutions when plating.

For characterisation of agonist induced tracer binding by NanoBRET, required HEK293 membranes were incubated (amount as defined in relevant chapter methods) with a single concentration of fluorescent tracer as indicated, furimazine and 14 decreasing concentrations of corresponding orthosteric ligands of interest. NSB and total binding responses were defined by inclusion of either vehicle or defined unlabelled NSB ligand at saturating concentrations.

For kinetic assays, membrane-furimazine suspension was added to the assay plate by smart online injection using BMG PHERAstar FS injectors, 5 minutes after furimazine incubation. Diluted membrane/furimazine mix was loaded into PHERAstar FS injector system and primed to equilibrate system and remove bubbles from injection lines. A PHERAstar injector protocol was used to inject 10 $\mu$ L of membrane per well using smart dispensing to generate final well volumes as described. Fluorescent ligand output and donor emission were both measured using PHERAstar FS filters of corresponding wavelengths as stated in the corresponding chapters, using an internal temperature of 37°C unless otherwise stated. Data was recorded across a range of timepoints as stated for both endpoint and kinetic reads.

### 3.6.2. *Characterisation of unlabelled ligand binding through fluorescent ligand competition*

For both TR-FRET and BRET assays, increasing concentrations of competing ligands were incubated with single concentrations of HEK293 cell membranes and fluorescent tracer as previously indicated. Where required, a single saturating concentration of orthosteric agonist was also included across the plate to ensure sufficient receptor activation and subsequent tracer binding. For BRET assays employing C terminally fused thermostable Nanoluciferase receptors, a single concentration of Nanoluc substrate was included either within the assay plate or within defined membrane suspensions (kinetic assays only) as previously described. Unlabelled ligand affinity was then derived through application of the Cheng-Prusoff correction (see section 3.7).

### 3.7. Data analysis

TR-FRET and NanoBRET assays were performed in either triplicate or duplicate unless otherwise indicated and were routinely expressed as the respective acceptor / donor emission ratios (ratio x 10,000 for TR-FRET data). In competition binding studies, individual experiment data were normalised to total binding in the absence of competing ligands (100 %), while in agonist-stimulated recruitment assays, data were normalised to a maximal concentration of stimulating reference agonist (100%) and vehicle control (0%).

For FI-ligand association kinetic data, specific binding traces for FI-ligand (defined as total binding – NSB) were fit to a one site association model. Global fitting of this model across multiple fluorescent ligand concentrations from the same experiment enabled estimation of FI-ligand association ( $k_{on}$ ) and dissociation rate constants ( $k_{off}$ ), together with the kinetically derived  $K_D$  ( $=k_{off}/k_{on}$ ) using the equations:

$$Bound = B_{plateau} \cdot (1 - e^{-k_{obs} \cdot t})$$

Where, the  $B_{plateau}$  is the equilibrium level of tracer binding, and the observed association rate constant  $k_{obs}$  is related to the binding rate constants for Fl-ligand in a single site model by:

$$k_{obs} = [Fl\_ligand] \cdot k_{on} + k_{off}$$

Endpoint saturation analysis also enabled calculation of the equilibrium dissociation constant ( $K_D$ ) for fluorescent tracer, as well as total binding density as  $B_{max}$  in TR-FRET and BRET experiments, based on:

$$Specific\ binding = B_{max} \cdot \frac{[Tracer]}{[Tracer] + K_D}$$

Competition binding studies were fitted to determine competing ligand  $IC_{50}$  concentrations, using a four-parameter fit including the Hill slope (n)

$$Specific\ binding = Basal + Total\ Specific\ binding \cdot \frac{IC_{50}^n}{[Ligand]^n + IC_{50}^n}$$

Where appropriate, the Cheng-Prusoff equation was applied to convert  $IC_{50}$  estimates to the competing ligand dissociation constant as  $K_i$

$$K_i = \frac{IC_{50}}{1 + \frac{[FL]}{K_{FL}}}$$

$K_{FL}$  and  $[FL]$  represent the fluorescent probe dissociation constant and concentration respectively. The Cheng-Prusoff method allows for determination of unlabelled ligand inhibitory constants ( $K_i$ ) through competition derived  $IC_{50}$  values if, as in this case, the concentration and affinity of the competing ligand is known.

For endpoint agonist stimulation of Fl-ligand recruitment measured by NanoBRET and NanoBiT complementation assays, concentration response curve analysis was performed to obtain estimates of ligand potency ( $EC_{50}$ ) and maximal response  $R_{max}$ :

$$Response = Basal + R_{max} \cdot \frac{[Agonist]^n}{[Agonist]^n + EC_{50}^n}$$

Alternatively kinetic Fl-ligand recruitment data were fitted to a rise-to-steady state model, as described by Hoare et al (2020):

$$Response \text{ (at time } t) = Basal + Response_{steady \ state} \cdot (1 - e^{-k_{obs} \cdot t})$$

$$Initial \ rate = k_{obs} \cdot Response_{steady \ state}$$

In this analysis, concentration response data were analysed by defining the initial rate at each ligand concentration as the response.

All data analysis was performed using Prism 10.0 (GraphPad Software, San Diego). Parameter estimates were expressed as pX (-log X) where appropriate (e.g. p $EC_{50}$ ) and data from individual experiments were pooled as mean  $\pm$  s.e.m. Statistical significance

between two data groups was assessed by Student's unpaired or paired t-test as indicated in the text, with a level of significance defined as  $p < 0.05$ .

## **Chapter 4. Results I**

Identification of G $\alpha$  C-terminus peptides able to promote the GPCR high affinity state for orthosteric agonist binding.

## **4. Identification of G $\alpha$ C-terminus peptides able to promote the GPCR high affinity state for orthosteric agonist binding.**

### 4.1. Chapter introduction

The need for a more universal, high-throughput, method of characterising intracellular allosteric ligands calls for the development of novel tracers for the GPCR intracellular binding site. The recent advancements in the use of G $\alpha$ s derived peptides to bind and modulate receptor conformations makes these peptides an appealing template in the design of more universally applicable tracers for targeting the G protein interaction site. However, understanding of the exact nature of their modulatory capacity in regard to agonist binding, and the effects of peptide structure on their allosteric ability, remains limited. As such, the aims of this chapter were to establish an experimental system to monitor the influence of peptides on orthosteric ligand binding at G $\alpha$ s and G $\beta\gamma$  coupled receptors. This involved the development of a TR-FRET based approach to monitor effects on orthosteric ligand binding (the principles of which are introduced in section 4.2.1). This also required the identification of candidate G $\alpha$ s and G $\beta\gamma$  coupled receptors to act as examples within these studies. A brief background to these receptors ( $\beta_2$ -AR and Y1) is outlined in section 4.2.2 and 4.2.3.

### 4.2. Introduction to employed techniques and receptors within this chapter.

#### *4.2.1. Time-resolved Förster Resonance Energy Transfer (FRET) assays for GPCR ligand binding.*

As previously discussed in chapter 1, luminescence and fluorescence-based biosensors or ligands are emerging as widely used methodologies for characterisation of ligand interactions at GPCRs (Soave et al., 2020c; Stoddart et al., 2018, 2015; Sykes et

al., 2019). The techniques available are fast expanding to encompass all stages of GPCR signalling, from detecting initial ligand binding interactions, to downstream signalling responses. The development of fluorescent ligands in particular has allowed for a revolution in the measurement of ligand binding within a homogeneous assay system, allowing for real-time readout of receptor-ligand interactions both visually and through application of light-based plate readers (Soave et al., 2020c; Stoddart et al., 2015).

Foremost amongst the new light-based techniques available is FRET. Initial FRET studies relied on the application of fluorescent protein pairs, such as Cyan and Yellow-fluorescent-protein (CFP / YFP), which required measurement of acceptor emissions at the same time as donor excitation. Application of fluorescent proteins allowed for cellular based assays, employing genetically encoded sensors, with the capacity to detect intracellular protein-protein interactions through resonance energy transfer (Anton et al., 2022b; Hoffmann et al., 2005). More recently this technique has been further expanded using intramolecular FRET sensors to allow for direct spatial measurement of cellular microenvironments and changes in secondary messenger concentrations as a result of receptor activation (Anton et al., 2022b; Comeo et al., 2020; Halls, 2019; Navarro et al., 2018; Soave et al., 2020c).

One disadvantage of standard FRET methodologies is that the donor excitation can generate background autofluorescence, and therefore “noise” within emission data collected at the same time. Often the specific signal to noise in FRET experiments is therefore limited, particularly for quantitative investigations of pharmacology. One method to overcome this limitation involves the use of lanthanide elements, including Europium (Eu) and Terbium (Tb) as the donor fluorophores in a FRET assay. Following excitation (typically at 337 nm), these ions have a long emission lifetime, allowing a persistent FRET signal if present after the excitation pulse is completed. FRET measurements can be made

following a short delay after excitation (known as time resolved FRET (TR-FRET), roughly in the microsecond range)(Degorce et al., 2009). This reduces the background from short-lived fluorescence emission and improves the detection range, increasing the overall signal-to-noise ratio for the specific FRET signal and increasing assay sensitivity. A second advantageous property of lanthanides is their discrete emission spectra with multiple peaks, allowing the use of well separated acceptor fluorophores from the donor excitation (Figure 4.1).

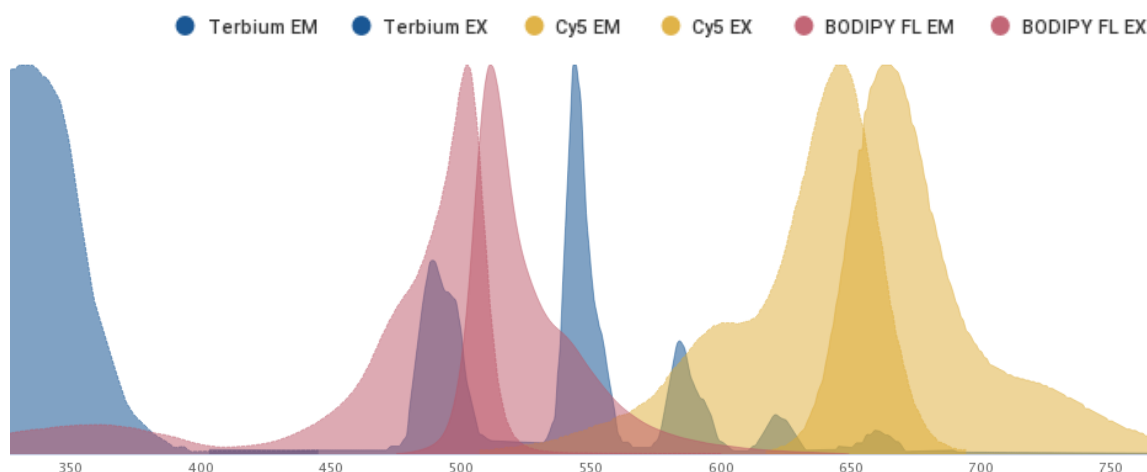


**Figure 4.1.** Excitation/Emission spectra of Terbium compared with the classical fluorophores BODIPY-FL and Cyanine5 (Cy5).

Clearly one issue with application is the ability to tag targets of interest with a lanthanide fluorophore, however, this was made possible with the development of caged lanthanide chelates and their modification with reactive groups suitable for protein labelling technologies, such as SNAP-tag technology. SNAP-tag technology utilises the irreversible and specific reaction of O<sup>6</sup>-alkylguanine-DNA alkyl transferase (AGT) tag with O<sup>6</sup>-benzylguanine (BG) derivatives, leading to the transfer of the synthetic probe to a reactive cysteine residue on the tagged target

protein(Keppler et al., 2004). The combination of TR-FRET technology and suitable Tb donor labelling of the receptor proteins, together with the generation of fluorescent ligand probes, then provides routes to powerful high-throughput, homogenous, assays for kinetic and endpoint receptor binding studies, both for the fluorescent probes themselves, and also unlabelled ligands through probe competition studies (Figure 4.2)(Fyfe et al., 2019; Sykes et al., 2017; Sykes and Charlton, 2018).

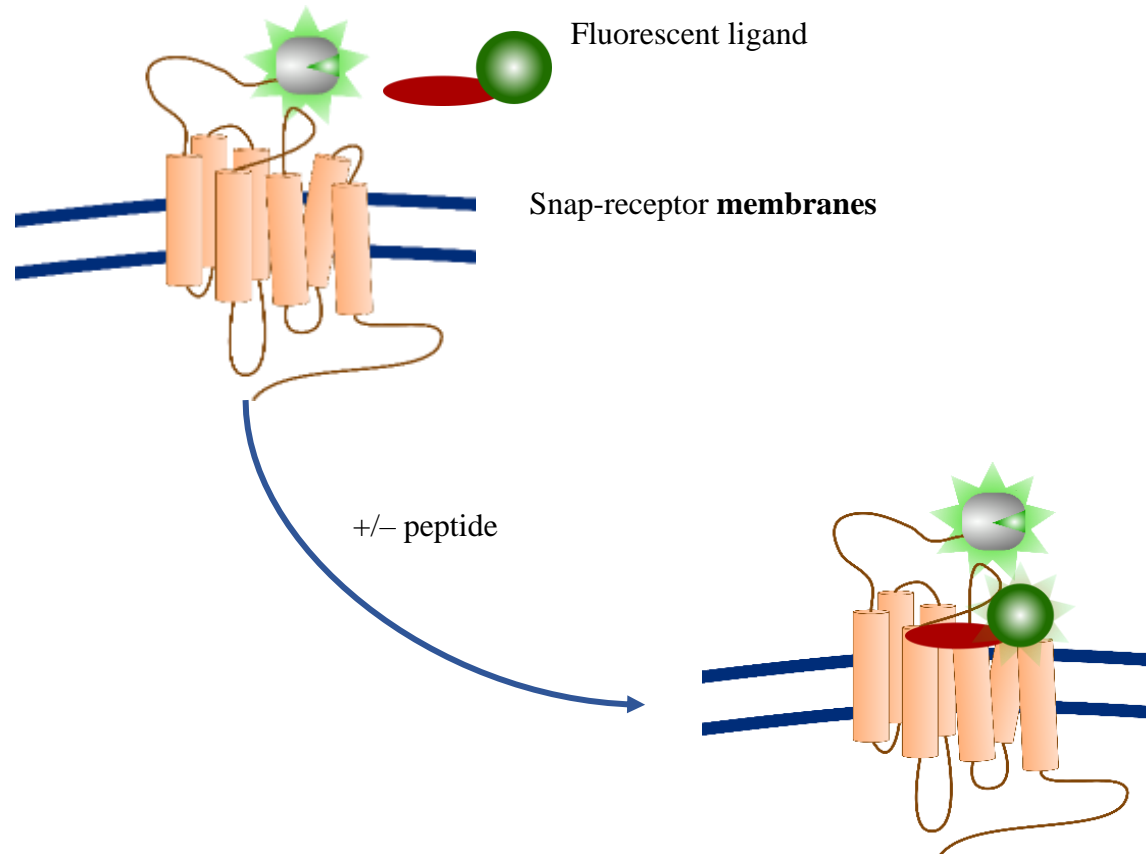


**Figure 4.2. Principle of TR-FRET.** Upon orthosteric ligand binding, stimulation of the N-terminally fused donor Tb, attached with reaction of BG-Tb with the extracellular SNAP tag, allows energy transfer to ligand fluorophores within 10 nm distance, producing a FRET ratio increase indicating specific binding.

The draw of fluorescent ligand technology is its ability to be combined with resonance energy transfer technology. This facilitated the development of homogeneous assay formats, removing the need to separate bound from free ligand when measuring ligand interactions, thus enabling true equilibrium assay systems. This can further be extended to include multiple timepoints, allowing more accurate evaluation of ligand kinetics within a single assay well. In addition, beyond its homologous real-time benefits, is that it eliminates the primary concern with the use, and disposal, of radiolabelled ligands and provides a significantly faster system for ligand binding measurements. As such, it also facilitates the means to measure acute changes in agonist affinity as a result of GPCR conformational dynamics at a range of timepoints (see section 6.5.1). The coupling of native G proteins to receptors is known to promote conformational change towards the active-conformation (high-affinity state) and application of FRET based studies has allowed for exploration of this phenomenon (section 4.5.2). Additionally, their sensitivity allows characterisation of how assay environments (e.g. pH, buffer composition) can have subtle effects on receptor-ligand interactions (Farmer et al., 2022). These advantages highlight TR-FRET using orthosteric ligand probes as a suitable approach for the exploration and characterisation of synthetic G $\alpha$  C-terminus peptides and their effects on GPCR-agonist interactions.

#### 4.2.2. *Targeting the $\beta_2$ -Adrenoceptor.*

Of the hundreds of class A GPCRs, the most well studied are the adrenoceptor family (AR). This family carries out their function upon the binding of catecholamines (e.g., adrenaline, noradrenaline) and can be subdivided into nine receptor subtypes:  $\alpha_{1A}$ ,  $\alpha_{1B}$ ,  $\alpha_{1D}$ ,  $\alpha_{2A}$ ,  $\alpha_{2B}$ ,  $\alpha_{2C}$ ,  $\beta_1$ ,  $\beta_2$  and  $\beta_3$ , with their expression being widespread across the body (Ahlquist, 1948; Hill, 2006). Of the nine receptors,

the  $\beta$  receptors couple primarily to Gs proteins, facilitating their function through the accumulation of cAMP and subsequent activation of PKA. This response has diverse functional consequences at a phenotypic level, dependent on tissue specific receptor location.

Clinically, the  $\beta_2$ -AR has a longstanding association with the pathology and treatment of asthma and chronic obstructive pulmonary disease (COPD), which highlights the diverse roles these receptors display. Asthma and COPD represent a diseased state of restricted airflow driven by inflammation, airway smooth muscle pro-contractile agents, together with luminal occlusion by mucus and plasma, and airway wall thickening. As of 2019, it is believed that asthma has affected an estimated 262 million people worldwide and caused 455,000 deaths on record, with COPD affecting a similar 292 million people and is the fourth leading cause of death worldwide (Adeloye et al., 2022). Despite their similar presented symptoms, COPD and asthma have distinct pathophysiological differences. Asthma is generally considered to be associated with hyperresponsiveness of the airways which leads to recurrent, fully reversible, inflammation. Conversely, COPD is the umbrella term used for a group of lung diseases, including emphysema and chronic bronchitis, defined as a disease state characterised by airflow limitation that is not fully reversible. Within healthy tissue,  $\beta_2$ -AR activation drives relaxation of the airway smooth muscle to promote opening of the airway. As such, within the smooth muscle tissue of the lungs, application of  $\beta_2$ -AR agonists acts to alleviate the effects of COPD and asthma and promotes relaxation of the muscle, resulting in dilation of the airways. Initially, observation of this relationship led to the treatment of asthma using high-efficacy, short-acting,  $\beta_2$ -AR agonists such as isoprenaline, however, this was later linked to a high degree of asthma-mortality and subsequently discontinued. This was believed to be due not only to the high efficacy of these

ligands, but also due to the lack of selectivity between the  $\beta_2$ -AR and  $\beta_1$ -AR which are primarily found in cardiac tissue. Additionally, the systemic application of these ligands was further believed to drive adverse drug reactions, particularly at the heart, due to poor clearance and tissue selectivity, resulting in alternative application techniques being explored (Salpeter et al., 2004; Walker et al., 2011; Wendell et al., 2020). Subsequently, the treatment of choice was then changed to employ long-acting  $\beta_2$ -AR partial agonists, such as salmeterol, which were able to reduce the incidence of on/off-target side-effects while also reducing the need for repeat dosing beyond once a day.

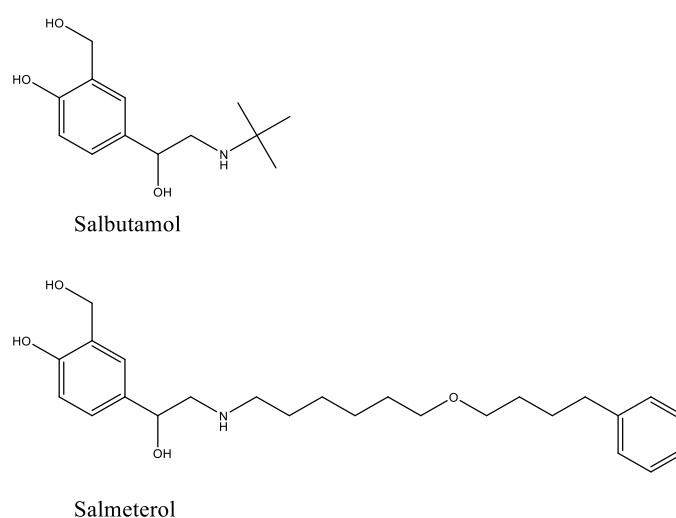


**Figure 4.3.** Structures of  $\beta_2$ -AR short and long-acting partial agonists.

Additionally, the majority of patients rely on short acting partial-agonists such as salbutamol for fast alleviation of symptoms in the case of severe onset of symptoms (Burggraaf et al., 2001; Cullum et al., 1969; D'Alonzo and Tolep, 1998; Walker et al., 2011). The pharmacological profile of these ligands is believed to be related to their corresponding chemical structure (Figure 4.3). In the cases of salbutamol and salmeterol, both share an identical head group, with salmeterol containing a long carbon chain compared to the small

tert-butyl group of salbutamol. This large alkyl chain provides salmeterol with a greater hydrophobicity, likely resulting in increased membrane localisation and a subsequent slower pharmacokinetic profile, facilitating its role as a long-acting agonist.

However, the application of these long and short acting partial agonists is still implicated in the development of severe side-effects over prolonged use. Foremost amongst the side-effects associated with prolonged use of  $\beta_2$ -AR agonists is the detrimental effects on cardiac and vasculature function. Prolonged use of  $\beta_2$ -AR agonists (even when applied topically via inhalation) is associated with greater risk of hypertension, ischaemia, myocardial depression, atrial fibrillation and sudden cardiac related death through its role of increasing heart rate through off-target interactions at the  $\beta_1$ -AR (Salpeter et al., 2004). These negative cardiac implications are further exacerbated by potential on-target side-effects within the skeletal muscle vascular beds, resulting in vasodilation, a subsequent drop in cardiac venous return, and compensatory tachycardia (Lulich et al., 1986). Another example of the potential negative impact of  $\beta_2$ -AR orthosteric agonists is through stimulation of  $\beta_2$ -AR within the immune system. Recent studies have found stimulation of  $\beta_2$ -AR to produce asthma-like allergic airway disease in mice through its role in activating  $T_H2$  cells.  $T_H2$  cells drive inflammation through the activation and recruitment of adaptive immune cells (B cells) and macrophages through release of IL4 and IL13, thus having potential detrimental consequences for those suffering with inflammatory driven diseases, such as COPD and Asthma (Walker et al., 2011).

The diverse functionality of the  $\beta_2$ -AR in particular has driven its extensive targeting by therapeutics for treating a plethora of diseases. As stated before, development of  $\beta_2$ -AR agonists has played a pivotal role in the treatment of asthma, particularly with the development of salbutamol, used to alleviate

bronchoconstriction (Cullum et al., 1969). Similarly, the discovery of  $\beta_2$ -AR antagonists ( $\beta$ -blockers) such as propranolol has lowered the risk of severe heart conditions for uncountable patients through its ability to reduce the effects of hypertension and cardiac arrhythmia through inhibition of the  $\beta_1$ -AR response. However, limited selectivity for the  $\beta_1$ -AR against the  $\beta_2$ -AR, and the systemic application of these antagonists, can result in severe effects in asthma patients through promotion of bronchoconstriction. Subsequently, more selective  $\beta_1$ -AR antagonists, such as atenolol, have mitigated cardiac risks while having reduced side effects within the airways (Quirke, 2006).

The treatment of both asthma/COPD and cardiovascular disease highlight the desirable effects of developing selective adrenoceptor ligands in order to reduce the incidence of therapeutic side effects. However, due to high variability in function yet conserved structural homology within the adrenoceptor family, development of selective therapeutics with limited on- and off-target side effects remains challenging (Rasmussen et al., 2011; Rosenbaum et al., 2009; Toyoda et al., 2023; Xu et al., 2021). In particular, structural studies highlight a high degree of conservation of key residues between  $\beta_2$ -AR and  $\beta_1$ -AR involved in ligand binding, particularly aspartate (TM3) serine (TM5) residues and suggest that ligand selectivity is driven by variations in extracellular regions, altering ligand access to the binding pocket. This complexity has led to the exploration of alternative targeting mechanisms, such as allosteric modulation.

Compound 15 and Compound 6 were first described in 2019 as novel intracellular modulators of  $\beta_2$ -AR. Compound 15 was shown to bind to a site within the G protein binding pocket and thus inhibit signalling, while promoting the receptor inactive conformation, although its low affinity limits its therapeutic utility. In contrast, Compound 6 was shown to bind via the intracellular loop 2 region and displays an ability to stabilise the active conformation of the

receptor through interactions with TM3&4(Heng et al., n.d.; Liu et al., 2017a). Application of these allosteric ligands is believed to hold greater potential for reduced side effect burden due to not only providing greater target selectivity, but also relying on endogenous hormone levels for activity, thereby limiting the effects at off-target tissues with reduced receptor activation (e.g.,  $\beta_2$ -AR in TH2 cells) (as discussed in section 1.2.1).

#### 4.2.3. *Targeting the Neuropeptide Y Y1 receptor.*

Neuropeptide Y (NPY) and its corresponding receptors Y1,2,4 and 5 are expressed throughout the body with locations including various regions of the central and peripheral nervous system(Yi et al., 2018). NPY itself is a 36 amino acid peptide that acts as a neurotransmitter, having involvement on a plethora of homeostatic and physiological functions, particularly within the control of appetite and satiety. It is the most abundant neuropeptide in the central nervous system; however, it shares a high proportional (70%) homology with hormones peptide YY (PYY), released from colonic endocrine l cells, and islet released pancreatic polypeptide (PP, 50%). All four known NPY receptors are class A GPCRs and mediate their activity through employment of  $G\alpha_i$  G proteins, resulting in a reduction in cellular cAMP production, modification of gene expression and a reduction in  $Ca^{2+}$  channel function(Yi et al., 2018; Zhang et al., 2011). The Y1 receptor shows equivalent affinity and responses to NPY and PYY, but not the circulating 3-36 metabolites produced by the action of dipeptidyl peptidase IV(Grandt et al., 1996).

Dysregulation of the NPY signalling pathway has been implicated in both psychological and physiological diseases, including obesity, blood pressure, GI and bone function, and certain forms of cancer(Baldock et al., 2009; Chen and Zhang, 2022; Holzer et al., 2012; Qin et al., 2019; Zhang et al., 2011; Zukowska-Grojec et al.,

1991). The central role of NPY in the hypothalamic circuits controlling appetite has received particular attention historically. Activation of NPY Y1 signalling in hypothalamic arcuate neurones has been shown to induce food intake and promote obesity, primarily identified through behavioural studies using the rodent model system (Zhang et al., 2011). Upregulation of NPY and stimulation using NPY agonists was shown to produce a marked increase in feeding behaviour (Beck, 2006; Nguyen et al., 2012). These studies subsequently led to development of several selective Y1 antagonists, able to promote satiety within additional *in vivo* studies. BIBO3304 is a key example Y1 peptidomimetic antagonist developed in an attempt to reduce Y1 driven feeding, however, the *in vivo* efficacy of BIBO3304 and other selective antagonists has remained limited due to poor bioavailability, limiting their use to purely pharmacological studies (H. A. Wieland et al., 1998). Additionally, the role of Y1 signalling in promoting vasoconstriction may result in orthosteric ligands displaying detrimental effects within the circulatory system. A further barrier limiting the effectiveness of selective Y1 antagonists is the presence of compensatory mechanisms within the NPY signalling pathways. In particular, Y5 signalling in the paraventricular nucleus of the hypothalamus has been implicated in moderating food intake, and, upon Y1 knockout or inhibition, overcompensates to counteract the reduction in feeding behaviour as a result of loss of Y1 signalling (Nguyen et al., 2012). Subsequently, the ability to modulate endogenous levels of Y1 signalling, particularly at sites of peak NPY responses driving appetite and feeding behaviour, through application of use-dependent ligands would potentially provide increased effectiveness in reducing feeding behaviour. This makes the identification of alternative, allosteric, ligands with an improvement bioavailability and CNS penetration profile an appealing strategy for tackling Y1 mediated responses. Additionally, application of use-dependent allosteric ligands could further provide site and receptor selectivity, thereby reducing the

occurrence of on- and off-target side effects, particularly within the circulatory system and sympathetic nervous system (Schneider et al., 2007).

#### 4.3. Chapter aims:

Overall, the objective of this chapter was to indirectly assess the function of candidate Gs and Gi peptides through a predicted ability to enhance orthosteric agonist affinity at relevant GPCRs, based on the Ternary-Complex Model (see chapter 1). For each of the example receptors studied ( $\beta_2$ -AR – Gs, Y1 – Gi), this involved the generation of a suitable TR-FRET orthosteric ligand binding assay, its validation, and use to assess peptide impacts.

#### 4.4. Methods

##### 4.4.1. *Cell line generation and membrane preparation.*

HEK293 cell lines were generated as previously described (section 3.3 & 3.5) expressing p3.1neo(+)-SNAP- $\beta_2$ -AR or p3.1(+) SNAP-rY1. Cells were initially screened for SNAP-receptor membrane expression by labelling with membrane impermeant fluorophore SNAP-surface AF488 prior to fixing and imaging, as described previously (section 3.5). Upon validation of cell line stability and receptor expression, cells were grown in four T175 flasks to 90% confluency before being used to generate Tb labelled Hek-SNAP-receptor cell membranes as described (section 3.5).

##### 4.4.2. *TR-FRET assessment to derive BODIPY-FL-PEG8-(S)-Propranolol affinity at the $\beta_2$ -adrenoceptor.*

To determine the ability of various Gas derived G $\alpha$  C-terminal peptides to modulate agonist affinity at  $\beta_2$ -AR, the binding of the fluorescent ligand BODIPY-FL-PEG8-(S)-Propranolol (Hello Bio

Ltd, Bristol, UK) was first characterised in saturation and kinetic association binding studies. All assays were run in 384-well, white, Optiplates (product number: 6007290, PerkinElmer LAS Ltd, UK).

Fluorescent probe association kinetics were determined using seven different concentrations of BODIPY-FL-PEG8-(S)-Propranolol (Fl-propranolol) ranging from 100nM – 1.56nM (final assay concentrations), initially made up to be 3-fold more concentrated, accounting for dilution upon addition to assay plate. Assays were run in both sodium rich assay buffer was composed of 1x Hank's balanced salt solution (CaCl<sub>2</sub>·2H<sub>2</sub>O[185.4mg/L], MgSO<sub>4</sub>·7H<sub>2</sub>O[200mg/L], KCl[400mg/L], KH<sub>2</sub>PO<sub>4</sub>[60mg/L] MgCl<sub>2</sub>·6H<sub>2</sub>O[8g/L], Na<sub>2</sub>HPO<sub>4</sub>[90mg/L], NaHCO<sub>3</sub>[350mg/L]), NaCl[8g/L], 1% DMSO, 0.1mg/ml Saponin, 0.02% w/v Pluronic acid F<sub>127</sub> and 20mM HEPES and 0.2% bovine serum albumin [BSA], pH 7.4) or low sodium buffer (25mM HEPES, 1% DMSO, 0.1mg/ml Saponin, 0.02% w/v Pluronic acid F<sub>127</sub>, 1mM MgCl<sub>2</sub> and 0.2% BSA, pH 7.4). The appropriate concentrations of Fl-propranolol were incubated with Tb-Hek-ssβ<sub>2</sub>-AR cell membranes (1µg/well) in assay buffer (final volume, 30µL), in the absence or presence of 10 µM ICI118551 to determine non-specific binding. Prior to reading the assay plate was spun at 200rpm for 10 seconds to ensure equal well volume and mixing. The amount of bound Fl-propranolol to Tb-labelled receptors was determined by HTRF detection using a PHERAstar FS (BMG), using real time measurements during incubations at 37°C. Tb donor was stimulated using three flashes with incorporated laser at 337nm and dual fluorescence was measured, measuring emission wavelengths of 520nm (acceptor, Fl-propranolol) and 490nm (donor, Tb), to generate a HTRF ratio (520/490nm x 10000). Readings were taken at 10 second intervals, on a row-by-row basis, within a 30-minute range allowing for construction of association kinetics curves. The resulting specific binding data were fitted to a one site association kinetic model as described in data analysis (section 3.7) to

determine best-fit estimates for  $k_{on}$  and  $k_{off}$ , as well as kinetic derivation of Fl-propranolol  $K_D$ . Assays employing non-hydrolysable GTP-analogues incorporated 100 $\mu$ M Gpp(NH)p within the assay buffer, in order to minimise native G-protein interaction with the receptor.

A similar experimental setup was used for the characterisation of the Y1 receptor fluorescent orthosteric antagonist BIDA84(Liu et al., 2016). The binding affinity of BIDA84 was again characterised in saturation binding studies. Assay buffer (low sodium) consisted of 25mM HEPES, 1% DMSO, 0.1mg/ml Saponin, 0.02% w/v Pluronic acid F127, 1mM MgCl<sub>2</sub> and 0.2% BSA, pH 7.4 either with or without the addition of 2.5mM CaCl<sub>2</sub>, reported to improve Y1 ligand binding(Heike A. Wieland et al., 1998). Tb-Hek-ssY1 membranes (1 $\mu$ g/well) were incubated at 37°C with increasing concentrations of BIDA84 ranging from final assay concentration 200nM-1.6nM (decreasing by half concentration, and either assay buffer or 1 $\mu$ M NPY/BIBO3304 (NSB), which defined NSB (final well volume: 30 $\mu$ L). BIDA84 binding to labelled receptors was recorded measuring wavelengths of 665nm (acceptor, BIDA84) and 620nm (donor, Tb), to generate a HTRF ratio (665/620 x 10000). Readings were taken over a 2-hour timecourse with readings every 30 minutes. Final specific binding data were derived by removal of measured NSB from total binding data and BIDA84 affinity ( $K_D$ ) was determined as described in methods, data analysis section 3.7.

#### *4.4.3. TR-FRET assessment to determine allosteric behaviour of unlabelled $G\alpha_s$ C-terminal peptides.*

Having derived the affinity of fluorescent tracers, the allosteric behaviour of  $G\alpha_s$  and  $G\alpha_i$  peptides Gas11, Gas24, Gas19cha18, Gai24 and Gai19cha18 was assessed indirectly (Sequences within section 3.4). Binding affinities of various orthosteric receptor agonists and antagonists was measured through competition with

the labelled tracers at their respective receptors, in the presence or absence of the G protein peptides.

For  $\beta_2$ -AR investigations, assays were run in both high and low sodium conditions, with high sodium conditions incorporating Gpp(NH)p as previously described, and low sodium assays run both with and without Gpp(NH)p present. Tb labelled Hek-ss $\beta_2$ -AR membranes (1 $\mu$ g/well) were incubated with increasing concentrations of orthosteric ligands (salbutamol, isoprenaline, salmeterol, formoterol and ICI118551 ranging from 1 $\mu$ M to 0.01nM final assay concentration decreasing in half log steps, 10 $\mu$ L/well), vehicle or 10 $\mu$ M corresponding peptide (10 $\mu$ L/well), and 20nM Fl-propranolol. The addition of the ss $\beta_2$ -AR-Hek cell membranes was done last by injection using BMG PHERAstar injectors to ensure equivalent competition between labelled vs unlabelled ligand binding over the time to equilibrium. The assay plate (final assay volume 30 $\mu$ L [all dilutions accounted for 3x dilution upon addition to assay plate]) was then incubated at 37°C between reads using a benchtop incubator. HTRF endpoint plate reads (using BMG Pherastar, settings as described in above) were taken after 30-, 60- and 120-minutes post membrane addition and. NSB was again defined by 10 $\mu$ M ICI118551 (10 $\mu$ L/well) and total binding was determined by vehicle control and used to define 0% and 100% binding respectively when normalizing response data.

Y1 receptor assays were again run using low sodium assay buffer as was previously described, with or without the addition of 2.5mM CaCl<sub>2</sub>. Initial optimisation assays, not including test peptides, compared the effect of Ca<sup>2+</sup> ions in the assay buffer on agonist affinity, comparing this new buffer with Ca<sup>2+</sup> deficient buffer as previously described. Tb labelled Hek-ssY1 membranes (1 $\mu$ g/well) were incubated with increasing concentrations of orthosteric ligands (NPY, PYY, [Leu31, pro34]PYY, and the dimeric peptide antagonist 1229U91 / GR231118(Liu et al., 2016; Mountford et al., 2014) ranging from 3 $\mu$ M to 0.01nM decreasing in half log steps,

10 $\mu$ L/well), vehicle or 10 $\mu$ M corresponding C terminal G protein peptide (10 $\mu$ L/well), and 20nM BIDA84. NSB was again defined by 1 $\mu$ M BIBO3304 (10 $\mu$ L/well) and total binding was determined by vehicle control and used to define 0% and 100% binding respectively when normalizing response data.

In both  $\beta_2$ -AR-Gs peptide and rY1-Gi peptide assays, normalized data were used to determine ligand IC<sub>50</sub> values +/- peptide and values were then converted into derived pK<sub>i</sub> values using the Cheng and Prusoff correction as described in data analysis (section 3.7).

## 4.5. Results

### 4.5.1. Validation of the HEK SNAP- $\beta_2$ -AR cell line and Fl-propranolol for use in TR-FRET ligand binding assays.

Following transfection of p3.1neo(+)-SNAP- $\beta_2$ -AR, generating the Hek-ss $\beta_2$ -AR cell line, receptor expression was validated by SNAP surface-AF488 labelling of live cells. Visualisation of whole cells post labelling showed high receptor expression, localised to the cell plasma membrane.

The effect of G protein mimetic peptides binding to the intracellular domains of GPCRs can be assessed indirectly from their impact on orthosteric ligand binding (Mannes et al., 2021). For example, peptides which stabilise an active conformation would be expected to enhance the observed affinity of orthosteric agonists. Initially therefore, a TR-FRET assay was established to monitor orthosteric ligand binding to the  $\beta_2$ -adrenoceptor, using the fluorescent ligand BODIPY-FL-PEG8-(S)-Propranolol (Fl-propranolol) as a tracer, to then allow characterisation of unlabelled ligand affinities through competition binding experiments.

Binding of the Fl-propranolol tracer to ss $\beta_2$ -adrenoceptors, in Hek293 membranes, was first characterised in two distinct buffers, high sodium Hank's based buffer containing Gpp(NH)p (Figure

4.4A), which promotes the G protein uncoupled receptor conformation, and Gpp(NH)p deficient low sodium buffer (Figure 4.4B), reported to promote a shift in equilibrium towards the active conformation for the  $\beta_2$ -adrenoceptor (Boguth et al., 2010; Hubner et al., 2016; Lefkowitz and Williams, 1977; Selent et al., 2010). In both cases the binding association kinetics of seven concentrations of Fl-propranolol were monitored, and the observed association rates ( $k_{obs}$ ) from specific binding traces showed a linear relationship with antagonist concentration, as would be expected for single site binding. Initial assays, carried out to determine the optimal quantity of membrane required for sufficient donor fluorescent output, identified 1  $\mu$ g/well produced adequate HTRF signal without incorporating additional noise within the signal.

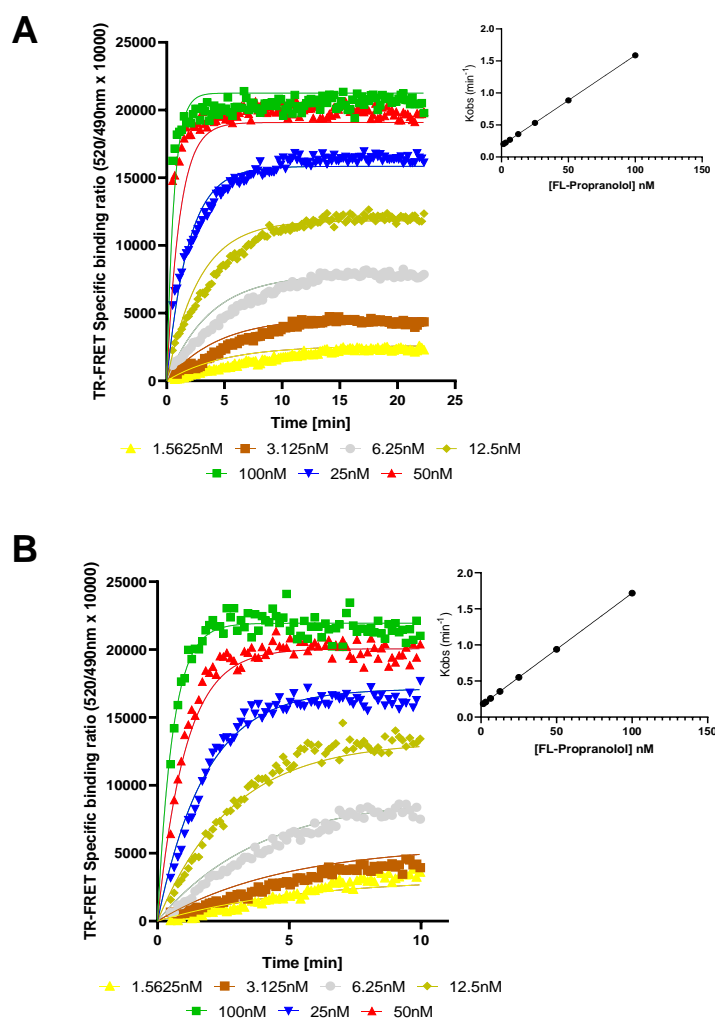


**Figure 4.4. Determination of Fl-propranolol kinetic binding parameters in HEK-β<sub>2</sub>-AR membranes.** (A) (left) Observed association of Fl-propranolol specific binding to the β<sub>2</sub>-adrenoceptor under high sodium conditions, including 100 μM Gpp(NH)p. (right) plot of Fl-propranolol concentration against  $k_{obs}$  showing binding following a simple law of mass action model with  $k_{obs}$  increasing with concentration in a linear manner. In both A and B data is presented in singlet from a representative of five experiments, in membranes at 37°C. (B)(left) Fl-propranolol specific binding under low sodium conditions. (right) plot of Fl-propranolol concentration against  $k_{obs}$  showing binding following a simple law of mass action model with  $k_{obs}$  increasing with concentration in a linear manner. Data in singlet from a representative of five experiments. Non-specific binding was in all cases determined through inclusion of 10 μM ICI118551 and deducted from plotted data to determine specific binding.

Global fitting of the FL-propranolol association time courses to a single site binding model allowed for characterisation of  $k_{on}$  and  $k_{off}$  values for FL-propranolol at the  $\beta_2$ -AR. In a sodium rich environment binding displayed an interaction best described with a single population of binding sites, with a  $k_{on}$  of  $7.98 \pm 1.56 \times 10^6 \text{ M}^{-1} \text{ min}^{-1}$  and  $k_{off}$  of  $0.092 \pm 0.023 \text{ min}^{-1}$  ( $n=5$ ). This allowed for the calculation of the equilibrium dissociation constant ( $K_D$ ) as  $11.2 \pm 0.6 \text{ nM}$ . In low sodium buffer FL-propranolol was shown to have a similar affinity, as would be expected for an antagonist / inverse agonist that did not favour the active conformation. Using the same model FL-propranolol displayed a  $k_{on}$  of  $1.3 \pm 0.18 \times 10^7 \text{ M}^{-1} \text{ min}^{-1}$ ,  $k_{off}$  of  $0.18 \pm 0.02 \text{ min}^{-1}$  and subsequently a  $K_D$  of  $16.1 \pm 3.1 \text{ nM}$  ( $n=5$ ).

FL-propranolol competition analysis was performed to determine the affinities of four representative agonist ligands (isoprenaline, formoterol, salbutamol and salmeterol) and the unlabelled antagonist ICI118551 in both high and low sodium assay buffers as described in the methods – and later to examine the potential allosteric effect of different G $\alpha$ s derived peptides. For these assays, 20 nM FL-propranolol tracer was chosen as  $1 - 2 \times K_D$  concentration in the assay. Where appropriate,  $IC_{50}$  values were converted to estimates of the competing ligand affinity using the Cheng-Prusoff correction. The hypothesis is that the G $\alpha$ s derived G $\alpha$ C-terminal peptide may increase the affinity of orthosteric  $\beta_2$ -adrenoceptor agonists, leading to a shift to a more potent  $IC_{50}$ , potentially accompanied by a shallower Hill slope (which would reflect the presence of both high and low affinity receptor populations within the assay). Specific binding was monitored at a number of timepoints to ensure the 2 h endpoint shown represented equilibrium conditions.

For control measurements in the absence of G $\alpha$ s peptides, the measured affinity of the example ligands was as expected from literature data (Table 4.1), with an order of affinity of salmeterol >

ICI118551 > formoterol > isoprenaline > salbutamol, within low sodium environment assays. The addition of both Gpp(NH)p and a high sodium environment was hypothesised to cause a reduction in agonist affinity. This is due to the inclusion of a non-hydrolysable GTP-analogue resulting in  $G\alpha$ -GppNHp and  $G\beta\gamma$  dissociation, uncoupling of the native G protein from the receptor ternary complex with agonist, causing a conformational shift to the low-affinity agonist state further driven by the negative allosteric action of sodium (Warne et al., 2019). This was observed within comparison assays (Table 4.2, Figures 4.5&4.6), indicating high sodium buffer in combination with Gpp(NH)p is able to produce lower affinity binding. Removal of sodium and Gpp(NH)p from the assay resulted in increased affinity across all higher affinity agonists (10-fold formoterol, 7-fold salmeterol). However, a four-fold increase in antagonist affinity was also observed for ICI118551 (df=7, p=0.0002).

Additionally, within both high and low sodium conditions, all agonist competition curves displayed a Hill slope between 0.6 – 1.4 consistent with single site binding, suggesting there was no detectable influence of the mixed populations of receptors in high / low affinity conformations (which would display as a two-site model)(Student's t-test comparing hillslope deviation from -1, low sodium: p = 0.51, high sodium: p = 0.65).

Additionally, the effect of solely Gpp(NH)p addition on measured agonist affinity was explored. In assessing the competition between Fl-propranolol and unlabelled isoprenaline for the  $\beta_2$ -AR, addition of 100  $\mu$ M Gpp(NH)p in low sodium buffer had a small, statistically significant, effect in reducing the affinity of isoprenaline, but to a lesser extent than in combination with heightened sodium (pKi isoprenaline =  $6.50 \pm 0.15$ , pKi isoprenaline + Gpp(NH)p =  $6.11 \pm 0.06$ , p=0.04, df=3 [Student's t-test], n=4, data shown later in Figure 4.8).

4.5.2. *Measuring the allosteric effects of G $\alpha_s$  C-terminus peptides on ligand binding at the  $\beta_2$ -Adrenoceptor.*

The allosteric effects of G $\alpha$  C-terminus peptides were assessed through TR-FRET competition binding studies. To compare the effects of different extents of the G $\alpha$   $\alpha 5$  helix coverage, peptides comprised either the final 11 (G $\alpha s 11$ ), 24 (G $\alpha s 24$ ) or 19 (G $\alpha s 19 cha 18$ ) amino acids of the G $\alpha s \alpha 5$  helix. G $\alpha s 19 cha 18$  also incorporated a cyclohexylalanine (cha) substitution of leucine 18 reported to increase peptide affinity for the  $\beta_2$ -AR receptor (see section 1.4)(Mannes et al., 2021).

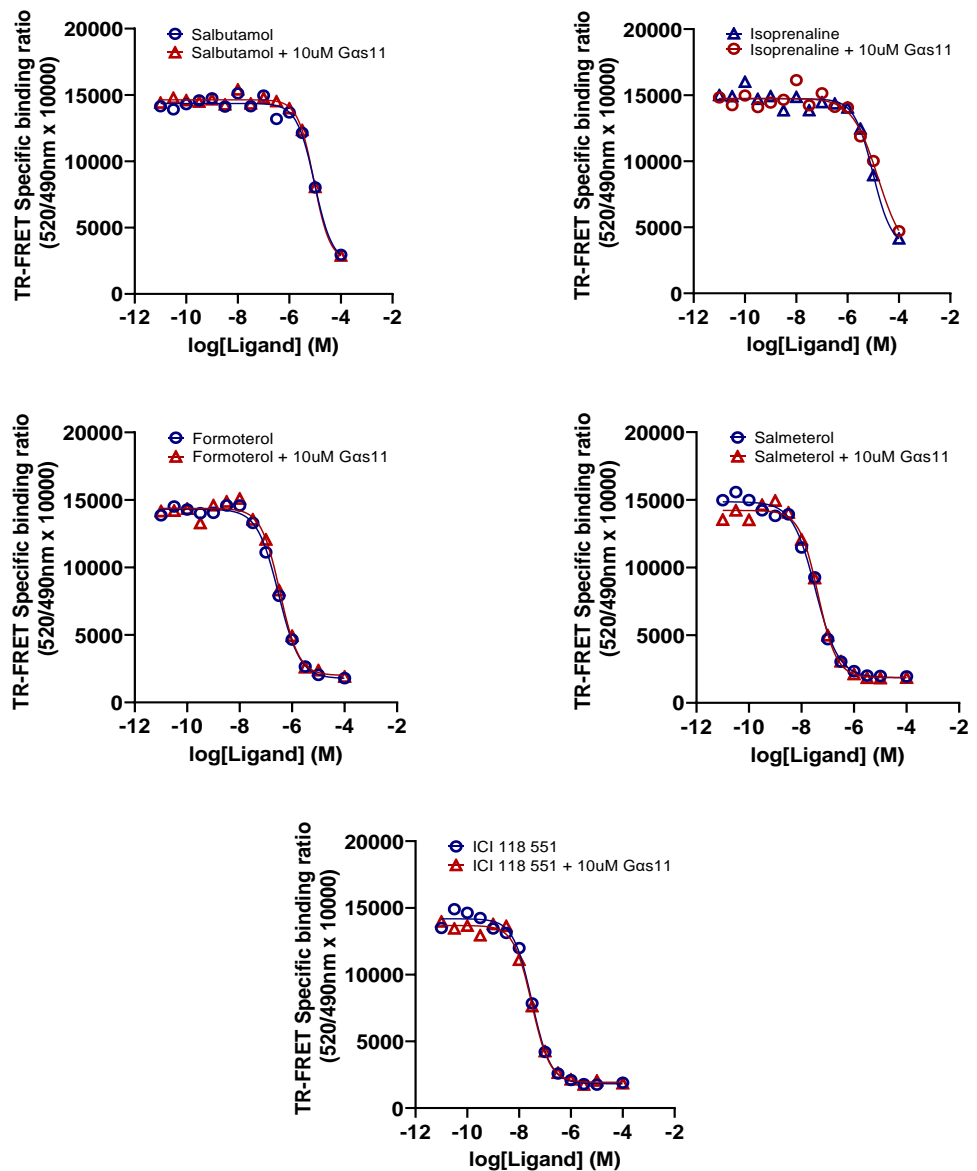


**Figure 4.5. The effect of Gas11 on competition between 20nM Fl-propranolol and  $\beta_2$ -adrenoceptor agonists for  $\beta_2$ -AR binding in HEK  $\beta_2$ -AR membranes in High Sodium conditions.** Data in duplicate as mean  $\pm$  s.e.m from a representative of five experiments. Non-specific binding was in all cases determined through inclusion of 10 $\mu$ M ICI118551 and deducted from plotted data to determine specific binding. All assays run at 37°C for 2 hours.

In initial studies run in Gpp(NH)p containing high sodium buffer (Figure 4.5), the G $\alpha$ s11 peptide had no effect on agonist or ICI118551 IC<sub>50</sub>s. Furthermore, in comparison studies using low sodium buffer, 10 $\mu$ M G $\alpha$ s11 peptide remained insufficient to increase agonist affinity (Table 4.2, Figure 4.6) or produce a significant change in Hill slope across all agonists, with all agonists displaying comparable K<sub>i</sub> values to previously characterised inhibitory constants (Table 4.1)(Baker, 2010, 2005). This shows that even under conditions predicted to promote the high affinity state, G $\alpha$ s11 is unable to produce sufficient positive modulation of agonist binding. In addition, no effect of G $\alpha$ s11 on F-propranolol binding was observed as the total specific binding HTRF ratio was similar +/- G $\alpha$ s11 under the buffer conditions tested (Figure 4.5, 4.6).

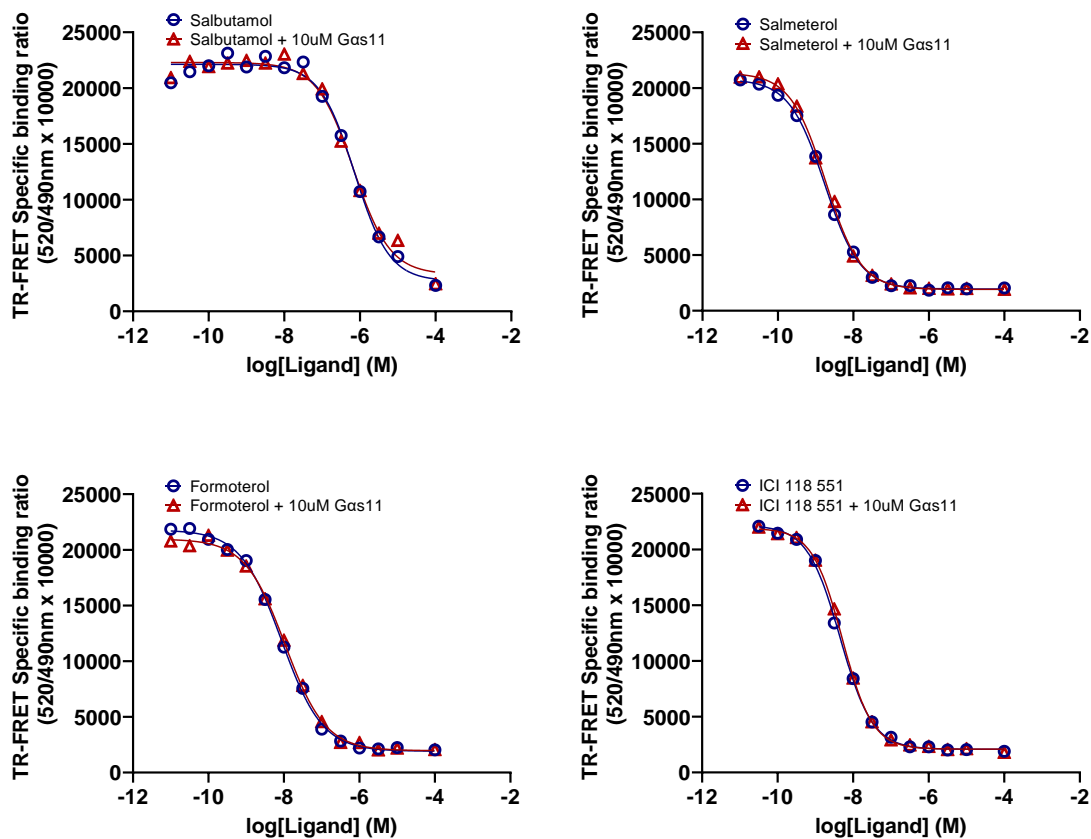


**Figure 4.6. The effect of Gas11 on competition between 20nM Fl-propranolol and  $\beta_2$ - adrenoceptor agonists in Low Sodium conditions.**

Data in duplicate as mean  $\pm$  s.e.m from a representative of five experiments.

Non-specific binding was in all cases determined through inclusion of 10 $\mu$ M ICI118551 and deducted from plotted data to determine specific binding. All assays run at 37°C for 2 hours.

**Table 4.1.** Literature values of  $\beta_2$ -AR orthosteric ligands

Compounds	Literature(Baker, 2010, 2005)	Low Na assay data
	pK <sub>i</sub> or pK <sub>D</sub>	pK <sub>i</sub> ±s.e.m
Salbutamol	6.01	5.92 ±0.18
Isoprenaline	6.40	6.18 ± 0.18
Salmeterol	8.83	8.74 ±0.21
Formoterol	8.63	8.05 ±0.18
<i>ICI 118 551</i>	9.26	8.56 ±0.12

**Table 4.2:** Summary of binding parameters of  $\beta_2$ -adrenoceptor ligands derived from TR-FRET based competition assays, comparing high / low Na buffers and the effect of *Gas11*.

Compounds	High Na + Gpp(NH)p	Low Na
	pK <sub>i</sub> ±s.e.m	pK <sub>i</sub> ±s.e.m
Salbutamol	5.15 ±0.24	5.92 ±0.18
<i>Salbutamol + Gas11</i>	5.64 ±0.08	5.78 ±0.22
Isoprenaline	5.43 ±0.07	
<i>Isoprenaline + Gas11</i>	5.41 ±0.09	
Salmeterol	7.99 ±0.07	8.74 ±0.21*
<i>Salmeterol + Gas11</i>	7.93 ±0.10	8.73 ±0.19*
Formoterol	6.97 ±0.08	8.05 ±0.18*
<i>Formoterol + Gas11</i>	6.92 ±0.07	7.95 ±0.18*
<i>ICI 118 551</i>	7.90 ±0.02	8.56 ±0.12*
<i>ICI 118 551 + Gas11</i>	7.90 ±0.03	8.53 ±0.12*

Data are presented as mean ± s.e.m from 5 different experiments.

Test for significance using log(K<sub>i</sub>) data: \* P < 0.05 high versus low sodium buffer, Student's unpaired t test

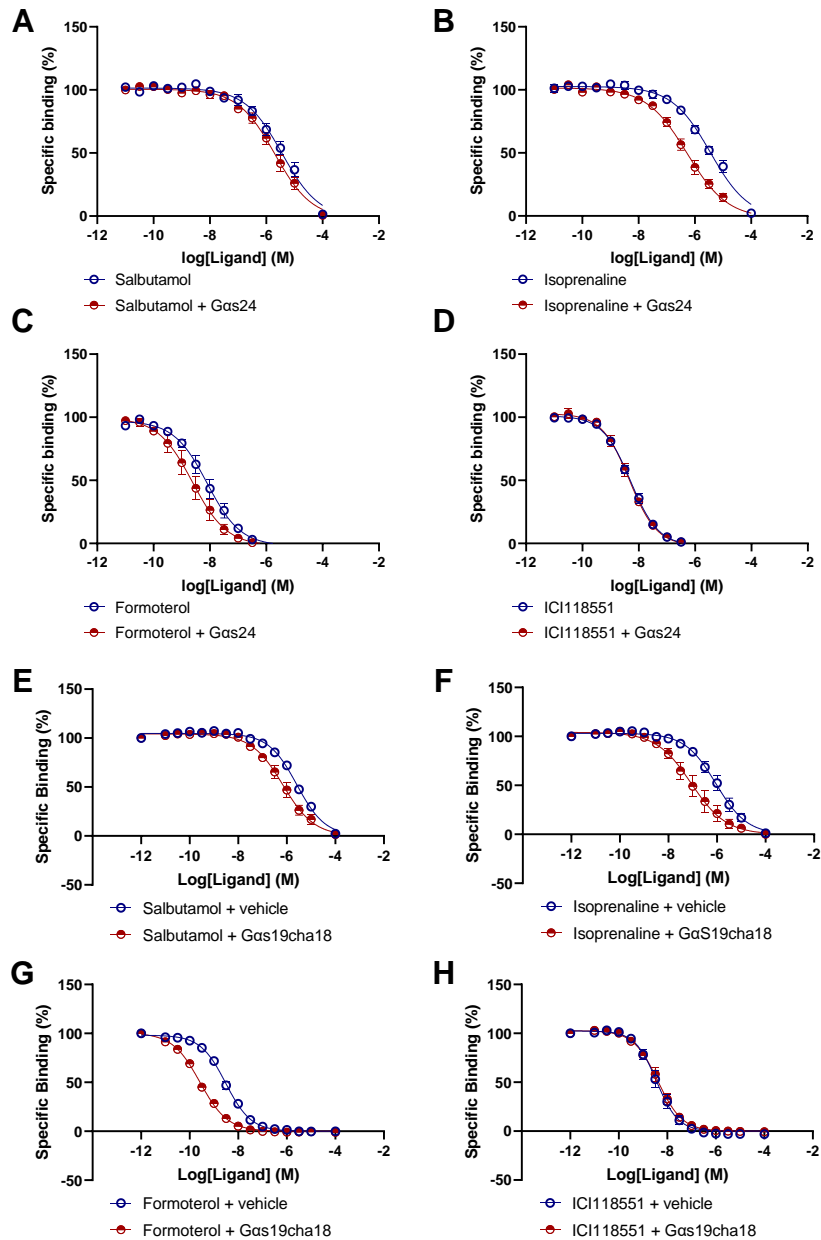


**Figure 4.7. Competition between 20nM Fl-propranolol and  $\beta_2$ -adrenoceptor agonists incorporating Gas24 (A-D) or Gas19cha18 (E-H), in Low Sodium conditions.** Data is pooled normalized data from five experiments normalized to maximum and minimum Fl-propranolol binding, plotted as mean  $\pm$  s.e.m. Non-specific binding was in all cases determined through inclusion of 10 $\mu$ M ICI118551 and deducted from plotted data to determine specific binding. All assays run at 37°C for 2 hours.

**Table 4.3:** Binding affinities (pK<sub>i</sub>) of β<sub>2</sub>-adrenoceptor ligands in the absence and presence of 10μM Gas C terminal peptides in low sodium conditions

Ligand	Gas24			Gas19cha18		
	Vehicle	10 μM peptide	Fold change	Vehicle	10 μM peptide	Fold change
<b>Isoprenaline</b>	5.81 ± 0.17	6.54 ± 0.19*	5.4	6.18 ± 0.18	6.93 ± 0.30**	5.60
<b>Formoterol</b>	8.30 ± 0.18	8.92 ± 0.18***	4.2	8.85 ± 0.07	9.90 ± 0.08***	11.2
<b>Salbutamol</b>	5.64 ± 0.12	5.78 ± 0.22	1.4	5.89 ± 0.07	6.36 ± 0.17**	3.00
<b>ICI118551</b>	8.62 ± 0.12	8.60 ± 0.12	1.0	8.70 ± 0.14	8.67 ± 0.13	0.90

pK<sub>i</sub> data are presented as mean ± s.e.m and are from 5 different experiments per peptide, with paired vehicle controls for each peptide. Significant differences between control and peptide assay conditions are indicated by \* P<0.05, \*\* P<0.01, \*\*\* P<0.001 (paired Student's t-test).

In contrast, 10 $\mu$ M Gas24 and 10 $\mu$ M Gas19cha18 each promoted a significant increase in measured affinity for three example orthosteric agonists (Figure 4.7; Table 4.3). The extent of the shift in affinity was highest for the high efficacy agonists isoprenaline and formoterol and reduced for the lower efficacy agonist salbutamol. However, Gas24 and Gas19cha18 had no significant effect on the affinity of the representative antagonist IC1118551. Similarly to Gas11 assays, these peptides had no effect on Fl-propranolol binding, displaying similar HTRF ratios +/- Gas peptide and having no effect on Fl-propranolol affinity.

Interestingly, within this experimental set both G peptide inclusive and control agonist curves showed a shallower Hill slope compared to high sodium conditions, especially in the case of salbutamol and isoprenaline, with slopes between -0.50 and -0.58, compared to high sodium condition range (-0.8 to -1; Figure 4.5), suggesting a greater proportion of receptors in the high-affinity state. As such, the addition of a G protein mimetic peptide is hypothesised to cause a shift within the assay to produce a greater number of receptors in the high-affinity conformation, displayed as a change in Hill slope closer to -1, however, in both cases Hill slopes did not change significantly across all tested agonists (paired t-test,  $p \geq 0.05$ ) with the inclusion of the peptide.

The effect of Gpp(NH)p was explored in more detail for the isoprenaline curves +/- Gas19cha18, as shown in Figure 4.8. These paired experiments were all performed in low sodium buffer. Compared to isoprenaline control, the addition of 100  $\mu$ M Gpp(NH)p was associated with a modest reduction in isoprenaline affinity. However, 10  $\mu$ M Gas19cha18 produced a similar increase in observed isoprenaline affinity, whether or not Gpp(NH)p was present.

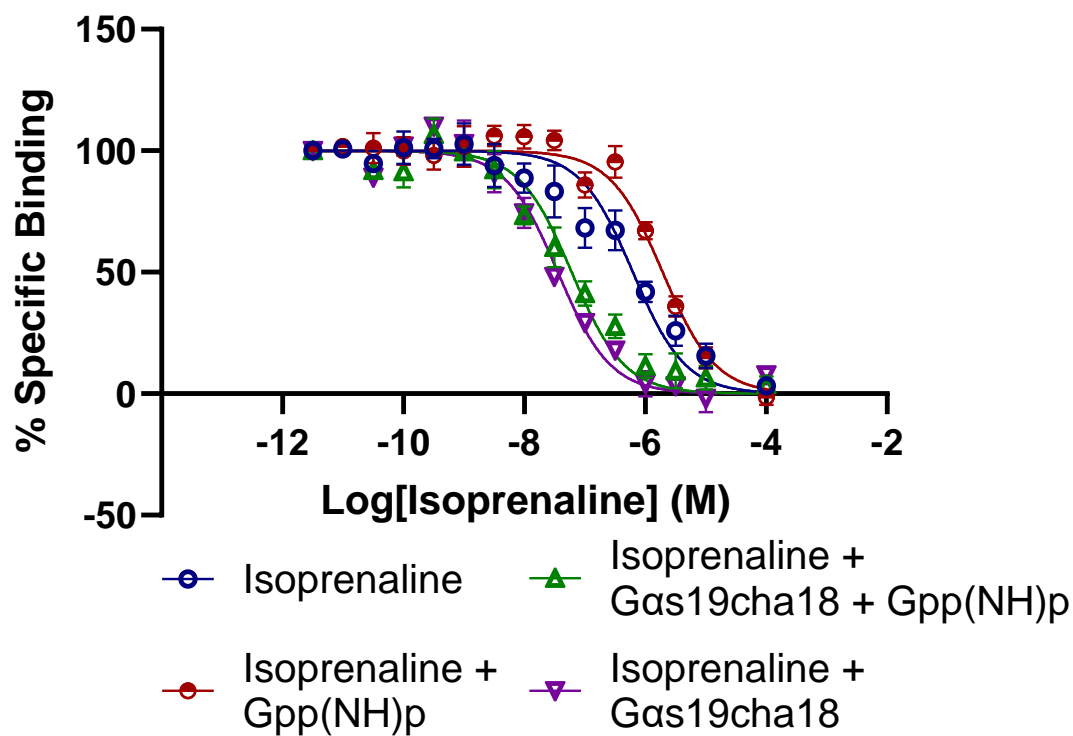


**Figure 4.8.** The effect of 10  $\mu\text{M}$  Gas19cha18 on competition binding between 20nM Fl-propranolol and isoprenaline in HEK ss $\beta_2$ -AR membranes, in the absence and presence of 100 $\mu\text{M}$  non-hydrolysable GTP analogue Gpp(NH)p in low sodium assay buffer (60 min timepoint) Data are pooled and normalized from three independent experiments, plotted as mean  $\pm$  s.e.m.

Finally, selectivity assays were performed for a paired comparison of the effects of *Gas11* against *Gas24*, and *Gas24* against 24aa *Gai* peptides (*Gai24*) at the  $\beta_2$ -adrenoceptor under low sodium conditions (Figure 4.9&4.10). Incubation with 10 $\mu$ M *Gai24* had no effect on agonist affinity compared to negative controls, whereas incubation with *Gas24* displayed similar shifts in agonist affinity to those previously observed. Similarly, running side-by-side comparison with differing *Gas* peptides showed no effect upon incubation with 10 $\mu$ M *Gas11* but a similar shift in affinity with incorporation of longer peptide.

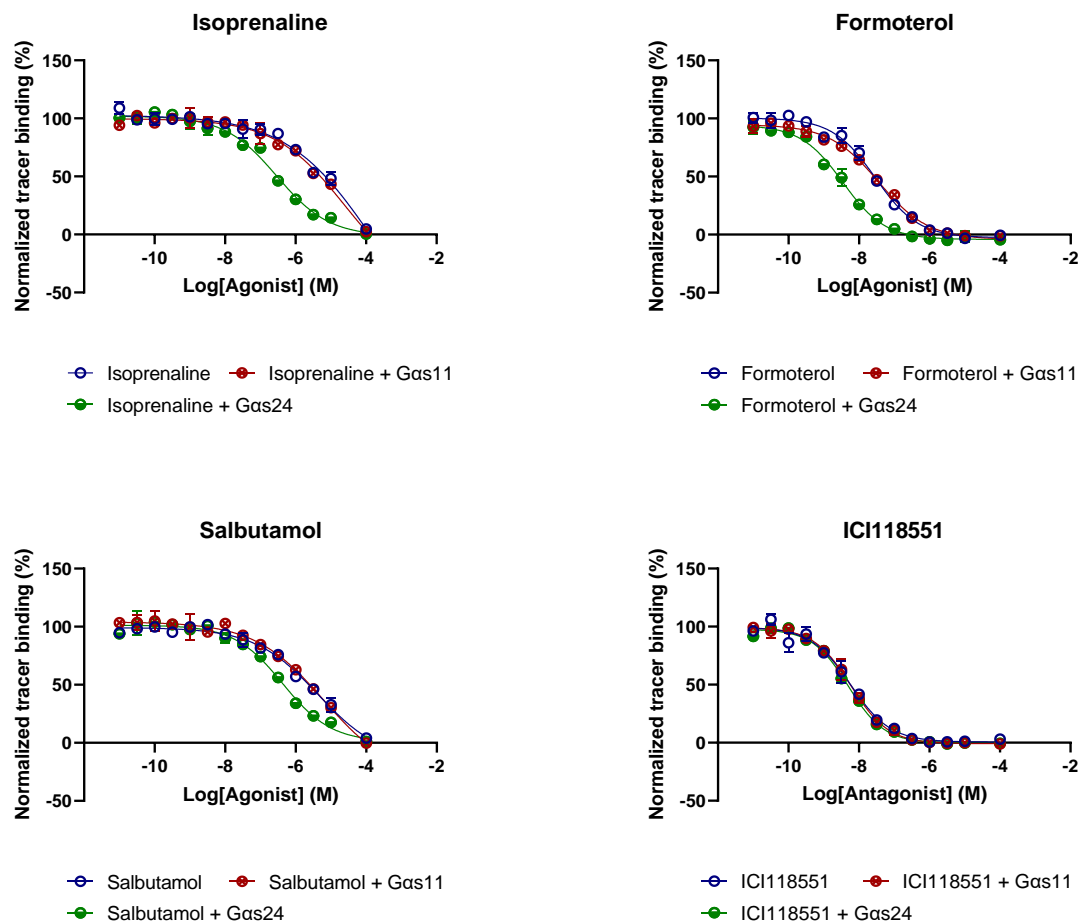


**Figure 4.9. Competition analysis of  $\beta_2$ -adrenoceptor agonists in HEK ss $\beta_2$ -AR membranes, comparing the effects of incubation with 10 $\mu$ M Gas11 or Gas24 peptides.** Normalized data were expressed as % Fl-propranolol binding in the absence of competing ligand. Non-specific binding was in all cases determined through inclusion of 10 $\mu$ M ICI118551. Assays were performed at 37°C for 2 hours using 20nM Fl-propranolol tracer, in low sodium buffer. Data are pooled from 2 independent experiments, plotted as mean  $\pm$  s.e.m.

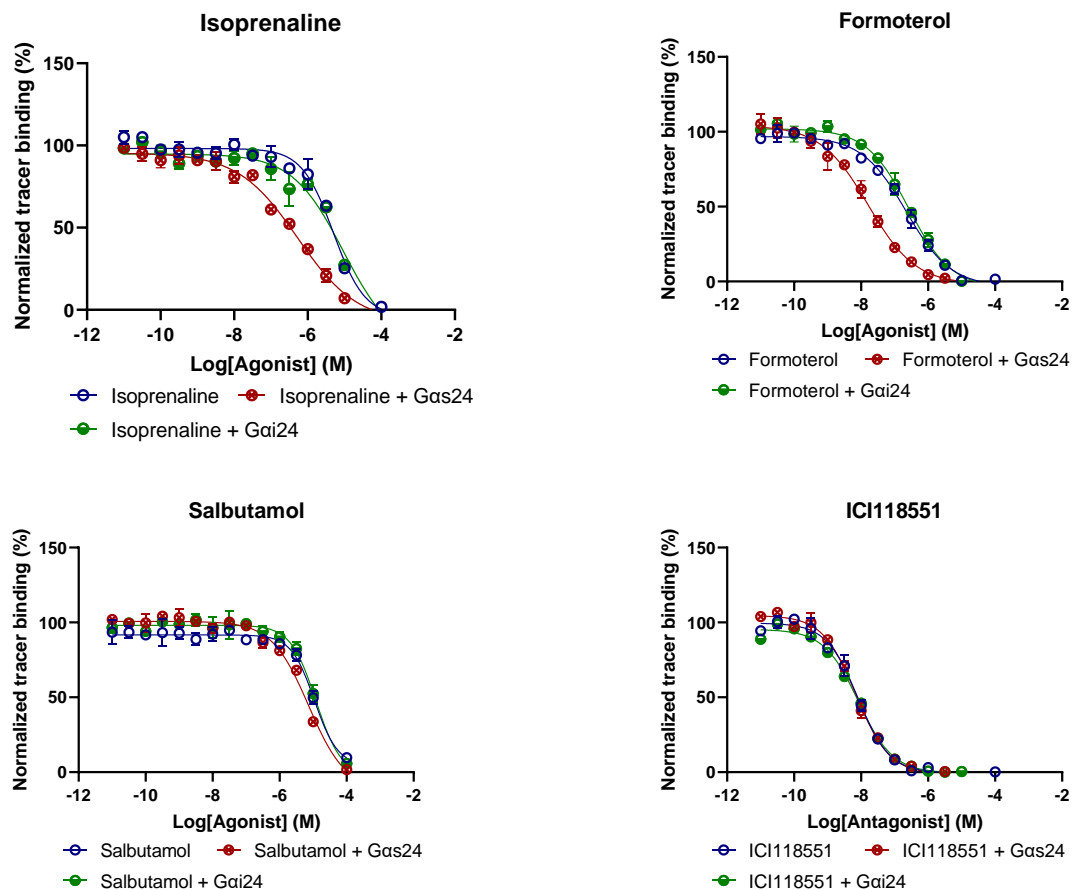


**Figure 4.10. Competition analysis of  $\beta_2$ -adrenoceptor agonists post incubation with 10 $\mu$ M Gas24 or Gai24 peptides.** Normalized data were expressed as % F1-propranolol binding in the absence of competing ligand. Non-specific binding was in all cases determined through inclusion of 10 $\mu$ M ICI118551 and defines 0% tracer binding. Assays were performed at 37°C for 2 hours using 20nM F1-propranolol tracer, in low sodium buffer. Data are pooled from 2 independent experiments, plotted as mean  $\pm$  s.e.m.

Taken together these data supported the binding of Gas24 and Gas19cha18 to the  $\beta_2$ -AR, and their allosteric stabilisation of the active conformation selectively promoting high agonist affinity, as previously observed in radioligand binding assays by Mannes et al (2021)(Mannes et al., 2021).

#### 4.5.3. *Characterisation of Gi derived peptide allosteric actions on NPY Y1 receptor ligand binding.*

The ternary GPCR complex promoting high affinity agonist binding in the presence of effector G proteins is a feature of GPCRs coupled to all G protein classes(De Lean et al., 1980; García-Nafriá et al., 2018; Samama et al., 1993; Wan et al., 2018; Warne et al., 2019). In order to explore whether allosteric actions extended beyond G $\alpha$ s-based peptides, the G $\alpha$ i coupled NPY Y1 receptor was chosen as a system to investigate the actions of G $\alpha$ i peptides on ligand binding.

A TR-FRET assay was first established using the fluorescent antagonist peptide probe BIDA84 ([Lys(2)(sCy5), Arg(4)]BVD-15) previously characterised by Liu et al., 2016. Using buffer either containing or lacking 2.5mM CaCl<sub>2</sub>, the affinity of BIDA84 to Y1 membranes was determined by analysis of endpoint saturation data measuring increasing concentrations of BIDA84 binding at the orthosteric binding site. The addition of CaCl<sub>2</sub> to the buffer had no significant effect on the binding affinity of BIDA84 (-CaCl<sub>2</sub>, K<sub>D</sub>: 5.4nM  $\pm$  1.8, +CaCl<sub>2</sub>, K<sub>D</sub>: 14.5nM  $\pm$  8.3, p= 0.08, n=4, Figure 4.11A&B).

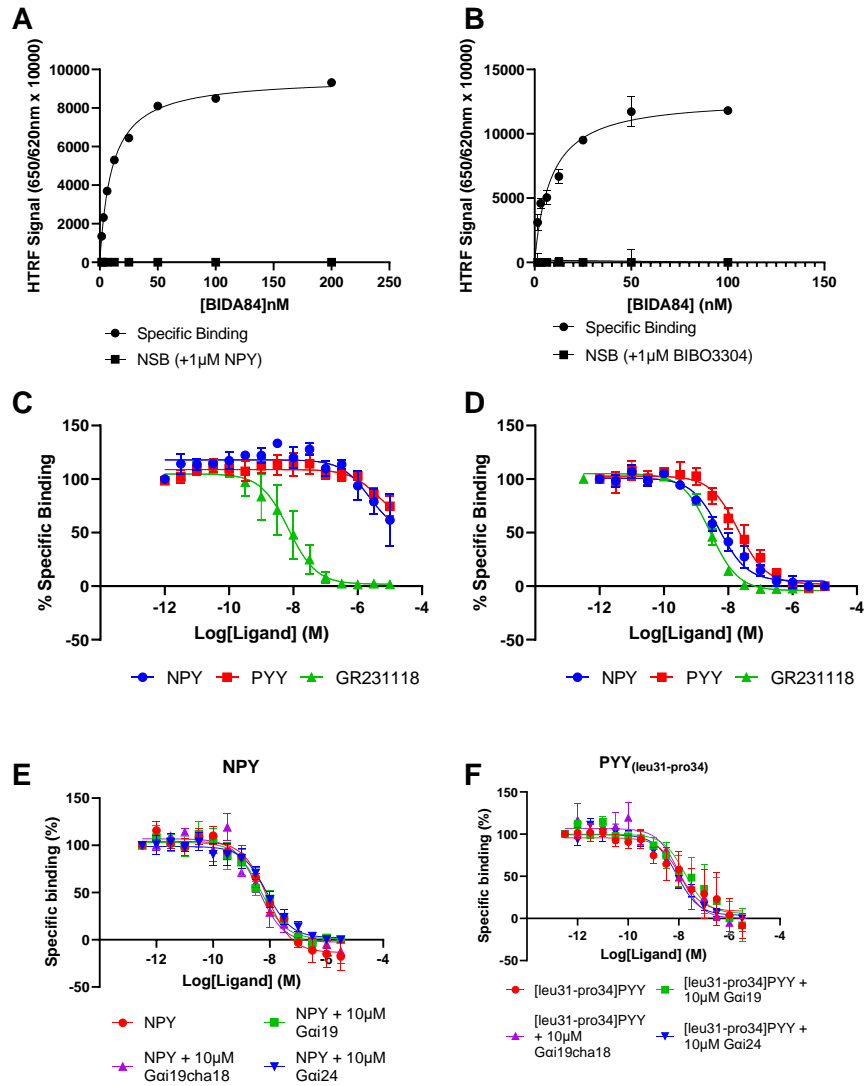


**Figure 4.11. Characterisation of TR-FRET binding assays in Y1 receptor membranes and the effects of Gai derived peptides.** A) Saturation binding of BIDA84 in a  $\text{Ca}^{2+}$  free environment, data are an example from 4 independent experiments. B) Binding of BIDA84 in a  $2.5 \text{ mM Ca}^{2+}$  environment C) Competition binding between BIDA84 and control ligands in a  $\text{Ca}^{2+}$  free environment. D) Competition binding between BIDA84 and control ligands in a High  $\text{Ca}^{2+}$  environment. E-F) Competition analysis for peptide agonists in absence and presence of different  $10 \mu\text{M}$  Gai derived peptides in high  $\text{Ca}^{2+}$  conditions. Data are pooled, normalized data from 3-5 independent experiments incubated for 2-hours at  $37^\circ\text{C}$ , plotted as mean  $\pm$  s.e.m.

The affinities of NPY, PYY, [leu31,pro34]PYY, PYY3-36 and the peptide antagonist GR231118 were determined by competition with BIDA84 fluorescent ligand and subsequent conversion of resulting  $IC_{50}$ s to  $pK_i$  values using the Cheng and Prusoff correction.

Optimisation assays measuring binding affinity of NPY and PYY were run in both assay buffers as previously described, allowing characterisation of the role of  $Ca^{2+}$  in promoting agonist binding. The inclusion of calcium caused a 100-fold increase in the affinity of both NPY and PYY, bringing their relative affinities in line with previous reports (Gehlert et al., 1997; Krause et al., 1992) (NPY: - $CaCl_2$ ,  $pK_i = 6.30 \pm 0.2$ , + $CaCl_2$ ,  $pK_i = 8.64 \pm 0.15$ , PYY: - $CaCl_2$ ,  $pK_i = 6.02 \pm 0.07$ , + $CaCl_2$ ,  $pK_i = 8.09 \pm 0.25$ ). However, the presence of buffer calcium had little effect on GR231118 affinity (Figure 4.11C&D; - $CaCl_2$ ,  $pK_i = 9.14 \pm 0.34$ , + $CaCl_2$ ,  $pK_i = 8.92 \pm 0.13$ ,  $n=4$ ).

Having validated the use of BIDA84 TR-FRET competition binding to determine agonist affinity,  $G_{\alpha i}$  derived peptides were incorporated into assays employing a  $Ca^{2+}$  rich buffer. However, in contrast to  $G_s$  findings, the presence of 10  $\mu M$   $G_{\alpha i24}$ ,  $G_{\alpha i19}$  or  $G_{\alpha i19cha18}$  did not significantly change NPY or [Leu31, Pro34]PYY binding affinity, as assessed by similar binding  $IC_{50}$  values in the absence and presence of each peptide (Figure 4.11E&F).

#### 4.6. Discussion

The aim of this chapter was to determine whether different  $G_{\alpha C}$  terminal peptides, mimicking the  $\alpha 5$  helix, were able to affect the affinity of orthosteric ligands at candidate  $G_s$  ( $\beta_2$ -AR) and  $G_i$  (Y1) coupled receptors. For each receptor, membrane-based TR-FRET binding assays were established using fluorescent antagonist probes, which allowed estimation of unlabelled agonist and antagonist affinities in the absence and presence of  $G_{\alpha C}$  peptide. For the  $\beta_2$ -AR, longer  $G_s$  derived C terminal peptides (but not  $G_i$ )

were demonstrated to enhance agonist affinities selectively, demonstrating an allosteric action. However equivalent Gi peptides did not directly alter Y1 agonist binding. This study provided the groundwork for the selection of the most active G $\alpha$  C terminal peptides as fluorescent affinity probes for investigation in later chapters.

#### *4.6.1. Initial validation of employing TR-FRET techniques for measuring ligand binding*

In both cases, initial TR-FRET assays were successfully established as a system for the derivation of ligand binding at target receptors  $\beta_2$ -AR and Y1. For  $\beta_2$ -AR assays, employment of the fluorescent antagonist BODIPY-FL-Propranolol facilitated measurement of orthosteric ligand affinities via TR-FRET. However, the measured affinity of an agonist can be influenced by the experimental environment. In particular, receptor conformation can have a profound impact on agonist affinity, as implicated by the ternary-complex model (see section 1.2.5), causing experimental variation as a result of the proportions of high (G protein coupled) vs low (G protein uncoupled) affinity receptor populations. In the case of the  $\beta_2$ -AR, the proportion of high/low affinity populations can be influenced by the addition of sodium ions within assay buffer (negative allosteric modulator of class A GPCRs) and destabilisation of the receptor-Gs complex by non-hydrolysable GTP analogues (e.g., Gpp(NH)p) (Agasid et al., 2021; Katritch et al., 2014; Selent et al., 2010; Sykes et al., 2019). Subsequently, application of high sodium conditions in the presence of Gpp(NH)p allowed derivation of affinity values in line with literature measurements, derived using alternative techniques including radioligand binding (Baker, 2010, 2005). Removal of these low affinity promoting factors was hypothesised to increase agonist affinity. Employment of low sodium conditions resulted in an

increase in control formoterol and salmeterol affinities, indicative of increased high affinity binding, with no change in Fl-propranolol affinity. The degree of affinity enhancement from high to low sodium environments correlated with the reported efficacy (formoterol > salbutamol > salmeterol) since high efficacy activation is linked to higher affinity for coupled active versus uncoupled inactive receptors(Kent et al., 1980). Interestingly, a slight increase in ICI118551 affinity was observed in the low sodium environment, an unexpected characteristic for an antagonist. However, with no change in antagonist tracer binding this may be an artifact of ICI118551's binding mode compared to other antagonists, given its reliance on ionic interactions within the binding pocket(Wacker et al., 2010). Furthermore, the inclusion of Gpp(NH)p to this low sodium environment allowed characterisation of the positive allosteric effect of native G protein coupling on agonist affinity. By employing Gpp(NH)p to remove the native G protein, a reduction in agonist affinity is observed, indicating a change in receptor conformation to the low-affinity state.

Similarly, employment of the fluorescent peptide probe BIDA84 facilitated use of TR-FRET at the Y1 receptor for the first time. Initial binding experiments allowed for derivation of BIDA84's binding affinity in line with previous findings employing direct imaging approaches(Liu et al., 2016). Further application of BIDA84 facilitated derivation of orthosteric ligand affinities similar to those described within radioligand binding assays(Gehlert et al., 1997; Krause et al., 1992). These assays also provided the means to explore the effects of environmental calcium levels on ligand binding at the Y1 receptor. Previous reports have indicated calcium ions facilitate high affinity binding at the Y1 orthosteric binding site(Keller et al., 2015). Removal of calcium from the assay buffer resulted in a reduction in agonist affinity, highlights its important role in Y1 function.

#### 4.6.2. Using TR-FRET binding to determine the allosteric effects of G protein mimetic peptides.

Having validated the ability of TR-FRET binding studied to accurately derive orthosteric agonist affinity at the  $\beta_2$ -AR and Y1 receptors, this was used to probe the allosteric effects of G protein mimetic peptides. The allosteric effects of G $\alpha$  C-terminal peptides were first characterised at the  $\beta_2$ -AR through measurement of the affinity of multiple agonists, and the antagonist ICI118551, determined through competition with Fl-propranolol under high and low sodium conditions. G $\alpha$ s19cha18 and G $\alpha$ s24, but not G $\alpha$ s11 or G $\alpha$ i24, enhanced agonist affinity (but not antagonist ICI118551) binding at the  $\beta_2$ -adrenoceptor. The largest shift observed (all peptides were used at highest available concentration, 10  $\mu$ M) was with the inclusion of G $\alpha$ s19cha18, causing a 11.2-fold increase in formoterol affinity. The inability of these peptides to alter ICI118551 affinity is in line with the hypothesis that these peptides are promoting conformational change towards the high-affinity state, thereby influencing agonist binding but not antagonist binding due to antagonists having no conformational preference for the high-affinity conformation. Additionally, reintroduction of Gpp(NH)p within these assays (maintaining a low sodium environment) further highlights the overall sensitivity of the assay for receptor conformation. Addition of Gpp(NH)p resulted in the reduction in isoprenaline control affinity (by removing the coupling of native G protein within the system) but had no effect on the modulatory effect of G $\alpha$ s19cha18. This indicates G $\alpha$ s19cha18 is able to stabilise the high affinity state independently of the native G protein's stabilizing effect and does not simply substitute for the native G protein.

The observed structure activity relationship, displaying increased activity with longer peptide length, is consistent with G peptide binding data produced by Mannes *et al* and may highlight a key role of the alpha helical secondary structure(Mannes et al., 2021).

The increase in length (from Gs11 – to Gs24) provides greater structural integrity of the peptides within the assay. Previous findings suggest that shorter peptides (around 10 amino acids) do not display any significant secondary structure when in an aqueous experimental environment (Koehl et al., 2018; Mant et al., 2007). This is in line with presented findings showing Gas11 had no effect on agonist affinity. This suggests that, as the elongation allows for an additional number of rotations and subsequently a greater number of hydrogen bonds, the native  $\alpha$ -helical structure is better maintained. This therefore allows the peptides to maintain a greater structural homology to the native G $\alpha$ 5 helix, putatively increasing their affinity for the intracellular binding site. Similarly, as displayed previously by Mannes *et al*, the increased efficacy of Gas19cha18 is believed to be due both to the additional length, and the subsequent stability this provides, and due to the substituted cyclohexylalanine residue providing a greater hydrophobic interaction between peptide and receptor than the corresponding leucine thereby increasing the affinity for the G protein binding site. Further characterisation and comparison against the G $\alpha$ i24 peptide indicated the allosteric effect displayed by the Gas24 peptide was a selective process, with incubation with G $\alpha$ i24 peptides having no effect on agonist affinity. This highlights that variation in amino acid sequence seen within the final C-terminal region of alpha subunits (see section 3.4) is sufficient to provide selective G protein coupling, indicating that selective peptide binding can be achieved with only a small fragment of the C-terminal region (Gilchrist et al., 1998; Rasenick et al., 1994).

These findings paved the way for the exploration of G $\alpha$ <sub>i</sub> derived peptides, employing the Y1 receptor as a representative Gi coupled class A GPCR. With accurate measurement of BIDA84 affinity and defined competition curves of control agonists, able to accurately determine their respective affinities, peptides G $\alpha$ i24, G $\alpha$ i19 and G $\alpha$ i19cha18 were employed as initial modulators. G $\alpha$ i19cha18 was

designed as a putative higher affinity ligand due to the conservation of the substituted leucine residue at the -2 position between the  $G\alpha_s$  and  $G\alpha_i$   $\alpha$ 5-helix sequences and the comparable, hydrophobic, nature of G protein binding sites between  $G_s$  and  $G_i$  coupled receptors (Figure 4.12)

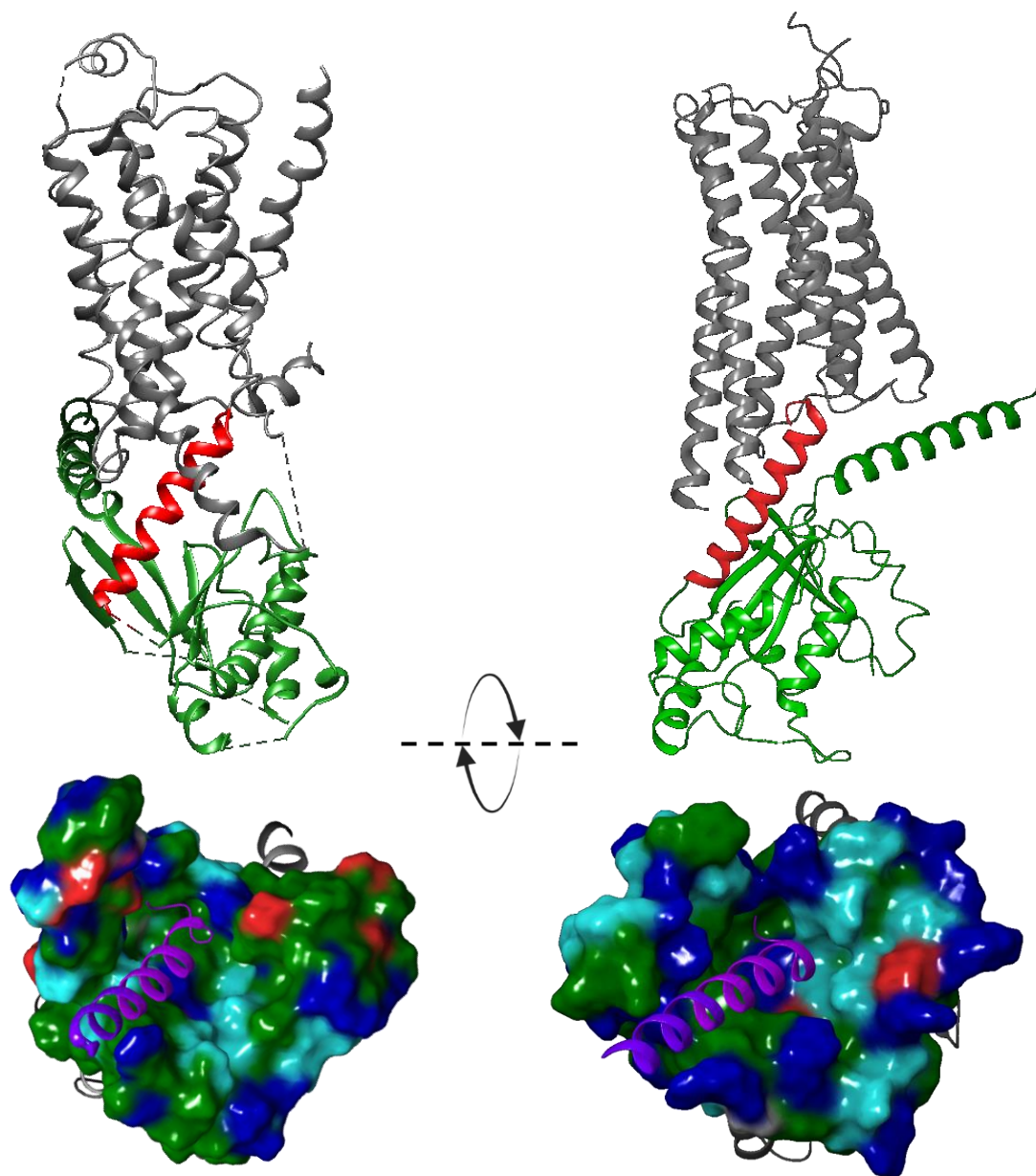


**Figure 4.12. Structural representation of G protein  $\alpha 5$  helix binding to  $\beta 2$ -AR (left, PDB:7DHR) and Y1 (right, PDB:7VGX).** (Top)  $G\alpha$  subunit (green),  $\alpha 5$  Helix (red), receptor (grey). (Bottom)  $\alpha 5$  helix (purple), positive charge side chain (Royal blue), Negative charge side chain (Red), Polar residue (Light blue), Hydrophilic sidechain (Green). Models were generated from PDB files (Park et al., 2022; F. Yang et al., 2021) using Maestro (Schrodinger, Reading, UK)

This conservation, along with recent structural studies and previous Gs peptide data, suggests this modification provides a greater hydrophobic interaction between the  $\alpha 5$  helix and GPCR, as has been previously reported (Mannes et al., 2021; Yang et al., 2018). However, Gai24, Gai19 and Gai19cha18 all displayed an inability to modulate agonist peptide affinity, with peptide + and peptide - agonist curves displaying similar  $IC_{50}$  values. It is hypothesised that if these peptides preferentially couple to the active receptor state with greater affinity, they will subsequently promote the high-affinity state as seen in Gs receptor studies, increasing agonist affinity. However, there is some evidence to suggest that this is not always evident within experimental systems, especially when employing G protein mimetic peptides (Gilchrist et al., 1998). This suggests these findings may not represent a lack of peptide binding, just a lack of allosteric efficacy. Findings by Gilchrist *et al* in 1998 identified the use of 11 amino acid  $G\alpha_i$  peptides as competitive inhibitors of Adenosine receptor 1 - G protein binding, but also indicated that peptide binding inhibited radiolabelled orthosteric agonist binding (Gilchrist et al., 1998). This is in contrast to what would be expected upon stabilisation of the high-affinity state as indicated previously (Mannes et al., 2021).

It is also worth noting that in these assays direct binding of the  $G\alpha$  C terminal peptide is not being measured and any action is only indirectly revealed by the allosteric influence on agonist binding. It is possible that, as previously suggested (Gilchrist et al., 2002, 2001, 1998), shorter peptides, or  $G_i$  peptides are capable of binding receptors and competing with native G protein. However, they are unable to promote the receptor high-affinity conformation to a significant degree as to alter global agonist affinity and subsequent binding measurements (Gilchrist et al., 2002; Mannes et al., 2021). This is explored further in later chapters.

Similarly, more recent molecular dynamic simulations and employment of Systematic Protein Affinity Strength Modulation

(SPASM)  $G\alpha$  peptide linked sensors have alluded to the variability in binding mechanisms between the types of G protein. Findings by Sandhu *et al* identified that binding of the same G protein can vary significantly from receptor to receptor (see chapter 6), however, their main focus lay in calculation of the various insertion angles used by the respective  $G\alpha$  helices for binding to active state receptors(Sandhu et al., 2019). Their proposed models indicate that the angle, combined with the amino acids make up, is a key driver in G protein selectivity. In relation to  $G_i$  binding and the lack of receptor conformational change seen in these assays, their findings indicate that  $G\alpha_i$  inserts at a much shallower angle than the respective  $G_s$  and  $G_q$  models presented, thus displaying reduced receptor entry. This reduction in sterical interaction may result in  $G\alpha_i$  displaying a weaker interaction with its respective receptors, and the corresponding C terminal peptides may then have a reduced allosteric action as is indicated here. Without additional methodologies for detecting peptide binding directly, the role of  $G\alpha$  C-terminal peptides for  $G\alpha_i$  coupled peptides remains elusive. Hence the objective in the following chapters was to establish whether  $G_s$  and  $G_i$  C terminal peptide sequences could be used as the basis for the generation of fluorescent probes, and enable direct binding assays at the G protein interaction site to be performed.

## **Chapter 5. Chemistry**

A click-chemistry approach facilitating peptide-fluorophore coupling for the generation of fluorescent G $\alpha$  C-terminus peptides.

## 5. A click-chemistry approach facilitating peptide-fluorophore coupling for the generation of fluorescent Gα C-terminus peptides.

### 5.1. Introduction

The growing appreciation for fluorescence technology has driven an increase in experimental diversification within both biological and molecular chemistry settings. The need for single target selective tracer ligands for biological application has led to the need for more structurally complex fluorescent ligands. Especially in the context of peptide/protein-based biosensors, this requires more classical chemical synthesis approaches to be tailored to accommodate the great number of reactive groups present in such amino acid sequences. The application of “click-chemistry” allows for the addition of fluorophores to larger, more complex, molecules without the need for large scale functional group protection and deprotection steps (introduced in 5.1.1)(Kolb et al., 2001). In this chapter, the ability to generate fluorescent Gα C-terminus peptides employing solution-based click-chemistry is explored.

#### 5.1.1. *Click chemistry and the advancement of fluorescent ligand technology and development.*

Click-chemistry was originally described by K. B. Sharpless in 2001, for which he was awarded the Nobel Prize in Chemistry in 2022, to describe reactions that give high yields, create only by-products that can be removed without chromatography, are stereospecific, simple to perform, and can be conducted in easily removable or benign solvents(Rostovtsev et al., 2002; Tornøe et al., 2002). The original expression of a Click reaction utilized alkyne/azide cycloaddition, made feasible by the employment of a copper catalyst, and was termed “Copper(I)-catalysed Azide-Alkyne Cycloaddition” (CuAAC, Figure 5.1). The use of copper catalysis greatly reduces the overall time relative to the

corresponding uncatalyzed, thermal, process and allows for reactions to be run at, or below, room temperature. This is achieved by converting the reaction into a series of discrete steps, forming a 5-triazolyl copper intermediate, culminating in the formation of a 1,2,3-triazole heterocycle. This 1,2,3-triazole heterocycle has the benefit of being highly chemically stable (inert to severe hydrolytic, oxidizing and reducing conditions, even at high temperatures). However, one drawback to the original reaction conditions used is the required  $\text{Cu}^+$  ions are highly susceptible to oxidation to the respective  $\text{Cu}^{2+}$  ion. For this reason, it has become common practice to generate  $\text{Cu}^+$  ions through reduction of a Cu(II) salt. A common approach employed is the reduction of  $\text{CuSO}_4$  by ascorbic acid, which allows for a continuous supply of  $\text{Cu}^+$  without the need to isolate reactions from environmental oxygen.

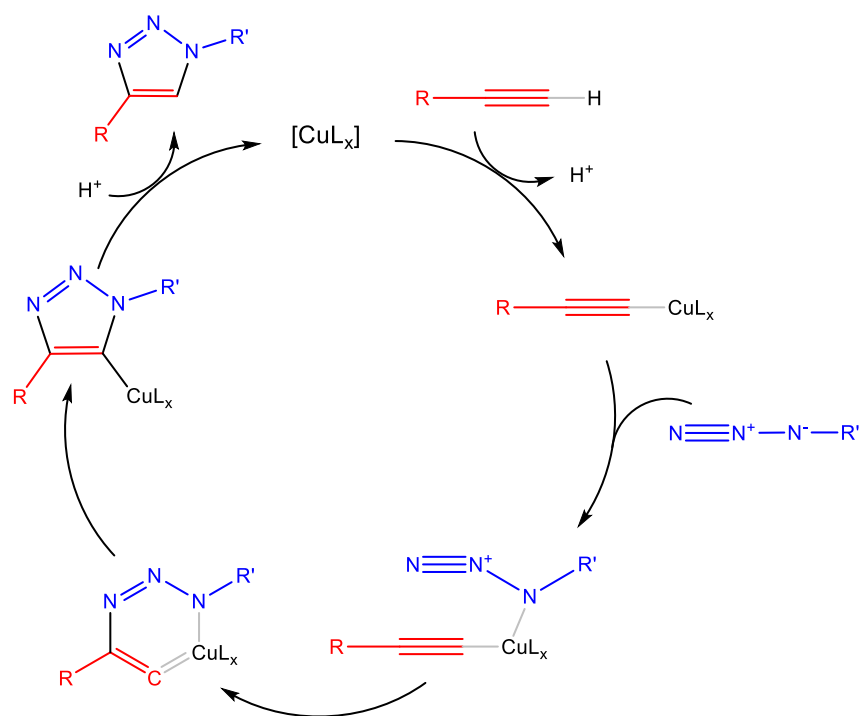


**Figure 5.1.** Reaction mechanism for copper-catalysed azide-alkyne cycloaddition for the combining of two compounds (R and R') via a ligand bound  $\text{Cu}^{1+}$  catalyst ( $\text{CuL}_x$ ).

The use of the CuAAC reactions has allowed for the development of novel fluorescent ligands previously hindered by additional reactive groups within the ligand pharmacophore. Recent examples include the generation of peptide linker-based fluorescent ligands for the histamine H<sub>1</sub> receptor (Kok et al., 2022).

## 5.2. Application of CuAAC for the generation of varied fluorescent Gas19cha18 peptide tracers.

### 5.2.1. General methods

Chemicals and solvents were purchased from standard suppliers and used without further purification. Sulfo-cyanine5-azide and Alexafluor-488-azide were purchased from Lumiprobe (Hunt Valley, MD) (5mg, >95% purity) and stored at -20°C.

Propargylglycine-Gas19cha18 peptide (Pra-Gas19cha18) was purchased from GenScript Biotech (New Jersey, USA) (4 mg, >95% purity) and stored at -20°C. Reactions were carried out in 1mL LC/MS glass vials and monitored by thin layer chromatography on commercially available precoated aluminium-backed plates (Merck Kieselgel TLC Reverse-phase-C8 Silica gel 60 Å F<sub>254</sub>) using a 50% CH<sub>3</sub>CN/50% H<sub>2</sub>O mobile phase.

Visualization was by examination under UV light (254 and 366 nm) followed by staining with ninhydrin. Organic solvents were evaporated under reduced pressure at ≤40°C (water bath temperature). Analytical RP-HPLC was performed using YMC-Pack C8 column (150 mm x 4.6 mm x 5 µm) at a flow rate of 1.0 mL/min over a 30 min period (gradient method of 10%-90% solvent B; solvent A = 0.01% formic acid in H<sub>2</sub>O, solvent B = 0.01% formic acid in CH<sub>3</sub>CN), UV detection at 254 nm and 320 nm spectra were analysed using Shimadzu LabSolutions software (modified from methodologies presented by Mannes *et al.* (Mannes et al., 2021)). LC/MS was carried out using a Phenomenex Gemini-NX C18 110 Å, column (50 mm × 2 mm x 3 µm) at a flow rate

0.5mL/min over a 5 min period (gradient method of 5%-95% solvent B; solvent A = 0.01% formic acid in H<sub>2</sub>O, solvent B = 0.01% formic acid in CH<sub>3</sub>CN). LC/MS spectra were recorded on a Shimadzu UFLCXR system combined with an Applied Biosystems API2000 electrospray ionization mass spectrometer and visualized at 254 nm (channel 1) and 320 nm (channel 2).

### 5.2.2. Experimental procedures

**Table 5.1: Procedures for the attempted synthesis of fluorophore tagged Gas19cha18 by copper-catalysed azide-alkyne cycloaddition.**

Procedure	Reactants	CuSO <sub>4</sub> :C <sub>6</sub> H <sub>7</sub> NaO <sub>6</sub> (Eq)	Solvents/additional reagents	Conditions
1	sulfo-cyanine5-azide / Pra-Gas19cha18 (1:1Eq)	5:25	95% H <sub>2</sub> O : 5% (CH <sub>3</sub> ) <sub>2</sub> NCH	20°C, 5 minutes
2	sulfo-cyanine5-azide / Pra-Gas19cha18 (1:1Eq)	5:25	95% H <sub>2</sub> O : 5% (CH <sub>3</sub> ) <sub>2</sub> NCH	20°C, 24 hours
3	sulfo-cyanine5-azide / Pra-Gas19cha18 (1:1Eq)	5:25	55% H <sub>2</sub> O : 5% (CH <sub>3</sub> ) <sub>2</sub> NCH : 40% (CH <sub>3</sub> ) <sub>2</sub> SO	20°C, 24 hours
4	benzyl azide / propargyl amine (1:1Eq)	5:25	55% H <sub>2</sub> O : 5% (CH <sub>3</sub> ) <sub>2</sub> NCH : 40% (CH <sub>3</sub> ) <sub>2</sub> SO	20°C, 60 minutes
5	sulfo-cyanine5-azide / Pra-Gas19cha18 (1:1Eq)	5:25	55% H <sub>2</sub> O : 5% (CH <sub>3</sub> ) <sub>2</sub> NCH : 40% (CH <sub>3</sub> ) <sub>2</sub> SO : TBTA (5 Eq)	20°C, 24 hours
6	sulfo-cyanine5-azide / Pra-Gas19cha18 (1:1Eq)	5:25	55% H <sub>2</sub> O : 5% (CH <sub>3</sub> ) <sub>2</sub> NCH : 40% (CH <sub>3</sub> ) <sub>2</sub> SO : TBTA (5 Eq)	50°C, 24 hours
7	sulfo-cyanine5-azide / Pra-Gas19cha18 (1:1Eq)	10:25	55% H <sub>2</sub> O : 5% (CH <sub>3</sub> ) <sub>2</sub> NCH : 40% (CH <sub>3</sub> ) <sub>2</sub> SO	20°C, 24 hours
8	Alexafluor-488-azide / Pra-Gas19cha18 (1:1Eq)	5:25	55% H <sub>2</sub> O : 5% (CH <sub>3</sub> ) <sub>2</sub> NCH : 40% (CH <sub>3</sub> ) <sub>2</sub> SO	20°C, 24 hours
9	sulfo-cyanine5-azide / Pra-Gas19cha18 (1:1Eq)	5:25	55% H <sub>2</sub> O : 5% (CH <sub>3</sub> ) <sub>2</sub> NCH : 40% (CH <sub>3</sub> ) <sub>2</sub> SO : 20% TFE	20°C, 24 hours

General procedure: In all cases, solutions of Reactants and CuSO<sub>4</sub>/ C<sub>6</sub>H<sub>7</sub>NaO<sub>6</sub> pairs were made with solvents as described, before combining and stirring in an LC/MS vial in the dark under stated conditions. All reactions were analysed by LC/MS and RP-HPLC as described previously.

### 5.2.3. Results

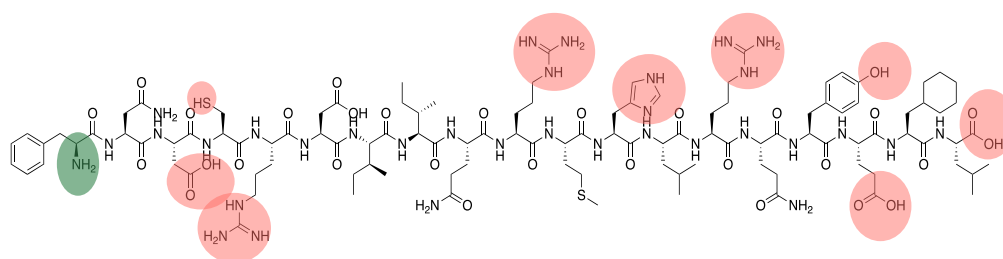


**Figure 5.2.** Skeletal structure of Gas19cha18 indicating potential reactive side groups (Red) and putative site available for fluorophore addition (Green).

Having established Gas19cha18 as the peptide with the greatest ability to positively modulate agonist affinity at the  $\beta_2$ -AR, Gas19cha18 was chosen as the basis for the development of fluorescent peptidic tracers. The nature of peptides, being formed from amino acid sequences, results in their possessing a high number of reactive groups as a result of amino acid side chains. Gas19cha18 is no exception. Analysis of Gas19cha18's skeletal structure (Figure 5.2) identifies multiple residues commonly exploited within standard coupling reactions within organic chemical synthesis, including amide and carboxyl groups. Subsequently, it is necessary to derive a coupling method which allows for these groups to remain independent of the coupling reaction, preferable without the need for side chain protection steps. Exploitation of the CuAAC reaction has the potential to allow efficient coupling of complex fluorophores to  $\alpha$  C-terminal peptides without the formation of unwanted impurities or side products. To facilitate the use of this reaction, Gas19cha18 derivatives *N*-terminally modified with the non-native amino acid propargyl glycine were acquired along with azido-bearing analogues of common red-emitting fluorophores sulfo-cyanine5 (sulfo-cy5-azide) and Alexafluor-488 (AF-488-azide). Propargyl glycine provides an alkyne reactive group connected to the alpha

carbon of the amino acid, providing the means for fluorophore cycloaddition without interference with the peptide chain.

CuAAC reactions have been shown to occur under a variety of conditions with varying degrees of efficiency. Studies carried out by Byrne *et al* employing peptides within CuAAC reactions identified a  $\text{CuSO}_4 \cdot 5\text{H}_2\text{O}/\text{Na Ascorbate}$  equivalent ratio of 5:25, under aqueous conditions supplemented with 5% N,N-Dimethylformamide (DMF), to provide a 90% conversion efficiency after 5 minutes at room temperature (Byrne *et al.*, 2011). Using these conditions as a starting point, to a 250  $\mu\text{L}$  aqueous solution of  $\text{CuSO}_4 \cdot 5\text{H}_2\text{O}/\text{Na Ascorbate}$  (5:25) was added 1 equivalent (Eq) Pra-Gas19cha18 pre-mixed with 1 Eq sulfo-cy5-azide in 225  $\mu\text{L}$   $\text{H}_2\text{O}$  + 25  $\mu\text{L}$  DMF (Figure 5.3, Table 5.1 [1]). The mixture was stirred at room temperature for 5 minutes before sampling via RP-TLC and LC/MS as previously described. RP-TLC identified two distinct spots indicative of unreacted peptide and fluorophore. Similarly, LC/MS traces indicated the presence of both peptide and fluorophore reactants, with no significant identification of expected product peaks ( $m/z$  calculated:  $[\text{M}+\text{H}]^+$ : 3323.58,  $[\text{M}+2\text{H}]^+$ : 1662.29,  $[\text{M}+3\text{H}]^+$ : 1108.5,  $[\text{M}+4\text{H}]^+$ : 831.65). Subsequently, the reaction was allowed to continue for 24 hours (Table 5.1 [2]).

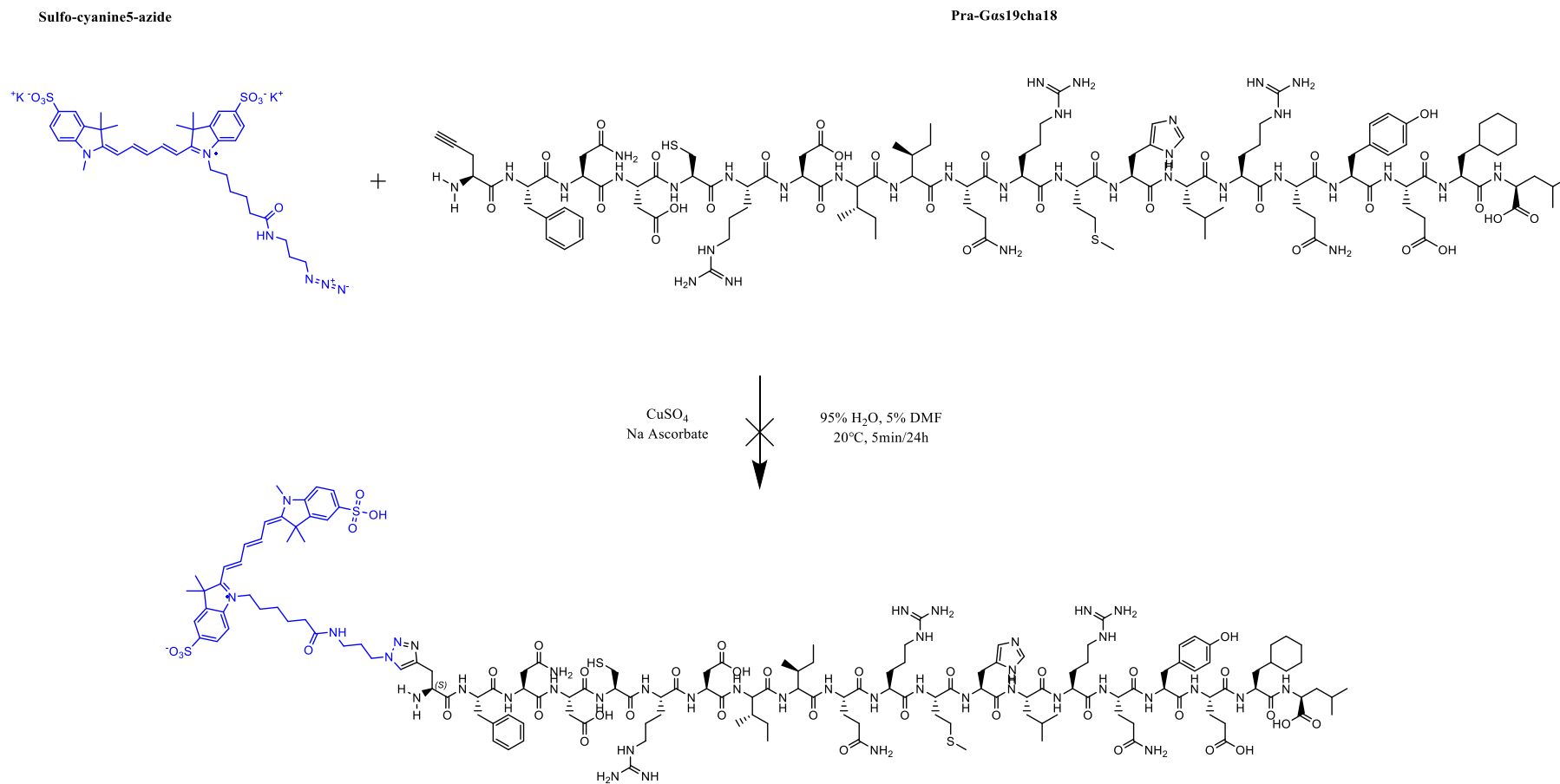


**Figure 5.3.** Attempted reaction between Pra-Gas19cha18 and Sulfo-cyanine5-azide under initial conditions (Table 5.1 [2/3]).

LC/MS analysis post 24-hour incubation again failed to identify product formation; however, UV 254 nm absorption traces indicated the formation of a new peak at  $t_R = 2.44$  min producing mass peaks within similarly large mass ranges to those expected for product formation, suggesting formation of an unknown product. Analytical reverse-phase HPLC was carried out on a 50  $\mu$ L sample of reaction mixture (as described above) to identify and isolate reaction components. HPLC traces indicated a wide peak between  $t_R = 5.5 - 7.5$  min and a large single peak at  $t_R = 9.52$  min (Figure 5.4). Collection of the single later peak afforded a blue solution, while collection across the entire smaller, wider peak resulted in a colourless sample.

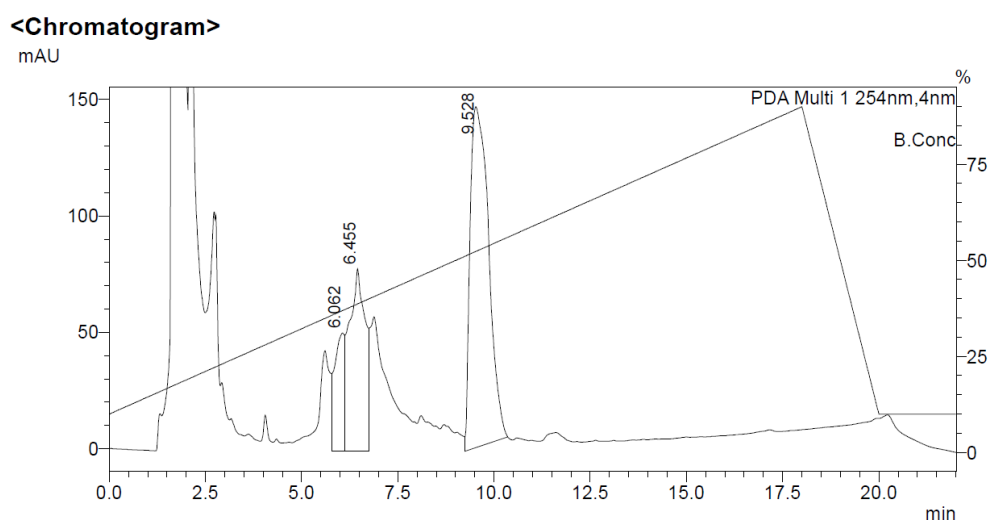


**Figure 5.4.** RP-HPLC analysis 254nm detection trace of Pra-G $\alpha$ s19cha18/Sulfo-cy5-azide CuAAC reaction mixture sample after 24 hours. Right axis indicates % CH<sub>3</sub>CN + 0.01% formic acid in water, with solvent gradient depicted over UV trace, measured using the right-hand Y-axis.

Collected samples were prepared for analysis by first removing the CH<sub>3</sub>CN solvent using reduced pressure evaporation, before freeze drying the remaining solution. Solid samples obtained were then solubilized in MeOH and analysed by LC/MS. Analysis identified

the wide peak ( $t_R = 5.5 - 7.5$  min) collected to contain unreacted peptide while the 9.5-minute peak contained unreacted sulfo-cy5-azide, with neither sample containing product or traces of the previously identified unknown species. Together, these findings indicate that the reaction is unable to proceed under these conditions. Additionally, incorporation of 40% DMSO to ensure solubility was not an underlying limitation gave similar results identifying solubility is not the limiting factor (Table 5.1 [3]).

In order to determine if the CuAAC reaction itself is the underlying limiting factor, a small-scale test reaction was carried out under the same conditions (with the inclusion of DMSO to maintain solubility) between benzyl azide and propargyl amine (Figure 5.6, Table 5.1 [4]) for 60-minutes.

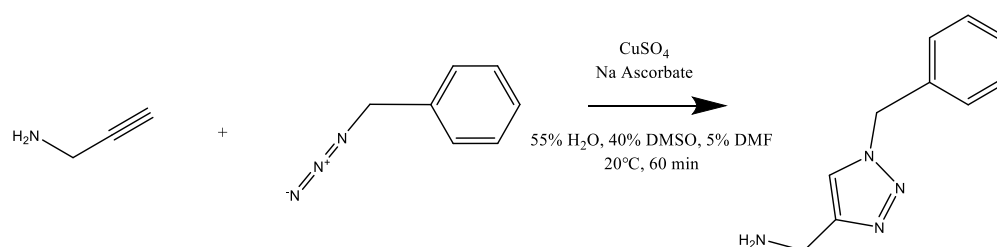


**Figure 5.6.** CuAAC test reaction.

Under these conditions, TLC and LC/MS analysis identified highly efficient product generation. This suggests that the reaction conditions are adequate to allow for efficient click reactions to occur between these reactive groups, therefore indicating that the inefficiency of the peptide-fluorophore coupling is likely the result of particular reactant properties within this environment.

The addition of a Copper-chelating ligand has previously been used to enhance the speed and efficiency of CuAAC reactions by providing a continuous supply of Cu<sup>+</sup> ions within the reaction mix. Foremost amongst the various ligands available is *tris*-((1-benzyl-4-

triazolyl)methyl)amine (TBTA), a tertiary amine containing the 1,2,3-triazole moiety. Addition of 5 Eq TBTA to the primary reaction mixture was hypothesised to increase the availability of  $\text{Cu}^+$  ions, thus driving the reaction to completion (Table 5.1 [5]). However, similar negative results were obtained upon LC/MS and RP-HPLC analysis of resulting reaction mixture post 5-minute and 24-hour incubations at room temperature. Similarly, increasing the reaction temperature to  $50^\circ\text{C}$  had no positive effect on product formation, nor did the inclusion of 10 Eq  $\text{CuSO}_4$  (Table 5.1 [6&7]).

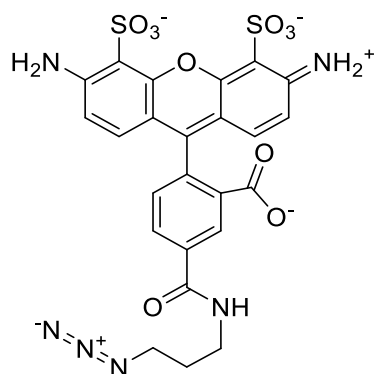


**Figure 5.7.** Structure of Alexafluor-488-azide

In order to determine if the reaction was hindered by properties of the reacting fluorophore, sulfo-cy5-azide was substituted for AF488-azide (Figure 5.7, Table 5.1 [8]) under the same conditions (excluding TBTA). TLC and RP-HPLC both failed to identify product formation despite fluorophore substitution, implicating the Pra-Gas19cha18 as the primary limiting factor within the reaction. 2,2,2-Trifluoroethanol (TFE) has previously been identified to disrupt intramolecular protein hydrogen bonding (Roccatano et al., 2002). With this in mind, TFE (20%) was added to reaction mixture to negate any detrimental effects of peptide secondary structure which might sterically shield the ability of the cycloaddition to take

place (Table 5.1 [9]). Unfortunately, this also appeared to have no effect on reaction efficiency.

#### 5.2.4. Discussion

Within this section, the viability of peptide click reactions to label peptides was explored. Extensive literature examples exist highlighting the high diversity in conditions available which facilitate CuAAC reactions, however, there are limited examples of solution-based click reactions being exploited for long-chain peptide chemistry. Test reactions exploiting small-molecule reactants demonstrated the efficiency of the click-reaction under initial reaction conditions, implying the displayed inefficiency of the target reaction is directly related to the larger compounds being employed. Additionally, the inability of different solvent systems to alter reaction efficiency rules out the possibility of solubility limitations within the system. This therefore required more extensive exploration of reaction/reactant properties which may be hindering product formation.

The use of CuAAC was chosen to overcome the limitations of multiple reactive groups on the Gas19cha18 peptide. However, these reactive sidechains may also be hindering the efficiency of the reaction due to their ability to chelate  $\text{Cu}^+/\text{Cu}^{2+}$  ions. The presence of Arginine and Cysteine residues in particular may have a detrimental effect on reaction efficiency due to the polar nature of the arginine side groups facilitating metal ion interactions and the sulfhydryl group of Cysteine promoting oxidation of  $\text{Cu}^+$  ions to  $\text{Cu}^{2+}$ . Together these interactions were hypothesised to reduce the availability of the  $\text{Cu}^+$  catalyst, thereby limiting the reaction. However, addition of excess amounts of  $\text{Cu}^+$  had no obvious effect on product formation. Further addition of a  $\text{Cu}^+$ -chelating ligand was believed to allow a greater proportion of  $\text{Cu}^+$  to be available for catalysis(Hein et al., 2008), however again this had no positive

impact on product formation, suggesting catalyst availability is unlikely to be the primary limiting factor in product formation.

The nature of the medium/long-chain peptide molecule backbone allows for a high degree of inter- and intra-molecular hydrogen-bonding, facilitating formation of protein/peptide secondary structure. As such, the resulting molecule can have drastically varied molecular geometry which can have significant impacts on molecular properties with a high degree of variability depending on solvent system employed (Kossoń et al., 2023). Employing this knowledge to the presented reactions provides an alternative explanation for why product formation is not occurring. The ability for the peptide starting material to form alpha helical secondary structures may have the negative impact of hiding the required alkyne reactive group, thereby hindering the reaction between the alkyne and azide. This phenomenon is one of the primary reasons peptide synthesis is carried out using a solid phase scaffold as it limits the stability of intra-molecular interactions (Merrifield, 1963). Disruption of hydrogen bonding by the addition of TFE was hypothesised to promote a greater efficiency of product formation by allowing access to the alkyne functional group, however, TFE had little effect on product formation, even under test scale conditions. Together with previous exploratory reactions, this suggests that a combination of presented confounding factors may be limiting product formation within these experiments.

There are a number of alternative approaches which may overcome some of the limitations encountered to facilitate peptide-fluorophore CuAAC reactions. Primary among these is the exploration of non-amino acid-based linker chemistry (Figure 5.8A).

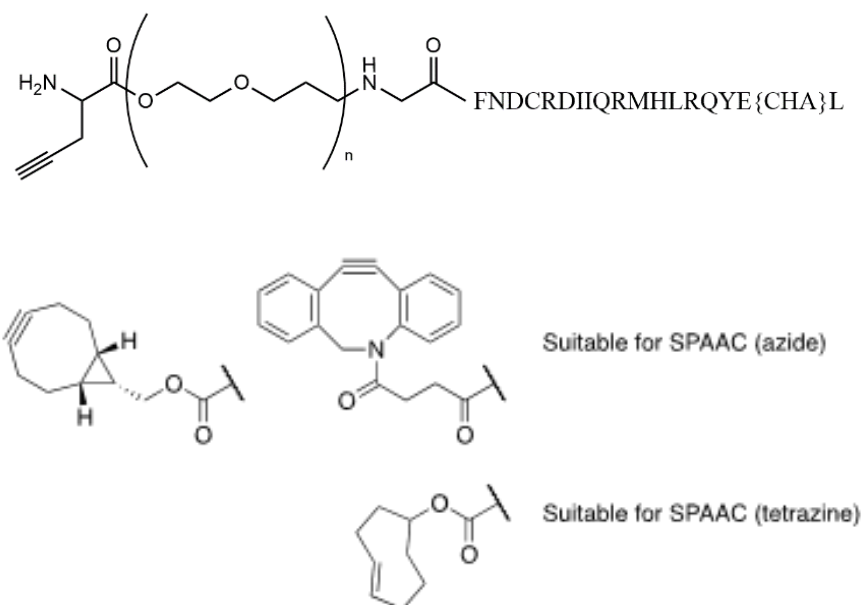


**Figure 5.8. Example alternative approaches.** (A) Alternative linker chemistry, this example depicts a PEG-type linker extending away from the amino acid chain of *Gas19cha18*. (B) Examples of alternative reactive groups applicable within strained click reactions with their reactive partner indicated in brackets.

This would allow for extension of the alkyne group away from the structurally dynamic amino acid chain and therefore limit the effects of steric hindrance on reaction efficiency while maintaining a solution-based reaction process. Similarly, the employment of alternative click partners may provide greater efficiency, such as use of strain-promoted azide-alkyne cycloaddition. This technique relies on much bulkier reactive groups, therefore limiting hiding of the alkyne group. Strain-promoted azide-alkyne cycloaddition provides the reactive alkyne within a strained difluoroalkyne, in which the electron withdrawing gem-difluoro moiety acts together with the ring strain to destabilize the alkyne (Figure 5.8B). This destabilization increases the reaction driving force and the desire of the cycloalkyne to relieve its ring strain through cyclisation with nearby azides (Agard et al., 2006). This process has the added benefit of being catalyst free, thus removing copper from the

reaction process completely. Copper is known to have a high degree of cellular toxicity which can have significant detrimental effects on future pharmacological assays. This is primary due to the chelating properties of copper discussed within this chapter, which can disrupt the complex protein interactions required for cellular function. Additionally, trace levels of copper ions are essential for the function of certain proteins (particularly cytochrome c oxidase, a key transporter within the electron-transport chain involved in ATP production), which can be disrupted under high copper conditions. Furthermore, there is evidence that high levels of copper ions are able to promote formation of reactive oxygen species which can have a severe impact on cellular function (Tsukihara et al., 1995; Zu et al., 2000).

This toxicity is of limited consequence within the membrane-based assays presented within this thesis, however, future exploration utilizing synthesised fluorescent peptides may be affected, making catalyst free reactions a preferred methodology.

## **Chapter 6. Results II**

Development of fluorescent G $\alpha$ -C terminal peptides as GPCR binding and signalling biosensors through intracellular NanoBRET.

## **6. Development of fluorescent G $\alpha$ -C terminal peptides as GPCR binding and signalling biosensors through intracellular NanoBRET.**

### 6.1. Chapter introduction:

The aim of this chapter was to establish a NanoBRET-based method (introduced in 6.2.1) to develop fluorescent G $\alpha$  C-terminus peptides as binding probes for intracellular modulator receptor sites, and as sensors for G protein coupled receptor activation. With the overall thesis aim being to develop universally applicable use-dependent tracers, particular attention was paid towards characterising the role of orthosteric agonist binding on tracer recruitment. Binding was explored using the previously described  $\beta_2$ -AR and NPY Y1 as primary candidate Gs and Gi coupled receptors, as well as across a range of example receptors each identified to potentially benefit from IAM development (briefly introduced in section 6.2.3 and 8.2.1). Selected G $\alpha$  C fluorescent peptides were then tested in their capacity to act as both intracellular tracers, and as receptor conformational biosensors, to probe unlabelled ligand interactions both at the intracellular and extracellular binding sites.

### 6.2. Introduction

#### *6.2.1. NanoBRET as a method of detecting receptor-ligand interactions.*

An emerging alternative technique to the previously discussed FRET technology is Bioluminescence resonance energy transfer (BRET) technology. BRET employs the same physical principles of energy transfer as describe within FRET assays (Section 4.2.1), however, donor luminescence is provided by the chemical reaction catalysed by a luciferase enzyme rather than a stimulated fluorophore. BRET provides advantages over FRET techniques by providing a simplified method for producing detectable

fluorescence output, while maintaining reliance on resonance energy transfer with similar distance constraints (<10 nm). This allows BRET to retain homogeneous detection of protein-protein/protein-ligand interaction in real time. The use of a luciferase to generate donor emission further removes the need for laser-based donor excitation, which can have negative effects in producing experimental artefacts due to light damage (e.g., photobleaching). The recent advance in BRET technology upon the discovery of NanoLuc (Nluc), engineered from the luciferase found in deep sea shrimp *Oplophorus gracilirostris*, allowed for greater signal definition than previous iterations of the technique (Stoddart et al., 2018). This method exploits the higher luminescence output generated by the luciferase than that produced by more traditional luciferases (e.g., Rluc8) to reduce noise within the assay system and expand the range of compatible fluorophore acceptor wavelength spectra (Stoddart et al., 2015). Additionally, the reduced size of the Nluc makes it more easily employed within plasmid-based vectors and limits the possibility of steric hindrance of protein interactions when applied to target proteins. The Nluc luciferase generates a donor luminescence emission of 450-80nm as a result of catalysing an oxidation reaction between the substrate furimazine and oxygen, generating furimamide. The high Nluc emission intensity centred on this wavelength allows for stimulation of a wide variety of fluorophores. The Nluc / furimazine reaction is itself longer lasting than traditional BRET luciferases using coelenterazine as substrate. In addition, luciferase substrates (e.g., endurazine) whose active moieties are released over time by cellular esterase activity, can provide additional capacity for longer read times within cellular assays. This is especially useful for real time kinetic characterisation of ligand binding with long residency times and slow approach to equilibrium (Meyrath et al., 2022).

NanoBRET has been exploited to explore receptor-ligand interactions through fusion of the Nluc tag to the extracellular region of receptors, much like SNAP-tag-based approaches (Roberts et al., 2020; Vasta et al., 2021, 2018). However, Nluc-based NanoBRET has a potential advantage over SNAP-based approaches due to its ability to function intracellularly. The luciferase substrate is cell permeable which is in contrast to SNAP-tag labels. This means that NanoBRET has potential to monitor the intracellular binding of GPCR ligands (as has been readily demonstrated for many GPCR-G protein and GPCR-arrestin BRET studies (Casella et al., 2023; Huber et al., 2022; Johnstone et al., 2022; Toy et al., 2022; White et al., 2020b, 2017)). However, for a whole cell intracellular ligand-GPCR NanoBRET application, the fluorescent tracer would also be required to be cell permeable and so access the binding site.

Further to ligand-based approaches, advances in BRET-based biosensors measuring protein recruitment (e.g., G protein, GRK, arrestin recruitment) have expanded our understanding of receptor-effector interactions (Charest et al., 2005; Galés et al., 2005). Additionally, this has allowed development of biosensors designed for detection of specified receptor conformations, including fluorescently tagged miniG protein and Nanobody technologies (Dijon et al., 2021; Soave et al., 2020d; Wan et al., 2018). Given their original design purpose within the field of structural biology, one of the inherent benefits of these sensors is their ability to detect and stabilise the active conformation. However, as probes to assess competition binding with small molecules at intracellular binding sites, this also limits their utility within more traditional binding assays, due to very high receptor affinity, prolonged occupancy and potential ability to stabilise active receptor states alone without participation of the orthosteric agonist (Wan et al., 2018). Consequently, there is a need for

kinetically fast, lower affinity tracers that bind in a receptor conformation dependent manner .

### 6.2.2. *Current methods for characterisation of intracellular allosteric modulator binding*

The rapid discovery of allosteric ligands has previously been hindered by a lack of tools available for direct characterisation of modulator binding at the target allosteric binding site. Historically, research has relied on characterisation of allosteric ligands through measurement of their modulatory capacity within functional or orthosteric binding assays(Casadó-Anguera and Casadó, 2022; Kenakin, 2010; Kruse et al., 2013; May, 2003). The use of radioligands to characterise intracellular ligand binding has also been utilised for exploration of intracellular ligand binding in a small number of cases(Gonsiorek et al., 2007b; Salchow et al., 2010). With the advancements in BRET technologies highlighted previously (section 6.2.1), and the concurrent development of fluorescent allosteric ligands, there has been an increasing opportunity to characterise direct allosteric ligand binding interactions using real time resonance energy transfer technology.

Of the small number of available fluorescent allosteric ligands targeting the intracellular binding site, the majority are those targeted to the CXCR/CCR chemokine receptor families(Huber et al., 2023, 2022). Work by Casella *et al*, Toy *et al* and Huber *et al* highlights the unique perspective fluorescent ligands can provide when characterising allosteric ligands through real-time kinetic analysis of ligand-receptor interactions(Casella et al., 2023; Huber et al., 2023; Toy et al., 2022). In particular, application of the CXCR2 selective fluorescent ligand presented in these studies allowed for a greater understanding of both labelled and unlabelled modulator binding characteristics, both through equilibrium binding and through employment of Motulsky-Mahan competition kinetics

analysis within a homogeneous assay system. This, for example, illustrated that the non-surmountable mode of action of navarixin (a CXCR2 selective NAM) is the result of a long residency time (defined as  $1/k_{\text{off}}$ ), rather than the non-competitive allosteric mechanism alone. These studies highlight that use of fluorescent IAMs allows for real-time identification of ligand binding characteristics and opens the possibility of screening ligands which not only compete for intracellular sites, but also have favourable binding properties for particular receptor conformations.

### 6.2.3. *Background to additional alternative candidate Gi coupled receptors used in this study.*

The development of the fluorescent peptide BRET approach used the  $\beta_2$ -AR (Gs) and NPY Y1 (Gi) systems as previously introduced in chapter 4. However, further Gi-coupled receptors were also explored in this chapter to determine tracer selectivity. A brief introduction to these subtypes is provided below (prostaglandin EP<sub>4</sub> is introduced in section 8.2.1).

#### 6.2.3.1. CXCR2:

Chemokines are key players in the innate immune response. CXC chemokines specifically are involved in several important mechanisms promoting immune cell responses to damaged tissue including immune cell survival, leukocyte chemotaxis and activation of the inflammatory response (Viola and Luster, 2008). The majority of chemokines are released by macrophages, endothelial cells or smooth muscle cells upon detection of, or as a consequence of cell damage (D. Scholten et al., 2012). All chemokines are peptide ligands and therefore are made of single amino acid chains able to fold into complex secondary, tertiary and quaternary structures, allowing for complex receptor binding interactions (Allen et al., 2007; Liu et al., 2022). All chemokines have a shared tertiary structure stabilised by disulphide bridges

between conserved cysteine residues. CXC chemokines are defined by the inclusion for a conserved cysteine-X-cysteine motif (X indicating a single amino acid separation between cysteines) at their N terminus. The N terminus of chemokines is highly flexible and the first two cysteines are located within the anterior region followed by a coil region termed the N-loop. The N-loop region is important for interactions with receptor N termini upon binding (D. Scholten et al., 2012). The core domain of chemokines consists of three antiparallel  $\beta$  strands, and the C terminus consists of an  $\alpha$  helix (Miller and Mayo, 2017; D. Scholten et al., 2012).

In order to carry out their function chemokines are required to bind to cell surface receptors, including CXCR1 and CXCR2. CXCR1 and CXCR2 belong to the C-X-C chemokine receptor family distinguished through their binding to C-X-C family chemokine ligands. Due to their similar structure, multiple related chemokines (such as CXCL8 and CXCL1) are able to act as agonists for the same receptor, maximising their effectiveness in innate immune responses (Alexander et al., 2011; D. Scholten et al., 2012). The use of peptide ligands allows for a high degree of mechanistic complexity within the ligand binding site, involving multi-site interactions to facilitate receptor activation. Additionally, chemokines employ a two-step binding method, with initial receptor-ligand interactions occurring between the receptor N-terminus and chemokine N-loop region. This then facilitates binding within a secondary binding site formed by the extracellular loop 2 and TM4, 5, and 6 in the receptor transmembrane domain (Burg et al., 2015; Kufareva et al., 2014; Zheng et al., 2017).

Targeting of CXCR2 in particular has been proposed to be a potential novel approach for the treatment of multiple diseases, particularly in the case of inflammatory disease. CXCR2 expression on neutrophils drives chemotaxis towards sites of acute inflammation, following the CXCL8 (and other chemokines)

gradient. The role of neutrophils and CXCL8-CXCR1/2 mediated chemotaxis is essential for the successful clearance of pathogens, with knock-out mice displaying significantly delayed wound healing and compromised neutrophil chemotaxis (Del Rio et al., 2001; Devalaraja et al., 2000). However, inappropriate or prolonged expression of CXCL8 and/or its receptors CXCR1/2, drives an excessive infiltration of immune cells into damaged tissue and can confer chemokine sensitivity to cells that are normally not responsive to chemokines, resulting in chronic inflammation and autoimmune disease (Balkwill, 2004; Koelink et al., 2012). Most notably, CXCL8 has been shown to be upregulated in COPD patients (Keatings et al., 1996). This promotes excessive recruitment of macrophages and neutrophils to the lungs, resulting in alveolar and epithelial cell damage. CXCL8 also promotes the contraction of the epithelium to increase its immune cell permeability, however, this further contributes to airway obstruction and inflammatory cell accumulation. This accumulation results in further release of inflammatory mediators leading to sustained tissue damage (Reutershan et al., 2006). Additionally, CXCR2's role in driving chemotaxis has also been attributed to its role in promoting increased cell survival and metastasis with tumours overexpressing CXCR2. As such, the ability to inhibit CXCR2 signalling has the potential to limit the progression of tumour metastasis and inflammatory diseases such as COPD. However, the combination of ligand multi-site interactions, shared endogenous ligands (therefore poor selectivity) and the two-step binding process makes classical therapeutic targeting difficult and produces a high degree of on- and off-target side-effects. Use of orthosteric antagonists has produced severe side-effects, particularly neutropenia as a result of inhibiting the chemotaxis of neutrophils from the bone marrow into the bloodstream. Subsequently, an approach which limits inhibition to sites of high receptor activation (such as allostery) may prove more effective at reducing therapeutic side-effects. Exploitation of the CXCR intracellular binding site has proved to be a suitable

approach for achieving high target selectivity with the recent development of the IAM navarixin, able to achieve 100-fold selectivity for CXCR2 over CXCR1 (Gonsiorek et al., 2007b; Holz et al., 2010; Liu et al., 2022; Norman, 2013; Salchow et al., 2010). The success of intracellular binding ligands at these receptors makes CXC chemokine receptors attractive examples as a case-study for the utility of novel intracellular binding tracers.

#### 6.2.3.2. Metabotropic glutamate receptor 2:

Metabotropic glutamate receptors (mGluRs) are receptors found within the central nervous system (CNS) which belong to the family of class C GPCRs (in contrast to the other GPCRs explored in this thesis). This family is distinguished by the presence of a large extracellular domain (Venus flytrap domain) extending from the N terminus (compared with the more common class A receptor structure) which contains the endogenous ligand, L-glutamate, binding domain. Physiological activation of these receptors relies on receptor dimerization, both as homo- and heterodimers. G protein binding has been shown within cryo-EM structures to again occur through use of the G $\alpha$   $\alpha$ 5 helix, however at a structurally distinct site (and orientation) to that seen with Class A GPCRs (Seven et al., 2021). Targeting the metabotropic glutamate receptor 2 (mGluR2) in particular has been proposed to aid in the treatment of schizophrenia and other related neurological/neurodegenerative diseases (Kammermeier, 2012; Li et al., 2022). Glutamate is widely utilized within the CNS as an excitatory neurotransmitter for both metabotropic (GPCRs) and ionotropic (ion channels e.g., NMDA) receptors and therefore the employment of classical orthosteric agonists/antagonists has the potential to produce a plethora of on- and off-target side-effects (Arsova et al., 2021; Cacabelos et al., 1999; Gómez-Santacana et al., 2022; Planells-Cases et al., 2006; Seven et al., 2021). Additionally, mGluR2 is widely expressed across multiple

brain regions, therefore modulation of mGluR2 response to glutamate, rather than direct activation/inhibition of mGluR2, via use of allosteric ligands is likely to achieve increased target selectivity and reduce potential side-effects(Liau et al., 2022).

Initial PAMs developed were shown to have a high degree of success in producing antipsychotic-like and pro-cognitive effects in preclinical models, making them attractive methods of intervention for schizophrenia, however, these were later associated with serious side-effects including neurotoxicity and seizure(Bridges et al., 2013; Kinney et al., 2005). These adverse effects were further attributed to modification of the receptor signalling bias through stabilisation of particular receptor conformations(Kenakin and Christopoulos, 2013). This proposes the possibility of deriving novel allosteric modulators able to stabilise preferable conformations and therefore promote particular signalling pathways through modification of receptor bias(Sengman et al., 2017). The use of intracellular binding ligands has the potential to not only provide increased target selectivity at the mGluRs for therapeutic exploitation, but also would allow for probing of the relationships underpinning mGluR homo/heterodimer signalling and allosteric driven biased signalling through detection of particular receptor conformations.

#### 6.2.3.3. $\mu$ opioid receptor:

The  $\mu$  opioid receptor (MOR) is the primary target for opioid analgesics, the current gold standard in pain relief therapeutics(Koehl et al., 2018). MOR activation alters neuronal function through classical  $G\alpha_i$  protein signalling mechanisms, including postsynaptic activation of G protein coupled inwardly rectifying potassium channels (GIRK), allowing for hyperpolarization and inhibition of neuronal signalling(Williams et al., 1982). However respiratory depression is a well-documented

on-target side effect, and is the leading cause of opioid related deaths, particularly resulting from prolonged use of MOR agonist treatments(Stahl et al., 2021). The risk of developing severe side-effects is further driven by the rapid development of opioid tolerance, whereby greater therapeutic doses are needed to replicate the desired analgesia while producing a heightened side-effect profile. Alternative methods of targeting the MOR have aimed to reduce either the generation of opioid tolerance or limit the production of on-target side-effects. Foremost among these methods is the development of biased agonists able to promote G protein verses arrestin signalling to different degrees, however, more recent findings suggest this method may prove ineffective in reducing side-effect profiles(Gillis et al., 2020; Guttridge et al., 2020; Schmid et al., 2017; Stahl et al., 2021). The ability to exploit the intracellular binding site of the MOR may provide an alternative mechanism for targeting opioid signalling and reducing the severe side-effect burden of current therapies. The use of intracellular modulators has thus far exclusively produced antagonists, an outcome unfavourable in the case of targeting the MOR for analgesia. However, the identification of IAMs able to selectively compete with particular effectors (as seen with alternative allosteric ligands(Bolognini et al., 2016; D. J. Scholten et al., 2012)) may provide an alternative route for the study and exploitation of biased signalling and therapeutic tolerance. Similarly, IAMs may provide an alternative strategy to the current naloxone treatment for overdone patients.

### 6.3. Chapter aims:

Overall, the objective of this chapter was to characterise the binding of selected Gas and Gai derived peptides directly via NanoBRET. Initial binding characteristics used candidate receptors introduced in chapter 4 ( $\beta_2$ -AR and Y1), exploring the role of orthosteric agonists on tracer recruitment. The utility of these fluorescent tracers was then utilised to determine their ability to bind multiple GPCRs and to characterise both intracellular and orthosteric ligand binding.

### 6.4. Methods

#### 6.4.1. *Cell line generation and validation*

HEK293 cell lines were generated as previously described expressing either: p3.1neo(+)-SNAP- $\beta_2$ -AR-tsNluc, p3.1neo(+)- $\beta_1$ -AR-LgBiT, p3.1(+) rY1-tsNluc, p3.1neo(+)-EP<sub>2</sub>-tsNluc, p3.1neo(+)-EP<sub>4</sub>-tsNluc, p3.1neo(+)-A<sub>2A</sub>-tsNluc, p3.1neo(+)-MOR-tsLgBiT, P3.1neo(+)-mGlu2-tsNluc and p3.1neo(+)-SNAP-CXCR2-tsNluc (Generating: Hek-ss $\beta_2$ AR-tsNluc, Hek-ss $\beta_1$ AR-LgBiT, Hek-rY1-tsNluc, Hek-EP<sub>2</sub>-tsNluc, Hek-EP<sub>4</sub>-tsNluc, Hek-ssA<sub>2A</sub>-tsNluc, Hek-MOR-LgBiT, Hek-mGluR2-tsNluc and Hek-ssCXCR2-tsNluc). Cells were initially screened for SNAP-receptor plasma membrane expression by labelling with membrane impermeant fluorophore SNAP-surface AF488 prior to fixing and imaging, as described previously (section 3.3.4), or for functional luciferase by addition of furimazine solution (1/1440 manufacturer's stock) and measurement of 450 nm luminescence output. Upon validation of stable cell line transfection and receptor expression, cells were grown in four T175 flasks to 90% confluency before being used to generate Hek-receptor cell membranes as described (section 3.5).

6.4.2. *Bioluminescence resonance energy transfer (NanoBRET) assays to monitor fluorescent G protein peptide recruitment.*

NanoBRET assays used either low sodium assay binding buffer (including 2.5mM CaCl<sub>2</sub> for Y1 assay), or an extracellular Hank's balanced saline solution, with the constituents as described for TR-FRET binding measurements (section 4.4.2). TMR- G $\alpha$  peptide binding was first characterised by addition of increasing fluorescent probe concentrations (8 – 5000 nM) to 1 $\mu$ g/well Hek cell membranes, in which donor luciferase luminescence was stimulated with the addition of furimazine (1/960 dilution from Promega manufacturer's stock) in the additional absence or presence of the orthosteric agonist ( $\beta_2$ -AR: 10  $\mu$ M isoprenaline, Y1: 100 nM PYY)[final assay volume, 40 $\mu$ l [all dilutions accounted for 4x dilution upon addition to assay plate]]. Fluorescent peptide NSB was defined by the inclusion of 10 $\mu$ M unlabelled G $\alpha$ s19cha18/G $\alpha$ i19cha18 peptide. Endpoint reads at 10-, 30- and 60-min incubation at 37°C were taken using a PHERAstar as the BRET ratio between donor luminescence (450 nm emission) and acceptor TMR- G $\alpha$ s19cha18/TMR- G $\alpha$ s19 / TMR-G $\alpha$ i19cha18 recruitment fluorescence (550 nm) to determine peptide binding. Data was analysed using endpoint saturation analysis to derive tracer K<sub>D</sub> as described in section 3.7.

For quantitative analysis of TMR- G $\alpha$ s19cha18 / TMR- G $\alpha$ s19 / TMR-G $\alpha$ i19cha18 recruitment by orthosteric agonists, 500nM tracer peptide was incubated with 1 $\mu$ g/well Hek cell membranes, 1/960 dilution furimazine, and a selection of the following ligands at the indicated final concentrations;  $\beta_2$ -AR: salbutamol, salmeterol, isoprenaline, formoterol, or ICI118551; Y1: NPY, PYY, [Leu31,Pro34]NPY. To initiate the recruitment, membranes were separately preincubated (5 min) with furimazine to establish luminescence output, prior to their online injection using the PHERAstar to assay buffer containing the probe peptide and stimulating ligands. NanoBRET was monitored for 30 min every

1.16 (TMR- G $\alpha$ s19cha18), 2.61 (TMR- G $\alpha$ s19), or 1.3 (Y1) minutes on the PHERAstar, using the BRET ratiometric measurements described above. In experiments to determine TMR- G $\alpha$ s19cha18 selectivity, agonist binding, assays were repeated using the same protocol employing Hek- $\beta$ <sub>1</sub>-AR-LgBiT (incorporating 10 $\mu$ M HiBiT peptide [VSGWRLFKKIS] to assay plate to form complemented NanoBiT), Hek-A<sub>2A</sub>-tsNluc, Hek-EP<sub>2</sub>-tsNluc, Hek-EP<sub>4</sub>-tsNluc or Hek-ssCXCR2-tsNluc cell membranes, stimulated with isoprenaline, NECA (Sigma-Aldrich, Pool, UK), PGE<sub>2</sub> (Sigma-Aldrich, Pool, UK) or CXCL8 28-99 (Strattech Scientific, Cambridge, UK) respectively, or vehicle. For experiments to determine TMR- G $\alpha$ i19cha18 selectivity, membrane suspensions of selected cell lines were validated for receptor expression and luminescence output by addition of 1/960 furimazine solution as previously described (incorporating 10 $\mu$ M HiBiT peptide in the assay media to form complemented Nanoluc where required). TMR-G $\alpha$ i19cha18 binding assays were undertaken employing similar protocols to previous Y1 binding assays, making use of saturating concentrations of respective receptor agonists where required [MOR: 10  $\mu$ M DAMGO (Sigma-Aldrich, Pool, UK), CXCR2: 10  $\mu$ M CXCL8 28-99, mGlu2R: 20  $\mu$ M LY395756 (Sigma-Aldrich, Pool, UK)]. In these experiments the extent of recruitment was assessed 30 min after membrane addition at 37°C. Endpoint agonist stimulation of tracer peptide recruitment was assessed by concentration response curve analysis, performed to obtain estimates of ligand potency (EC<sub>50</sub>) and maximal response R<sub>max</sub> as described in data analysis. Alternatively, kinetic recruitment data were fitted to a rise-to-steady state model, as described by Hoare et al (2020) to identify the kinetically derived EC<sub>50</sub> (described in section 3.7)(Hoare et al., 2020).

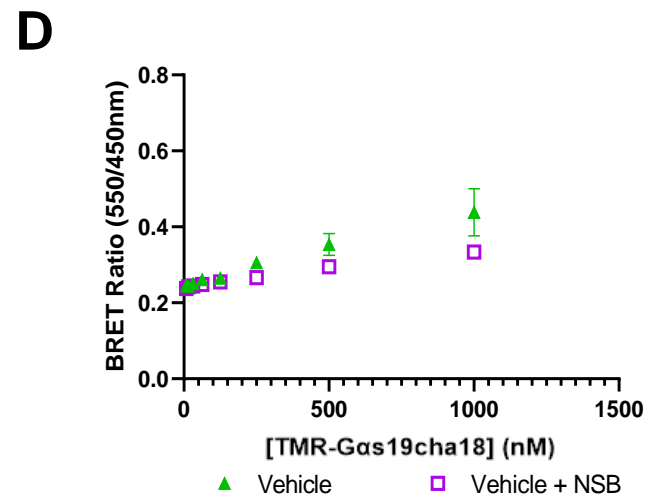
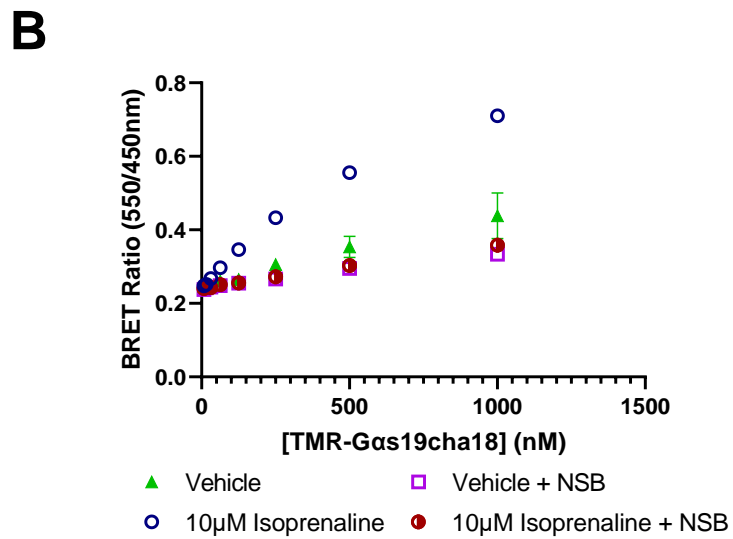
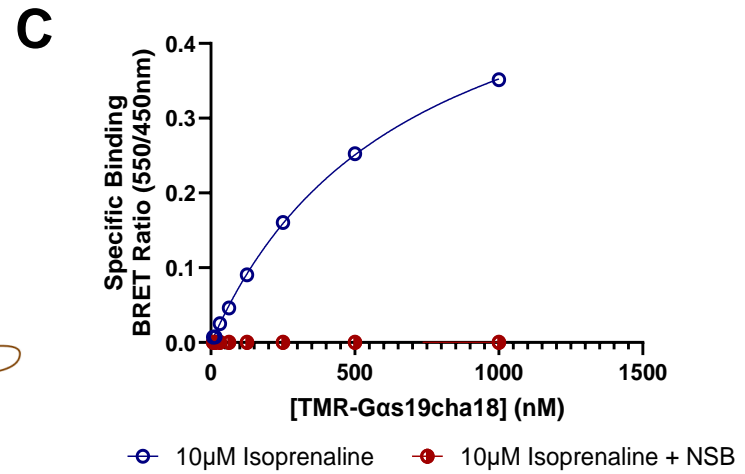
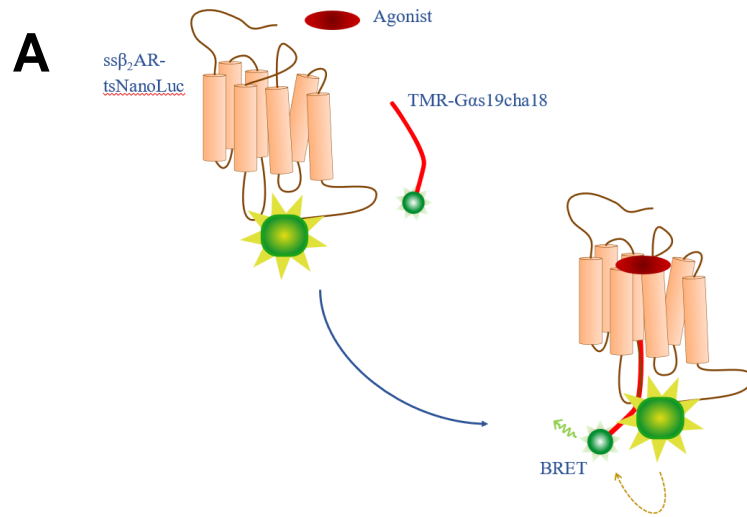
To determine unlabelled ligand affinities using competition binding, 1  $\mu$ g/well Hek-  $\beta$ <sub>2</sub>-AR/Y1-tsNluc cell membranes were incubated with 500nM / 125nM TMR- G $\alpha$ s19cha18 or 1  $\mu$ M TMR-

G $\alpha$ i19cha18, a range of competing concentrations of unlabelled peptides (G $\alpha$ s19cha18, Palmitoylated(Palm)G $\alpha$ s19cha18, G $\alpha$ s19, G $\alpha$ s24, G $\alpha$ s11, G $\alpha$ i19, G $\alpha$ i24 or G $\alpha$ i19cha18), 10 $\mu$ M isoprenaline or 800nM NPY and 1/960 dilution of flurimazine as indicated above (final volume, 50 $\mu$ l). Incubations were performed at 37°C and BRET measurements were taken every 30 minutes over a 2-hour interval, using the PHERAstar (550 nm / 450 nm ratio). Data was analysed using the Cheng-Prusoff correction as described in section 3.7.

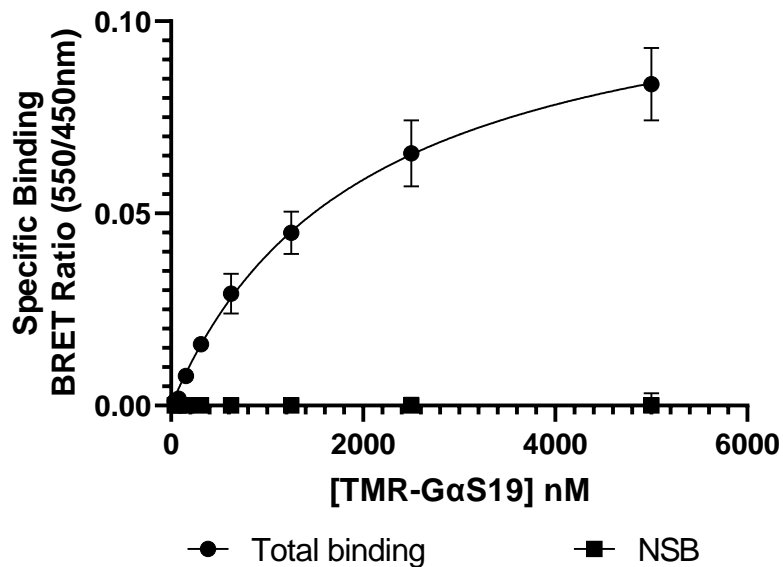
## 6.5. Results

### 6.5.1. *Establishing a NanoBRET binding assay to directly monitor TMR- Gas19cha18 recruitment to the $\beta_2$ -Adrenoceptor in HEK293 cell membranes.*

Chapter 4 highlighted the role the  $G\alpha_{\alpha 5}$  helical peptide sequence has on their positive enhancement of agonist binding affinity in the  $\beta_2$ -AR. Of the various peptides explored,  $G\alpha_{s19cha18}$  displayed the greatest modulatory capacity, supporting previous studies indicating the  $\beta_2$ -AR allosteric modulation by this modified  $G\alpha_s$  peptide (Mannes et al., 2021). However, this allosteric analysis of the effects of the  $G\alpha$  C terminal peptides relied on measuring their properties indirectly, rather than direct demonstration of binding and peptide affinity for the  $\beta_2$ -AR-G protein interaction site. Given the knowledge that the peptide C terminus was likely to make close contact with the  $\alpha 5$ -helix binding site, fluorescent probes predicted to retain  $\beta_2$ -AR affinity through N terminal modification of the sequence with the BRET compatible fluorophore tetramethylrhodamine (TMR-  $G\alpha_{s19}$ / TMR-  $G\alpha_{s19cha18}$ ) were generated. The ss $\beta_2$ -AR was fused at the C terminus with a thermostable (ts) Nanoluciferase (ss $\beta_2$ -AR-tsNluc, described in section 3.2) thereby providing a source of intracellularly located donor luminescence and providing opportunity to detect TMR-peptide binding to the expressed ss $\beta_2$ -AR-tsNluc in membranes by NanoBRET (Figure 6.1A).

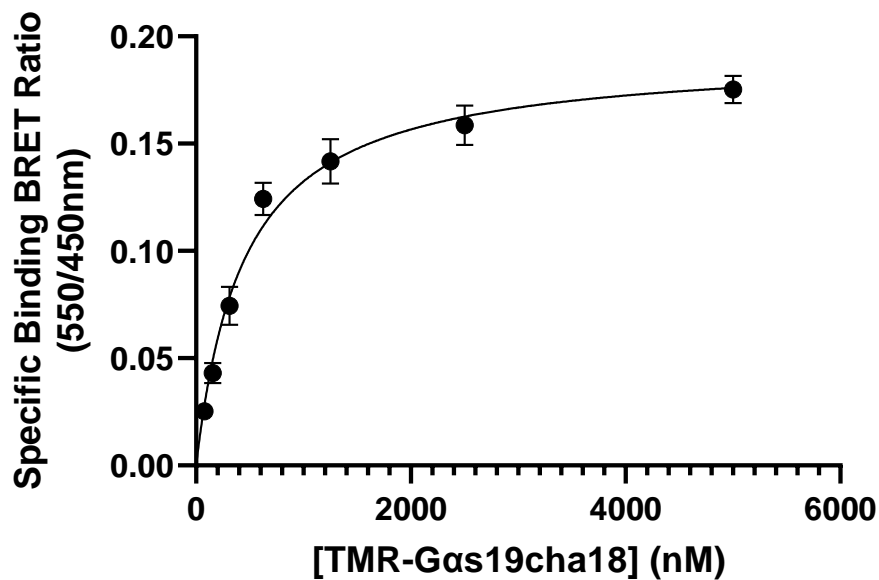


**Figure 6.1. Agonist-dependent binding of TMR-G $\alpha$ s19cha18 to the  $\beta$ <sub>2</sub>-adrenoceptor determined by NanoBRET.** (A) Diagram of TMR-peptide interaction with ss $\beta$ <sub>2</sub>-AR-tsNluc, generating NanoBRET signal, in the presence of an orthosteric agonist. (B) Saturation binding of TMR-G $\alpha$ s19cha18, demonstrating the increased specific binding observed in the presence of 10  $\mu$ M isoprenaline to Hek-ss $\beta$ <sub>2</sub>-AR-tsNluc membranes. (C) Specific binding data in the presence of isoprenaline fitted with a one-site specific binding model to determine TMR-G $\alpha$ s19cha18 affinity ( $K_D$ ). (D) Saturation binding measurements for TMR-G $\alpha$ s19cha18 to ss $\beta$ <sub>2</sub>-AR-tsNluc membranes in an agonist-free environment and low sodium buffer. In B and D, total and nonspecific binding (NSB) were defined by the absence and presence of 10  $\mu$ M unlabelled G $\alpha$ s19cha18. Data shown are single examples from five independent experiments, taken after 60-minutes incubation at 37°C in a low sodium environment.



**Figure 6.2. Agonist-dependent binding of TMR-Gas19 to the  $\beta_2$ -adrenoceptor determined by NanoBRET.** Specific binding data, using Hek-ss $\beta_2$ -AR-tsNluc membranes in the presence of isoprenaline, fitted with a one-site specific binding model to determine TMR-Gas19 affinity ( $K_D$ ). Total and nonspecific binding (NSB) were defined by the absence and presence of 10  $\mu$ M unlabelled Gas19cha18. Data shown are a single example from three independent experiments, with assay conditions as per Figure 6.1

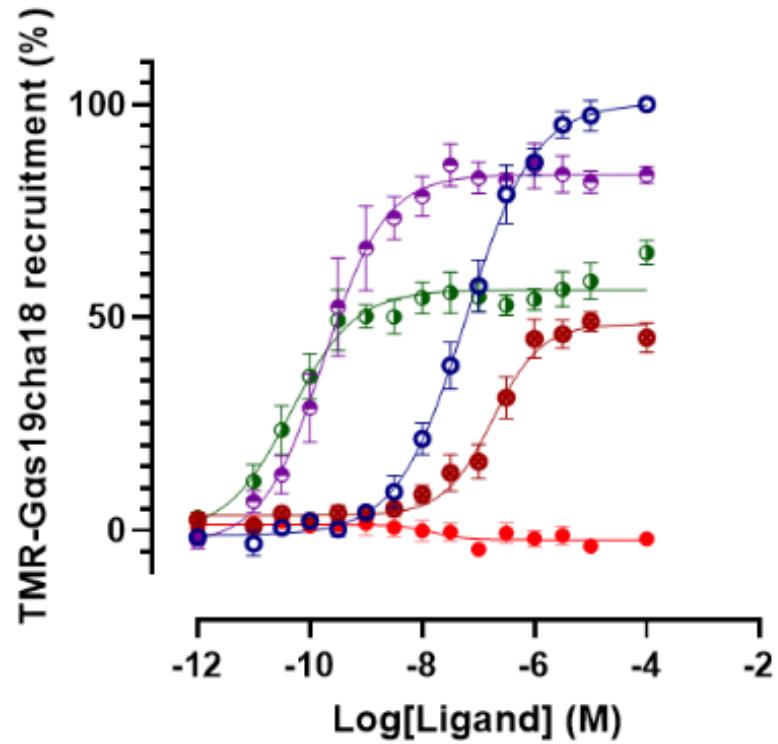
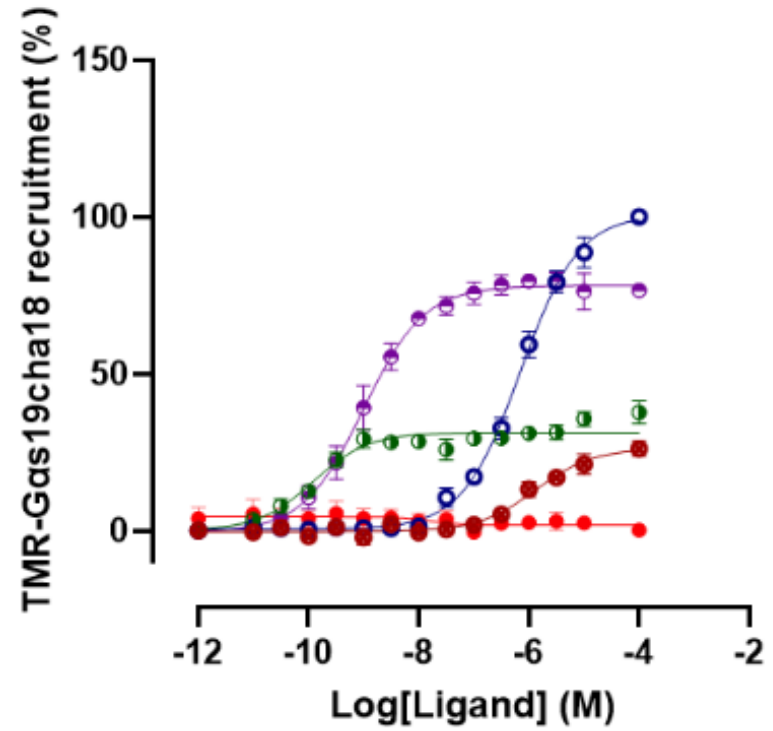
Initial saturation studies performed using TMR- Gas19cha18 and TMR- Gas19, with otherwise unstimulated ss $\beta_2$ -AR-tsNluc membranes (in low sodium buffer after 60-minutes incubation at 37°C used for previous TR-FRET measurements), failed to detect significant specific binding using up to 1  $\mu$ M or 5  $\mu$ M of labelled peptide respectively (Figure 6.1D). As highlighted by previous TR-FRET binding assays performed in chapter 4, it was hypothesised that  $G\alpha_s$  peptides would preferentially bind to the receptor active state. In line with this hypothesis, TMR- Gas19cha18 and TMR- Gas19 recruitment was only observed in the presence of 10  $\mu$ M isoprenaline, in which a substantive specific BRET measurement was observed that was effectively competed by unlabelled Gas19cha18 peptide (Figure 6.1B, Figure 6.1C). Under these agonist-stimulated conditions and low sodium environment, the TMR- Gas19cha18 affinity ( $K_D$ ) for the  $\beta_2$ -AR was  $K_D = 599 \pm 25$  nM (n=5) and  $3.0 \pm 0.75$   $\mu$ M for TMR- Gas19 ( $B_{max}$  (as BRET ratio) =  $0.29 \pm 0.05$ , n=5 and  $0.12 \pm 0.005$ , n=3, Figure 6.2). The use of an extracellular Hank's-based buffer (with higher sodium concentration) did not significantly affect TMR-Gas19cha18 affinity or  $B_{max}$  ( $K_D = 446 \pm 123$  nM, p=0.16,  $B_{max} = 0.21 \pm 0.01$ , p=0.20 n=4, Figure 6.3). These data demonstrated that, in line with previous peptide structure activity relationships in chapter 4 and Mannes *et al.* (Mannes *et al.*, 2021), TMR- Gas19cha18 was the most suitable probe for the  $\beta_2$ -AR intracellular G protein binding site, whose binding could be detected by NanoBRET, and appeared dependent on the active receptor conformation promoted by orthosteric  $\beta_2$ -AR agonists.



**Figure 6.3: Saturation binding of TMR-Gαs19cha18 to the  $\beta_2$ -adrenoceptor in high sodium conditions.** Data in duplicate, taken after 60 minutes, are from a representative of four experiments. Non-specific binding was in all cases determined through inclusion of 10 $\mu$ M Gαs19cha18 and deducted from plotted data to determine specific binding. All assays run at 37°C for 2 hours.

#### 6.5.1.1. $\beta_2$ -Adrenoceptor orthosteric agonist pharmacology revealed by TMR- G $\alpha$ s19cha18 NanoBRET recruitment assays.

Given the agonist dependence of TMR- G $\alpha$ s19cha18 recruitment, the ability of this NanoBRET assay to function as a  $\beta_2$ -AR activation sensor for ligands of known differences in efficacy was explored. Using 500 nM TMR- G $\alpha$ s19cha18 tracer, kinetic and endpoint NanoBRET measurements were performed in ss $\beta_2$ -AR-tsNluc membranes in response to agonists and antagonist, also comparing the low sodium binding buffer initially used with a high sodium buffer with higher "extracellular" sodium concentrations. Endpoint concentration response data (Figure 6.4A; Table 6.1) clearly ranked the agonists isoprenaline, formoterol, salbutamol and salmeterol in the expected order of potency and maximal response (Baker, 2005), with salbutamol and salmeterol both identified as partial agonists relative to isoprenaline. The effect of the high sodium buffer environment was a reduction in agonist potency (Figure 6.4B, Table 6.1) as would be expected due to the nature of the negative allosteric effect of sodium on GPCR signalling. This was further highlighted by the enhanced partial agonism (reduced  $R_{max}$  compared to isoprenaline) apparent for those ligands (salmeterol, salbutamol) with lower intrinsic efficacy.

**A****B**

—○— Isoprenaline    —○— Formoterol    —●— Salbutamol  
—●— Salmeterol    —●— ICI118551

**Figure 6.4. Agonist-dependent recruitment of TMR-G $\alpha$ s19cha18 to ss $\beta$ 2-AR-tsNluc measured by NanoBRET.** Assays were performed using 500 nM TMR-G $\alpha$ s19cha18 with endpoint binding measured after 30 min, 37°C exposure to different  $\beta$ <sub>2</sub>-AR orthosteric ligands, to construct concentration–response relationships. (A and B) represent pooled data from five experiments, performed in low sodium and high sodium buffers, respectively, plotted as mean  $\pm$  s.e.m. In each case, agonist responses were normalized to 100  $\mu$ M isoprenaline.

**Table 6.1:** Agonist potencies and maximal responses derived from TMR-G $\alpha$ s19cha18 binding in Low sodium buffer or extracellular high sodium media.

Ligands	Low Sodium				High Sodium			
	pEC <sub>50</sub>	±s.e.m	R <sub>max</sub>	±s.e.m (%)	pEC <sub>50</sub>	±s.e.m	R <sub>max</sub>	± s.e.m (%)
<b>Salbutamol</b>	6.84	±0.16	49.2	±2.7	5.91	±0.22**	26.6	±3.4***
<b>Salmeterol</b>	10.32	±0.18	57.1	±3.5	9.85	±0.21	32.4	±1.6***
<b>Isoproterenol</b>	7.25	±0.12	100.6	±1.3	6.15	±0.09**	101.1	±1.2
<b>Formoterol</b>	9.68	±0.18	83.7	± 3.1	9.02	±0.21*	78.0	±3.2
<b>ICI118551</b>	-		-3.14	±1.6	-		1.50	±1.4

Data parameters are presented as mean ± s.e.m and are from 5 different experiments per environment. For ICI118551, the effect at 10 mM antagonist is recorded as R<sub>max</sub>. Significant differences between pEC<sub>50</sub> or R<sub>max</sub> data in the two buffers are indicated by \* P<0.05, \*\* P<0.01, \*\*\* P<0.001 (unpaired Student's t-test).

A further advantage of the NanoBRET methodology was the homogeneous assay format and the ability to collect the time dependent kinetics data of TMR- Gas19cha18 recruitment for the different agonists, and subsequent receptor activation, over time (Figure 6.5). Fitting the rise to steady-state observed in the data enabled calculation of the initial rate of fluorescent G peptide probe recruitment at each agonist concentration, and to construct concentration-initial response rate relationships for the agonists as shown in Figure 6.5D, Table 6.2.

These data provided equivalent agonist potency and maximal response measurements to the endpoint concentration-response measurements performed under the same buffer conditions. This utility within kinetics-based assays, primarily as a result of the relative low affinity of the peptide tracer and rapid binding kinetics, provides TMR- Gas19cha18 with the ability to follow changes in receptor conformation faithfully during activation. This may prove beneficial compared to previously reported sensors that detect the active receptor conformation with very high affinity, including miniG proteins or Nb80 nanobody recruitment, or where the sensor is tethered in close proximity to the G protein binding site through fusion to the receptor C terminus (e.g. SPASM sensors)(Culhane et al., 2022; Gupte et al., 2017; Sadler et al., 2023; Touma et al., 2020).

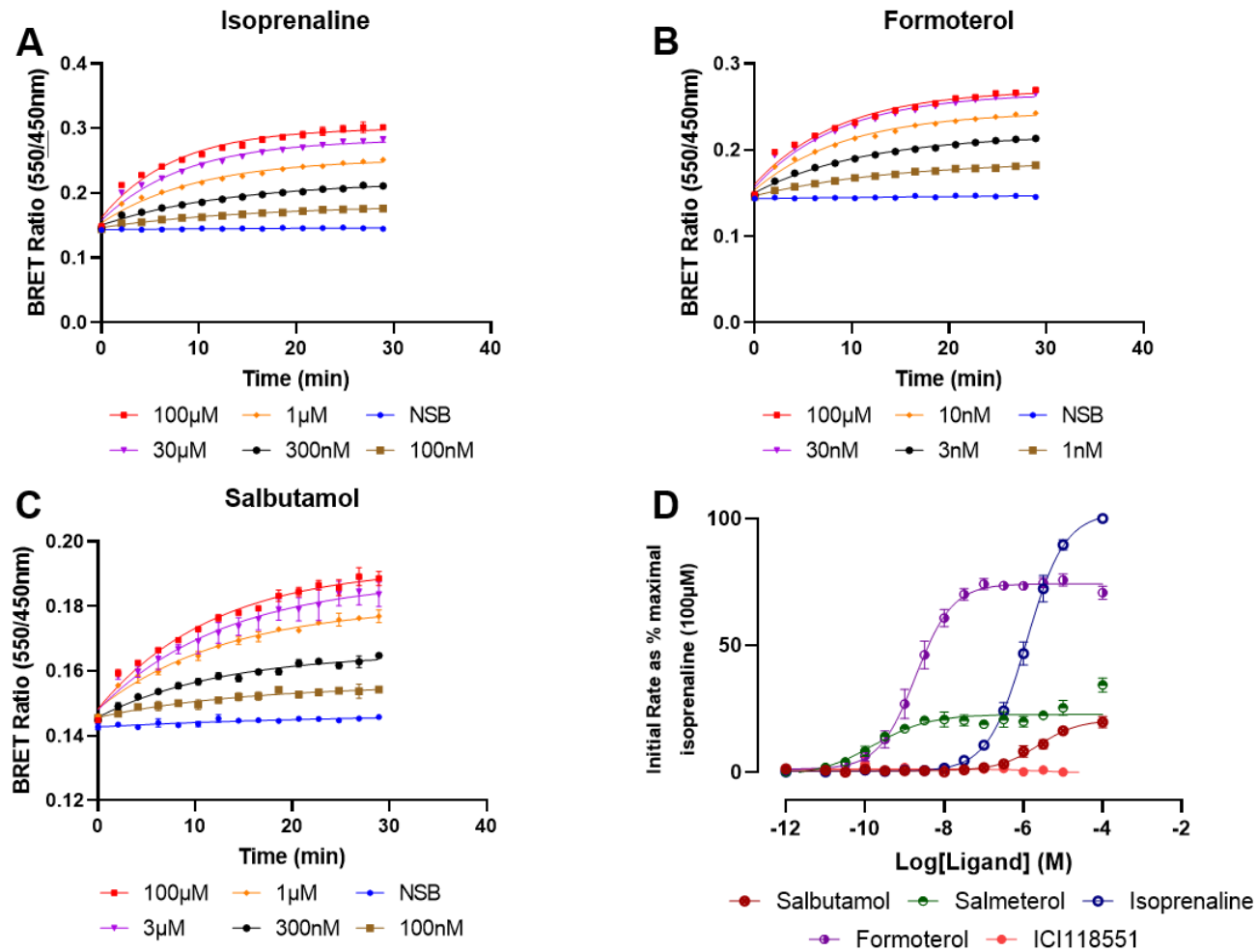


**Figure 6.5. The kinetics of TMR-*Gas9cha18* stimulated recruitment to the  $\beta_2$ -AR.** (A–C) show the concentration-dependent time courses of TMR-*Gas9cha18* recruitment measured by NanoBRET in high sodium buffer. Data are representative examples from five independent experiments. (D) Initial rates of TMR-*Gas9cha18* recruitment at each agonist concentration were calculated based on a rise to steady-state model and plotted to generate the pooled concentration–initial rate curves. Normalized data, plotted as mean  $\pm$  s.e.m, from four independent experiments are shown, to the 100  $\mu$ M isoprenaline response.

**Table 6.2:** Agonist potencies and maximal responses derived from TMR-G $\alpha$ s19cha18 binding using endpoint or kinetically derived data from high sodium experiments.

<b>Compounds</b>	<b>Endpoint</b>				<b>Kinetics rate</b>			
	pEC <sub>50</sub>	±s.e.m	R <sub>max</sub>	±s.e.m (%)	pEC <sub>50</sub>	±s.e.m	R <sub>max</sub>	±s.e.m (%)
<b>Salbutamol</b>	5.91	±0.22	26.57	±3.36	5.66	±0.20	20.18	±2.34
<b>Salmeterol</b>	9.85	±0.21	32.39	±1.57	10.02	±0.34	22.28	±2.51
<b>Isoproterenol</b>	6.15	±0.09	101.10	±1.15	5.92	±0.10	102.50	±0.87
<b>Formoterol</b>	9.02	±0.21	78.00	±3.23	8.73	±0.16	74.10	±1.73
<b>ICI118551</b>	-		1.5	±1.40	-		1.21	±0.59

Data are presented as mean ± s.e.m and are from 4-5 different experiments. Kinetic R<sub>max</sub> calculated as mean steady-state response at maximal concentration of ligand, Endpoint R<sub>max</sub> taken as response at maximal concentration of ligand.

Similarly, employment of unmodified TMR- *Gαs19* within these recruitment assays highlighted a similar tracer utility, with TMR- *Gαs19* also able to define both the full and partial agonism of isoprenaline and salmeterol respectively with comparable measurements to TMR-*Gαs19cha18*. Comparison of the tracers TMR- *Gαs19* and TMR- *Gαs19cha18* within the same assay indicated that the higher affinity ligand TMR- *Gαs19cha18* gave a greater  $R_{max}$  for both isoprenaline and salmeterol responses than the lower affinity peptide (TMR- *Gαs19cha18*, isoprenaline:  $R_{max}[\text{BRET ratio}] = 0.41 \pm 0.05$ ,  $pEC_{50} = 6.91 \pm 0.12$ , salmeterol:  $R_{max} = 0.28 \pm 0.03$ ,  $pEC_{50} = 9.14 \pm 0.16$ , TMR- *Gαs19* isoprenaline:  $R_{max} = 0.20 \pm 0.01$ ,  $pEC_{50} = 6.74 \pm 0.22$ , salmeterol:  $R_{max} = 0.18 \pm 0.01$ ,  $pEC_{50} = 9.18 \pm 0.07$ ,  $n=3$ , Figure 6.4&6.6). This change in  $R_{max}$  may be due to alterations in peptide structure changing the relative distance or orientation between the Nluc and TMR in each case. Despite this variability in  $R_{max}$ , both peptides were able to characterise the relative efficacies of agonists to the same degree – indicated by limited variation in  $pEC_{50}$  values – and both were able to produce maximal responses to salmeterol with a roughly 50% reduction in signal compared to the corresponding isoprenaline response.

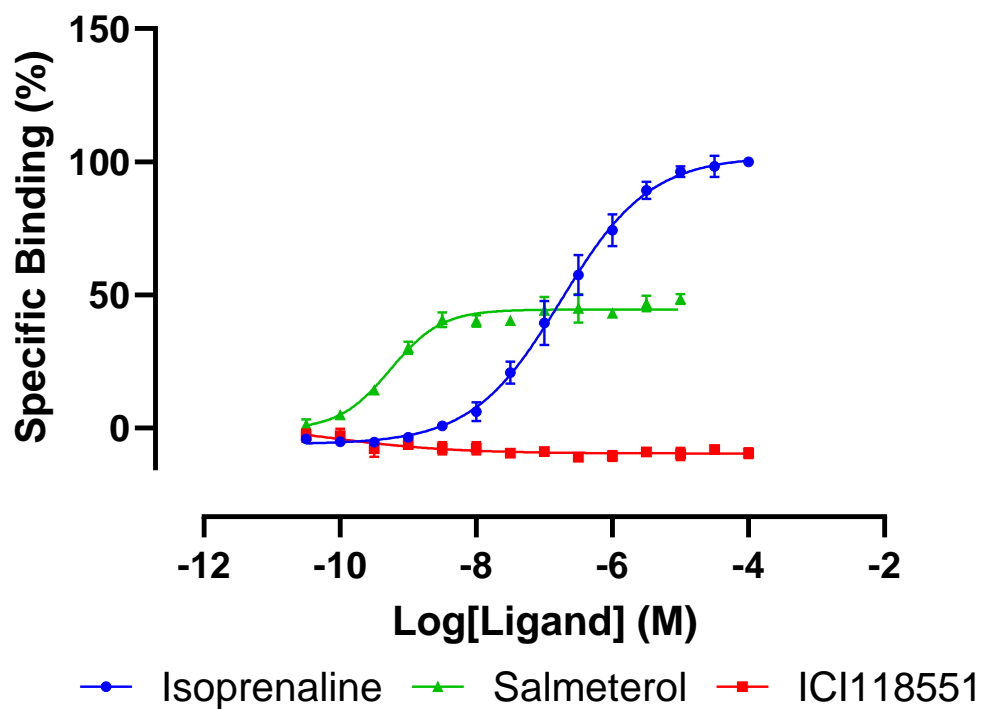


**Figure 6.6. Agonist-dependent recruitment of TMR-Gas19 to ss $\beta$ 2-AR-tsNluc measured by NanoBRET.** Assays were performed using 500 nM TMR-peptide with endpoint binding measured after 30-minutes, 37°C, exposure to different  $\beta$ <sub>2</sub>-AR orthosteric ligands, to construct concentration–response relationships. Data are pooled, normalized, data from three independent experiments, plotted as mean  $\pm$  s.e.m. Normalization defined by isoprenaline response.

#### 6.5.1.2. Characterising TMR- G $\alpha$ s19cha18 selectivity for example G $_s$ and G $_i$ coupled receptors

NanoBRET binding assays employing chemokine receptor CXCR2, a G $_i$  selective GPCR, or G $_s$  selective prostanoid receptors EP $_2$ /EP $_4$ , Adenosine receptor 2A (A $_{2A}$ ) and  $\beta_1$ -adrenoceptors indicated the selectivity of TMR- G $\alpha$ s19cha18 binding and recruitment for G $_s$  coupled GPCRs (Figure 6.7). Stimulation of CXCR2-tsNluc membranes with its peptide agonist CXCL8 28-99 did not increase TMR- G $\alpha$ s19cha18 recruitment above basal levels. Conversely, PGE $_2$  stimulation of the EP $_2$ -tsNluc receptor and isoprenaline stimulation of  $\beta_1$ -adrenoceptors in membranes demonstrated an agonist concentration-dependent increase in TMR- G $\alpha$ s19cha18 NanoBRET (pEC $_{50}$ = 6.55  $\pm$  0.14, n=3), with levels of specific binding similar to previous  $\beta_2$ -AR responses.

Interestingly, initial screening of G $_s$  coupled receptors failed to identify TMR-G $\alpha$ s19cha18 binding to EP $_4$  or A $_{2A}$  regardless of agonist stimulation (Figure 6.8). Structural data mapping the G $\alpha_s$  binding site highlights both receptors having similar hydrophobic pockets able to house  $\alpha 5$  helices, however, alterations within the C terminal region of the GPCR, especially in the case of elongations of the C terminus, may reduce measurement of peptide binding. Both EP $_4$  and A $_{2A}$  have C terminal tails considerably longer than the other G $_s$  receptors tested, which, when fused with the luciferase, increases both the flexibility and distance between acceptor and donor potentially attenuating the measurable BRET signal. Additionally, recent findings have alluded to the role of both ICL3 and C terminal tail regions in sterically hindering G protein binding (Sadler et al., 2023). Potentially subtype differences in these regions outside the C terminal peptide binding site may have additional impacts in the tracer binding observed.

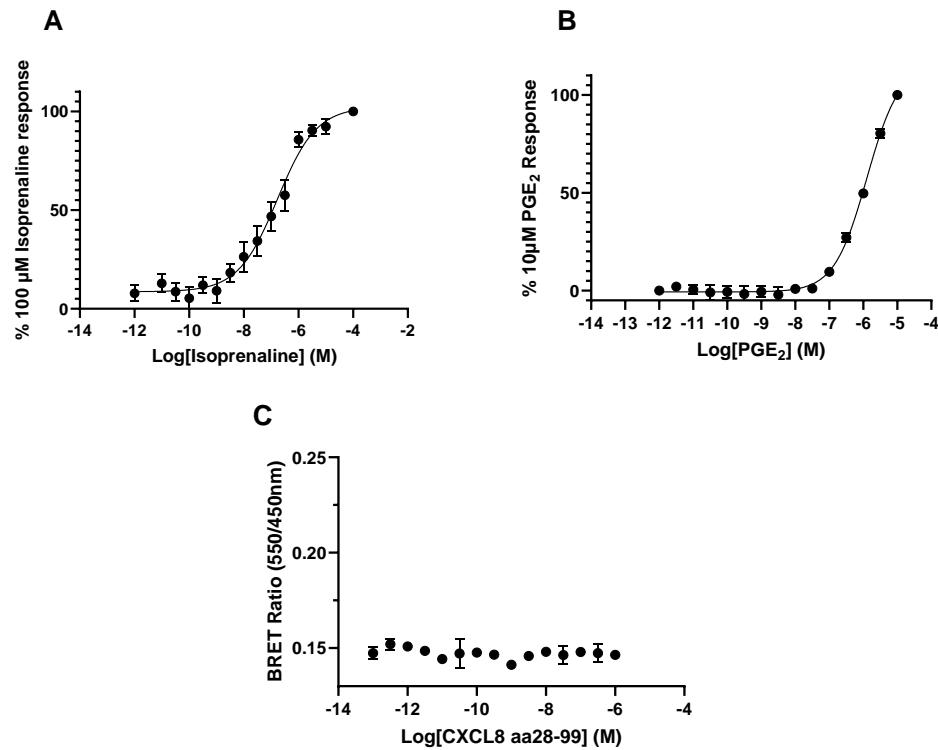


**Figure 7. Agonist-dependent binding of TMR-Gas19cha18 to various GPCRs.** (A) Agonist stimulated recruitment of TMR-Gas19cha18 to the  $\beta_1$ -adrenoceptor. Data are pooled, normalised data from 5 independent experiments. (B) Recruitment of TMR-Gas19cha18 to EP<sub>2</sub>-tsNluc measured by NanoBRET after PGE<sub>2</sub> stimulation (30 min). (C) TMR-Gas19cha18 NanoBRET measurements performed in ssCXCR2-tsNluc membranes in the absence or presence of the chemokine CXCL8 28-99(30 min). For each receptor, data represent an individual duplicate experiment displaying mean  $\pm$  SD, from three performed.

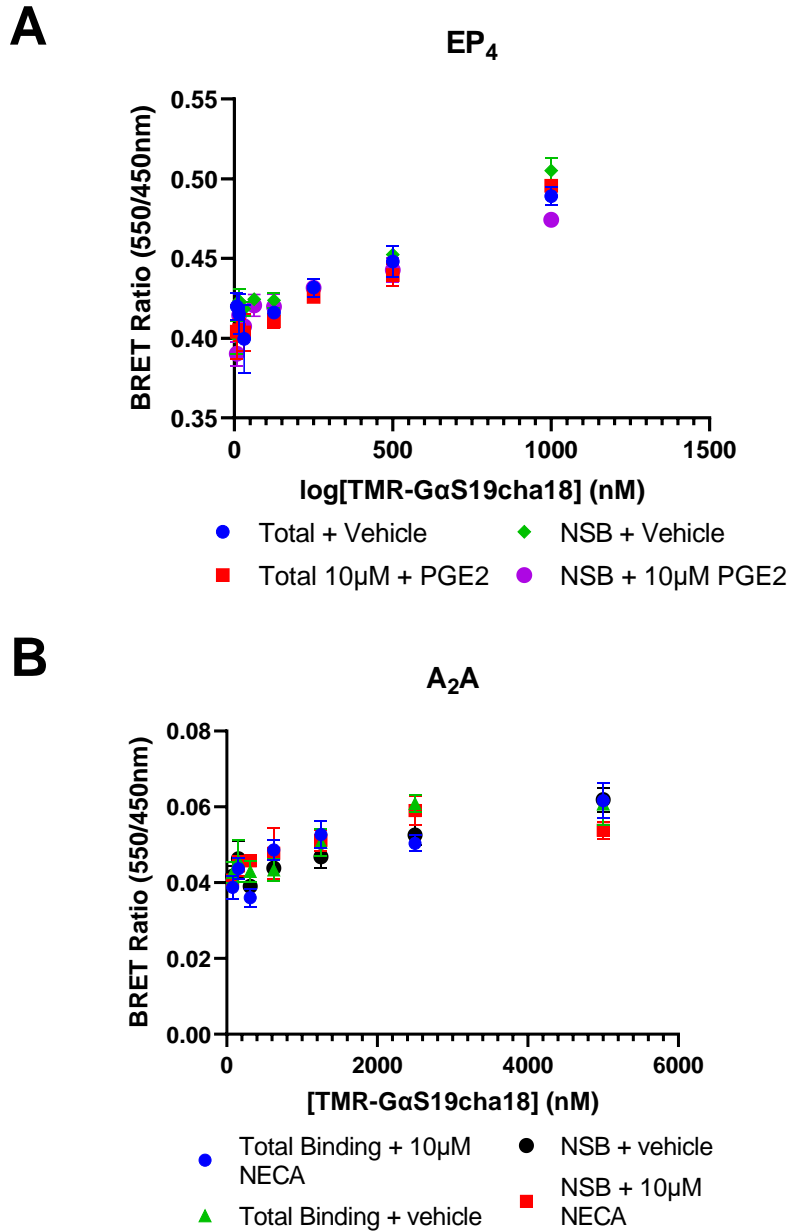


**Figure 6.8. Saturation binding studies to explore the binding capabilities of TMR-Gαs19cha18 at the prostaglandin EP<sub>4</sub> and Adenosine A<sub>2A</sub> receptors.** (A) Saturation binding of TMR-Gαs19cha18 at the EP<sub>4</sub> receptor under vehicle and agonist (10 µM PGE<sub>2</sub>) conditions. (B) Saturation binding of TMR-Gαs19cha18 at the A<sub>2A</sub> receptor under vehicle and agonist (10µM NECA) conditions. In both cases, Data are examples from two independent assays.

6.5.1.3. Using TMR- G $\alpha$ s19cha18 binding competition as a detection method for ligands binding the GsGPCR-G protein interaction site.

To determine whether TMR- G $\alpha$ s19cha18 could be used as a tracer in binding studies to obtain rank orders of affinity for putative IAMs, NanoBRET competition binding was performed in ss $\beta$ <sub>2</sub>-AR-tsNluc membranes, using the candidate unlabelled G $\alpha$  C-terminal peptides G $\alpha$ s19cha18, G $\alpha$ s19, G $\alpha$ s24, G $\alpha$ s11, G $\alpha$ i24 and PalmG $\alpha$ s19cha18 (Table 6.3), in the presence of isoprenaline (Figure 6.9). The inclusion of an N terminal palmitic acid modification (PalmG $\alpha$ s19cha18) was hypothesised to bring about an increase in peptide affinity due to an increase in peptide translocation to the plasma membrane.

Table 6.3. Amino acid sequences of screened G $\alpha$  C-terminus peptides

Name	Sequence (N-C terminus left to right)
<b>G<math>\alpha</math>s11</b>	Q RMHLR QYELL
<b>G<math>\alpha</math>s24</b>	NIRR VFNDC RDIIQ RMHLR QYELL
<b>G<math>\alpha</math>s19</b>	FNDC RDIIQ RMHLR QYELL
<b>G<math>\alpha</math>s19cha18</b>	FNDC RDIIQ RMHLR QYE{CHA}L
<b>PalmG<math>\alpha</math>s19cha18</b>	palmitoyl-FNDC RDIIQ RMHLR QYE{CHA}L
<b>G<math>\alpha</math>i24</b>	NVQFVFDVAV TDVI IKNNLKDCGLF
<b>G<math>\alpha</math>i19cha18</b>	FDAV TDVI IKNNLKDCG{CHA}F

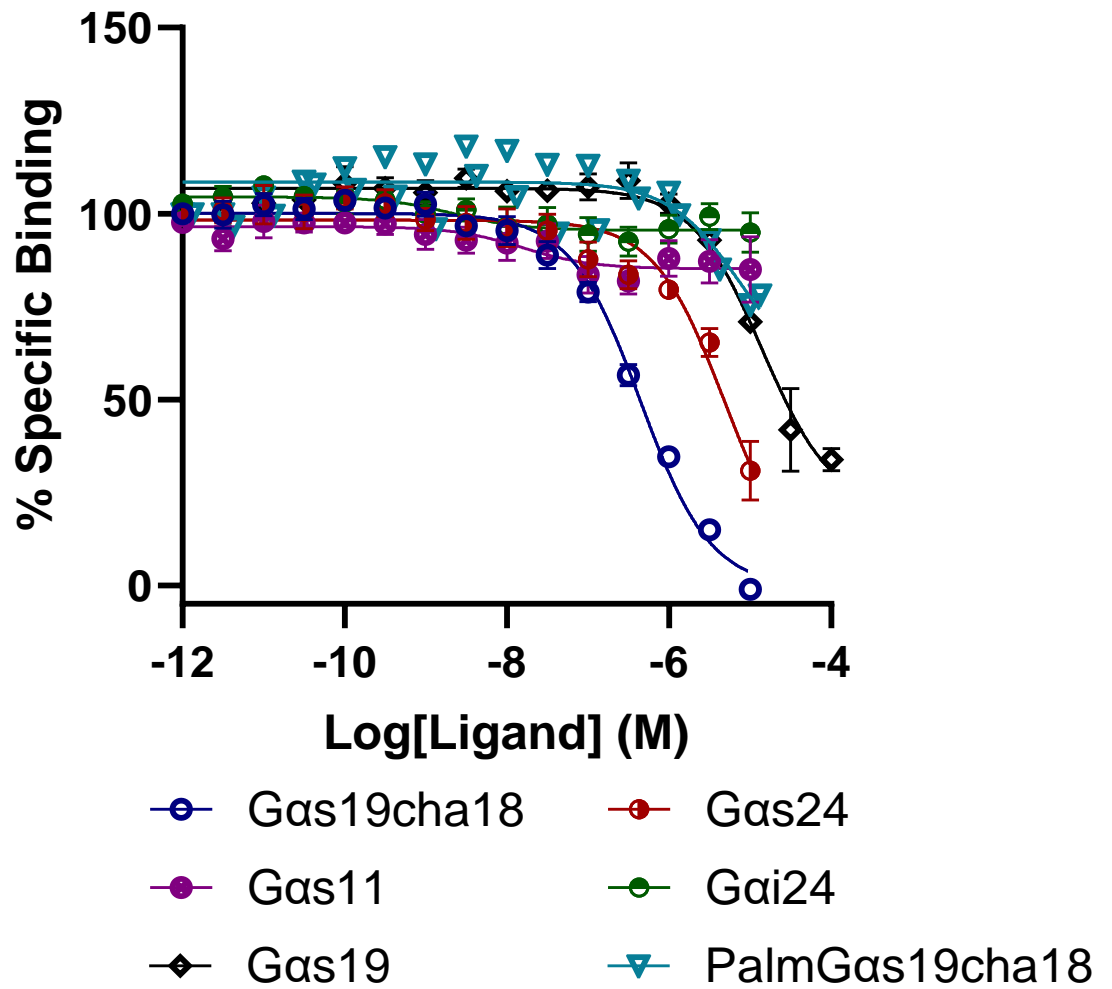


**Figure 6.9.** NanoBRET competition binding assays using TMR-Gas19cha18 to determine affinities of unlabelled Ga C terminal peptides for the ssβ<sub>2</sub>-AR-tsNluc receptor in membranes. Assays were performed in low sodium buffer, for 2h at 37°C using 500nM fluorescent tracer. Data are pooled and normalized from five independent experiments plotted as mean ± s.e.m. IC<sub>50</sub> curves were fitted based on an assumption of maximal competition (0%) defined by the high concentrations of Gas19cha18 peptide.

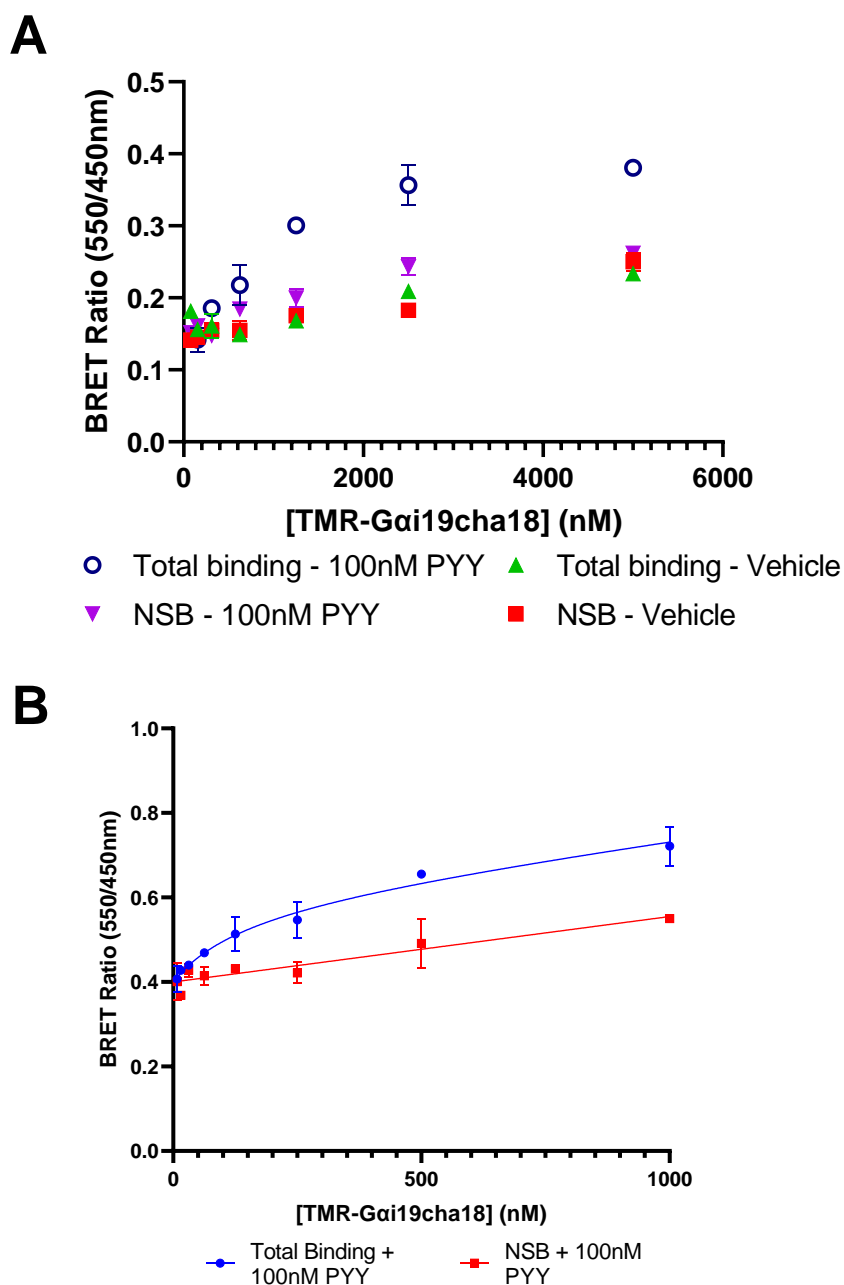
Gas19cha18, PalmGas19cha18, Gas19 and Gas24 successfully competed for the G protein binding site labelled by TMR-Gas19cha18, allowing derivation of their respective affinities (Gas19cha18 > Gas24 > Gas19 & PalmGas19cha18). The determined pK<sub>i</sub> for unlabelled Gas19cha18 (6.62 ± 0.06, n=5) was equivalent to that directly measured for the TMR-Gas19cha18 probe. Similarly, the reduction in affinity seen with the unmodified peptides follows the hypothesised order of allosteric efficacy displayed within TR-FRET studies, that elongation of the peptide sequence results in greater allosteric modulation. Gas24 provided a greater affinity for the intracellular site than the shorter, unmodified, Gas19 peptide. This unmodified peptide further validates our previous findings highlighting the role of the C terminal region within the context of GPCR binding, indicating the substitution of leucine18 for cyclohexylalanine results in a 41-fold increase in peptide affinity.

In contrast Gas11 and Gai24 did not display any detectable competition with the tracer peptide, even with a reduction in tracer concentration (Figure 6.9), supporting the predicted order of selectivity of the different peptides for α5 helix binding site for Gs coupled receptors. However, measurement of PalmGas19cha18 affinity indicated a similar affinity to the unmodified Gas19, and a 14-fold reduction in affinity compared to the unmodified Gas19cha18 peptide. This reduction in affinity, suggests that the addition of the palmitate may hinder the peptide's access to the G protein binding site, and / or does not perform as a lipid anchor to increase local concentration at the membrane as hypothesised .

#### 6.5.2. *Establishing a NanoBRET assay to directly monitor TMR-Gai19cha18 recruitment to the Y1 receptor*

In order to determine if these peptides couple to the Y1 intracellular region, the fluorescent tracer TMR-Gai19cha18 was produced. This peptide is formed from the final 19 amino acids of the Gα<sub>i2</sub> subunit,

again substituting the (conserved) penultimate leucine for a cyclohexylalanine residue. Initial assays utilised TMR-G $\alpha$ <sub>i</sub>19cha18 concentrations ranging from 5 $\mu$ M to 8nM, with the inclusion of 10 $\mu$ M unlabelled G $\alpha$ <sub>i</sub>19cha18 to define non-specific binding. TMR-G $\alpha$ <sub>i</sub>19ch18 specific binding was only evident with the inclusion of 100 nM PYY, an equivalent high affinity agonist of the Y1 receptor to NPY (Gehlert et al., 1997; Sheikh and Williams, 1990), with these data showing a small increase in BRET over vehicle and NSB controls. However, despite this high concentration range, comparison of multiple timepoints from 10 min to 2 h (not shown) measurements of peptide binding remained highly variable due to the inability of the NSB ligand to fully displace fluorescent ligand binding (resulting in a hyperbolic NSB curve), making derivation of true specific binding, and subsequently peptide K<sub>D</sub> inaccurate (Figure 6.10). The effect of the NSB ligand produced variable inhibition on an assay-to-assay basis (with no change to the experimental protocol) suggesting that it may be a result of poor peptide solubility, which is in line with the higher lipophilicity of the G $\alpha$ <sub>i</sub> peptide than that seen with the previous G $\alpha$ <sub>s</sub> peptide.



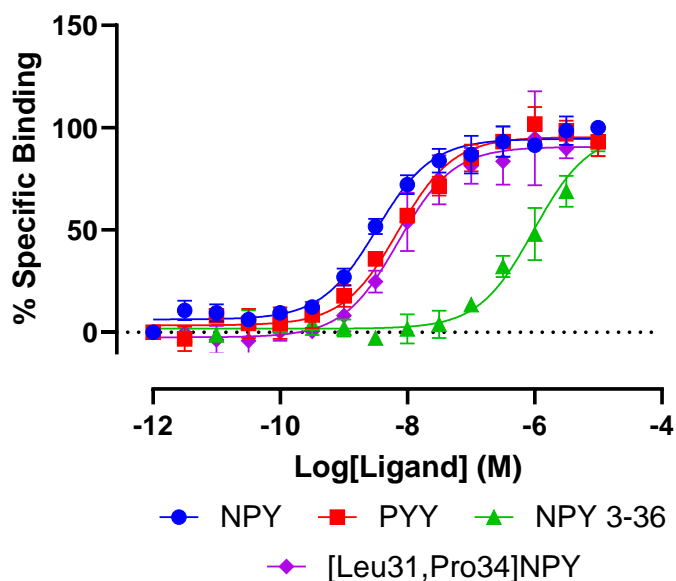


**Figure 6.11.** Agonist-dependent recruitment of TMR-G $\alpha$ i19cha18 to Y1-tsNluc measured by NanoBRET. Assays were performed using 1  $\mu$ M TMR-G $\alpha$ i19cha18 with endpoint binding measured after 10 min exposure to the Y1 endogenous agonists NPY, PYY, [Leu31, Pro34]NPY and NPY<sub>3-36</sub> to construct a concentration–response relationship. Data represent pooled, normalized, data from 3-4 individual experiments, plotted as mean  $\pm$  s.e.m.

**Table 6.4:** Agonist potencies derived from TMR-G $\alpha$ i19cha18 binding using 10-minute endpoint derived data.

Peptide	pEC <sub>50</sub>	$\pm$ s.e.m
NPY	8.45	$\pm$ 0.08
PYY	8.13	$\pm$ 0.06
NPY <sub>3-36</sub>	6.30	$\pm$ 1.53
[Leu31, Pro34]NPY	7.05	$\pm$ 1.12

Data are presented as mean  $\pm$  s.e.m and are from 3-4 different experiments.

Despite an inability to quantify the probe affinity with a high degree of accuracy, further exploration of the agonist dependent recruitment of TMR-G $\alpha$ i19cha18 was merited. 1 $\mu$ M tracer was used to probe receptor activation and relative efficacy of known agonists at rY1. TMR-G $\alpha$ i19cha18 was incubated with varying concentrations of NPY, PYY, NYY<sub>3-36</sub> and both endpoint and kinetic NanoBRET measurements were taken over a 30-minute interval. Endpoint data allowed for the ranking of the agonists in the expected order of efficacy, with NPY, [Leu31, Pro34]NPY and PYY displaying similar pEC<sub>50</sub> profiles and NPY<sub>3-36</sub> displaying a marked decrease in pEC<sub>50</sub> (Figure 6.11, Table 6.4)(Gehlert et al., 1997). Kinetic analysis (as described for  $\beta_2$ -AR data) was also attempted however, due to the small measurement window obtained within these NanoBRET assays, small variations in assay conditions resulted in a large amount of signal variation and subsequently result in the kinetic data having insufficient quality for robust measurements to be obtained (data not shown).

Through employment of TMR-G $\alpha$ i19cha18, the relative binding affinities of unlabelled peptides G $\alpha$ i19, G $\alpha$ i19cha18 and G $\alpha$ i24 were compared in real time by direct competition analysis, in the presence of 800nM NPY (Figure 6.12). Only G $\alpha$ i19cha18 displayed complete competition with the fluorescent probe for the G protein binding site with a pIC<sub>50</sub> of  $6.36 \pm 0.22$ . This was not further converted to a K<sub>i</sub> using the Cheng-Prusoff correction in the absence of an accurate tracer K<sub>d</sub> value. Nevertheless, the observed capacity for G $\alpha$ i19cha18 to compete highlights the conserved beneficial effects the CHA modification has on peptide affinity at both G<sub>s</sub> and G<sub>i</sub> classes of receptor, and indicates the lower affinity of the unmodified G $\alpha$ i19 and G $\alpha$ i24.

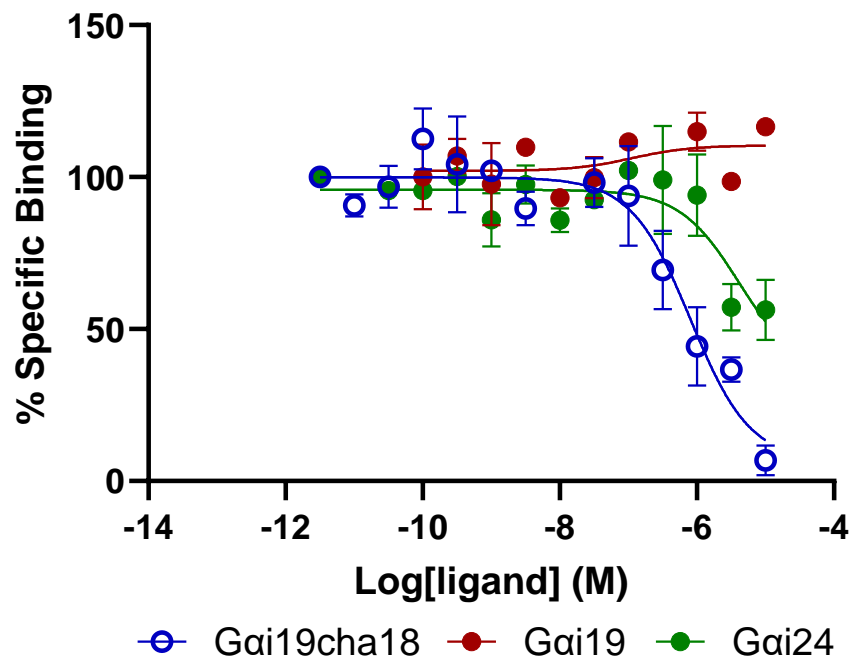


**Figure 6.12.** NanoBRET competition binding assays using TMR-Gai19cha18 to determine affinities of unlabelled Gα C terminal peptides for the ssY1-tsNluc receptor in membranes. Assays were performed in high calcium, low sodium buffer, for 2 h at 37°C using 1 μM fluorescent tracer under 800nM NPY conditions. Data are representative from four independent experiments.

In combination, these NanoBRET data highlights the ability of  $G\alpha_i$  C terminal peptides to bind to the G protein binding site of Y1, with specific binding in the presence of orthosteric agonist peptides, but a reduced window compared to the  $\beta_2$ -AR-TMR-Gs19cha18 peptide system. The earlier TR-FRET study (chapter 4) did not reveal a significant impact of  $G\alpha_i24$  or  $G\alpha_i19$  peptides on orthosteric agonist affinity (in contrast to  $G\alpha_s$  C terminal peptide allosteric behaviour at the  $\beta_2$ -AR system). Collectively this may indicate that  $G_i$  peptide binding affinity is not greatly increased by activation of the Y1 receptor conformation using NPY. This is in line with previous findings indicating high basal levels of  $G\alpha_i$  G protein-GPCR coupling to inactive receptors and the inability of shorter  $G\alpha_i$  peptides to promote receptor conformational change (Gilchrist et al., 1998; Seifert and Wenzel-Seifert, 2002). Clearly other factors, including the lower  $G_i$  peptide affinity, and the relative orientation and distance of the NanoLuc and TMR- $G\alpha_i19cha18$  bound biosensor, might also contribute to lower BRET signal for the Y1 biosensor. However, these results do demonstrate the principle that  $G_i$  peptidomimetics can also be produced as biosensors for the measurement of receptor activation and relative agonist efficacy, and identification of intracellular allosteric modulators at  $G\alpha_i$  coupled receptors.

### 6.5.3. *Characterisation of TMR-Gai19cha18 binding at alternate GiPCRs*

The observations seen within the  $\beta_2$ -AR/G $\alpha_s$  peptide system show that G $\alpha_s$  derived peptides have the potential to act as more universally applicable biosensors. This is hypothesised to hold true for G $\alpha_i$  derived peptides due to their displaying similar characteristics when employed at the Y1 receptor. Using alternative G $\alpha_i$  selective receptors: Mu opioid receptor (MOR), CXCR2, and mGluR2, the broader utility of the TMR-G $\alpha_i$ 19cha18 was examined.

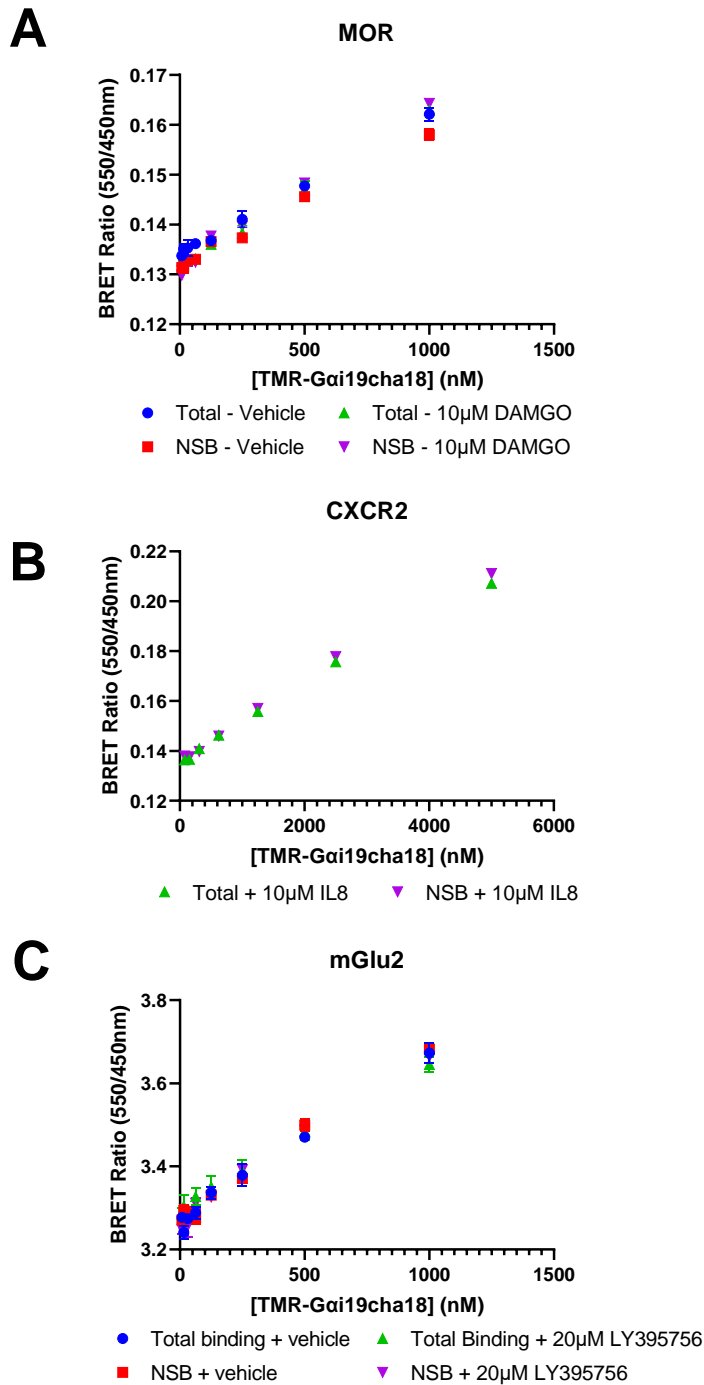


**Figure 6.13. TMR-*Gas19cha18* binding at alternate  $G\alpha_i$  coupled receptors. CXCR2 and mGlu2, in membrane preparations (A) MOR binding under vehicle and agonist conditions. (B) CXCR2 binding under agonist conditions. (C) mGlu2 binding under vehicle and agonist conditions. In all cases, data are representative experiments from three performed, taken after 30-minutes incubation at 37°C. In all cases, raw luminescence (NanoLuc) output was monitored to ensure suitable receptor expression.**

Initial saturation binding experiments at Y1 suggest TMR-G $\alpha$ <sub>i19cha18</sub> has a much lower affinity than the G $\alpha$ <sub>s</sub> counterpart. Given the variability in agonist dependent TMR-G $\alpha$ <sub>s19cha18</sub> peptide binding displayed across members of the G $\alpha$ <sub>s</sub> receptor family in section 6.5.1.2, it is likely a similar variation may be present across G $\alpha$ <sub>i</sub> coupled receptors.

Analysis of TMR-G $\alpha$ <sub>i19cha18</sub> binding across additional G $\alpha$ <sub>i</sub> coupled receptors showed no significant binding for all receptors tested at chosen tracer concentrations in the presence of predicted maximal concentrations of the chosen agonist. For the MOR and mGluR2, it was also observed that no specific binding was evident in the absence of DAMGO or LY395756. The inability of TMR-G $\alpha$ <sub>i19cha18</sub> to couple to mGlu2 is not unexpected (Figure 6.13A). mGlu2 is a member of the Class C family of GPCRs which employing alternative G protein binding methods to the more classical Class A family. Structurally, Class C receptors maintain the classical 7TM structure, however, have additional N-terminal, extracellular, venus-flytrap domains used for endogenous ligand binding (Cacabelos et al., 1999; Gómez-Santacana et al., 2022; Kammermeier, 2012). Furthermore, G $\alpha$ <sub>5</sub> helix binding is thought to be more topographically arranged at the receptor intracellular surface and less embedded within the mGluR2 receptor which, along with alternative conformational changes as a result of receptor activation, suggests peptide interactions are likely to be distinct to class A responses (Seven et al., 2021).

In regard to the MOR, previous data presented by Kossoń *et al* suggested 24 amino acid long G $\alpha$ <sub>i</sub> derived peptides are able to couple, and modulate, MOR agonist interactions (Kossoń et al., 2023). However, the data presented showed no significant differences between agonist affinities in the absence or presence of G $\alpha$ <sub>i24</sub> 100 $\mu$ M peptide environments, bearing in mind the use of a competition binding methodology in which both the radiolabelled DAMGO tracer and competing ligands were agonists potentially

susceptible to allosteric modulation. This is in agreement with the binding data generated using TMR-G $\alpha$ i19cha18, which displayed no binding under vehicle or saturating agonist conditions (Figure 6.13C). Additionally, incorporating the displayed lack of binding at CXCR2 (Figure 6.13B) suggests that Gi peptide binding is much more variable across receptor types compared with its Gs counterpart.

## 6.6. Chapter discussion

Previous TR-FRET findings in Chapter 4 highlighted a potential role for G $\alpha$  derived peptides in directly monitoring the GPCR-G protein binding site through binding in an agonist dependent manner. This led in this Chapter to the generation of fluorescent G peptide probes able to couple to various GPCRs (in a G protein selective manner) in an agonist-dependent manner. For the Gs,  $\beta_2$ -AR system, the generation of both a modified and unmodified 19 amino acid peptide allowed for exploration of the findings put forward by Mannes et al, allowing characterisation of peptide affinity for the  $\beta_2$ -AR directly (Mannes et al., 2021). TMR-peptide saturation binding studies displayed clear specific binding to the  $\beta_2$ -AR using NanoBRET and indicated the necessity for an agonist to be present to facilitate tracer recruitment. These findings highlight incorporation of the non-native amino acid cyclohexylalanine residue at the 18 position (-2 G $\alpha_s$  position) results in a five-fold increase in affinity over the unmodified peptide, corroborating previous TR-FRET data and indicating an increase in allosteric efficacy upon CHA inclusion. This strengthens evidence for the importance of the hydrophobicity provided by this terminal amino acid region in the binding mechanism employed by Gs coupled GPCRs (Mannes et al., 2021).

The displayed agonist dependent binding observed by both Gs peptides provides an interesting insight into G $\alpha$ - $\alpha$ 5 interactions.

Recent molecular dynamic simulations by Amirhossein Mafi *et al* (2023) suggests the  $\alpha 5$  helix displays reduced receptor interactions (at the  $\beta_2$ -AR) when binding with the inactive state, however, upon receptor activation, embeds deeper within the binding pocket and forms stronger interactions, facilitating receptor conformational change towards the active state (Mafi *et al.*, 2023). Assimilation of these findings in the context of presented peptidomimetic tracers provides evidence in support of these simulations and may allow greater understanding of the mechanisms driving the displayed agonist dependent binding. The inability to detect peptide tracer binding without receptor activation suggests these tracers do not provide strong enough interactions with the inactive state to allow significant binding above non-specific measurements, however, the increased binding at (and therefore affinity for) the active conformation. This can be explained through incorporation of knowledge seen within active state GPCR X-ray and cryo-EM structures, which display a widening of the intracellular binding site on activation. This allows greater access to the binding pocket and therefore a greater number of interactions between  $G\alpha\text{-}\alpha 5/G\alpha\text{-}$  peptide and receptor, an explanation corroborated within these simulations (Mafi *et al.*, 2023; Weis and Kobilka, 2008).

From a practical sense, this agonist dependent binding provides these peptide tracers an additional utility to that originally hypothesised. This relationship is indicative of the peptide's ability to exclusively couple to the receptor active conformation and, therefore, application of a single concentration of peptide allows for direct measurement of orthosteric agonist potency and efficacy at the level of receptor activation. The ability of peptide recruitment to facilitate distinction between full agonist and partial agonist responses validated this functionality as an activation sensor, much in the same way as alternative tracers such as miniG proteins and nanobodies (Heukers *et al.*, 2019). Where these peptides differ is in the relatively low affinity they display compared with these

predefined methodologies. The initial role of miniG proteins and nanobodies was within structural studies, allowing stabilisation of particular receptor conformations, has resulted in their having much higher, semi-irreversible binding mechanisms which limits their utility in the context of ligand kinetics. The lower affinity afforded by these peptides allows for their fast rate of association and therefore employment in the characterisation of agonist response kinetics, allowing collection of both equilibrium and time-dependent agonist behaviour.

Similar profiling of the  $G\alpha_i$  derived fluorescent tracer indicates the binding model displayed by TMR- $G\alpha_s$ 19cha18 is applicable more universally in the case of  $G\alpha$  C terminal peptides. TMR- $G\alpha_i$ 19cha18 displayed specific binding at the intracellular binding site of the Y1 receptor, however, with a reduced affinity and  $B_{max}$  than that seen in  $Gs$ - $\beta_2$ -AR assays. This is not unexpected when in combination with the lack of allosteric efficacy seen in previous TR-FRET assays, and in the context of literature regarding  $G\alpha_i$  binding more generally (Seifert and Wenzel-Seifert, 2002).  $G\alpha_i$  is the most common secondary messenger (excluding arrestins) utilised by class A GPCRs, and it has been shown to have greater constitutive activity in comparison with  $G\alpha_s$  and  $G\alpha_q$  coupled receptors (Seifert and Wenzel-Seifert, 2002). Gilchrist *et al* (1998) further highlight the ability of  $G\alpha_i$  peptides to inhibit GPCR function without displaying a change in receptor conformation towards the active state, in line with presented TR-FRET findings (Gilchrist *et al.*, 1998). Together, this suggests a weaker interaction is present between  $G\alpha_i$  subunits and GPCRs compared to other G protein subtypes, which is reflected in the binding and modulatory profiles displayed by our  $G\alpha_i$ 19cha18 peptide. Additionally, the inability of TMR- $G\alpha_i$ 19cha18 to bind to alternative  $G\alpha_i$  coupled receptors corroborates more recent findings suggesting  $G\alpha_i$  protein binding in particular employs much greater reliance on alternative sites of interaction beyond the  $\alpha 5$  helix (e.g.,

ICLs), thus limiting the putative affinity of the G $\alpha$ 5 helix peptides further depending on receptor type (Ham et al., 2021; Huang et al., 2022).

A key application of TMR-G $\alpha$ s19cha18 NanoBRET assays would be the ability to directly determine the affinities of unlabelled ligands at the G protein binding site through competition analysis, for example, in the identification of new lead IAMs. Previously, such studies have only been achieved through the generation of specific radioligand IAM probes for particular receptors, such as CXCR2, or through structural studies with limited pharmacological evaluation (Liu et al., 2017a; Salchow et al., 2010). Establishing a NanoBRET competition screening assay for  $\beta_2$ -AR-Nluc (in the presence of saturating concentrations of isoproterenol) provided a proof of concept to this peptide's role in ligand identification, with complementary G $\alpha$ i peptide/Y1 assays suggesting this relationship extends to alternative G $\alpha$  peptides. This allowed quantitative affinity estimation for the unlabelled peptides G $\alpha$ s19cha18, G $\alpha$ s19 and G $\alpha$ s24, and confirmed the lack of affinity of G $\alpha$ s11 and G $\alpha$ i24 for the  $\beta_2$ -AR intracellular site—dovetailing with the indirect measurements of their action on orthosteric agonist binding in chapter 4. Additionally, this allowed for further exploitation of alternative peptide modifications and their effect on peptide binding. The addition of a palmitoyl residue at the peptide N-terminus was hypothesised to increase peptide recruitment to the receptor, however, competition analysis indicates a large reduction in affinity compared to G $\alpha$ s19cha18 (Covic et al., 2002). This reduction is thought to be the result of the palmitoylation resulting in increased steric hindrance, limiting peptide binding within the G protein binding site, or not driving membrane association as expected. Additional competition experiments employing TMR-G $\alpha$ i19cha18 at the Y1 receptor also displayed the ability for competition at the G $\alpha$ i binding site. The limitations presented in TMR-G $\alpha$ i19cha18's saturation binding characterisation limits the

ability for accurate derivation of unlabelled ligand affinity via the Cheng-Prusoff correction, nevertheless, these assays do provide a proof of concept for the employment of Gi derived peptides within similar screening assays.

One consequence of the observed probe selectivity for the agonist-occupied receptor conformation is that, in future screening efforts, such binding assays are likely to reveal negative allosteric modulators with a preference for the receptor active state, which would provide them with a use-dependent mode of action(Jiang et al., 2020). This provides an additional route for therapeutic selectivity by allowing therapeutic targeting to particular regions (e.g., neuronal synapses or sites of inflammation) where the target receptors are highly active, avoiding a more general inhibitory profile that might lead to undesired on-target effects due to the uncompetitive ligand potency increasing at the target site(Boulton et al., 2018).

It is important to note, however, that despite displaying an ability to determine the affinity of unlabelled peptides of similar chemical size, there is a distinct possibility that competition may be limited in the context of small-molecule ligands. Therefore, it is essential to further characterise the ability of G $\alpha$  peptidomimetics to compete with small-molecule allosteric modulators (see chapter 8).

**Chapter 7. Results III**  
Employing Fluorescence  
Correlation Spectroscopy (FCS) to  
determine TMR-Gαs19cha18  
stoichiometric binding  
relationships and GPCR low-  
affinity conformation binding.

## **7. Employing Fluorescence Correlation Spectroscopy (FCS) to determine TMR-Gas19cha18 stoichiometric binding relationships and GPCR low-affinity conformation binding.**

### 7.1. Chapter introduction.

The utility of fluorescent ligands extends beyond the binding assays described thus far. Despite the growing number of luminescence and fluorescence-based plate reader assays available, these techniques are limited in their ability to characterise ligand interactions at a receptor microdomain level. Such limitations result in these assays being unable to accurately address questions relating to changes in ligand-receptor complex distribution, composition and stoichiometry, and multiple ligand-receptor binding events within microdomains. The application of fluorescence technology has facilitated a rapid expansion in light microscopy techniques, allowing for a plethora of approaches to explore a diverse range of biological functions. In particular, advancements in confocal microscopy have facilitated the development of highly sensitive biophysical techniques for the exploration of receptor-ligand interactions at the molecular level, including fluorescence correlation spectroscopy (FCS) and photon counting histogram (PCH) analysis (introduced in section 7.2.1). This chapter aims to explore the utility of fluorescent G protein mimetic tracers within these highly sensitive systems, allowing a greater understanding of peptide-GPCR interactions at the allosteric G protein binding site, and providing a basis to facilitate future exploitation of these tracers within microscopy-based assays.

## 7.2. Introduction

### 7.2.1. *Fluorescence correlation spectroscopy as an approach to measure receptor-ligand interactions.*

Fluorescence correlation spectroscopy (FCS) offers a highly sensitive methodology for the detection of molecular dynamics at the single receptor level. Initially described in 1972 (Magde et al., 1972), FCS did not become a technique for mainstream biological research until its integration with confocal microscopy in 1993 (Rigler et al., 1993), allowing for much smaller observation volumes (around 0.25 fL) to probe microdomain regions of biological samples. FCS is a quantitative technique with single molecule sensitivity which exploits the fluctuations in detected photons emitted (fluorescent intensity) from a fluorescent source (e.g. a labelled ligand or receptor protein) moving in and out of a stationary confocal volume over a set time period. These fluctuations are then used to determine the speed and number of the fluorescent species within the sample volume. Statistical analysis of the time-dependency of these fluctuations using autocorrelation analysis allows the average dwell time ( $\tau_D$ ) of the fluorescent moiety within the detection volume, and consequently its diffusion coefficient, to be determined (Goulding et al., 2021). Similarly, the amplitude of the autocorrelation curve is inversely proportional to the average number of fluorescent particles in the detection volume, from which particle concentration may be calculated. The inverse relationship makes FCS particularly sensitive for investigating low concentrations of particles, being especially useful as this methodology can be applied both to interactions occurring within a freely diffusing solution, or within a cellular system in situ. A variety of autocorrelation models can be fitted to the data, to account for 2D (e.g. within a cell membrane) and 3D models of diffusion, and multiple components with different rates of diffusion ( $\tau_{D1}$ ,  $\tau_{D2}$ ...) within the same sample volume. One influence on the diffusion coefficient of a fluorescent species is its size (for

unrestricted diffusion, a 2-fold change in  $\tau_D$  is representative of an 8 fold change in molecular mass). Thus, separation of multiple components can provide quantitative information on events which change the size and behaviour of receptor complexes (for example the change between free and bound small molecule ligands in receptor interaction (Stephen J. Briddon et al., 2004; Kilpatrick and Hill, 2016; Middleton et al., 2007)).

Additionally, the fluorescence intensity fluctuations over time captured during FCS can be analysed via the photon counting histogram (PCH) (Huang et al., 2004). PCH analysis is used to determine the molecular brightness of a fluorescent species, as well as its abundance. PCH analyses the fluctuation traces in respect to amplitude. The trace is divided into time bins, with the number of photons per bin counted and a frequency histogram generated. The resultant distribution is a combination of a number of Poissonian processes including the point-spread function of the microscope, the distribution of the fluorescent species, and the detector response characteristics. When the bin time used is less than the dwell time of the species within the volume, the resultant histogram deviation from the expected Poissonian distribution can be fitted to obtain the molecular brightness ( $\epsilon$ ; photons per second per molecule) and a particle number ( $N$ ) of the fluorescent species to be determined. This allows for the identification of particles of varying brightness, and when normalised to a control of known organisation, can provide evidence for different stoichiometries of ligand-receptor signalling complexes (e.g., transient or agonist induced changes in receptor dimerization or agonist-induced formation of aggregates within clathrin coated pits) (S. J. Briddon et al., 2004; Cordeaux et al., 2008; Ilien et al., 2009; Kufareva et al., 2014; Parmar et al., 2017; Philip et al., 2007). In comparison to FCS analysis of diffusion co-efficient changes, PCH molecular brightness is more sensitive to changing stoichiometry (a 2:1 versus 1:1 change in fluorescent ligand binding produces a 2x change in  $\epsilon$ ). Together

FCS and PCH combined allow estimation of particle relative concentrations and brightness, allowing for analysis of intricate interactions between labelled and unlabelled species at low concentrations (Briddon et al., 2018; Grime et al., 2020; Huang et al., 2004).

By employing these analyses in the context of fluorescent ligand interactions, it is possible to determine both ligand binding in the presence of receptors, and the number of fluorescent species interacting per receptor in either a solution-based system or whole cell environment (Grime et al., 2020; Lay et al., 2022). Particular examples of the utility of this technique can be demonstrated by Lay *et al* (2022), whereby solution-based FCS is used to determine populations of mono- or multi-labelled TMR-IL-23 within a single reaction sample, and Briddon *et al* (2004), which employs FCS to determine fluorescent ligand binding at the A<sub>1</sub>-AR receptor at a single cell level both at the cell membrane and intracellularly (Briddon et al., 2004; Lay et al., 2022). In the case of solution-based FCS for detecting ligand binding, it is necessary to provide all interacting partners within a freely moving environment. Practically, this relies on isolation of receptors from cell membranes, thereby providing the mobility necessary for accurate derivation of ligand binding.

### *7.2.2. Current methods for the solubilization of cell surface receptors*

The plasma membrane is a complex network of protein and lipid/phospholipid molecules, forming a distinct environment in which cell surface receptors carry out their function. Whilst receptor structure and function is determined primarily by the receptor amino acid sequence, a synergistic relationship must be established between membrane-spanning residues and membrane environment to maintain a stable conformation and function. Exploration of the interactions between receptors and their

surrounding environment have highlighted the importance of the lipid environment in facilitating receptor signalling. In particular, the formation receptor containing of “lipid rafts”, small (10–200 nm) domains enriched with cholesterol and sphingolipids that compartmentalize cellular processes, along with the identification of cholesterol binding sites in multiple class A GPCRs has highlighted potential routes for receptor signalling variability. For example, variation in  $\beta_{1/2}$ -AR vs EP<sub>2</sub> receptor driven adenylyl cyclase 6 activation in cardiac myocytes, with EP<sub>2</sub> signalling having reduced capacity to activate AC6 despite shared G $\alpha_s$  signalling through exclusion from lipid raft regions or driving particular changes in receptor-ligand interactions(Awasthi-Kalia et al., 2001; Hanson et al., 2008; Oates and Watts, 2011; Ostrom et al., 2001; Schwencke et al., 1999; Shamri et al., 2002). Subsequently, exploration and derivation of receptor structure and function using highly sensitive technologies, such as FCS and cryo-EM, requires the ability to extract single receptor proteins for study, while maintaining these in conformations that are functionally relevant to study ligand binding and signalling complexes.

A number of methods for isolating purified receptor proteins have been developed, which vary in the extent to which the native phospholipid membrane context around the receptor is preserved. to simulate the membrane environment. Pure detergent-based techniques disrupt membranes and solubilise receptors, for example using n-dodecyl- $\beta$ -D-maltopyranoside (DDM)(Harwood et al., 2021; Postis et al., 2015). DDM and other related detergents structurally mimic but are different from membrane phospholipids, containing polar head group and single alkyl chain, and remove receptors into detergent-based micelles with high efficiency while maintaining suitable aqueous solubility(Seddon et al., 2004). These have been used to great effect within structural biology to facilitate effective removal of membrane proteins without employing methodologies which may restrict or alter protein

conformation(Koehl et al., 2018; Liu et al., 2017a; Rasmussen et al., 2011; Thal et al., 2016). However, due to detergents having limited abilities to effectively mimic the native environment, the conformations of purified receptor proteins under study from those which are physiologically relevant. The stability of detergent extracted membrane proteins has also been shown to be highly variable depending on the protein of interest(Breyton et al., 1997; Helenius and Simons, 1975; Lee, 2011; Popot, 2010; Seddon et al., 2004). This led to exploration of alternative techniques for the extraction of membrane proteins without complete removal of surrounding membrane lipids, such as employing synthetic nanodiscs.

Polymer-based nanodiscs are typically 8-16nm in diameter and consist of a native phospholipid bilayer derived from the cell context in which the receptors are expressed, encircled by a helical membrane scaffold, such as polymerised styrene maleic-acid (SMA/SMALPs)(Knowles et al., 2009; Ratkeviciute et al., 2021). Polymer-based nanodiscs provide the advantage of allowing greater control over nanodisc size compared with micelle/detergent extraction and allow incorporation of varying degrees of the surrounding membrane environment. However, the sensitivity of SMA to ion concentrations (e.g.  $Mg^{2+}$ ), acidic pH below 7 and UV irradiation can be a limitation for certain types of experiment (Oluwole et al., 2017; Popot, 2010). Additionally, there is evidence that the conformational dynamics of GPCRs within SMALPs particularly is restricted, and therefore that the conformational dynamics of the SMALP encapsulated protein may differ from that of the native protein(Mosslehy et al., 2019; Routledge et al., 2020). Development of di-isobutylene maleic acid (DIBMA/DIBMALPs) based nanodiscs has also been explored to produce larger nanodiscs that may better allow conformational flexibility and complex formation in the encircled membrane proteins. DIBMALPs are believed to have a larger nanodisc diameter (~29nm), with the

hypothesis that DIBMALPs will have a reduced effect on membrane lipid packing and therefore less receptor constriction. Additionally, they display reduced UV absorption and greater tolerability of pH variation(Oluwole et al., 2017).

### 7.2.3. Chapter aims:

The overall aim of this chapter is to test TMR-Gas19cha18 as a probe to bind active GPCR conformations that can be detected and analysed using FCS / PCH -based approaches. Using the  $\beta_2$ -adrenoceptor as an example receptor, the binding of TMR-Gas19cha18 is explored to measure the interaction of the Ga peptide tracer with the receptor, and assess the nature of the TMR-Gas19cha18 species through their diffusion characteristics, relative abundance and molecular brightness. Additionally, this facilitated exploration of the effects of solubilization techniques, using either DDM or DIBMA methodologies, on the properties of the purified  $\beta_2$ -adrenoceptors as assessed by TMR-Gas19cha18 interaction.

## 7.3. Methods

### 7.3.1. Characterisation of the effect of Bovine Serum Albumin (BSA) on measured TMR-peptide concentration in solution-based FCS

TMR-Gas19cha18 was diluted to 50nM, 100nM, 200nM or 400nM in 500  $\mu$ L. assay buffer ( 20mM HEPES, 1mM MgCl<sub>2</sub> and 1% DMSO, pH 7.4) with or without the addition of 0.2% BSA. Tracer dilutions were initially generated in a single step dilution from 10mM (in DMSO) stock solution to minimise peptide exposure to plastic prior to addition to the assay plate, however, where required this method was updated to include a 1mM intermediate step (in DMSO) that underwent a 3-minute sonication prior to a final dilution step to generate a final concentration. 200 $\mu$ L/well tracer solution was allowed to incubate in the assay plate for 5 minutes at room temperature (in the dark) prior to measurement. Collected

TMR-Gαs19cha18 FCS autocorrelation data were fitted to a one-or two-component, free 3D, Brownian diffusion model including a pre-exponential for triplet state of the fluorophore to determine the relative diffusion coefficients and concentrations of multiple moving particles as defined in data analysis(Kilpatrick and Hill, 2016).

### 7.3.2. *Solubilization of ssβ<sub>2</sub>-AR-tsNluc receptors for use in FCS-based binding experiments.*

Solubilization buffers were first generated consisting of 20mM HEPES, 150mM NaCl, 5% glycerol and either 1% n-dodecyl-β-D-maltopyranoside (DDM) or 3% di-isobutylene maleic acid (DIBMA), pH: 8. For the generation of DIBMA or DDM solubilized ssβ<sub>2</sub>-AR-tsNluc receptor samples, Hek-ssβ<sub>2</sub>-AR-tsNluc membranes were first generated as previously described (section 3.5) and membrane samples were diluted to 37μg/μL into respective buffers (final volume, 1mL). For both DDM and DIBMA preparations, samples were incubated on a shaking plate for two-hours (on ice) before being transferred into 1.0 mL, thick-wall, polycarbonate, Beckman ultracentrifuge tubes. Samples were centrifuged using a Beckman Optimax ultracentrifuge, TLA-120.2 rotor, at 55,000g for one-hour at 4°C and supernatants were collected, flash-frozen, and store at -80°C prior to use(Harwood et al., 2021). Protein content of both DDM and DIBMA receptor particles was determined Protein concentration was determined using the bicinchoninic acid assay kit (Sigma-Aldrich, Pool, UK) using bovine serum albumin (BSA) as standard, as described in section 3.5.

### 7.3.3. *Characterisation of TMR-Gas19cha18 binding to DIBMA or DDM solubilized $\beta_2$ -Adrenoceptors by FCS.*

To assess TMR-ligand binding by FCS, the following samples were compared, using, 400nM TMR-Gas19cha18 incubations: receptor free DIBMA/DDM buffer only (DIBMA/DDM w/o  $\beta_2$ AR, 20mM HEPES, 1mM MgCl<sub>2</sub>, 0.2% BSA), DIBMA/DDM w/o  $\beta_2$ AR buffer +10 $\mu$ M isoprenaline, 3  $\mu$ g/well DIBMA/DDM containing a nominal 3  $\mu$ g/well  $\beta_2$ AR protein, or 3  $\mu$ g/well DIBMA/DDM  $\beta_2$ AR +10 $\mu$ M isoprenaline. Additional no BSA controls were run during the experiment for the receptor free conditions. In the case of DDM containing experiments, DDM assay buffer was supplemented with 0.1% DDM to maintain a critical micelle concentration above 0.15mM. In some experiments the competition for probe binding by 50 $\mu$ M unlabelled Gas19cha18 was assessed, and for this the unlabelled competitor peptide was incubated with solubilized receptors for five minutes prior to addition to assay plate containing tracer. Samples were then allowed to incubate in the assay plate (in the dark) for five minutes prior to measurement, taken as described previously for calibration and solution FCS (final volume, 200 $\mu$ L per well). Collected TMR-Gas19cha18 autocorrelation data were again fitted to a two-component, free 3D, Brownian diffusion model as well as to a one-component photon counting histogram (PCH) model to explore the possibility of mono- to multi-labelled particles (see data analysis)(Chen et al., 1999).

### 7.3.4. *General FCS acquisition setup.*

FCS assay plates were 8-well chambered Nunc Labtek coverglasses (No. 1.0 borosilicate glass bottom; ThermoFisher Scientific, Paisley, UK), and data were acquired using a Zeiss LSM 880 microscope with a 40X c-Apochromat 1.2 NA water-immersion objective (Carl Zeiss, Germany) at 24°C. Soluble samples containing TMR-Gas19cha18 species were excited with a Diode

pumped solid state (DPSS) 561 nm laser and emission light collected through a 553-695 nm band pass onto a GaAsP detector using a pinhole set at 1 Airy unit. The confocal volume was set to 200  $\mu\text{m}$  above the coverslip surface and beam paths were calibrated using a solution of 20 nM TAMRA (5-6 carboxy mixed isomers;  $D = 2.88 \times 10^{-10} \text{m}^2/\text{s}$ ) prepared in high performance liquid chromatography grade water (Sigma-Aldrich, Missouri, USA). Calibration measurements were collected using ten 10s reads at a laser power of 2.4-2.8% and used to define structural parameter and first order correction of brightness measurements per day (see section 7.3.6). Experimental measurements were collected using three, 30s, reads using 1% laser power in all cases.

#### *7.3.5. NanoBRET binding assay for the characterisation of DDM and DIBMA solubilized receptors*

NanoBRET binding assays were carried out in low sodium buffer, (25mM HEPES, 1% DMSO, 0.1mg/ml Saponin, 0.02% w/v Pluronic acid F<sub>127</sub>, 1mM MgCl<sub>2</sub> and 0.2% BSA, pH 7.4, final assay volume of 50  $\mu\text{L}$ ). 1  $\mu\text{g}$ /well ss $\beta_2$ -AR-tsNluc samples, either solubilized via DDM, DIBMA, or as Hek cell membrane samples, were treated with various concentrations of TMR-G $\alpha$ s19cha18 under vehicle or 10  $\mu\text{M}$  isoprenaline conditions. In all cases, NSB was defined by inclusion of 10  $\mu\text{M}$  unlabelled G $\alpha$ s19cha18 and donor luminescence was generated through addition of 1/960 furimazine dilution. Donor and acceptor outputs were measured every 0.8 minutes over a 30-minute timeframe at 25°C. Generated BRET ratio (550/450nm) data from the 30-minute timepoint were used to determine TMR-G $\alpha$ s19cha8 binding through endpoint saturation analysis as described in section 3.7.

### 7.3.6. FCS data analysis

In fluorescence correlation spectroscopy the pinhole of the microscope objective can be positioned to create a Gaussian shaped confocal detection volume (~0.25fl) on a region of interest, such as the plasma membrane of a cell or, as in this case, within a defined section of a sample solution. As fluorescently tagged moieties diffuse through this volume they produce time dependent fluctuations in fluorescent intensities. Autocorrelation analysis compares the size of a fluctuation ( $\delta I$ ) with the mean fluorescent intensity ( $I$ ) at time  $T$  with that of a subsequent fluctuation at time  $T+\tau$ . Using the entire range of  $\tau$  values, the autocorrelation function ( $G(\tau)$ ) can be determined, which is then normalised to the square of the mean intensity measured ( $I$ ). The autocorrelation function is thus:  $G(\tau) = 1 + \langle \delta I(T) \cdot \delta I(T + \tau) \rangle / \langle I \rangle^2$  (Figure 7.1A&B).

Nonlinear curve fitting of data derived from the autocorrelation function using a biophysical model, was used to produce an autocorrelation decay curve (Figure 7.1B). From this curve, specific parameters of the fluorescent particles within the confocal detection volume can be defined, namely the average dwell time ( $\tau D$ ) representing the halfway point of the  $G(\tau)$  decay and the average particle number  $N$ , from its inverse relationship to the autocorrelation function at time zero ( $G_0$ ) (Briddon and Hill, 2007).

FCS data was analysed using Zen Black 2012 software (Carl Zeiss, Germany). Initial calibration data was used to define the confocal volume by:

$$V = \pi^{\frac{3}{2}} \cdot (\omega_1)^2 \cdot \omega_2$$

Where  $V$ = volume,  $\omega_1$  is the radius of the confocal volume, determined from  $\omega_1 = (4 \cdot D \cdot \tau_{D1})^{1/2}$ , where  $D$  and  $\tau_{D1}$  are the diffusion coefficient and dwell time of TAMRA, respectively.  $\omega_2$

represents half the height of the confocal volume and is calculated by multiplying  $\omega_1$  by the structural parameter ( $S$ ), which thus represents the ratio of the height to the waist radius of the confocal volume (set as a constant [ $S = 5$ ] for 3D solution analysis as described below) The diffusion co-efficient  $D$  for TAMRA is known ( $D = 2.88 \times 10^{-10} \text{m}^2/\text{s}$ ), therefore measurement of the experimental dwell time ( $\tau_{D1}$ ) during the calibration provides  $\omega_1$ ,  $\omega_2$  and so the confocal volume. This volume, in conjunction with individual  $\tau_D$  values allowed the diffusion coefficients ( $D$ ) of the fluorescently tagged receptor or complex to be calculated using the equation  $D = \omega_1^2 / 4\tau_D$ . The concentration of fluorescent particles within the confocal detection volume was derived using the equation  $N / (\pi\omega_1^2)$ .

Experimental autocorrelation data were fitted to a 1-component or 2-component 3D diffusion model (i.e.  $m=1$  or  $2$ ), defined by:

$$G(\tau) = 1 + \frac{1}{N} \cdot \sum_{i=1}^m f_i \cdot \left(1 + \frac{\tau}{\tau_{Di}}\right)^{-1} \cdot \left(1 + \frac{\tau}{S^2 \cdot \tau_{Di}}\right)^{-\frac{1}{2}}$$

Where  $N$  = particle number,  $f_i$  is a fraction of  $i^{\text{th}}$  component,  $\tau_{Di}$  is dwell time of  $i^{\text{th}}$  component,  $S$  = structure parameter. The first triplet state arriving from TMR photo-physics was also accounted for in a pre-exponential term not shown in the equation above. Fit quality was assessed on residuals to the fit by  $\chi^2$  analysis (Figure 7.1D). The concentrations of free and bound components were then calculated directly from their relative contributions to the amplitude of the autocorrelation function.

Raw fluctuation measurements were also exported and analysed using photon counting histogram (PCH) analysis (Chen et al., 1999). PCH analysis measures the variations that occur in the amplitude of

excitation intensity in different parts of the confocal volume. PCH analysis can provide information on molecular brightness ( $\epsilon$ ) and an alternative calculation of particle concentration. When performing PCH analysis, the fluorescence trace is divided into bins of a specific time. For diffusion of the fluorescent peptide TMR-Gas19cha18, a bin time of 20 $\mu$ s was chosen, to be less than the dwell time of the fluorescent species but to exclude more rapid time dependent fluctuations attributed to the photophysics of the fluorophore. The photon counts in each bin were counted, with a frequency histogram generated with the x axis representing the number of photon counts, k, and the y axis the number of bins containing those counts. This histogram deviates from an expected Poisson distribution due to the uneven illumination of the confocal volume, whereby the greatest excitation is found in the centre of the volume. This deviation from the ideal Poisson distribution can be measured in PCH analysis, and a fit modelled on the number (N) and the molecular brightness ( $\epsilon$ ) of fluorescent species. PCR calibration reads (TAMRA) were fitted to a 1 component model. The purpose of this calibration was to provide a first order correction value (F), which accounts for deviation from a Gaussian observation volume when using single photon rather than 2 photon excitation (Huang et al., 2004). This value was then used in the analysis of experimental data, using 1 or 2 component PCH models with a bin time set to 20 $\mu$ s.

## 7.4. Results and Discussion

### 7.4.1. *Characterisation of TMR-Gas19cha18 in solution within Fluorescence correlation spectroscopy.*

The use of labelled G protein peptidomimetics, with agonist dependent binding properties, in fluorescence correlation spectroscopy has the potential to provide insights into the composition of labelled active receptor complexes with a technique that reports ensemble behaviours based on single molecule sensitivity. .

In initial experiments the diffusion characteristics and experimental measured concentrations of TMR-Gas19cha18 were assessed in solutions in the absence and presence of 0.2 % bovine serum albumin (BSA). The nature of peptide amino acid side chains facilitates a high degree of potential interactions with surrounding plastic and glass and can result in non-specific binding, thus reducing the actual free concentration exposed to receptor preparations in the experiment. By coating plastic surfaces with bovine serum albumin (BSA), the loss of the labelled peptide to these surfaces might be minimised. Conversely, BSA may also affect the pharmacology of other ligands in the assay, for example small molecules which may bind BSA directly (Blecher, 1964; Sykes et al., 2016; Tummino and Copeland, 2008).

To determine the effects of BSA's inclusion within experimental setups, and to gain a better understanding of the nature of TMR-Gas19cha18's behaviour in solution, initial FCS experiments were carried out to compare peptide free concentration under BSA positive and BSA negative buffer conditions.

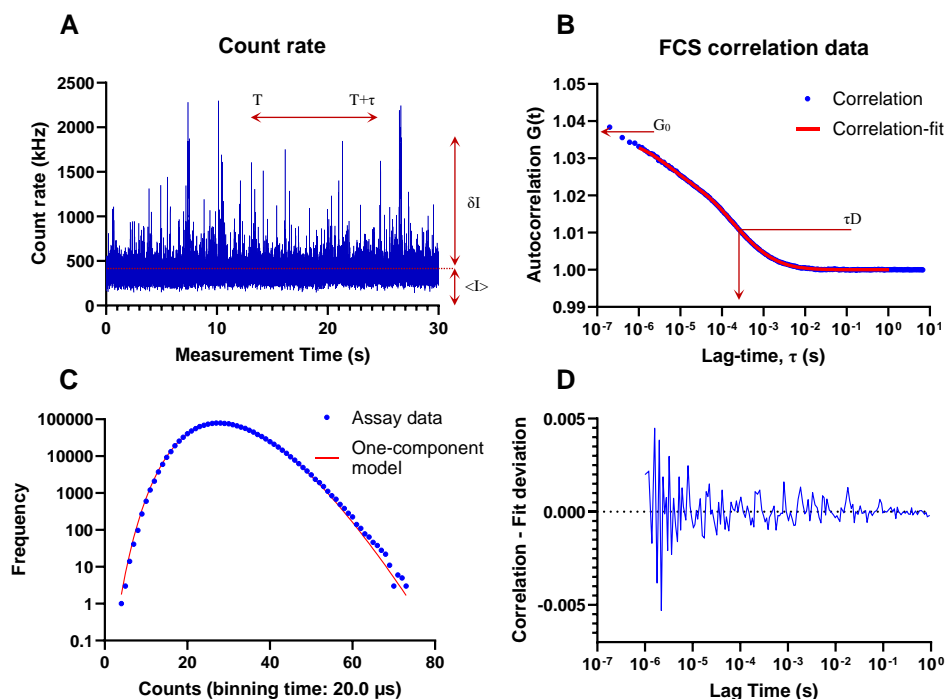


**Figure 7.1. FCS and PCH analysis of 200nM TMR-Gas19cha18 in solution to determine free concentration, diffusion co-efficient and molecular brightness** (A) Fluctuations in fluorescent intensity over time, measuring 200 nM TMR-Gas19cha18 in the presence of 0.2% BSA, used to derive auto-correlation curves and photon counting histograms. (B) Autocorrelation curve for TMR-Gas19cha18 in the presence of 0.2% BSA, fitted to a single-component 3D diffusion model. (C) Photon-counting histogram (PCH) of the data presented in (A) fit with a one-component model (red line). (D) Deviation of data presented in (B) from the single-component FCS model fitted curve to determine model suitability. In all cases, data are representative experiments from three performed at 24°C.

Initial experiments were designed to test three concentrations of TMR-G $\alpha$ s19cha18 (50nM, 100nM and 200nM), comparing their theoretical assay concentration with that determined through FCS analysis under 0% or 0.2% BSA conditions. Autocorrelation curves were determined through analysis of fluorescence fluctuation data obtained over time (Figure 7.1A) and in turn used to determine respective fluorescent species concentrations. In all cases the observed concentrations indicated a significant reduction over calculated theoretical concentrations. This relationship was particularly pronounced in the absence of BSA, with each dilution resulting in an average concentration of  $\sim$  1nM, indicating an almost complete loss of free peptide (Figure 7.2A). Addition of BSA resulted in an increase in observed concentration, but did not rescue the large difference between this and the test concentrations applied (Figure 7.2A). This indicated that while BSA may limit NSB binding for the peptide, it is insufficient alone to prevent the reduction in free TMR-G $\alpha$ s19cha18 concentration. To test whether peptide aggregation in solution was also a factor, Figure 7.2B illustrates the additional effect of sonication and use of an intermediate, 100 % DMSO dilution, to prepare the FCS assessed ligand solutions. These conditions improved the availability of the tracer for autocorrelation analysis. Notably, this analysis was now best fitted by a two-component model, with the first component 1 having a dwell time of  $87.65 \pm 7.9 \mu\text{s}$ , and the second component 2 having a dwell time of  $476.80 \pm 38.1 \mu\text{s}$ . The respective concentrations for each component (Figure 7.2B) were  $147.30 \pm 16.21 \text{ nM}$ , and  $98.59 \pm 14.63 \text{ nM}$ , which when combined reflected the majority of the calculated peptide concentration used (400 nM). Clearly, FCS analysis does not identify directly the species underpinning the components identified. Component 1, with the shorter dwell time and faster diffusion, may represent the free TMR-peptide in solution. For freely diffusing species, a 2-fold change in  $\tau D$  is obtained with an 8-fold change in MW, For component 2 (diffusing 5.5 times slower than component 1), this

suggests ~64 times change in MW of the TMR-Gas19cha18 diffusing species involved. It is tempting to speculate that this reflects BSA (molecular weight 66 kD) bound TMR-Gas19cha18 (MW 2.9 kD) – and this would also account for the preservation of much of the calculated ligand concentration, given a 1:1 BSA:TMR-Gas19cha18. However, it is not entirely possible to exclude alternatives for component 2, such as TMR-Gas19cha18 aggregated complexes present in the solution.

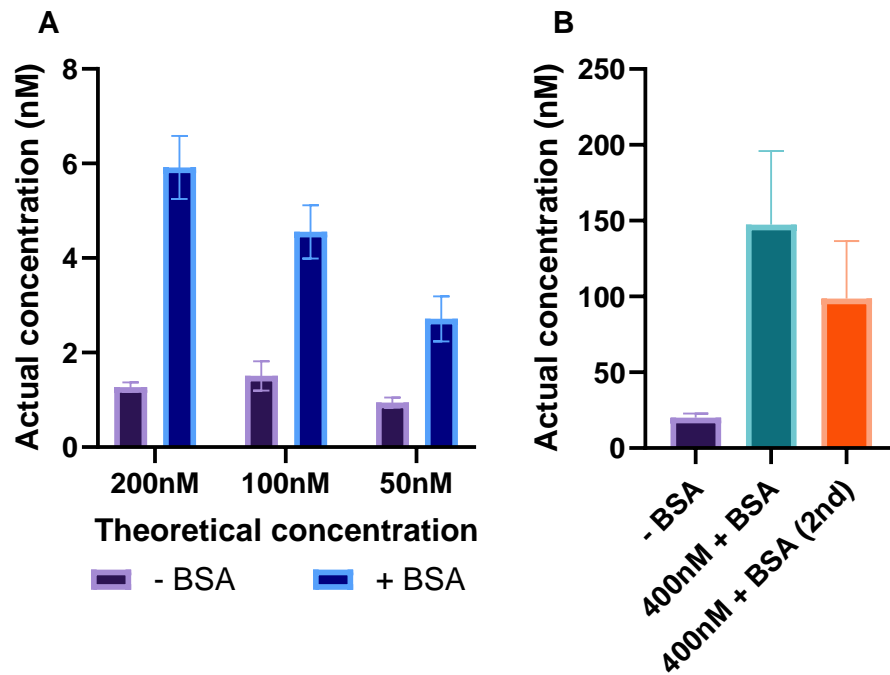


**Figure 7.2. Determination of the effects of 0.2% BSA on TMR-Gas19cha18 component concentrations by fluorescent correlation spectroscopy.** (A) initial concentration data derived from a single-component auto-correlation analysis comparing the effects of 0.2% BSA on increasing concentrations of TMR-Gas19cha18, without sonication. (B) Concentration data derived from single (-BSA) or two-component auto-correlation analysis comparing the effects of 0.2% BSA in low sodium buffer on of the observed concentration from 400 nM TMR-Gas19cha18 input, after exposure to sonication for 3 minutes and employing intermediate DMSO dilution. In both cases data are pooled data from three independent experiments, defining components on mean dwell time observed (+400nM BSA [ $\tau$ D1] dwell =  $87.65 \pm 7.9 \mu\text{s}$ , +400nM BSA (2<sup>nd</sup>) [ $\tau$ D2] dwell =  $476.8 \pm 38.1 \mu\text{s}$ ).

#### 7.4.2. *Application of FCS-based techniques to determine fluorescent ligand-receptor binding.*

Having determined the FCS characteristics of TMR-G $\alpha$ s19cha18 in solution, and optimised the conditions to maximise the observed concentration, the effect of adding solubilized  $\beta_2$ -Adrenoceptors (Hek-ss- $\beta_2$ -AR-tsNluc) on the FCS behaviour of TMR-G $\alpha$ s19cha18 was investigated. Theoretically, the addition of solubilized receptors known to couple to TMR-G $\alpha$ s19cha18 should produce a mixed population of bound versus free ligand, distinguishable through a two-component analysis separating species with differing dwell times on the basis of altered molecular weight. As previously discussed (see chapter 6), the expected agonist dependent binding mechanism of the G $\alpha$ s peptide-receptor interaction should also increase the proportion of bound ligand in the presence of an orthosteric agonist, such as isoprenaline. A complicating factor, as discussed above, is that even in the absence of receptor, the presence of BSA leads to two-component fitting of the free fluorescent species.

This hypothesis was first tested employing  $\beta_2$ -AR-tsNluc particles from Hek cell membranes through use of an alternating polymer of di-isobutylene and maleic acid (DIBMA). DIBMA is designed to extract lipid-encased membrane proteins from cell membranes in a detergent-free environment, yielding discoidal DIBMA-lipid particles (DIBMALPs) larger than the more traditional SMALPs (Oluwole et al., 2017). Co-incubation of DIBMA extracted  $\beta_2$ -AR-tsNluc with TMR-G $\alpha$ s19cha18 in assay buffer containing 0.2 % BSA, including or excluding a saturating concentration of isoprenaline (10  $\mu$ M), resulted in FCS autocorrelation curves that were best modelled with two component analysis across all conditions tested (Figure 7.3A&B; Table 7.1).

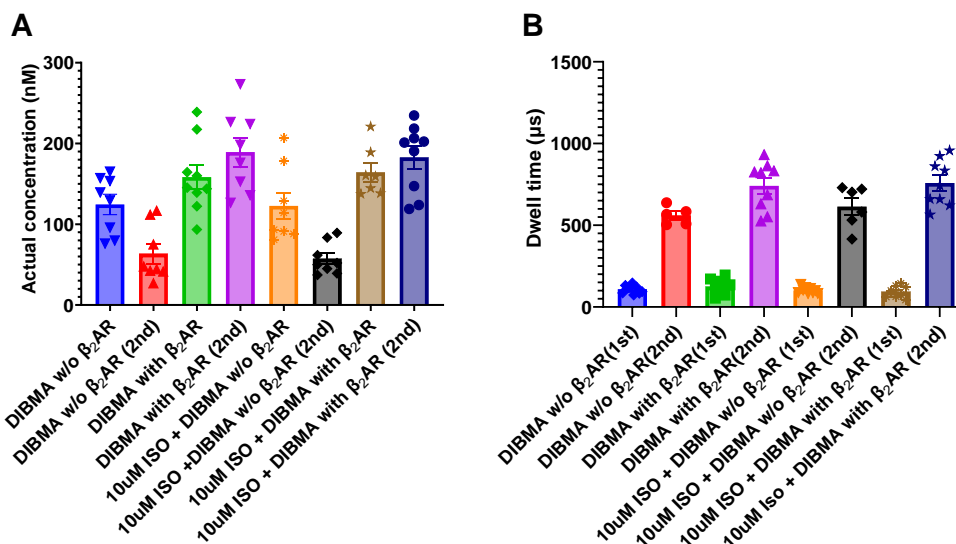


**Figure 7.3. FCS analysis of 400 nM TMR-G $\alpha$ s19cha18 binding to DIBMA  $\beta_2$ -Adrenoceptor particles.** Experiments were performed in assay buffer + 0.2 % BSA and FCS measurements were fitted with two component autocorrelation analysis to distinguish faster (1<sup>st</sup>) and slower (2<sup>nd</sup>) diffusing TMR probe species (A) Component concentrations in the absence or presence of DIBMA solubilized receptors, with or without 10  $\mu$ M isoprenaline (ISO) also present (B) Component dwell times in the absence or presence of DIBMA solubilized receptors, with or without 10 mM isoprenaline (Iso) also present. In all cases data were pooled from 3 independent experiments in a low sodium assay buffer + 0.2 % BSA.

**Table 7.1. FCS autocorrelation analysis of TMR-G $\alpha$ s19cha18 binding at DIBMA solubilized  $\beta$ <sub>2</sub>-AR.**

Condition	% Component 1	Component 1				Component 2			
		<i>Conc</i>	$\pm$ s.e.m (nM)	$\tau D1$	$\pm$ s.e.m ( $\mu$ s)	<i>Conc</i>	$\pm$ s.e.m (nM)	$\tau D2$	$\pm$ s.e.m ( $\mu$ s)
<b>DIBMA w/o <math>\beta</math><sub>2</sub>AR</b>	<b>74.3<math>\pm</math>2.3</b>	124.5	$\pm$ 12.7	109.0	$\pm$ 8.5	63.3	$\pm$ 12.1	559.8	$\pm$ 25.0
<b>DIBMA with <math>\beta</math><sub>2</sub>AR</b>	<b>52<math>\pm</math>5.2</b>	158.3	$\pm$ 15.1	124.6	$\pm$ 15.6	189.3	$\pm$ 18.0*	741.0	$\pm$ 48.7*
<b>DIBMA w/o <math>\beta</math><sub>2</sub>AR + ISO</b>	<b>70.3<math>\pm</math>2.2</b>	122.7	$\pm$ 16.4	101.5	$\pm$ 6.3	57.2	$\pm$ 6.9	613.6	$\pm$ 51.6
<b>DIBMA with <math>\beta</math><sub>2</sub>AR + ISO</b>	<b>47.34<math>\pm</math>3.7</b>	164.3	$\pm$ 11.6	92.7	$\pm$ 12.9	182.6	$\pm$ 14.0*	758.4	$\pm$ 47.0*

Data are pooled data from three independent experiments, performed in assay buffer using 400 nM TMR-G $\alpha$ s peptide in the presence of 0.2 % BSA. \* P<0.05 comparing DIBMA  $\pm$   $\beta$ <sub>2</sub>AR using paired Student's t-tests. No significant difference in the absence and presence of 10  $\mu$ M isoprenaline (ISO) was observed regardless of whether  $\beta$ <sub>2</sub>AR particles were present.

As previously discussed, 400nM TMR-G $\alpha$ s19cha18 in solution without any receptor (DIBMA reagent only [DIBMA w/o  $\beta$ <sub>2</sub>AR]) still produced two component autocorrelation curves representing species of differing diffusion times. This was interpreted as the presence of BSA bound, as well as free TMR-G $\alpha$ s19cha18. However, addition of DIBMA receptor particles resulted in a significantly higher second component concentration and longer dwell time (Table 7.1, Figure 7.3A&B), suggesting the presence of additional high molecular weight TMR peptide complexes and consistent with receptor particle binding. Surprisingly, this difference was observed consistently whether isoprenaline was present (Table 7.1, Figure 7.3A&B), suggesting receptor particle-ligand binding detectable by FCS occurred whether or not the orthosteric agonist was present.

Previous NanoBRET studies (chapter 6) demonstrated predominantly agonist dependent binding of the TMR-G $\alpha$ s19cha18 peptide in  $\beta$ <sub>2</sub>-AR membranes. However, this does not rule out the possibility of a low level of G $\alpha$ s19cha18 peptide binding at unoccupied receptors, not readily detected using BRET techniques, but identified through the sensitive measurements of FCS. However, the absence of isoprenaline regulated G $\alpha$ s peptide binding suggests that the associated  $\beta$ <sub>2</sub>-AR conformational changes in DIBMA particles may be impeded. This is in agreement with previous findings by Harwood *et al*, Mosslehy *et al.*, and Routledge *et al* (Harwood *et al.*, 2021; Mosslehy *et al.*, 2019; Routledge *et al.*, 2020) in which it was determined that addition of a polyolefin based solubilization agent (e.g., SMA/DIBMA) has a restrictive effect on receptor conformational change, thus limiting conversion between the inactive and active states. On the basis of the data generated, it is not possible to distinguish whether DIBMA particles containing “inactive” empty  $\beta$ <sub>2</sub>-AR are able to bind the TMR probe, or whether  $\beta$ <sub>2</sub>-AR purified in this manner show a more constitutively active conformational state (with respect to the G $\alpha$  C

terminus binding site) that supports TMR probe binding compared to the NanoBRET membrane studies, but is not further regulated by isoprenaline.

If the component 2 species identified in the DIBMA  $\beta_2$ -AR studies represents TMR probe binding to the receptor, it should theoretically be possible to compete for this binding with unlabelled probe. To this end, DIBMA  $\beta_2$ -AR samples were pretreated with 50  $\mu$ M unlabelled G $\alpha$ s19cha18 for 5 min, before addition of 400 nM TMR-G $\alpha$ s19cha18 and FCS measurements. In the presence of unlabelled peptide, the dwell times for component 1 and component 2 did not change significantly from the controls (DIBMA  $\beta_2$ -AR only  $\tau$ D1 = 178.3 $\pm$ 18.2  $\mu$ s, DIBMA  $\beta_2$ -AR+G $\alpha$ s19cha18  $\tau$ D1 = 190.9 $\pm$ 12.8  $\mu$ s, DIBMA  $\beta_2$ -AR only  $\tau$ D2 = 831.6 $\pm$ 78.5  $\mu$ s, DIBMA  $\beta_2$ -AR+G $\alpha$ s19cha18  $\tau$ D2 = 962.7 $\pm$ 100.5  $\mu$ s). The presence of unlabelled G $\alpha$ s19cha18 selectively lowered the measured component 2 concentration to a similar level displayed within receptor free samples, however this difference was not statistically significant compared to vehicle positive controls (Figure 7.4A, DIBMA  $\beta_2$ -AR only  $\tau$ D2 component concentration 167.5 $\pm$ 17.9 nM, DIBMA  $\beta_2$ -AR+G $\alpha$ s19cha18 [ $\tau$ D2] 126.2 $\pm$ 14.3 nM, one-tailed paired Student's t-test, p=0.19, t=0.92, df=6). Thus, these data are consistent with  $\beta_2$ -AR specific binding being observed in DIBMA particles, but the interpretation is complicated by the likely additional contribution to component 2 of TMR-G $\alpha$ s19cha18 bound BSA. In addition, the presence of unlabelled peptide might not only compete for  $\beta_2$ -AR bound probe, but also TMR probe bound to BSA in the assay, thereby altering its free concentration regulating receptor binding which may be an additional confounding factor.

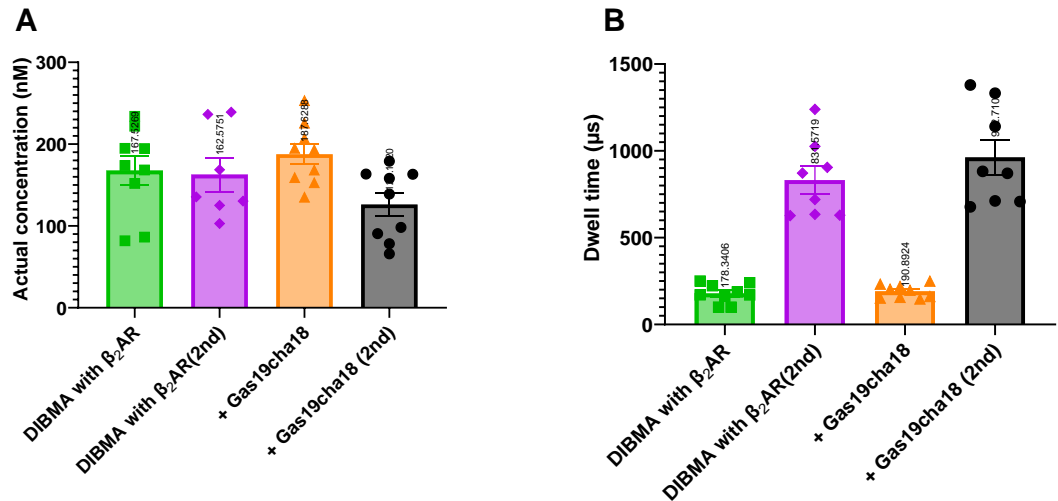


**Figure 7.4. FCS analysis of TMR-Gas19cha18 binding to DIBMA  $\beta_2$ -AR in the absence or presence of 50  $\mu$ M unlabelled Gas19cha18 peptide. (A) Component concentrations in the absence or presence of 50  $\mu$ M unlabelled Gas19cha18. (B) Component dwell times in the absence or presence of 50  $\mu$ M unlabelled Gas19cha18. In all cases data were pooled from 3 independent experiments in a low sodium assay buffer + 0.2 % BSA.**

#### 7.4.3. PCH analysis of TMR- probe species in the absence and presence of $\beta_2$ -AR DIBMA particles.

The alternate PCH analysis of FCS recordings enable the molecular brightness of the fluorescent species passing through the confocal volume to be determined. Where multiple species of differing binding stoichiometry are present, this may be detected by PCH as multiple components with differing brightness. For example, this might occur through multi peptide binding to a single DIBMA receptor particle (for example if receptor oligomers were present), or to BSA in solution. Equally, types of non-specific interaction (peptide aggregates, or interactions with the DIBMA lipid disc) might create multimeric, brighter particles compared to the TMR-peptide in solution. However, PCH analysis of the DIBMA  $\beta_2$ -AR experiments indicated only a single brightness component for the TMR-Gas19cha18 binding, which was similar in all conditions including the BSA only controls (Figure 7.1C and Figure 7.4A). A likely interpretation is that binding of the peptide to the DIBMA  $\beta_2$ -AR, or to BSA is at 1:1 stoichiometry such that the brightness of the bound species does not change compared to the free unbound peptide in solution. This would further indicate that the fluorescent  $G\alpha$  probe can bind single receptors (rather than e.g. an oligomeric complex). This conclusion is supported by previous literature that suggests GPCR isolated preparations in nanodiscs, are primarily monomeric in nature, such that only one  $G\alpha_s$  peptide binding site per DIBMA  $\beta_2$ -AR particle would be expected (Bayburt et al., 2011, 2007).

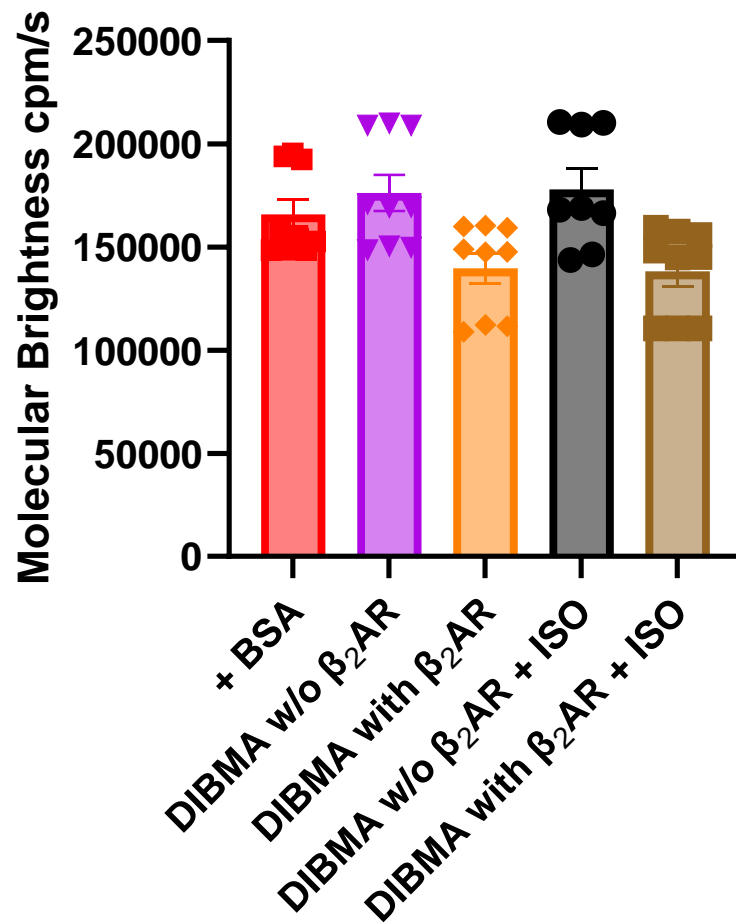


**Figure 7.5. PCH analysis of TMR-*Gαs19cha18* interactions under DIBMA extracted  $\beta_2$ -AR conditions.** Data (from FCS measurements also providing Figure 7.3) comparing the relative molecular brightness of 400 nM TMR-*Gαs19cha18* in the presence of DIBMA solubilized  $\beta_2$ -AR receptors, and in their absence (but including 0.2 % BSA). Experiments were performed in the absence and presence of 10 mM isoprenaline

#### 7.4.4. *TMR-G<sub>s</sub> probe binding to DDM solubilised receptors can also be detected by FCS*

A common alternative method for solubilization of membrane proteins is through the employment of detergents, defined as any agent that consists of a polar hydrophobic head group and nonpolar hydrophilic tail, such as n-dodecyl- $\beta$ -D-maltopyranoside (DDM). Such techniques rely on the formation of detergent micelle particles able to embed in and disrupt the plasma membrane through their hydrophilic tail and substitute for phospholipids surrounding membrane proteins, thus allowing extraction of membrane proteins. The lack of a restricting polymer provides the extracted protein greater capacity for conformational flexibility by reduced lipid packing. It is also well established that, despite their role in mimicking the membrane phospholipid environment, detergent hydrophilic head-groups are far from able to recapitulate this advanced lipid environment (Harwood et al., 2021; Ratkeviciute et al., 2021). As such, this results in many detergents having a potential detrimental effect on the structure, function and stability of the proteins extracted. Indeed, previous studies employing DDM solubilized adrenoceptors have displayed large variations in agonist affinity and receptor functionality (Dawaliby et al., 2016; Harwood et al., 2021). One such example is work by Leitz et al, which identified solubilized  $\beta_2$ -AR (in the absence of effector coupling) displays isoprenaline affinities around 5  $\mu$ M, almost a 7-fold reduction in affinity than comparable measurements in whole cell binding assays within the wider literature (also, see chapter 4) (Leitz et al., 2006).

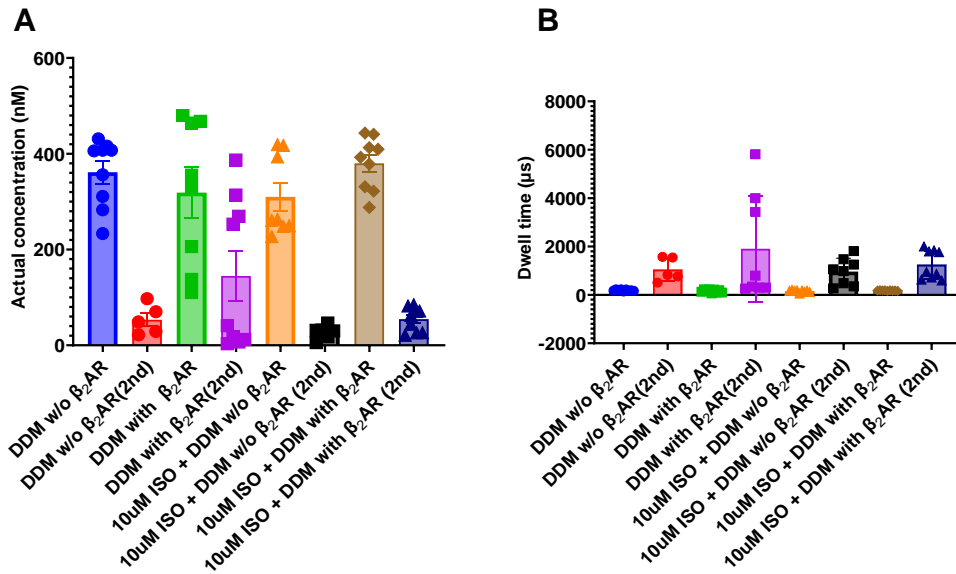


**Figure 7.6. FCS analysis of 400 nM TMR-Gas19cha18 binding to DDM solubilised  $\beta_2$ -Adrenoceptors.** (A) Component concentrations in the presence of DDM solubilized receptors under vehicle or agonist or orthosteric agonist conditions (B) Component dwell times in the presence of DDM solubilized receptors under vehicle or 10  $\mu$ M agonist conditions (E) In all cases data were pooled from 3 independent experiments in a low sodium assay buffer + 0.2 % BSA.

**Table 7.2. FCS autocorrelation analysis of TMR-Gas19cha18 binding at DDM solubilized  $\beta_2$ -AR.**

Condition	% Component 1	Component 1				Component 2			
		<i>Conc</i>	$\pm$ <i>s.e.m</i> (nM)	$\tau$ <i>D1</i>	$\pm$ <i>s.e.m</i> ( $\mu$ s)	<i>Conc</i>	$\pm$ <i>s.e.m</i> (nM)	$\tau$ <i>D2</i>	$\pm$ <i>s.e.m</i> ( $\mu$ s)
<b>DDM w/o <math>\beta_2</math>AR</b>	91.6 $\pm$ 3.4	361.2	$\pm$ 23.4	192.4	$\pm$ 10.7	53.4	$\pm$ 13.8	1024	$\pm$ 217.4
<b>DDM with <math>\beta_2</math>AR</b>	73.01 $\pm$ 11.4	318.8	$\pm$ 53.4	162.5	$\pm$ 22.0	144.8	$\pm$ 52.5	1906	$\pm$ 773.0
<b>DDM w/o <math>\beta_2</math>AR + Iso</b>	77.0 $\pm$ 8.4	309.9	$\pm$ 29.7	153.4	$\pm$ 15.0	27.22	$\pm$ 5.7	960.1	$\pm$ 196.3
<b>DDM with <math>\beta_2</math>AR + Iso</b>	87.67 $\pm$ 1.8	379.8	$\pm$ 18.3	179.2	$\pm$ 3.7	54.31	$\pm$ 8.4	1241	$\pm$ 197.7

Data are pooled data from three independent experiments.

The diffusion characteristics of TMR-G $\alpha$ s19cha18 were studied in the absence and presence of DDM solubilized  $\beta_2$ -AR-tsNluc, using assay buffer containing 0.2 % BSA, as for experiments employing DIBMA isolated receptors. As before FCS measurements generated autocorrelation curves that were best described by a two-component model, eliciting a first component with combined dwell times of mean  $171.9 \pm 7.4 \mu\text{s}$  (representing free ligand), and second slower diffusing component ( $1282.8 \pm 216.3 \mu\text{s}$ ) indicative of a higher molecular weight species. Across all tested environments, derived concentrations were higher, which may be due to the presence of 0.1% DDM within the assay buffer further limiting TMR-G $\alpha$ s19cha18 aggregation, potential BSA interaction and other forms of non-specific binding (Table 7.2). However, in contrast to DIBMA  $\beta_2$ -AR data, the increase in 2<sup>nd</sup> component concentration on addition of DDM  $\beta_2$ -AR was not clearcut or significant (given the variability in individual experiments). There was also no additional increase in 2<sup>nd</sup> component concentration in the presence of 10  $\mu\text{M}$  isoprenaline, compared to vehicle (Table 7.2, Figure 7.6). This means that although 2 components are present, it is difficult to make firm conclusions that the DDM  $\beta_2$ -AR receptor preparations preserve the TMR-G $\alpha$ s19cha18 site and support its specific binding from the current data. In contrast to DIBMA based preparations, it is also possible the DDM solubilisation provides greater variation in the size and nature of the  $\beta_2$ -AR micelles, and the number of receptors per particle, which could affect the accuracy of component separation in the FCS analysis. PCH analysis on the DDM receptor data (Figure 7.7, was fitted best with a single component model with equivalent molecular brightness of TMR-G $\alpha$ s19cha18 particles under all conditions. This suggests, that is G $\alpha_s$  peptide binding to the DDM solubilised  $\beta_2$ -AR is present, multi-receptor binding per micelle is not evident.

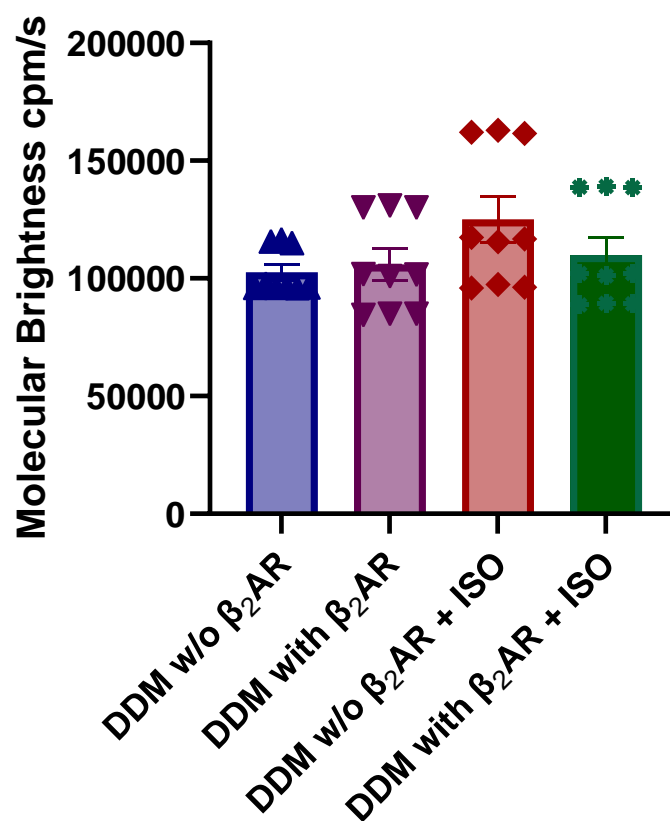


**Figure 7.7. PCH analysis of TMR-Gas19cha18 interactions under DDM solubilize  $\beta_2$ -AR conditions.** Data comparing the relative molecular brightness of TMR-Gas19cha18 in the presence of DDM solubilized  $\beta_2$ -AR receptors. In both cases data are pooled from three independent experiments, and the PCH histogram was sufficiently described by a single component brightness model.

7.4.5. *DIBMA and DDM purified  $\beta_2$ -AR do not show agonist-dependent TMR-Gas19cha18 binding in NanoBRET binding studies.*

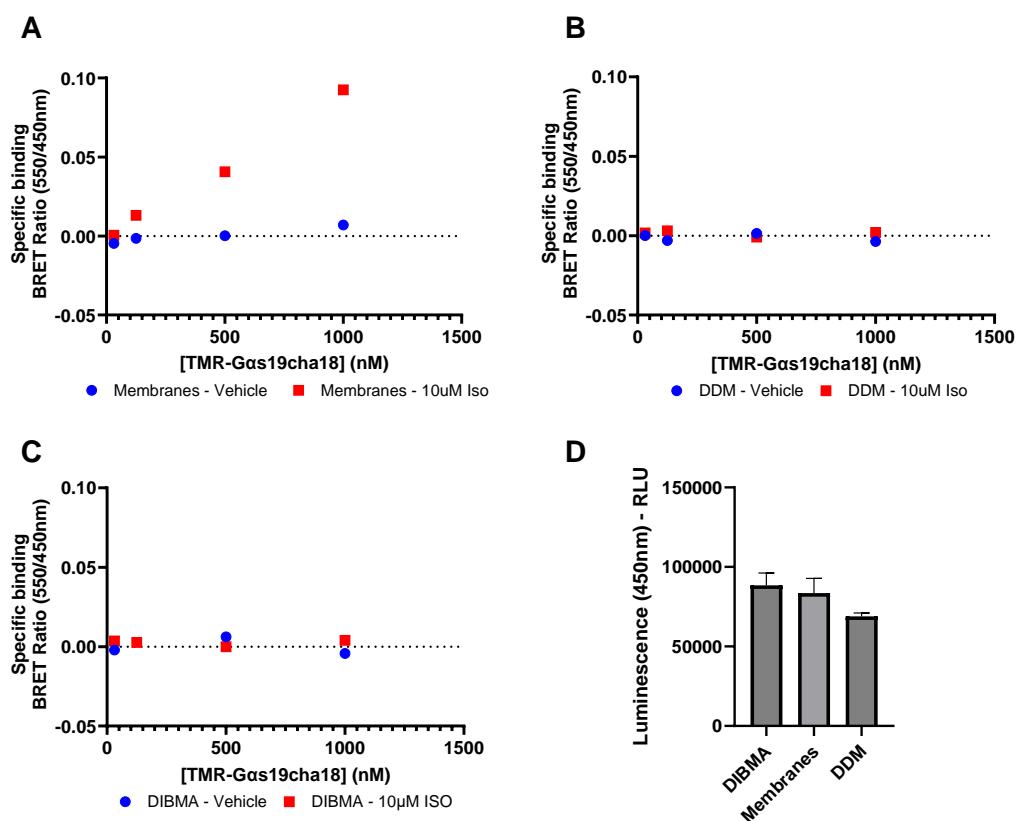


**Figure 7.8. TMR-Gas19cha18 binding to DIBMA, DDM or Membrane bound  $\beta_2$ -AR detected via NanoBRET.** (A) TMR-Gas19cha18 binding to  $\beta_2$ -AR in Hek cell membranes. (B) TMR-Gas19cha18 binding to DDM solubilized receptors. (C) TMR-Gas19cha18 binding to  $\beta_2$ -AR in DIBMA particles. (D) Raw Nanoluciferase donor luminescence (450nm) measurements from each receptor sample preparation. In all cases data depict measurements after 30 minutes incubation at room temperature and is a single example assay from three independent experiments performed, in the presence and absence of 10  $\mu$ M isoprenaline (ISO) using 1ug per well protein content for each sample prep per assay.

A common characteristic of both DIBMA and DDM solubilised preparations was that no change in TMR-G $\alpha$ s19cha18 binding could be detected by FCS in the presence of the orthosteric agonist isoprenaline. To assess whether this reflected a property of the receptor preparations used, rather than the FCS based measurement, it was explored whether DIBMA and DDM solubilized receptors could be used in a TMR-G $\alpha$ s19cha18 NanoBRET binding study (see Chapter 6). For each case, luciferase activity was evident on addition of furimazine substrate (Figure 7.8D, in comparison to  $\beta_2$ -AR membrane preparation controls). TMR-G $\alpha$ s19cha18 NanoBRET specific binding was enhanced in  $\beta_2$ -AR membrane preparations by the presence of isoprenaline to those seen previously in the case of membrane bound receptors (chapter 6), however, no significant tracer binding was observed at DIBMA or DDM isolated receptors regardless of the presence of isoprenaline (Figure 7.8). It should be noted that in all cases, luminescence output was used to ensure comparable levels of receptor within each environment, thereby limiting the effects of receptor concentration (although with sufficient donor emission the BRET ratio should account for this variation). The inability for DDM and DIBMA solubilised receptors to display specific tracer binding, even at almost  $2 \times K_D$  concentrations in the presence of agonist, suggests these methods do impair the receptor conformational changes that promote high level TMR-G $\alpha$ s19cha18 binding. This corroborates previous FCS data, indicating TMR-G $\alpha$ s19cha18 may display limited binding to the inactive receptor state, but employment of DIBMA or DDM isolation limits the ability of orthosteric agonists to enhance receptor activation and G $\alpha_s$  C terminal peptide binding. Nevertheless, the demonstration that some binding can be detected by FCS in DIBMA preparations, but not through NanoBRET, highlights the benefit provided by the added sensitivity of this technique for low concentrations of bound fluorescent species.

#### 7.4.6. Concluding remarks

In this chapter, the application of the fluorescent peptide TMR-Gas19cha18 within FCS-based approaches has been explored. Employment of TMR-Gas19cha18 within FCS has been optimised to determine the conditions needed to maximise observed tracer concentration and identified the likelihood of tracer-BSA binding. TMR-Gas19cha18 was then used to provide evidence that DIBMA isolated  $\beta_2$ -adrenoceptors can bind TMR-Gas19cha18, with PCH analysis suggesting this occurs in a 1:1 stoichiometric relationship. However, a similar relationship was not as clearly defined when employing DDM solubilisation techniques for receptor isolation, nor was either isolation technique able to elicit receptor samples able to mimic the orthosteric agonist dependent TMR-Gas19cha18 peptide binding seen in previous chapters. This appears to be a consequence of the isolated protein (e.g., restricted conformational change in DIBMA particles), rather than due to the FCS-based measurement technique, which is supported by maintained absence in agonist dependent tracer binding in NanoBRET measurements.

At present, the FCS studies presented using the TMR-Gas19cha18 tracer are limited to solution-based techniques, and purified receptors (with potential disadvantages), because of the membrane impermeability of these tracers. The ability to employ FCS within whole cells with a cell permeable Ga peptidomimetic, would greatly increase the experimental possibilities, and the biological questions that might be addressed. In particular, this would allow for the exploration of GPCR interactions and pharmacology within distinct cellular environments, such as question of active signalling receptors within endosomes as has been suggested through the use of nanobody 80 (Nb80, detects  $\beta_2$ -AR active conformation) by Von Zastrow *et al* (Irannejad *et al.*, 2013; Tsvetanova and von Zastrow, 2014). In relation to this thesis, this is of particular interest as the role of intracellular modulators in endosomal signalling is yet to be explored and may have implications in altering the

prolonged/distinct receptor signalling displayed with endosomal signalling, thereby expanding their therapeutic potential(Mohammad Nezhady et al., 2020; Tsvetanova and von Zastrow, 2014). Additionally, intracellular peptidomimetics may facilitate greater exploration of GPCR-effector/GPCR-GPCR interactions in relation to receptor dimerization via employment of FCS technology(Kilpatrick et al., 2015).

Overall, these findings provided new possibilities for probing complex receptor relationships using solution-based FCS, such as dual-fluorescent binding studies, and have the potential to facilitate exploration of previously undetectable interactions at the intracellular binding site of GPCRs.

## **Chapter 8. Results IV**

Identification of novel intracellular modulators of the prostaglandin EP<sub>2</sub> receptor.

## 8. Identification of novel intracellular modulators of the prostaglandin EP<sub>2</sub> receptor.

### 8.1. Chapter introduction:

Previous exploration of novel peptidomimetic tracers identified TMR-G $\alpha$ s19cha18's ability to characterise unlabelled peptide ligands able to compete for the intracellular binding site. However, application of peptide ligands within a clinical setting is hindered by their membrane impermeability, meaning that the future of intracellular ligands is reliant on the discovery of novel small molecule modulators. Therefore, this chapter aims to identify the capabilities of TMR-G $\alpha$ s19cha18 to identify small molecule intracellular binders at relevant GPCRs. Previous screening of alternative Gs coupled receptors identified that TMR-G $\alpha$ s19cha18 is able to bind to the prostaglandin EP<sub>2</sub> receptor as a biosensor. The prostaglandins represent a highly attractive family for therapeutic exploitation (introduced in 8.2.1) and, with a recent lead intracellular modulator having been identified, provide a clinically relevant candidate for the use of a TMR-G $\alpha$ s19cha18 NanoBRET binding assay to identify the affinities of candidate small molecule intracellular ligands. Further application of the NanoBiT arrestin complementation assay (introduced in 1.2.6.3) provides a functional method of characterising novel ligands to verify the predictions of the novel screening system.

### 8.2. Introduction

#### 8.2.1. *Prostaglandin receptors and the role of EP<sub>2</sub> in disease.*

Prostaglandins (PGs) are lipid-derived autacoids generated by sequential metabolism of arachidonic acid by the cyclooxygenase (COX) and prostaglandin synthase enzymes. They play key roles in regulation of various cellular functions, inflammation and immune cell regulation through the employment of a range of GPCRs (Hata and Breyer, 2004). There are five subtypes of prostaglandin

(Thromboxane A<sub>2</sub>, PGD<sub>2</sub>, PGE<sub>2</sub>, PGI<sub>2</sub>, and PGF<sub>2α</sub>) and each bind one or more of the nine prostaglandin receptors DP<sub>1-2</sub>, EP<sub>1-4</sub>, FP, IP and TP. Therapeutic exploitation of prostaglandin signalling has primarily been achieved through reduction of prostaglandin production by employment of COX-1/2 inhibitors (non-steroidal anti-inflammatory drugs, NSAIDs, e.g., ibuprofen)(Rouzer and Marnett, 2009). NSAIDs are known for their antipyretic, analgesic, and anti-inflammatory properties, however, these have been met with a high degree of deleterious side effects such as gastrointestinal bleeding(Stiller and Hjemdahl, 2022). Selective targeting of COX-2 was hypothesised to reduce the incidence of severe side effects, however, despite reducing the incidence of severe gastrointestinal off-target effects, selective inhibition of COX-2 was implicated in serious on-target cardiovascular effects (e.g., myocardial infarction, hypertension, arrhythmia)(Schjerning et al., 2020). Due to COX-2's activation during inflammation and observed side-effect profile, selective targeting of particular prostaglandin receptors is being explored as a method to further reduce off-target side effects(Ganesh, 2014). Activation of the prostaglandin receptor EP<sub>2</sub> by PGE<sub>2</sub> in particular has been shown to be involved in the progression of oxidative damage associated with the activation of the innate immune response, implicating its role in inflammatory diseases such as endometriosis and rheumatoid arthritis, as well as neurodegenerative diseases including Alzheimer's and Parkinson's(Ganesh, 2014; McCullough et al., 2004; Prasanna et al., 2011; Tani et al., 2001). Additionally, upregulation of COX, PGE<sub>2</sub> and EP<sub>2</sub> expression within cancer (particularly colon cancer) is associated with increased tumorigenesis and proliferation, while also having an immunosuppressive role within the tumour microenvironment, increasing tumour immune evasion. This proposes a new route for targeting tumorigenesis through development of selective EP<sub>2</sub> receptor antagonists able to attenuate tumour proliferation and

increasing immune responses at the tumour microenvironment(Sluter et al., 2021).

Dependent on the indication, both agonists and antagonists might be of therapeutic benefit, making EP<sub>2</sub> and other prostaglandin receptors attractive therapeutic targets. Subsequently, this has resulted in a selection of prostaglandin ligands being developed, primarily binding via an orthosteric mode of action. A number of EP<sub>2</sub> antagonists have been identified by *ex vivo* and limited *in vivo* studies, however, none are currently licenced for use clinically and only one is currently under investigation in phase I trials (TPST-1495)(Davar et al., 2022). EP<sub>2</sub> antagonism has shown positive results in animal models of colorectal cancer, with application of selective EP<sub>2</sub> antagonist PF-04418948 over 80 days producing marked suppression in tumour formation by inhibition of proliferation and pro-inflammatory immune cell migration, limiting subsequent shaping the tumour microenvironment(Ma et al., 2015). Additionally, EP<sub>2</sub> antagonism has been shown to reduce the generation of the neuroinflammatory phenotype within Alzheimer's disease, allowing increased amyloid plaque phagocytosis and slowing of disease progression(Fox et al., 2015).

The recent development of a selective EP<sub>2</sub> receptor intracellular modulator proposes a novel method of targeting prostanoid receptors with potentially reduced side-effects(Jiang et al., 2020). "Compound 1" has been identified to display insurmountable inhibition selectively at the EP<sub>2</sub> receptor with varying efficiency depending on the agonist employed (Structure 1, section 8.4.1). Compound 1 was identified through its ability to disrupt cAMP production using a cAMP FRET sensor assay, and subsequent computational docking simulations to determine its binding site.

Interestingly, compound 1 was shown to change in apparent modulatory capacity depending on the potency of agonist employed, with more potent agonists eliciting a greater allosteric

efficacy, suggesting compound 1 displays a use-dependent mechanism of action. The combination of both allostery and use-dependent functionality provided by compound 1 gives the unique advantage of combining the beneficial ceiling effect of allosteric modulators, and the increased affinity for sites of high receptor activation driving a reduction in on- and off-target side effects. This would allow a reduced side-effect burden beyond those seen in orthosteric ligands designed to reduce side-effects on a purely receptor selectivity basis and therefore is a promising mechanism for further therapeutic exploration. One consideration however is that the exact binding site of compound 1 has not been definitively shown. Jiang *et al* inferred that binding occurs at the intracellular binding site through computational docking models, however, no experimental evidence is provided. Therefore, a binding assay as described in previous chapters would provide essential evidence for the IAM/G protein site action of compound 1 and similar molecules.

### 8.3. Chapter aims:

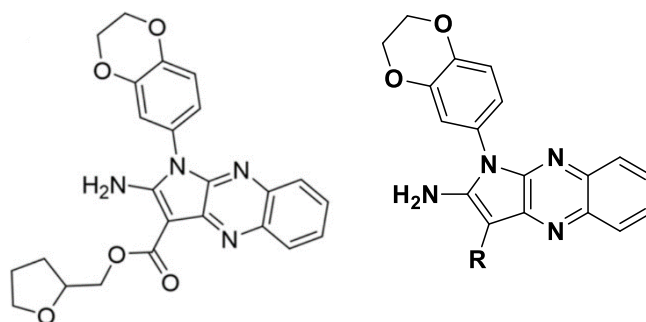
The EP<sub>2</sub> receptor is a current potential target for the antagonist treatment of inflammatory, CNS diseases and cancer, and is also the most recent GPCR with a candidate allosteric small-molecule ligand that may act intracellularly. This makes it a timely candidate for testing TMR-G $\alpha$ s19cha18's utility in screening at the intracellular site to guide modulator SAR. This chapter aims to characterise a number of novel EP<sub>2</sub> receptor IAMs derived from compound 1, within a small-scale competition screening assay, employing TMR-G $\alpha$ s19cha18 as the fluorescent probe in the NanoBRET binding assay. Characterisation of novel ligands via competition screening and subsequent functional characterisation provides experimental support for the action of Compound 1 as an IAM, and a greater understanding of EP<sub>2</sub> IAM structure-activity

relationships based on this series. It also validates the TMR-Gas19cha18 binding assay for small-molecule screening at intracellular GPCR sites.

## 8.4. Materials and Methods

### 8.4.1. Materials

Compounds CD006, CD012, CD026, CD064 and FI08, were designed using compound 1 (Structure 1) as a primary pharmacophore, with alterations at position R (Structure 2, see Table 8.1 for individual R groups):



**Structures 1 (Left) & 2 (Right).** (Left) Compound 1 as reported by Jieng *et al.*, (Right) Pharmacophore for the generation of compound 1-based analogues.

Compounds were synthesised by Constance Dalton (Mistry Lab, University of Nottingham) and verified by NMR spectra, recorded in deuterated solvent on a Bruker 400 spectrometer ( $^1\text{H}$  at 400.134 MHz,  $^{13}\text{C}$  at 100.624 MHz) at 293 K. RF-HPLC or Preparatory TLC purified samples were stored as 10mM stock solutions in DMSO at  $-20^\circ\text{C}$  in individual 2  $\mu\text{l}$  aliquots before use.

### 8.4.2. NanoBRET binding studies to monitor TMR-Gas19cha18 binding at the $\text{EP}_2$ receptor.

A Hek293 cell line and subsequent membrane preparations expressing p3.1neo(+)- $\text{EP}_2$ -tsNluc were each generated as described previously in sections 3.3&3.5. NanoBRET assays used low sodium assay binding buffer as described previously (section 4.4.2). TMR-

Gαs19cha18 binding was first characterised by addition of increasing fluorescent probe concentrations (78.125 – 10,000 nM) to 1µg/well Hek-EP<sub>2</sub>-tsNluc cell membranes, in which donor luciferase luminescence was stimulated with the addition of furimazine (1/960 dilution from Promega manufacturer's stock) in the additional absence or presence of the orthosteric agonist 10µM PGE<sub>2</sub> (final assay volume, 40µL [all dilutions accounted for 4x dilution upon addition to assay plate]). Fluorescent peptide NSB was defined by the inclusion of 10µM CD006. Endpoint reads at 30- and 60-min incubation at 37°C were taken using a PHERAstar as the BRET ratio between donor luminescence (450 nm emission) and acceptor TMR- Gαs19cha18 fluorescence (550 nm) to determine peptide binding.

For quantitative analysis of TMR- Gαs19cha18 recruitment by orthosteric agonist, 500nM tracer peptide was incubated with 1µg/well Hek-EP<sub>2</sub>-tsNluc cell membranes, 1/960 dilution furimazine, and incremental concentrations of PGE<sub>2</sub>. To initiate the recruitment, membranes were separately preincubated (5 min) with furimazine to establish luminescence output, prior to their online injection using the PHERAstar to assay buffer containing the probe peptide and stimulating ligands. NanoBRET was monitored after 30- and 60-minutes as above. Endpoint agonist stimulation of tracer peptide recruitment was assessed by concentration response curve analysis, performed to obtain estimates of ligand potency (EC<sub>50</sub>) and maximal response R<sub>max</sub> as described in data analysis (section 3.7).

To determine peptide tracer utility in small molecule competition screening and subsequent unlabelled ligand affinities, assays employed 500nM TMR- Gαs19cha18, a range of competing concentrations of unlabelled ligands ("compound 1", CD006, CD012, CD026, CD064, F108), 10µM PGE<sub>2</sub> and 1µg/well Hek-EP<sub>2</sub>-tsNluc cell membranes pre-incubated with 1/960 dilution of furimazine as indicated above (final volume, 50µL). Incubations

were performed at 37°C and BRET measurements were taken at 30 and 60 minutes, using a BMG PHERAstar FSX (550 nm / 450 nm ratio).

#### 8.4.3. *NanoBiT complementation assays to determine functional antagonism by candidate modulators.*

NanoBiT complementation was applied for the validation of the above novel unlabelled ligand CD006 within a functional assay system. Prior to ligand screening, Hek-EP<sub>2</sub>-LgBiT/SmBiT- $\beta$ -arrestin2 cells were seeded at 32,000 cells/well using poly-D-lysine coated 96-well, clear-bottom, white Greiner assay plates, and were incubated overnight at 37°C, 5% CO<sub>2</sub>. Post incubation, cells were washed, and growth media was replaced with 40  $\mu$ L pre-warmed assay buffer which consisted of HEPES buffered salt solution + 0.1% BSA (HBSS + 0.1% BSA) supplemented with 1/1320 dilution of furimazine and the CD006 concentrations as indicated in the results. The basal measure of luminescence was monitored for 5 minutes before the addition of 10  $\mu$ L vehicle (assay buffer) or varied concentrations of PGE<sub>2</sub> (10  $\mu$ M to 100 pM) to assay wells via online injection. Final assay volumes were 60  $\mu$ L per well [all dilutions accounted for 6x dilution upon addition to assay plate]. Luminescence measurements were obtained from 1 min post ligand addition as raw luminescence units (RLU), for 35 minutes, at 120 second intervals, maintained at 37°C throughout the assay.

## 8.5. Results and Discussion

### 8.5.1. Validation of TMR-Gas19cha18 as an intracellular probe for small-molecule screening at the prostaglandin EP<sub>2</sub> receptor

As shown in chapter 6, TMR-Gas19cha18 is able to bind the prostaglandin EP<sub>2</sub> receptor in an agonist dependent manner. However, the applicability of the fluorescent peptide NanoBRET assay in the context of small-molecule screening is yet to be established. To determine the ability of TMR-Gas19cha18 to identify novel unlabelled small-molecule modulators it is necessary to first determine the behaviour of the binding assay in verifying the affinity of a putative intracellular modulator. Previous data presented by Jiang *et al* identified the novel small-molecule EP<sub>2</sub> intracellular modulator “compound 1”, however, no data was presented to experimentally determine its binding at the intracellular binding site. Initial functional data by C Dalton (data not shown) identified CD006, a precursor in compound 1 synthesis, to be a potent EP<sub>2</sub> antagonist with similar modulatory capacity to compound 1. This makes CD006 a suitable candidate for determining TMR-Gas19cha18 capacity for small-molecule competition. Initially using a single high concentration of CD006 (10µM) against varied concentrations of TMR-Gas19cha18 yielded complete inhibition of tracer binding under agonist conditions (Figure 8.1C), indicating CD006 was indeed able to compete with the probe in competition binding and could be used more broadly in the assays to define tracer NSB.

Agonist-dependent binding of the probe to the EP<sub>2</sub>-Nanoluc receptor was briefly discussed in section 6.5.1.2, but in these initial studies EP<sub>2</sub>-probe binding had not been shown to be exclusively the result of receptor activation, nor had tracer EP<sub>2</sub> affinity been established, which is essential for deriving affinity estimates with competition screening. Therefore, initial saturation binding experiments compared the binding of increasing concentrations of

TMR-G $\alpha$ s19cha18 in both an agonist and vehicle environment, employing CD006 in defining NSB.

As with previous experiments employing the  $\beta_2$ -AR, peptide binding was exclusively observed upon inclusion of an orthosteric agonist, PGE<sub>2</sub>, with probe binding after vehicle treatment not significantly increased compared to non-specific binding (Figure 8.1A-B). In the presence of 10 $\mu$ M PGE<sub>2</sub> the affinity of TMR-G $\alpha$ s19cha18 for EP<sub>2</sub> was shown to be around 3-fold lower than that for the  $\beta_2$ -AR under similar conditions, with a  $K_D = 1.92 \pm 0.19 \mu$ M (Figure 8.1B, n=3). This variation in affinity across the G $\alpha_s$  coupled receptors is not unexpected. The ever-growing number of available GPCR-G protein structures are beginning to highlight the variability within G protein binding mechanisms across receptor subtypes. In particular, a review undertaken by Flock *et al* of multiple GPCR-G protein structural datasets across various receptor families, highlights multiple mechanism by which different G $\alpha_s$  coupled receptors interact and bind with the G $\alpha_s$  subunit (Flock *et al.*, 2017). Their review uses evolutionary history of receptor family sequences to highlight the variation in reliance on alternative interacting residues between the G $\alpha$   $\alpha$ 5 helix binding site and the receptor intracellular loop regions. Together, diversity of these inherent binding mechanisms and receptor- $\alpha$ 5 interactions presents an explanation for displayed variations in peptidomimetic interactions and affinity. Regarding the Gs-EP<sub>2</sub> binding site specifically, the cavity on the cytoplasmic side of the active EP<sub>2</sub> structure is narrower than that in the structure of the  $\beta_2$ -AR-Gs complex due to smaller separation of the TM3-TM6-TM7 bundles (Qu *et al.*, 2021). This potentially limits the binding of TMR-G $\alpha$ s19cha18 sterically, resulting in a reduced affinity. These variations in saturation binding (and apparent affinity) may also be influenced by the extent of competition between probe binding and native G protein in the assay. Incorporation of data presented by Flock *et al* implies this influence may also vary receptor to receptor

through variation in G protein affinity. Future studies may allow for exploration of these variations employing CRISPR cell lines lacking  $G\alpha_s$  expression (Inoue et al., 2019).

Further exploration of the concentration dependence for agonist induced recruitment of the  $G\alpha$  probe displayed previously produced data in line with previous adrenoceptor findings, indicating a  $pEC_{50}$  for  $PGE_2$  of  $5.89 \pm 0.07$  ( $n=3$ ; Figure 8.1D). This furthers the utility of the tracer peptide as a tool in determining orthosteric ligand efficacy. It is noteworthy that the displayed potency determined from tracer recruitment is significantly reduced when compared with previously presented functional (cAMP) data by Jieng *et al.* This is potentially due to differences signal amplification, with cAMP responses giving greater amplification (and therefore potency) at lower concentrations than is seen in direct probe binding experiments. Similarly, these variations may be the result of alterations in receptor function/conformation as a result of employing membrane preparations versus whole cells, or due to the C terminal NanoLuc modification employed for NanoBRET studies. There is also the possibility that, as with saturation experiments, an element of tracer competition with native G proteins is also driving a reduction in displayed potency (Gilchrist et al., 2001, 1998; Hamm et al., 1988).

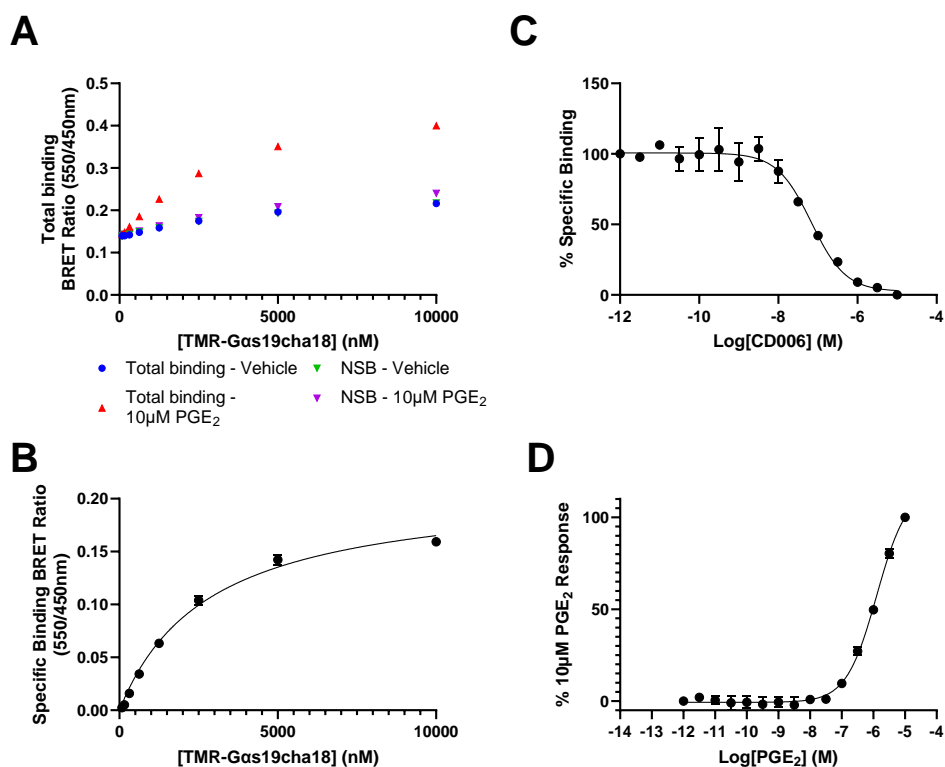


**Figure 8.1. Optimisation of a NanoBRET binding assay for validation of TMR-Gas19cha18 binding at the EP<sub>2</sub> receptor-tsNluc in HEK293 membranes.** (A) Saturation binding of TMR-Gas19cha18, demonstrating the increased specific binding observed only in the presence of 10 µM PGE<sub>2</sub>. Data are a representative experiment from three performed. (B) Validation of CD006 as a suitable NSB compound through NanoBRET competition displaying 100% displacement at high concentrations. Data are pooled, normalized, data from three experiments. (C) Derivation of TMR-Gas19cha18 affinity ( $K_D$ ) at EP<sub>2</sub> through saturation analysis of specific binding under orthosteric agonist stimulated conditions (10µM PGE<sub>2</sub>). Data are a representative experiment from three performed. (D) Concentration dependence of PGE<sub>2</sub> dependent recruitment of TMR-Gas19cha18 by NanoBRET, using 500nM TMR-Gas19cha18. In all cases measurements taken after 60-minutes, incubated at 37°C under low sodium conditions. Data are pooled, normalized, data from three experiments, plotted as mean  $\pm$  s.e.m.

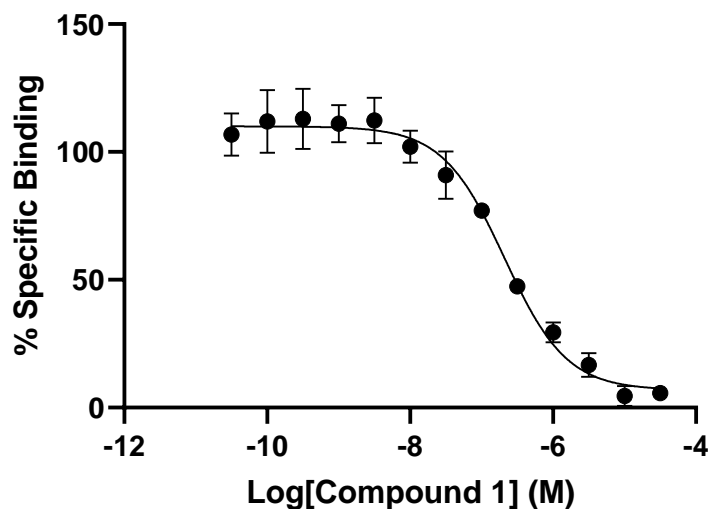
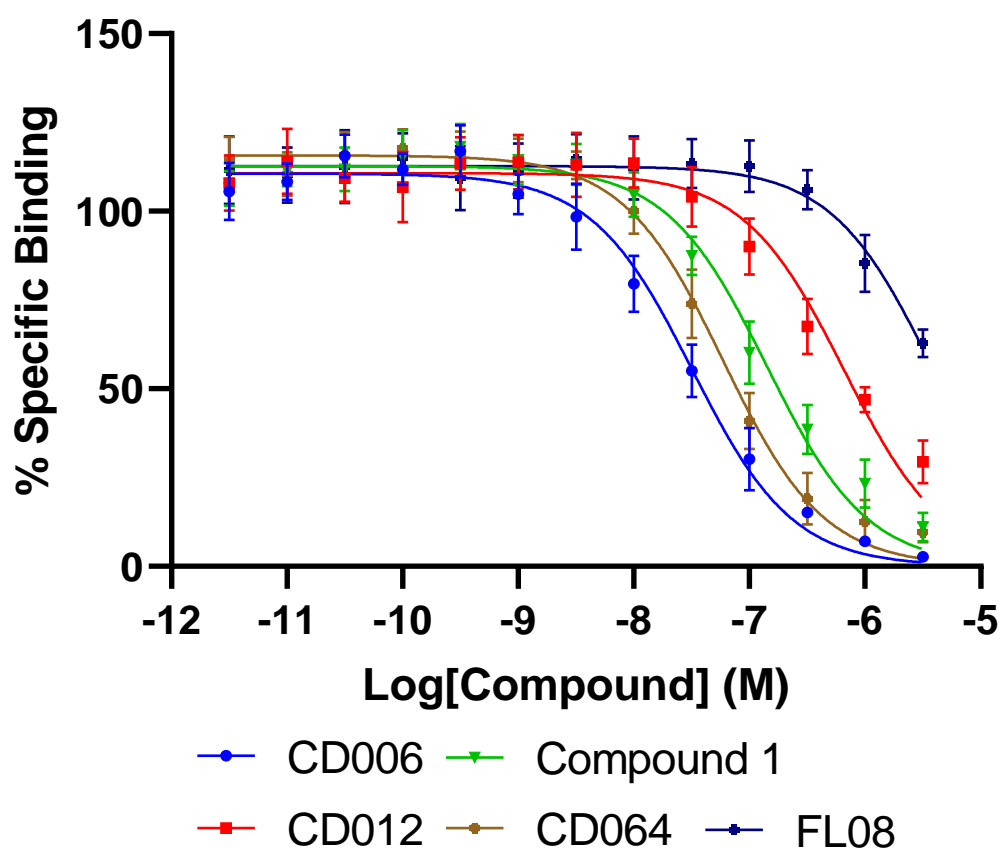


**Figure 8.2.** NanoBRET competition using TMR-G $\alpha$ s19cha18 to determine compound 1 affinity at EP<sub>2</sub>-tsNluc, measured at 60-minutes, 37°C incubation in low sodium buffer. Data are pooled, normalized, data from two-independent experiments run in duplicate, plotted as mean  $\pm$  s.e.m.

Having defined tracer binding affinity, the ability of TMR-G $\alpha$ s19cha18 to accurately determine unlabelled ligand binding parameters was initially investigated through competition against the EP<sub>2</sub> modulator compound 1. Employing a single concentration of tracer (1 $\mu$ M), at approximately 0.5 $\times$ K<sub>D</sub>, in the presence of a saturating concentration of PGE<sub>2</sub> (10 $\mu$ M) generated clear competition curves between TMR-G $\alpha$ s19cha18 and increasing concentrations of compound 1. The subsequent affinity derived for compound 1, estimated from the IC<sub>50</sub> value via the Cheng-Prusoff correction (Figure 8.2, pK<sub>i</sub> = 6.89 $\pm$ 0.01, n=2) is in line with estimates put forward by Jiang et al, validating TMR-G $\alpha$ s19cha18 as a suitable tracer for intracellular modulator characterisation(Jiang et al., 2020). Furthermore, this provides direct evidence that the location of compound 1 binding is indeed the intracellular G protein binding site of the EP<sub>2</sub> receptor, as predicted from homology modelling(Jiang et al., 2020).

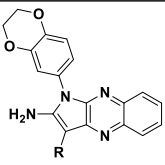
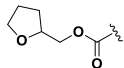
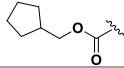
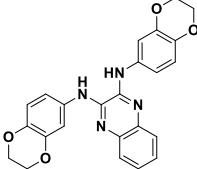
### 8.5.2. *Employing TMR-Gas19chal18 in the screening of novel EP<sub>2</sub> receptor intracellular allosteric modulators*

The ability of compound 1 to bind the EP<sub>2</sub> intracellular binding site presents an opportunity for rational, structural-based, design of a range of higher affinity small-molecule ligands, using compound 1 as a primary pharmacophore. Structural modelling by Jiang *et al* suggests the tetrahydrofuran species is the primary region of compound 1 involved in ligand binding. This region is orientated to allow extension of the species deeper into the centre of the intracellular pocket. Thus, modification of this region is hypothesised to have the greatest effect on ligand interactions and may allow generation of further modulators of greater selectivity and affinity. Medicinal chemistry efforts in this area were led by Constance Dalton, Shailesh Mistry and Charlie Laughton (University of Nottingham), with the pharmacological analysis presented below.



**Figure 8.3. NanoBRET competition screening to determine novel, small-molecule, EP<sub>2</sub> intracellular allosteric modulator affinities.** Screening employed Hek-EP<sub>2</sub>-tsNluc membranes incubated with 500nM TMR-G $\alpha$ s19cha18 and respective ligand concentrations in low sodium buffer at 37°C. Data was collected every 30-minutes over a one-hour interval. Data is pooled, normalised, 60-minute timepoint data from five independent experiments, plotted as mean  $\pm$  s.e.m.

**Table 8.1. Binding affinities of compound 1 analogues at the EP<sub>2</sub> receptor, measured using the TMR-Ga19cha18 NanoBRET binding assay.**

Compound	Structure/R group	pK <sub>i</sub> ± s.e.m
Pharmacophore		
Compound 1		7.03±0.15
CD006		7.64±0.18
CD012		6.59±0.16
CD064		7.51±0.1
FL08		5.84±0.13

pK<sub>i</sub> values are pooled, mean measurements derived from 4-5 independent experiments.

To test this hypothesis, four compounds were synthesised (by C Dalton) as shown in Table 8.1. These were then tested along with compound 1 in a NanoBRET competition screening assay, competing against TMR-Gas19cha18 for the intracellular binding site, to determine their respective affinities. All compounds tested competed against TMR-Gas19cha18, displaying a range of IC<sub>50</sub> and subsequent pK<sub>i</sub> values (Figure 8.3, Table 8.1), with an order of affinity of CD006 = CD064 > Compound 1 > CD012 > FL08. In line with previous predictions (Jiang et al., 2020), modification of the tetrahydrofuran group had the greatest effect on compound binding. The order of affinity seen in Table 8.1 of these modified ligands supports the hypothesis that it is primarily hydrophobic interactions involving the tetrahydrofuran group which drive ligand binding. CD012 has the weakest hydrophobic interaction through

the inclusion of a polar nitrile group. CD064 provides a 3-fold increase in affinity over compound 1 through the substitution for a cyclopentylmethyl ester residue, which, by omitting the oxygen, has a greater hydrophobicity while maintaining a similar group size. CD006 displayed a similar increase in affinity compared to compound 1, suggesting compound binding is primarily driven through both hydrophobic interactions and the ability for the modulator to embed in the pocket. In CD006, substitution of the tetrahydrofuran for an ethyl ester results in this region being smaller and therefore may reduce the potential for steric hindrance in ligand binding, allowing for potentially deeper and easier access to the binding pocket, while maintaining a high hydrophobicity. Finally, the reduced affinity displayed by FL08 provides evidence for greater steric hindrance to binding on substitution of an additional larger dihydrobenzodioxine group at the R position.

These data provide evidence that the TMR-G $\alpha$ s19cha18 EP<sub>2</sub> binding assay can identify small molecule intracellular modulators and help rank inhibitors in structure activity relationships through measurement of binding affinity. However, determination of ligand binding does not provide any evidence for the allosteric function of the compounds at the receptor. The binding of these ligands is hypothesised to bring about antagonism via direct competition with the native G protein or arrestins. Hence the use of a receptor-effector recruitment assay helps visualise the competition of intracellular ligands with intracellular effectors and explore their functional effects.

8.5.3. *Evaluation of CD006 efficacy in whole cell functional responses using NanoBiT complementation*

To determine the functional activity of the highest affinity analogue CD006 identified by EP<sub>2</sub> binding studies, PGE<sub>2</sub> dependent recruitment of  $\beta$ -arrestin2 was measured using an NanoBiT assay under control conditions or in the presence of different IAM concentrations.

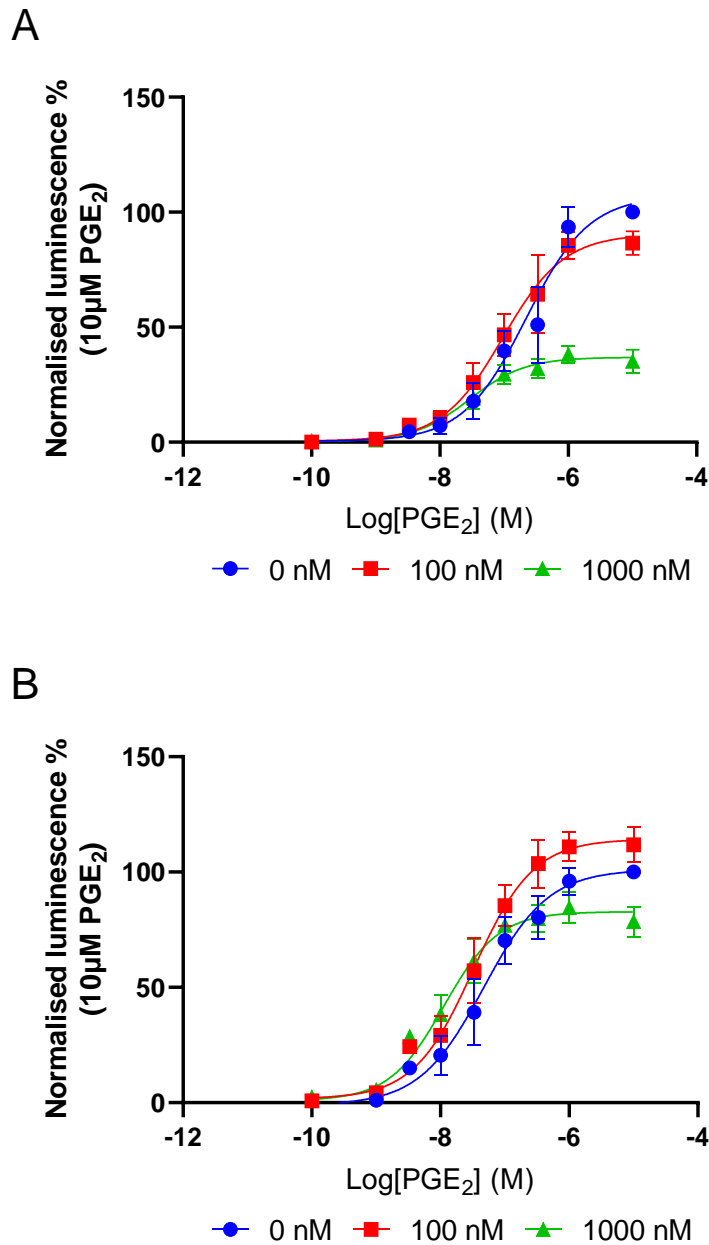


**Figure 8.4. PGE<sub>2</sub> driven  $\beta$ -arrestin2 recruitment to the EP<sub>2</sub> receptor under vehicle and CD006 conditions measured by NanoBiT complementation.** (A) Recruitment of  $\beta$ -arrestin2 as a result of receptor activation by PGE<sub>2</sub> in the presence of varied CD006 concentrations after 5-minute agonist incubation (B) Recruitment of  $\beta$ -arrestin2 as a result of receptor activation by PGE<sub>2</sub> in the presence of varied CD006 concentrations after 30-minute agonist incubation. Data are pooled, normalized data from 4 independent experiments, plotted as mean  $\pm$  s.e.m.

Initial control curves display effective recruitment of  $\beta$ -arrestin2 upon increasing concentration of PGE<sub>2</sub>, with only a small change in agonist potency between 5 and 30 minutes (pEC<sub>50</sub> 5 min:  $6.65 \pm 0.19$ , pEC<sub>50</sub> 31 min:  $7.34 \pm 0.02$ ,  $p=0.003$ [Student's t-test],  $df=3$ ,  $n=4$ ), indicative of rapidly equilibrating responses to orthosteric agonist stimulation. This is in contrast to PGE<sub>2</sub> mediated tracer recruitment data presented previously, indicating an increased potency of PGE<sub>2</sub>. This provides further evidence indicating the displayed potency determined from tracer recruitment is significantly reduced when compared with functional data, likely due to the presence of signal amplification in functional assays. Addition of CD006 had a minor effect on agonist EC<sub>50</sub> measurements, shifting curves to the left by 2 – 3 fold in potency, at both 100nM and 1  $\mu$ M concentrations across all timepoints (Figure 8.4, 31 minutes: vehicle pEC<sub>50</sub> =  $7.34 \pm 0.02$ , 1 $\mu$ M CD006 pEC<sub>50</sub> =  $7.89 \pm 0.13$ ,  $p=0.01$  [Student's t-test],  $df=3$ ,  $n=4$ ). This is indicative of an agonist dependent mechanism with positive co-operativity between the orthosteric and allosteric ligand binding. It suggests that modulators in this series, including compound 1 and CD006, may preferentially bind the active conformation and thus stabilise this high agonist affinity EP<sub>2</sub> receptor conformation. However, in addition to this positive cooperativity for agonist binding, 1  $\mu$ M CD006 produced a significant decrease in agonist R<sub>max</sub> at earlier timepoints. Initial readings taken after five minutes indicated a large reduction in R<sub>max</sub> verses control conditions (PGE<sub>2</sub> R<sub>max</sub> in presence of 1 $\mu$ M CD006 =  $37.4 \pm 3.5\%$  of control), however, this reduction became less pronounced upon additional measurement over 30-minutes (R<sub>max</sub> in presence of 1 $\mu$ M CD006 at 31-minutes =  $82.9 \pm 5.1\%$ ). As in Jiang et al (2021) analysis, this supports negative allosteric modulation on the basis of reduced receptor coupling efficiency to the effector ( $\beta$  co-operativity factor  $< 1$ ), due to the expected antagonism based on an IAM binding site of effector recruitment. Thus these functional data show initial evidence for a use dependent mechanism of the modulators (greater

binding / effect in the presence of agonist) which act to inhibit EP<sub>2</sub> as allosteric antagonists. Only two CD006 concentrations were assessed, but the functional effects observed at 100 nM and 1 μM are consistent with the measured binding affinity in the NanoBRET assay. Notably, the functional data are derived from a whole cell format, indicating that CD006 is sufficiently cell permeable (as might be expected from its lipophilicity) to access the IAM EP<sub>2</sub> site across the membrane. The greater effect of the modulator at early timepoints may reflect hemi-equilibrium conditions (at the 5 min timepoint, PGE<sub>2</sub> binding has had not sufficient time to re-establish a new equilibrium for agonist / modulator / EP<sub>2</sub> binding), or reflect the functional timecourse and location (e.g. plasma membrane versus endosomes at later timepoints) of EP<sub>2</sub>-arrestin recruitment by PGE<sub>2</sub>(Herenbrink et al., 2016; Hoare et al., 2020). Another factor driving this phenomenon may be due to the nature of the whole cell-based system, and how local concentrations of modulator might vary over the time of the assay, though it should be noted cells were pretreated with CD006 to establish an equilibrium prior to PGE<sub>2</sub> addition. Overall, these functional effect of CD006 highlight its role as an allosteric modulator of the EP<sub>2</sub> receptor, however, one limitation of the employed NanoBiT assay is it only provides functional characterisation of the effects on CD006 on arrestin recruitment. Given the high degree of overlap between the arrestin and G protein binding site, both employing the intracellular pocket inhabited by these intracellular ligands, it is likely that the arrestin response is similar to what would be seen with G protein binding. Additionally, the inhibition of cAMP production displayed previously for compound 1(Jiang et al., 2020) also suggests this relationship will be similar for EP<sub>2</sub>-G protein binding, however, it remains possible that CD006 may alter G protein and arrestin signalling to differing degrees. Future experiments exploring G protein recruitment directly, employing a range of modulators, would allow this possibility to be defined further. Additionally, employment of alternative orthosteric ligands,

and greater modulator concentrations, would facilitate a greater understanding of modulator function, and may allow global fitting of the allosteric operational model (in combination with derived modulator affinity data). This would provide greater quantitative characterisation of modulator function through measurement of their affinity ( $\alpha$ ) and efficacy ( $\beta$ ) co-operativity factors and will extend the evidence for a use dependent negative allosteric modulation of the EP<sub>2</sub> receptor across different effectors.

In conclusion, the binding of TMR-G $\alpha$ s19cha18 to the prostaglandin EP<sub>2</sub> receptor provides further evidence for its capacity to act as a more universal tracer for the Gs coupled GPCR intracellular binding site. Competition binding studies against novel small-molecule ligands show TMR-G $\alpha$ s19cha18 has the ability to identify ligands beyond the large peptide ligands described in chapter 6 and facilitates experimental validation of their intracellular mode of action. The application of these competition studies in combination with presented functional assays facilitated the identification of CD006 as a high affinity intracellular modulator able to compete for the intracellular binding site with native effector proteins. Subsequently, the functional validation of this identified small-molecule ligand provides strong verification for the use of TMR-G $\alpha$ s19cha18 as a tool for the identification and characterisation of small-molecule intracellular modulators within a high-throughput system. Ultimately, this provides an advantage in the easy ranking of novel modulators via binding affinity, and facilitates the use of the derived K<sub>i</sub>'s to improve fitting of functional data sets to allosteric models to estimate functional affinity, efficacy and co-operativity and provide evidence for use-dependent allosteric modulation. Together, this highlights an effective system for the identification of use-dependent modulators, particularly at the EP<sub>2</sub> receptor, with the potential to have greater target selectivity. Such compounds have the potential to provide greater therapeutic benefits over classical orthosteric antagonists in

targeting EP<sub>2</sub> as a strategy for treating cancer, inflammatory disease, and CNS disorders.

# **Chapter 9.**

## **General Discussion**

## 9. General Discussion

### 9.1. Thesis Discussion

GPCR therapeutics have been at the forefront of drug discovery since the purification of the opioid receptor agonist morphine from opium in 1804 (though this predated the concept of receptors, let alone GPCRs, by some 100 years). GPCR agonist and antagonist therapeutics have maintained their standing in drug discovery through the functional versatility of the receptors, which are involved in a wide variety of physiological processes. However, with increasing knowledge of cellular signalling and the nature of different GPCRs, barriers to further drug discovery have emerged, such as the difficulty of designing small molecules for larger peptide and protein hormone binding sites, and achieving suitable target selectivity between closely related receptors responsive to the same stimulating ligand. The identification of allosteric binding sites on GPCRs is rapidly broadening the potential for novel, selective, ligand development, enhanced by both advances in structural characterisation and pharmacological techniques to study the nature of allosterism (Changeux and Christopoulos, 2016; Leach et al., 2007; Thal et al., 2018). Sir James Black stated in his Nobel lecture “As analytical pharmacologists, what we are allowed to see of a new molecule's properties is totally dependent on the techniques of bioassay we use” (Black, 1989), a statement which, despite the growing number of methodologies being developed, still resonates with a continuing need for additional approaches in GPCR allosteric research. Growth of putative allosteric sites in GPCRs is likely to be spurred further by the expanding array of cryoEM and other structures, and their validation will require further additions to the assay toolbox to rapidly identify and fully evaluate allosteric ligand interactions. To date, techniques have relied heavily on functional interplay with orthosteric ligand binding and signalling and structural validation, which are limited in their capacity to identify a large array of ligands simultaneously

within a short timeframe and give limited direct understanding of allosteric ligand binding. Additionally, recent advancements in orthosteric ligand pharmacology have identified the importance of ligand binding kinetic relationships in therapeutic efficiency, an area currently underexplored in relation to allosteric pharmacology due to limited experimental capabilities (Cullum et al., 2023; Hill, 2006; Sykes et al., 2019).

This thesis aimed to address the need for a novel, high-throughput, approach to characterise allosteric ligands in the context of intracellular allosteric modulators, which target the receptor-effector interface and are applicable across a range of receptor targets (Andrews et al., 2008; Casella et al., 2023; Huber et al., 2023, 2022; Liu et al., 2017a; Nicholls et al., 2008; Oswald et al., 2016a; Salchow et al., 2010). Intracellular allosteric modulators have the capacity to rapidly advance the availability of highly receptor and target site-selective therapeutics. The combination of increased target selectivity through greater sequence heterogeneity within allosteric sites within receptor families, the allosteric “ceiling” that can limit maximal effect, and the potential for use-dependent binding mechanisms that limit drug action to conditions under orthosteric agonist stimulation, gives IAMs a unique advantage in reducing the adverse effects compared to more classical antagonist therapeutics. From a clinical perspective, these mechanisms have the potential to promote a positive impact on patient compliance and reduction in disease burden, particularly in cases where current treatments have severe adverse effects. Additionally, the ability of these ligands to directly compete with the effector (G proteins,  $\beta$ -arrestins) at the receptor binding provides these ligands with the ability to display allosteric antagonism with high negative co-operativity, and potentially in future discriminate between effector proteins to generate biased effects on signalling. Much of the pharmacology of IAMs remains of potential significance, rather than directly proven –

demonstration of high affinity, selective, IAM antagonists has been largely restricted to a few members of the chemokine receptor family to date (Andrews et al., 2008; Casella et al., 2023; Huber et al., 2023; Oswald et al., 2016a; Saha and Shukla, 2020; Salchow et al., 2010; Zweemer et al., 2014).

A characteristic of GPCR families is the ability of multiple diverse receptors to couple to the same class of G protein (e.g.  $G_s$ ,  $G_i$  or  $G_{q/11}$ ) and highlights a shared binding mechanism between receptor families that recognises the “right” G protein to maintain specificity of effector responses (Flock et al., 2015; Wingert et al., 2022; Zhou et al., 2019). It is this receptor-G protein binding site that is also targeted by a number of known IAMs. This underpinned the basic concept for the thesis, namely that probe tools could be developed that resembled the effector protein (e.g.,  $G\alpha_s$  versus  $G\alpha_i$ ) engaged by many different GPCRs, that could then be used in binding studies to assess interactions of novel allosteric ligands at the intracellular binding site. Previous research that focussed on G protein alpha subunit C termini (a key element involved in GPCR-G protein binding) suggested that peptides derived from this region would maintain a more universal binding relationship for GPCR intracellular binding sites (Dratz et al., 1993; Gilchrist et al., 1998; Hamm et al., 1988; Rens-Domiano and Hamm, 1995). This ability to recognise GPCRs based on G protein selectivity, in combination with their potentially ability to mimic the G protein’s ability to promote the agonist-receptor high affinity state, made these peptides a promising starting point for fluorescent probe development with utility at multiple GPCRs (Gilchrist et al., 2002, 2001; Mazzoni et al., 2000; Rasenick et al., 1994).

Initial characterisation of  $G\alpha$  C-terminus peptides in Chapter 4 aimed to establish their binding and modulatory capacity at both the  $G_s$  coupled  $\beta_2$ -adrenoceptor and  $G_i$  coupled Y1 receptor. The ability for various peptides, varying in length and amino acid sequence, to alter orthosteric agonist affinity within TR-FRET competition

binding studies was used as a measure of the peptide's ability to bind and promote the active conformation. From Gs peptide studies it was evident that peptide length, and by extension secondary structure due to the incorporation of additional alpha helical turns, has a large effect on modulatory capacity, with longer peptides displaying greater abilities to increase orthosteric agonist affinity. Additionally, the inclusion of a non-native amino acid (cyclohexylalanine, CHA) at the -2 position was shown to provide an increase in G $\alpha$ s19 peptide modulatory capacity similar to levels achieved by the longest peptide tested (G $\alpha$ s24), despite a reduction in peptide length. These studies confirmed the original activity of the peptides first described in Mannes et al (2021). However, when attempting to translate these peptide designs to G $_i$  receptor systems, multiple G $\alpha_i$  C terminus peptide variants had no significant effect on orthosteric agonist affinity, a result in line with previous findings by Gilchrist *et al* (Gilchrist et al., 1998). The nature of the assay used did not exclude the possibility that the G $\alpha_i$  peptides tested bound the Y1 receptor without influencing the affinity of the orthosteric peptide agonist NPY.

To directly determine G $\alpha$  peptide binding, and assess affinities of competing ligands at the intracellular modulator site, requires the generation of a functional fluorescent peptide probe. As such, Chapter 5 explored the utility of solution-based click-chemistry in the synthesis of fluorescent peptide probes. The ability to synthesise multiple derivatives using a single-step reaction would allow for rapid synthesis of optimised fluorescent peptides designed especially for particular experimental setups (e.g., far-red shifted fluorescent tracers for fluorescence correlation spectroscopy vs shorter wavelength tracers for BRET studies). Reactions undertaken proved ineffective in producing usable yields of tagged product, with variations in solvent system, temperature and collating ligand having no effect on reaction efficiency. Due to the alpha-helical structure of the peptide, it was hypothesised that the reacting group

of the propargylglycine may be hidden within the secondary structure. However, addition of trifluoroethanol, known to interrupt hydrogen bonding within protein secondary structure, had no effect on product yield. Subsequently, it was determined that in order to reduce the limiting effect of peptide secondary structure it is necessary to employ either an organic linker prior to fluorophore coupling or solid-phase peptide synthesis techniques. Generation of fluorescent TMR-G $\alpha$  peptides were therefore carried out commercially by solid-phase peptide synthesis.

Chapter 6 characterised the utility and characteristics of fluorescent G $\alpha$  C-terminus peptides within NanoBRET experiments. Again, employing the  $\beta_2$ -adrenoceptor and Y1 receptor as example Gs/Gi coupled receptors, peptide tracer binding was explored to determine respective affinities and binding mechanisms of fluorescent peptides. Initial experiments supported SAR relationships put forward in Chapter 4 and indicated that tracer binding relied on the presence of receptor orthosteric agonists in both  $\beta_2$ -AR and Y1 assays. However, G $\alpha_i$  derived peptide binding at the Y1 receptor appeared to display a lower affinity interaction than the G $\alpha_s$  counterpart. Further exploration of the agonist dependence displayed in association experiments identified the ability of labelled G $\alpha$  peptides to directly characterise orthosteric agonist efficacy as signalling biosensors, allowing clear distinction between various full and partial agonists. Additionally, comparison of various labelled and unlabelled G $\alpha_s$  peptides, varying in length and amino acid make-up, provided direct evidence supporting previous TR-FRET data, indicating increased affinity as a result of increased peptide length and hydrophobicity. Successive experiments employing alternative Gs/Gi coupled receptors indicated that TMR-G $\alpha_s$ 19cha18 in particular has the capacity to bind multiple Gs coupled receptors, whereas TMR-G $\alpha_i$ 19cha18's capability to bind alternative Gi coupled receptors appears more limited. In part this may reflect a reduced overall sensitivity of the assay due to the

reduced affinity of the Gi tracer compared to Gs. However, as discussed in chapter 6, it is also clear that the smaller size and nature of the Gi binding site in different GPCRs likely has a negative impact on the universal binding of Gα C terminal peptides.

Competition-based screening of unlabelled peptides using NanoBRET provided an initial indication that the fluorescent peptide probes may be applicable to establishing high-throughput screening at the intracellular binding site of multiple GPCRs. Chapter 8 carried these findings forward, demonstrating the utility of fluorescent G protein peptidomimetics in an initial small-molecule screen at the GPCR intracellular binding site.

Optimisation of TMR-Gαs19cha18 binding at the prostaglandin EP<sub>2</sub> receptor identified tracer affinity to be lower than the previously determined affinity for the β<sub>2</sub>-adrenoceptor, but with a sufficient PGE<sub>2</sub>-dependent assay window to be exploited in competition-based screening. Application of the known small molecule modulator “compound 1” indicated successful small-molecule competition able to provide measurements of compound 1 affinity consistent with the literature, and provide experimental validation of compound 1 intracellular binding (Jiang et al., 2020).

Subsequently, employment of TMR-Gαs19cha18 within a small-scale competition screen allowed identification of multiple novel intracellular allosteric modulators of the EP<sub>2</sub> receptor, with two, CD006 and CD064, displaying higher affinities for the intracellular binding site than the model compound, compound 1.

Having established a number of experimental uses for fluorescent G protein mimetics within plate-reader approaches, chapter 7 explored an alternative role for these tracers within microscopy-based experiments. Application of TMR-Gαs19cha18 within fluorescence correlation spectroscopy (FCS) established its capabilities for determining receptor binding using diffusion co-efficient based measurements. FCS auto-correlation analysis facilitated critical analysis of two common methods of receptor solubilization,

DIBMA particle formation or DDM micelle extraction, in the context of tracer binding. Evidence was provided for the binding of the probe to DIBMA  $\beta_2$ -AR particles, while observations with DDM solubilised  $\beta_2$ -AR were less clearcut. In addition, orthosteric-agonist dependent binding to solubilised receptors was not observed, in contrast to NanoBRET. The inability for DIBMA solubilized receptors, unlike membrane bound receptors, to display increased binding under agonist conditions implied a negative impact on native receptor conformation upon solubilization, either through loss of structural integrity or conformational restriction at the intracellular binding site. This ability to detect binding interactions at such a small scale demonstrates the putative power these probes have within FCS-based approaches for measuring intricate receptor dynamics, and future studies could explore whether the technique could be applied to native, unmodified receptor preparations

The aim of this thesis was to develop a novel toolset for the characterisation of intracellular allosteric modulators, applicable across multiple GPCRs. Exploiting the semi-universal binding mechanism displayed by G protein alpha subunits facilitated development of multiple peptidomimetic tracers able to selectively bind the GPCR intracellular binding site in a G protein, but not receptor, specific manner. Exploration of these fluorescent tracers has highlighted their capabilities within a range of different assay systems and provides strong evidence for their utility within a multitude of experimental scenarios. The nature of the G protein-GPCR interaction, and subsequent peptide-GPCR interaction, provided these novel tracers with the ability to not only act as a tool for high-throughput competition screening, but also as a novel sensor for detecting the GPCR active conformation. One future direction employing this characteristic could be to explore a wider range of agonists at candidate receptors, including not only orthosteric but other classes of allosteric (non IAM) ligand. Given

the fluorescent peptide probes are designed as G protein mimetics, it would also be useful to observe how the quantitative measures of agonist affinity and efficacy in this system relate to other measures for proposed G protein / arrestin biased ligands. Increasingly, structural data from receptor-arrestin and receptor-G protein complexes supports differences in active conformations between biased ligands that might be identified pharmacologically by a G protein mimetic intracellular probe(Liao et al., 2023).

One limitation of these tracers is their membrane impermeability and inability to be applied in whole cell experiments, which would allow for greater exploration of translational pharmacology and greater physiological relevance by maintaining the native receptor and cellular environment. Particular examples include application within primary cell assays and endogenous expression system, providing more representative measurements of modulator affinity and subsequent therapeutic effect at target tissues. Additionally, cell permeability would facilitate wider utility of the microscopy techniques employed in chapter 7, allowing for greater use of FCS and confocal microscopy to increase understanding of receptor-receptor interactions (e.g., dimerization). The large size of the peptide tracer prevents passive transmission across cellular membranes, however, there are potential solutions which could be explored in future work.

Foremost amongst these can be seen in work exploring antibody and nucleic acid (e.g., siRNA) employment within intracellular compartments. These are significantly larger than the peptide tracer described, and require complex methodologies for bypassing the cell membrane. There are a number of options available, the most experimentally simple of which is the employment of weak, reversable, detergent treatments, such as saponin(Medepalli et al., 2013; Wassler et al., 1987). This allows for the formation of small holes (roughly 100nm to 1µm in diameter) within the plasma membrane which allow for the translocation of proteins into and out

of the cytoplasm. However, the employment of saponin is known to have potential detrimental effects on the cellular environment and therefore may affect subsequent functional experimentation (Wassler et al., 1987). Alternative approaches make use of membrane permeable particles able to act as transporters of impermeable species, such as lipid or polymer-based nanoparticles. The exploitation of lipid nanoparticles in particular has become the gold standard in cell transfection (as described in section 3.3) by facilitating efficient transfer of DNA samples into test cell lines. Polymer-based nanoparticles function in a similar capacity, with initial systems designed to encase the desired cargo molecules for transport. However, unlike lipid particles which fuse with the cell membrane and release their contents intracellularly, polymer-based particles are designed to remain intact while crossing the cell surface before exploiting the intracellular machinery (e.g., proteases) to break down the transporter polymer and release the cargo (Yan et al., 2010). Alternatively, employment of cell penetrating peptides (such as the HIV-1 TAT protein) may provide a route across the membrane by applying these sequences as N-terminal modifications to Gα C terminal peptides, however, extensive peptide modification may have a negative impact on probe function (Zou et al., 2017). Exploration of these techniques and application of Gα peptides within whole cell assays would facilitate wider exploration of their role and applicability as tracers, particularly within primary cell assays and employment of allosteric operational models.

An alternative method for exploring this intracellular site, particularly within whole cell assays, is the use of miniG proteins or nanobodies. Such technologies would allow for DNA encoded luciferase/fluorescent protein-labelled binders able to target the intracellular binding site, however, these are not without their limitations, particularly in the context of high-throughput drug discovery. Foremost amongst these is the inability to easily

determine their intracellular concentration upon expression, meaning such probes can identify competition with unlabelled ligands, however, lack the required information for accurate derivation of ligand binding affinities (Carpenter et al., 2016; García-Nafría et al., 2018; Gilchrist et al., 2002; Robertson et al., 2022; Soave et al., 2020d; Wan et al., 2018). Additionally, when employing these alternative tracers within membrane-based approaches, the generation of purified nanobodies or miniG proteins requires time consuming and expensive experimental processes (namely generation of tracers through bacterial culture and subsequent purification steps) compared with short-chain peptide synthesis, which has the additional benefit of allowing incorporation of non-native amino acids and side-chain modifications. Together, presented findings utilising  $G\alpha$  C-terminus peptide tracers indicate similar limitations in cell permeability as does the use of miniG protein or nanobody technology, however, demonstrates a more accessible and highly modifiable system for the screening of intracellular binders.

Tackling these limitations represents one route to carry this research forward, providing greater utility of these peptidomimetics. Similarly, application of the key principles presented in this thesis would allow further exploration of similar peptide probes with wider employability. A related example would include similar characterisation of further G protein derived peptides, such as  $G\alpha_q$  or  $G\alpha_{12/13}$  for exploration of intracellular ligands able to interact with respectively coupled GPCRs. Furthermore, these principles are not exclusively applicable to GPCR ligand discovery and application of the core principles behind peptide selection can facilitate novel ligand discovery across all areas of protein research. By exploration of protein-protein interactions and identification of subsequent interacting region, it is possible to design putative peptide probes for a plethora of target proteins. This is particularly

promising for targeting structurally complex binding sites which remain elusive within small-molecule research.

## 9.2. Final Conclusions

Sponsored by the AJ Clark Scholarship (British Pharmacological Society), this thesis gives a stepwise account of the development and experimental validation of novel G protein peptidomimetic tracers for the intracellular binding site of Gs and Gi coupled G protein-coupled receptors.

The first three results chapters describe the initial identification and selection of lead peptides able to bind to a range of receptor subtypes. Initial assays identified peptides able to act as allosteric modulators of GPCR agonist binding, providing them with the putative ability to preferentially couple the receptor active conformation before exploration of their binding mechanisms directly via NanoBRET binding studies. These experiments highlighted the ability of these peptides to act not only as probes for the intracellular binding site, but also as activation sensors of GPCRs.

The final two results chapters provide contextual validation of the utility of described fluorescent probes across different experimental disciplines. Application of these probes within high-throughput screening was exemplified by the characterisation and identification of novel EP<sub>2</sub> receptor small-molecule modulators. In contrast, employment of these peptides within highly sensitive, microscopy-based, techniques was established through application within fluorescence correlation spectroscopy. Together, these chapters and this thesis provide a basis for the employment of G protein mimetic peptides within a range of pharmacological experiments for the characterisation of intracellular and extracellular ligands of GPCRs.

# **Chapter 10.**

## Bibliography.

## 10. Bibliography

- Aaij, C., Borst, P., 1972. The gel electrophoresis of DNA. *Biochimica et Biophysica Acta (BBA) - Nucleic Acids and Protein Synthesis* 269, 192–200. [https://doi.org/10.1016/0005-2787\(72\)90426-1](https://doi.org/10.1016/0005-2787(72)90426-1)
- Adeloye, D., Song, P., Zhu, Y., Campbell, H., Sheikh, A., Rudan, I., 2022. Global, regional, and national prevalence of, and risk factors for, chronic obstructive pulmonary disease (COPD) in 2019: a systematic review and modelling analysis. *Lancet Respir Med* 10. [https://doi.org/10.1016/S2213-2600\(21\)00511-7](https://doi.org/10.1016/S2213-2600(21)00511-7)
- Agard, N.J., Baskin, J.M., Prescher, J.A., Lo, A., Bertozzi, C.R., 2006. A comparative study of bioorthogonal reactions with azides. *ACS Chem Biol*. <https://doi.org/10.1021/cb6003228>
- Agasid, M.T., Sørensen, L., Umer, L.H., Yan, J., Robinson, C. V., 2021. The Effects of Sodium Ions on Ligand Binding and Conformational States of G Protein-Coupled Receptors-Insights from Mass Spectrometry. *J Am Chem Soc* 143, 4085–4089. [https://doi.org/10.1021/JACS.0C11837/ASSET/IMAGES/LARGE/JA0C11837\\_0002.JPEG](https://doi.org/10.1021/JACS.0C11837/ASSET/IMAGES/LARGE/JA0C11837_0002.JPEG)
- Ahlquist, R.P., 1948. A study of the adrenotropic receptors. <https://doi.org/10.1152/ajplegacy.1948.153.3.586> 153, 586–600. <https://doi.org/10.1152/AJPLEGACY.1948.153.3.586>
- Alexander, S., Mathie, A., Peters, J., 2011. *Guide to Receptors and Channels (GRAC)*, 5<sup>o</sup> Ed. *Br J Pharmacol*. <https://doi.org/10.1109/ISCAS.2009.5118218>
- Allen, S.J., Crown, S.E., Handel, T.M., 2007. Chemokine:Receptor Structure, Interactions, and Antagonism. *Annu Rev Immunol*. <https://doi.org/10.1146/annurev.immunol.24.021605.090529>

- Andersson, K.E., Campeau, L., Olshansky, B., 2011. Cardiac effects of muscarinic receptor antagonists used for voiding dysfunction. *Br J Clin Pharmacol* 72, 186. <https://doi.org/10.1111/J.1365-2125.2010.03813.X>
- Andrews, G., Jones, C., Wreggett, K.A., 2008. An Intracellular Allosteric Site for a Specific Class of Antagonists of the CC Chemokine G Protein-Coupled Receptors CCR4 and CCR5. *Mol Pharmacol* 73, 855–867. <https://doi.org/10.1124/mol.107.039321>
- Angers, S., Salahpour, A., Joly, E., Hilairret, S., Chelsky, D., Dennis, M., Bouvier, M., 2000. Detection of beta 2-adrenergic receptor dimerization in living cells using bioluminescence resonance energy transfer (BRET). *Proc Natl Acad Sci U S A* 97, 3684–3689. <https://doi.org/10.1073/PNAS.97.7.3684>
- Anton, S.E., Kayser, C., Maiellaro, I., Nemec, K., Möller, J., Koschinski, A., Zaccolo, M., Annibale, P., Falcke, M., Lohse, M.J., Bock, A., 2022a. Receptor-associated independent cAMP nanodomains mediate spatiotemporal specificity of GPCR signaling. *Cell* 185, 1130-1142.e11. <https://doi.org/10.1016/J.CELL.2022.02.011>
- Anton, S.E., Kayser, C., Maiellaro, I., Nemec, K., Möller, J., Koschinski, A., Zaccolo, M., Annibale, P., Falcke, M., Lohse, M.J., Bock, A., 2022b. Receptor-associated independent cAMP nanodomains mediate spatiotemporal specificity of GPCR signaling. *Cell* 185, 1130-1142.e11. <https://doi.org/10.1016/J.CELL.2022.02.011>
- Arsova, A., Møller, T.C., Hellyer, S.D., Vedel, L., Foster, S.R., Hansen, J.L., Bräuner-Osborne, H., Gregory, K.J., 2021. Positive Allosteric Modulators of Metabotropic Glutamate Receptor 5 as Tool Compounds to Study Signaling Bias. *Mol Pharmacol* 99. <https://doi.org/10.1124/MOLPHARM.120.000185>
- Aslam, M., Härtel, F. V., Arshad, M., Gündüz, D., Abdallah, Y., Sauer, H., Piper, H.M., Noll, T., 2010. CAMP/PKA antagonizes thrombin-induced inactivation of endothelial myosin light chain phosphatase: Role of CPI-17. *Cardiovasc Res* 87. <https://doi.org/10.1093/cvr/cvq065>

- ÅSTRÖM, A., PERSSON, N.H., 1961. Some pharmacological properties of o-methyl-alpha-propylaminopropioanilide, a new local anaesthetic. *Br J Pharmacol Chemother* 16, 32–44. <https://doi.org/10.1111/J.1476-5381.1961.TB00295.X>
- Awasthi-Kalia, M., Schnetkamp, P.P.M., Deans, J.P., 2001. Differential Effects of Filipin and Methyl- $\beta$ -cyclodextrin on B Cell Receptor Signaling. *Biochem Biophys Res Commun* 287, 77–82. <https://doi.org/10.1006/BBRC.2001.5536>
- Baillie, G.S., Adams, D.R., Bhari, N., Houslay, T.M., Vadrevu, S., Meng, D., Li, X., Dunlop, A., Milligan, G., Bolger, G.B., Klusmann, E., Houslay, M.D., 2007. Mapping binding sites for the PDE4D5 cAMP-specific phosphodiesterase to the N- and C-domains of  $\beta$ -arrestin using spot-immobilized peptide arrays. *Biochemical Journal* 404. <https://doi.org/10.1042/BJ20070005>
- Baker, J.G., 2010. The selectivity of beta-adrenoceptor agonists at human beta1-, beta2- and beta3-adrenoceptors. *Br J Pharmacol* 160, 1048–1061. <https://doi.org/10.1111/J.1476-5381.2010.00754.X>
- Baker, J.G., 2005. The selectivity of  $\beta$ -adrenoceptor antagonists at the human  $\beta$ 1,  $\beta$ 2 and  $\beta$ 3 adrenoceptors. *Br J Pharmacol* 144, 317–322. <https://doi.org/10.1038/sj.bjp.0706048>
- Baldock, P.A., Lee, N.J., Driessler, F., Lin, S., Allison, S., Stehrer, B., Lin, E.J.D., Zhang, L., Enriquez, R.F., Wong, I.P.L., McDonald, M.M., During, M., Pierroz, D.D., Slack, K., Shi, Y.C., Yulyaningsih, E., Aljanova, A., Little, D.G., Ferrari, S.L., Sainsbury, A., Eisman, J.A., Herzog, H., 2009. Neuropeptide Y knockout mice reveal a central role of NPY in the coordination of bone mass to body weight. *PLoS One* 4. <https://doi.org/10.1371/journal.pone.0008415>
- Balkwill, F., 2004. Cancer and the chemokine network. *Nat Rev Cancer* 4, 540–550. <https://doi.org/10.1038/NRC1388>
- Ballesteros, J.A., Weinstein, H., 1995. Integrated methods for the construction of three-dimensional models and computational probing of structure-

function relations in G protein-coupled receptors. *Methods in Neurosciences* 25, 366–428. [https://doi.org/10.1016/S1043-9471\(05\)80049-7](https://doi.org/10.1016/S1043-9471(05)80049-7)

- Bayburt, T.H., Leitz, A.J., Xie, G., Oprian, D.D., Sligar, S.G., 2007. Transducin Activation by Nanoscale Lipid Bilayers Containing One and Two Rhodopsins. *Journal of Biological Chemistry* 282, 14875–14881. <https://doi.org/10.1074/jbc.M701433200>
- Bayburt, T.H., Vishnivetskiy, S.A., McLean, M.A., Morizumi, T., Huang, C.C., Tesmer, J.J.G., Ernst, O.P., Sligar, S.G., Gurevich, V. V., 2011. Monomeric Rhodopsin Is Sufficient for Normal Rhodopsin Kinase (GRK1) Phosphorylation and Arrestin-1 Binding. *J Biol Chem* 286, 1420. <https://doi.org/10.1074/JBC.M110.151043>
- Beck, B., 2006. Neuropeptide Y in normal eating and in genetic and dietary-induced obesity. *Philosophical Transactions of the Royal Society B: Biological Sciences* 361, 1159. <https://doi.org/10.1098/RSTB.2006.1855>
- Bhatnagar, A., Willins, D.L., Gray, J.A., Woods, J., Benovic, J.L., Roth, B.L., 2001. The Dynamin-dependent, Arrestin-independent Internalization of 5-Hydroxytryptamine 2A (5-HT<sub>2A</sub>) Serotonin Receptors Reveals Differential Sorting of Arrestins and 5-HT<sub>2A</sub> Receptors during Endocytosis. *Journal of Biological Chemistry*. <https://doi.org/10.1074/jbc.M006968200>
- Black, J., 1989. Drugs from emasculated hormones: The principle of syntopic antagonism. *Science* (1979) 245. <https://doi.org/10.1126/science.2569237>
- Black, J.W., Leff, P., 1983. Operational models of pharmacological agonism. *Proc R Soc Lond B Biol Sci* 220, 141–162. <https://doi.org/10.1098/RSPB.1983.0093>
- Blecher, M., 1964. Serum protein-steroid hormone interactions I. Binding of deoxycorticosterone to serum proteins assayed in a metabolic system in vitro. *BBA - General Subjects* 93. [https://doi.org/10.1016/0304-4165\(64\)90270-3](https://doi.org/10.1016/0304-4165(64)90270-3)

- Boguth, C.A., Singh, P., Huang, C.C., Tesmer, J.J.G., 2010. Molecular basis for activation of G protein-coupled receptor kinases. *EMBO Journal* 29. <https://doi.org/10.1038/emboj.2010.206>
- Bolognini, D., Moss, C.E., Nilsson, K., Petersson, A.U., Donnelly, I., Sergeev, E., König, G.M., Kostenis, E., Kurowska-Stolarska, M., Miller, A., Dekker, N., Tobin, A.B., Milligan, G., 2016. A Novel Allosteric Activator of Free Fatty Acid 2 Receptor Displays Unique Gi-functional Bias. *J Biol Chem* 291, 18915–18931. <https://doi.org/10.1074/JBC.M116.736157>
- Bosier, B., Hermans, E., 2007. Versatility of GPCR recognition by drugs: from biological implications to therapeutic relevance. *Trends Pharmacol Sci*. <https://doi.org/10.1016/j.tips.2007.06.001>
- Boulton, S., Selvaratnam, R., Blondeau, J.P., Lezoualc'H, F., Melacini, G., 2018. Mechanism of Selective Enzyme Inhibition through Uncompetitive Regulation of an Allosteric Agonist. *J Am Chem Soc* 140. <https://doi.org/10.1021/jacs.8b05044>
- Breyton, C., Tribet, C., Olive, J., Dubacq, J.P., Popott, J.L., 1997. Dimer to monomer conversion of the cytochrome b6f complex: Causes and consequences. *Journal of Biological Chemistry* 272. <https://doi.org/10.1074/jbc.272.35.21892>
- Briddon, S.J., Hill, S.J., 2007. Pharmacology under the microscope: the use of fluorescence correlation spectroscopy to determine the properties of ligand–receptor complexes. *Trends Pharmacol Sci* 28, 637–645. <https://doi.org/10.1016/j.tips.2007.09.008>
- Briddon, S.J., Kilpatrick, L.E., Hill, S.J., 2018. Studying GPCR Pharmacology in Membrane Microdomains: Fluorescence Correlation Spectroscopy Comes of Age. *Trends Pharmacol Sci* 39, 158–174. <https://doi.org/10.1016/j.tips.2017.11.004>
- Briddon, S. J., Middleton, R.J., Cordeaux, Y., Flavin, F.M., Weinstein, J.A., George, M.W., Kellam, B., Hill, S.J., 2004. Quantitative analysis of the formation and diffusion of A 1-adenosine receptor-antagonist complexes

in single living cells. *Proc Natl Acad Sci U S A* 101, 4673–4678.

<https://doi.org/10.1073/pnas.0400420101>

Briddon, Stephen J., Middleton, R.J., Yates, A.S., George, M.W., Kellam, B., Hill, S.J., 2004. Application of fluorescence correlation spectroscopy to the measurement of agonist binding to a G-protein coupled receptor at the single cell level. *Faraday Discuss* 126, 197–207.

<https://doi.org/10.1039/B307407B>

Bridges, T.M., Rook, J.M., Noetzel, M.J., Morrison, R.D., Zhou, Y., Gogliotti, R.D., Vinson, P.N., Xiang, Z., Jones, C.K., Niswender, C.M., Lindsley, C.W., Stauffer, S.R., Conn, P.J., Daniels, J.S., 2013. Biotransformation of a novel positive allosteric modulator of metabotropic glutamate receptor subtype 5 contributes to seizure-like adverse events in rats involving a receptor agonism-dependent mechanism. *Drug Metabolism and Disposition* 41. <https://doi.org/10.1124/dmd.113.052084>

Budde, T., Meuth, S., Pape, H.C., 2002. Calcium-dependent inactivation of neuronal calcium channels. *Nat Rev Neurosci* 3.

<https://doi.org/10.1038/nrn959>

Burg, J.S., Ingram, J.R., Venkatakrisnan, A.J., Jude, K.M., Dukkipati, A., Feinberg, E.N., Angelini, A., Waghray, D., Dror, R.O., Ploegh, H.L., Garcia, K.C., 2015. Structural biology. Structural basis for chemokine recognition and activation of a viral G protein-coupled receptor. *Science* 347, 1113–1117. <https://doi.org/10.1126/SCIENCE.AAA5026>

Burggraaf, J., Westendorp, R.G.J., In't Veen, J.C.C.M., Schoemaker, R.C., Sterk, P.J., Cohen, A.F., Blauw, G.J., 2001. Cardiovascular side effects of inhaled salbutamol in hypoxic asthmatic patients. *Thorax*.

<https://doi.org/10.1136/thorax.56.7.567>

Byrne, C., McEwan, P.A., Emsley, J., Fischer, P.M., Cahn, W.C., 2011. End-stapled homo and hetero collagen triple helices: A click chemistry approach. *Chemical Communications* 47.

<https://doi.org/10.1039/c0cc04795c>

- Cacabelos, R., Takeda, M., Winblad, B., 1999. The glutamatergic system and neurodegeneration in dementia: Preventive strategies in Alzheimer's disease. *Int J Geriatr Psychiatry*. [https://doi.org/10.1002/\(SICI\)1099-1166\(199901\)14:1<3::AID-GPS897>3.0.CO;2-7](https://doi.org/10.1002/(SICI)1099-1166(199901)14:1<3::AID-GPS897>3.0.CO;2-7)
- Cao, C., Barros-Álvarez, X., Zhang, S., Kim, K., Dämgen, M.A., Panova, O., Suomivuori, C.M., Fay, J.F., Zhong, X., Krumm, B.E., Gumper, R.H., Seven, A.B., Robertson, M.J., Krogan, N.J., Hüttenhain, R., Nichols, D.E., Dror, R.O., Skinotis, G., Roth, B.L., 2022. Signaling snapshots of a serotonin receptor activated by the prototypical psychedelic LSD. *Neuron* 110, 3154-3167.e7. <https://doi.org/10.1016/j.neuron.2022.08.006>
- Carpenter, B., Nehmé, R., Warne, T., Leslie, A.G.W., Tate, C.G., 2016. Structure of the adenosine A2A receptor bound to an engineered G protein. *Nature* 536. <https://doi.org/10.1038/nature18966>
- Casadó-Anguera, V., Casadó, V., 2022. Unmasking allosteric-binding sites: novel targets for GPCR drug discovery. *Expert Opin Drug Discov* 17, 897–923. <https://doi.org/10.1080/17460441.2022.2085684>
- Casella, B.M., Farmer, J.P., Nesheva, D.N., Williams, H.E.L., Charlton, S.J., Holliday, N.D., Laughton, C.A., Mistry, S.N., 2023. Design, Synthesis, and Application of Fluorescent Ligands Targeting the Intracellular Allosteric Binding Site of the CXC Chemokine Receptor 2. *J Med Chem*. <https://doi.org/10.1021/acs.jmedchem.3c00849>
- Changeux, J.P., Christopoulos, A., 2016. Allosteric Modulation as a Unifying Mechanism for Receptor Function and Regulation. *Cell*. <https://doi.org/10.1016/j.cell.2016.08.015>
- Charest, P.G., Terrillon, S., Bouvier, M., 2005. Monitoring agonist-promoted conformational changes of beta-arrestin in living cells by intramolecular BRET. *EMBO Rep* 6, 334–340. <https://doi.org/10.1038/SJ.EMBOR.7400373>
- Chen, H.S.V., Pellegrini, J.W., Aggarwal, S.K., Lei, S.Z., Warach, S., Jensen, F.E., Lipton, S.A., 1992. Open-channel block of N-methyl-D-aspartate (NMDA) responses by memantine: therapeutic advantage against NMDA

receptor-mediated neurotoxicity. *J Neurosci* 12, 4427–4436.

<https://doi.org/10.1523/JNEUROSCI.12-11-04427.1992>

Chen, Q.C., Zhang, Y., 2022. The Role of NPY in the Regulation of Bone Metabolism. *Front Endocrinol (Lausanne)*.

<https://doi.org/10.3389/fendo.2022.833485>

Chen, Y., Müller, J.D., So, P.T.C., Gratton, E., 1999. The Photon Counting Histogram in Fluorescence Fluctuation Spectroscopy. *Biophys J* 77, 553–567. [https://doi.org/10.1016/S0006-3495\(99\)76912-2](https://doi.org/10.1016/S0006-3495(99)76912-2)

Cheng, X., Ji, Z., Tsalkova, T., Mei, F., 2008. Epac and PKA: A tale of two intracellular cAMP receptors. *Acta Biochim Biophys Sin (Shanghai)*.

<https://doi.org/10.1111/j.1745-7270.2008.00438.x>

Cherfils, J., Chabre, M., 2003. Activation of G-protein  $G\alpha$  subunits by receptors through  $G\alpha$ - $G\beta$  and  $G\alpha$ - $G\gamma$  interactions. *Trends Biochem Sci* 28, 13–17. [https://doi.org/10.1016/S0968-0004\(02\)00006-3](https://doi.org/10.1016/S0968-0004(02)00006-3)

Clark, A.J., 1937. Discussion on the chemical and physical basis of pharmacological action, 12 November, 1936. *Proc R Soc Lond B Biol Sci* 121, 580–609. <https://doi.org/10.1098/rspb.1937.0005>

Clark, A.J., 1933. The mode of action of drugs on cells / by A.J. Clark. | Wellcome Collection [WWW Document]. E. Arnold & Co. URL <https://wellcomecollection.org/works/nyvead3f> (accessed 7.15.23).

Clark, A.J., 1926. The reaction between acetyl choline and muscle cells. *J Physiol* 61, 530–546. <https://doi.org/10.1113/JPHYSIOL.1926.SP002314>

Comeo, E., Kindon, N.D., Soave, M., Stoddart, L.A., Kilpatrick, L.E., Scammells, P.J., Hill, S.J., Kellam, B., 2020. Subtype-Selective Fluorescent Ligands as Pharmacological Research Tools for the Human Adenosine A<sub>2A</sub> Receptor. *J Med Chem* 63, 2656–2672.

<https://doi.org/10.1021/acs.jmedchem.9b01856>

Conklin, B.R., Farfel, Z., Lustig, K.D., Julius, D., Bourne, H.R., 1993.

Substitution of three amino acids switches receptor specificity of G  $q\alpha$  to that of G  $i\alpha$ . *Nature* 363, 274–276. <https://doi.org/10.1038/363274a0>

- Cordeaux, Y., Briddon, S.J., Alexander, S.P.H., Kellam, B., Hill, S.J., 2008. Agonist-occupied A<sub>3</sub> adenosine receptors exist within heterogeneous complexes in membrane microdomains of individual living cells. *The FASEB Journal* 22, 850–860. <https://doi.org/10.1096/fj.07-8180com>
- Costa, T., Herz, A., 1989. Antagonists with negative intrinsic activity at delta opioid receptors coupled to GTP-binding proteins. *Proceedings of the National Academy of Sciences* 86, 7321–7325. <https://doi.org/10.1073/PNAS.86.19.7321>
- Covic, L., Gresser, A.L., Talavera, J., Swift, S., Kuliopulos, A., 2002. Activation and inhibition of G protein-coupled receptors by cell-penetrating membrane-tethered peptides. *Proc Natl Acad Sci U S A* 99, 643–648. <https://doi.org/10.1073/PNAS.022460899/ASSET/217B3341-43E8-42EB-A09C-176206FC7A6C/ASSETS/GRAPHIC/PQ0224608007.JPEG>
- Culhane, K.J., Gupte, T.M., Madhugiri, I., Gadgil, C.J., Sivaramakrishnan, S., 2022. Kinetic model of GPCR-G protein interactions reveals allosteric modulation of signaling. *Nat Commun* 13, 1202. <https://doi.org/10.1038/S41467-022-28789-5>
- Cullum, S.A., Veprintsev, D.B., Hill, S.J., 2023. Kinetic analysis of endogenous  $\beta$ 2-adrenoceptor-mediated cAMP GloSensor<sup>TM</sup> responses in HEK293 cells. *Br J Pharmacol* 180, 1304–1315. <https://doi.org/10.1111/BPH.16008>
- Cullum, V.A., Farmer, J.B., Jack, D., Levy, G.P., 1969. Salbutamol: a new, selective beta-adrenoceptive receptor stimulant. *Br J Pharmacol*. <https://doi.org/10.1111/j.1476-5381.1969.tb07975.x>
- D'Alonzo, G.E., Tolep, K., 1998. Salmeterol: a long-acting beta 2-agonist. *J Am Osteopath Assoc* 98.
- Davar, D., Powderly, J.D., Ulahannan, S.V., Johnson, M.L., Sharma, M., Krauss, J.C., Stagg, R., Francica, B., Moon, A., Jenkins, Y., Prasit, P., Dubensky, T.W., Whiting, S.H., Papadopoulos, K.P., 2022. A phase 1 study of TPST-1495 as a single agent and in combination with

pembrolizumab in subjects with solid tumors.

[https://doi.org/10.1200/JCO.2022.40.16\\_suppl.TPS2696](https://doi.org/10.1200/JCO.2022.40.16_suppl.TPS2696) 40, TPS2696–TPS2696. [https://doi.org/10.1200/JCO.2022.40.16\\_SUPPL.TPS2696](https://doi.org/10.1200/JCO.2022.40.16_SUPPL.TPS2696)

Dawaliby, R., Trubbia, C., Delporte, C., Masureel, M., van Antwerpen, P., Kobilka, B., Govaerts, C., 2016. Allosteric Regulation of GPCR Activity by Phospholipids. *Nat Chem Biol.* 12.

De Lean, A., Stadel, J.M., Lefkowitz, R.J., 1980. A ternary complex model explains the agonist-specific binding properties of the adenylate cyclase-coupled beta-adrenergic receptor. *Journal of Biological Chemistry* 255, 7108–7117. [https://doi.org/10.1016/S0021-9258\(20\)79672-9](https://doi.org/10.1016/S0021-9258(20)79672-9)

Degorce, F., Card, A., Soh, S., Trinquet, E., Knapik, G.P., Xie, B., 2009. HTRF: A technology tailored for drug discovery - a review of theoretical aspects and recent applications. *Curr Chem Genomics* 3, 22–32. <https://doi.org/10.2174/1875397300903010022>

Del Rio, L., Bennouna, S., Salinas, J., Denkers, E.Y., 2001. CXCR2 deficiency confers impaired neutrophil recruitment and increased susceptibility during *Toxoplasma gondii* infection. *J Immunol* 167, 6503–6509. <https://doi.org/10.4049/JIMMUNOL.167.11.6503>

Devalaraja, R.M., Nanney, L.B., Qian, Q., Du, J., Yu, Y., Devalaraja, M.N., Richmond, A., 2000. Delayed wound healing in CXCR2 knockout mice. *J Invest Dermatol* 115, 234–244. <https://doi.org/10.1046/J.1523-1747.2000.00034.X>

Dijon, N.C., Nesheva, D.N., Holliday, N.D., Aires, S., Martins, M., Miguel, D., 2021. Luciferase Complementation Approaches to Measure GPCR Signaling Kinetics and Bias. *Methods in Molecular Biology* 2268, 249–274. [https://doi.org/10.1007/978-1-0716-1221-7\\_17](https://doi.org/10.1007/978-1-0716-1221-7_17)

Dixon, A.S., Schwinn, M.K., Hall, M.P., Zimmerman, K., Otto, P., Lubben, T.H., Butler, B.L., Binkowski, B.F., Machleidt, T., Kirkland, T.A., Wood, M.G., Eggers, C.T., Encell, L.P., Wood, K. V., 2016. NanoLuc Complementation Reporter Optimized for Accurate Measurement of

Protein Interactions in Cells. ACS Chem Biol 11, 400–408.

<https://doi.org/10.1021/acscchembio.5b00753>

Dratz, E.A., Furstenau, J.E., Lambert, C.G., Thireault, D.L., Rarick, H., Schepers, T., Pakhlevanians, S., Hamm, H.E., 1993. NMR structure of a receptor-bound G-protein peptide. *Nature* 363, 276–281.

<https://doi.org/10.1038/363276a0>

DuBridge, R.B., Tang, P., Hsia, H.C., Leong, P.-M., Miller, J.H., Calos, M.P., 2023. Analysis of Mutation in Human Cells by Using an Epstein-Barr Virus Shuttle System. <https://doi.org/10.1128/mcb.7.1.379-387.1987> 7, 379–387. <https://doi.org/10.1128/MCB.7.1.379-387.1987>

Dwyer, M.P., Yu, Y., Chao, Jianping, Aki, C., Chao, Jianhua, Biju, P., Girijavallabhan, V., Rindgen, D., Bond, R., Mayer-Ezel, R., Jakway, J., Hipkin, R.W., Fossetta, J., Gonsiorek, W., Bian, H., Fan, X., Terminelli, C., Fine, J., Lundell, D., Merritt, J.R., Rokosz, L.L., Kaiser, B., Li, G., Wang, W., Stauffer, T., Ozgur, L., Baldwin, J., Taveras, A.G., 2006. Discovery of 2-hydroxy-N,N-dimethyl-3-{2-[[*(R)*-1-(5-methylfuran-2-yl)propyl]amino]-3,4-dioxocyclobut-1-enylamino}benzamide (SCH 527123): A potent, orally bioavailable CXCR2/CXCR1 receptor antagonist. *J Med Chem* 49. <https://doi.org/10.1021/jm0609622>

Edward Zhou, X., Melcher, K., Eric Xu, H., 2019. Structural biology of G protein-coupled receptor signaling complexes. *Protein Science*. <https://doi.org/10.1002/pro.3526>

Farmer, J.P., Mistry, S.N., Laughton, C.A., Holliday, N.D., 2022.

Development of fluorescent peptide G protein-coupled receptor activation biosensors for NanoBRET characterization of intracellular allosteric modulators. *The FASEB Journal* 36, e22576.

<https://doi.org/10.1096/FJ.202201024R>

Flock, T., Hauser, A.S., Lund, N., Gloriam, D.E., Balaji, S., Babu, M.M., 2017. Selectivity determinants of GPCR–G-protein binding. *Nature* 545, 317–322. <https://doi.org/10.1038/nature22070>

- Flock, T., Ravarani, C.N.J., Sun, D., Venkatakrishnan, A.J., Kayikci, M., Tate, C.G., Veprintsev, D.B., Babu, M.M., 2015. Universal allosteric mechanism for G $\alpha$  activation by GPCRs. *Nature* 524, 173–179. <https://doi.org/10.1038/nature14663>
- Förster, T., 1948. Zwischenmolekulare Energiewanderung und Fluoreszenz (Intermolecular energy migration and fluorescence). *Ann Phys* 2.
- Fox, B.M., Beck, H.P., Roveto, P.M., Kayser, F., Cheng, Q., Dou, H., Williamson, T., Treanor, J., Liu, H., Jin, L., Xu, G., Ma, J., Wang, S., Olson, S.H., 2015. A Selective Prostaglandin E2 Receptor Subtype 2 (EP2) Antagonist Increases the Macrophage-Mediated Clearance of Amyloid-Beta Plaques. *J Med Chem* 58, 5256–5273. [https://doi.org/10.1021/ACS.JMEDCHEM.5B00567/SUPPL\\_FILE/JM5B00567\\_SI\\_002.CSV](https://doi.org/10.1021/ACS.JMEDCHEM.5B00567/SUPPL_FILE/JM5B00567_SI_002.CSV)
- Fyfe, T.J., Kellam, B., Sykes, D.A., Capuano, B., Scammells, P.J., Lane, J.R., Charlton, S.J., Mistry, S.N., 2019. Structure–Kinetic Profiling of Haloperidol Analogues at the Human Dopamine D 2 Receptor. *J Med Chem* 62, 9488–9520. <https://doi.org/10.1021/acs.jmedchem.9b00864>
- Galés, C., Rebois, R.V., Hogue, M., Trieu, P., Breit, A., Hébert, T.E., Bouvier, M., 2005. Real-time monitoring of receptor and G-protein interactions in living cells. *Nat Methods* 2, 177–184. <https://doi.org/10.1038/NMETH743>
- Ganesh, T., 2014. Prostanoid receptor EP2 as a therapeutic target. *J Med Chem*. <https://doi.org/10.1021/jm401431x>
- Garbison, K.E., Heinz, B.A., Lajiness, M.E., Weidner, J.R., Sittampalam, G.S., 2004. Phospho-ERK Assays, *Assay Guidance Manual*.
- García-Nafría, J., Nehmé, R., Edwards, P.C., Tate, C.G., 2018. Cryo-EM structure of the serotonin 5-HT1B receptor coupled to heterotrimeric G $\alpha$ . *Nature*. <https://doi.org/10.1038/s41586-018-0241-9>
- Gehlert, D.R., Schober, D.A., Gackenheimer, S.L., Beavers, L., Gadski, R., Lundell, I., Larhammar, D., 1997. [125I]Leu31, Pro34-PYY is a high

affinity radioligand for rat PP1/Y4 and Y1 receptors: Evidence for heterogeneity in pancreatic polypeptide receptors. *Peptides (N.Y.)* 18. [https://doi.org/10.1016/S0196-9781\(96\)00346-4](https://doi.org/10.1016/S0196-9781(96)00346-4)

Gilchrist, A., Li, A., Hamm, H.E., 2002. G COOH-Terminal Minigene Vectors Dissect Heterotrimeric G Protein Signaling. *Sci Signal* 2002, p11–p11. <https://doi.org/10.1126/scisignal.1182002p11>

Gilchrist, A., Mazzoni, M.R., Dineen, B., Dice, A., Linden, J., Proctor, W.R., Lupica, C.R., Dunwiddie, T. V., Hamm, H.E., 1998. Antagonists of the Receptor-G Protein Interface Block G<sub>i</sub>-coupled Signal Transduction. *Journal of Biological Chemistry* 273, 14912–14919. <https://doi.org/10.1074/jbc.273.24.14912>

Gilchrist, A., Vanhauwe, J.F., Li, A., Thomas, T.O., Voyno-Yasenetskaya, T., Hamm, H.E., 2001. G<sub>α</sub> Minigenes Expressing C-terminal Peptides Serve as Specific Inhibitors of Thrombin-mediated Endothelial Activation. *Journal of Biological Chemistry* 276, 25672–25679. <https://doi.org/10.1074/jbc.M100914200>

Gillis, A., Gondin, A.B., Kliewer, A., Sanchez, J., Lim, H.D., Alamein, C., Manandhar, P., Santiago, M., Fritzwanker, S., Schmiedel, F., Katte, T.A., Reekie, T., Grimsey, N.L., Kassiou, M., Kellam, B., Krasel, C., Halls, M.L., Connor, M., Lane, J.R., Schulz, S., Christie, M.J., Canals, M., 2020. Low intrinsic efficacy for G protein activation can explain the improved side effect profiles of new opioid agonists. *Sci Signal* 13. <https://doi.org/10.1126/SCISIGNAL.AAZ3140>

Goldsmith, Z.G., Dhanasekaran, D.N., 2007. G Protein regulation of MAPK networks. *Oncogene*. <https://doi.org/10.1038/sj.onc.1210407>

Gómez-Santacana, X., Panarello, S., Rovira, X., Llebaria, A., 2022. Photoswitchable allosteric modulators for metabotropic glutamate receptors. *Curr Opin Pharmacol* 66, 102266. <https://doi.org/10.1016/j.coph.2022.102266>

Gonsiorek, W., Fan, X., Hesk, D., Fossetta, J., Qiu, H., Jakway, J., Billah, M., Dwyer, M., Chao, J., Deno, G., Taveras, A., Lundell, D.J., Hipkin, R.W.,

2007a. Pharmacological characterization of Sch527123, a potent allosteric CXCR1/CXCR2 antagonist. *Journal of Pharmacology and Experimental Therapeutics* 322. <https://doi.org/10.1124/jpet.106.118927>

Gonsiorek, W., Fan, X., Hesk, D., Fossetta, J., Qiu, H., Jakway, J., Billah, M., Dwyer, M., Chao, J., Deno, G., Taveras, A., Lundell, D.J., Hipkin, R.W., 2007b. Pharmacological characterization of Sch527123, a potent allosteric CXCR1/CXCR2 antagonist. *Journal of Pharmacology and Experimental Therapeutics*. <https://doi.org/10.1124/jpet.106.118927>

Goulding, J., Kondrashov, A., Mistry, S.J., Melarangi, T., Vo, N.T.N., Hoang, D.M., White, C.W., Denning, C., Briddon, S.J., Hill, S.J., 2021. The use of fluorescence correlation spectroscopy to monitor cell surface  $\beta$ 2-adrenoceptors at low expression levels in human embryonic stem cell-derived cardiomyocytes and fibroblasts. *FASEB Journal* 35. <https://doi.org/10.1096/FJ.202002268R>

Grandt, D., Schimiczek, M., Rascher, W., Feth, F., Shively, J., Lee, T.D., Davis, M.T., Reeve, J.R., Michel, M.C., 1996. Neuropeptide Y 3-36 is an endogenous ligand selective for Y2 receptors. *Regul Pept* 67. [https://doi.org/10.1016/S0167-0115\(96\)00104-8](https://doi.org/10.1016/S0167-0115(96)00104-8)

Gray, J.A., Bhatnagar, A., Gurevich, V. V., Roth, B.L., 2003. The interaction of a constitutively active arrestin with the arrestin-insensitive 5-HT<sub>2A</sub> receptor induces agonist-independent internalization. *Mol Pharmacol*. <https://doi.org/10.1124/mol.63.5.961>

Grime, R.L., Goulding, J., Uddin, R., Stoddart, L.A., Hill, S.J., Poyner, D.R., Briddon, S.J., Wheatley, M., 2020. Single molecule binding of a ligand to a G-protein-coupled receptor in real time using fluorescence correlation spectroscopy, rendered possible by nano-encapsulation in styrene maleic acid lipid particles. *Nanoscale* 12. <https://doi.org/10.1039/d0nr01060j>

Gupte, T.M., Malik, R.U., Sommese, R.F., Ritt, M., Sivaramakrishnan, S., 2017. Priming GPCR signaling through the synergistic effect of two G proteins. *Proc Natl Acad Sci U S A* 114, 3756–3761. <https://doi.org/10.1073/pnas.1617232114>

- Guttridge, A.M., Robins, M.T., Cassell, R.J., Uprety, R., Mores, K.L., Ko, M.J., Pasternak, G.W., Majumdar, S., van Rijn, R.M., 2020. G protein-biased kratom-alkaloids and synthetic carfentanil-amide opioids as potential treatments for alcohol use disorder. *Br J Pharmacol* 177, 1497–1513. <https://doi.org/10.1111/bph.14913>
- Halls, M.L., 2019. Localised GPCR signalling as revealed by FRET biosensors. *Curr Opin Cell Biol* 57, 48–56. <https://doi.org/10.1016/j.ceb.2018.11.001>
- Ham, D., Ahn, D., Ashim, J., Cho, Y., Kim, H.R., Yu, W., Chung, K.Y., 2021. Conformational switch that induces GDP release from Gi. *J Struct Biol* 213, 107694. <https://doi.org/10.1016/j.jsb.2020.107694>
- Hamm, H.E., Deretic, D., Arendt, A., Hargrave, P.A., Koenig, B., Hofmann, K.P., 1988. Site of G protein binding to rhodopsin mapped with synthetic peptides from the  $\alpha$  subunit. *Science* (1979) 241, 832–835. <https://doi.org/10.1126/science.3136547>
- Hanson, M.A., Cherezov, V., Griffith, M.T., Roth, C.B., Jaakola, V.-P., Chien, E.Y.T., Velasquez, J., Kuhn, P., Stevens, R.C., 2008. A Specific Cholesterol Binding Site Is Established by the 2.8 Å Structure of the Human  $\beta$ 2-Adrenergic Receptor. *Structure* 16, 897–905. <https://doi.org/10.1016/j.str.2008.05.001>
- Happ, J.T., Arveseth, C.D., Bruystens, J., Bertinetti, D., Nelson, I.B., Olivieri, C., Zhang, J., Hedeon, D.S., Zhu, J.F., Capener, J.L., Bröckel, J.W., Vu, L., King, C.C., Ruiz-Perez, V.L., Ge, X., Veglia, G., Herberg, F.W., Taylor, S.S., Myers, B.R., 2022. A PKA Inhibitor Motif within SMOOTHENED Controls Hedgehog Signal Transduction. *Nat Struct Mol Biol* 29, 990. <https://doi.org/10.1038/S41594-022-00838-Z>
- Harwood, C.R., Sykes, D.A., Hoare, B.L., Heydenreich, F.M., Uddin, R., Poyner, D.R., Briddon, S.J., Veprintsev, D.B., 2021. Functional solubilization of the  $\beta$ 2-adrenoceptor using diisobutylene maleic acid. *iScience* 24. <https://doi.org/10.1016/j.isci.2021.103362>

- Hata, A.N., Breyer, R.M., 2004. Pharmacology and signaling of prostaglandin receptors: Multiple roles in inflammation and immune modulation. *Pharmacol Ther* 103, 147–166.  
<https://doi.org/10.1016/J.PHARMTHERA.2004.06.003>
- Hauser, A.S., Attwood, M.M., Rask-Andersen, M., Schiöth, H.B., Gloriam, D.E., 2017. Trends in GPCR drug discovery: new agents, targets and indications. *Nat Rev Drug Discov* 16, 829–842.  
<https://doi.org/10.1038/nrd.2017.178>
- Hein, C.D., Liu, X.M., Wang, D., 2008. Click Chemistry, a Powerful Tool for Pharmaceutical Sciences. *Pharm Res* 25, 2216.  
<https://doi.org/10.1007/S11095-008-9616-1>
- Helenius, A., Simons, K., 1975. Solubilization of membranes by detergents. *BBA - Reviews on Biomembranes*. [https://doi.org/10.1016/0304-4157\(75\)90016-7](https://doi.org/10.1016/0304-4157(75)90016-7)
- Heng, J., Hu, Y., Pérez-Hernández, G., Inoue, A., Zhao, J., Ma, X., Sun, X., Kawakami, K., Ikuta, T., Ding, J., Yang, Y., Zhang, L., Peng, S., Niu, X., Li, H., Guixà-González, R., Jin, C., Hildebrand, P.W., Chen, C., Kobilka, B.K., n.d. Function and dynamics of the intrinsically disordered carboxyl terminus of  $\beta_2$  adrenergic receptor. <https://doi.org/10.1038/s41467-023-37233-1>
- Herenbrink, C.K., Sykes, D.A., Donthamsetti, P., Canals, M., Coudrat, T., Shonberg, J., Scammells, P.J., Capuano, B., Sexton, P.M., Charlton, S.J., Javitch, J.A., Christopoulos, A., Lane, J.R., 2016. The role of kinetic context in apparent biased agonism at GPCRs. *Nat Commun*.  
<https://doi.org/10.1038/ncomms10842>
- Heukers, R., De Groof, T.W.M., Smit, M.J., 2019. Nanobodies detecting and modulating GPCRs outside in and inside out. *Curr Opin Cell Biol*.  
<https://doi.org/10.1016/j.ceb.2019.01.003>
- Hilger, D., Masureel, M., Kobilka, B.K., 2018. Structure and dynamics of GPCR signaling complexes. *Nat Struct Mol Biol* 25, 4–12.  
<https://doi.org/10.1038/S41594-017-0011-7>

- Hill, S.J., 2006. G-protein-coupled receptors: past, present and future. *Br J Pharmacol* 147, S27. <https://doi.org/10.1038/SJ.BJP.0706455>
- Hill, A. V., 1909. The mode of action of nicotine and curari, determined by the form of the contraction curve and the method of temperature coefficients. *J Physiol* 39, 361–373.  
<https://doi.org/10.1113/JPHYSIOL.1909.SP001344>
- Hirsch, J.P., Dietzel, C., Kurjan, J., 1991. The carboxyl terminus of Scg1, the G $\alpha$  subunit involved in yeast mating, is implicated in interactions with the pheromone receptors. *Genes Dev* 5, 467–474.  
<https://doi.org/10.1101/gad.5.3.467>
- Hoare, S.R.J., 2018. Receptor binding kinetics equations: Derivation using the Laplace transform method. *J Pharmacol Toxicol Methods* 89, 26–38.  
<https://doi.org/10.1016/j.vascn.2017.08.004>
- Hoare, S.R.J., Tewson, P.H., Quinn, A.M., Hughes, T.E., Bridge, L.J., 2020. Analyzing kinetic signaling data for G-protein-coupled receptors. *Scientific Reports* 2020 10:1 10, 1–23. <https://doi.org/10.1038/s41598-020-67844-3>
- Hoff, M.J. b. van Den, Labruy ere, W.T., Moorman, A.F.M., Lamers, W.H., 1993. Mammalian gene expression is improved by use of a longer SV40 early polyadenylation cassette. *Nucleic Acids Res* 21, 4987.  
<https://doi.org/10.1093/NAR/21.21.4987>
- Hoffmann, C., Gaietta, G., B unemann, M., Adams, S.R., Oberdorff-Maass, S., Behr, B., Vilardaga, J.P., Tsien, R.Y., Ellisman, M.H., Lohse, M.J., 2005. A FIAsh-based FRET approach to determine G protein-coupled receptor activation in living cells. *Nat Methods* 2, 171–176.  
<https://doi.org/10.1038/NMETH742>
- Holz, O., Khalilieh, S., Ludwig-Sengpiel, A., Watz, H., Stryszak, P., Soni, P., Tsai, M., Sadeh, J., Magnussen, H., 2010. SCH527123, a novel CXCR2 antagonist, inhibits ozone-induced neutrophilia in healthy subjects. *European Respiratory Journal*.  
<https://doi.org/10.1183/09031936.00048509>

- Holzer, P., Reichmann, F., Farzi, A., 2012. Neuropeptide Y, peptide YY and pancreatic polypeptide in the gut–brain axis. *Neuropeptides* 46, 261.  
<https://doi.org/10.1016/J.NPEP.2012.08.005>
- Houslay, K.F., Christian, F., MacLeod, R., Adams, D.R., Houslay, M.D., Baillie, G.S., 2017. Identification of a multifunctional docking site on the catalytic unit of phosphodiesterase-4 (PDE4) that is utilised by multiple interaction partners. *Biochemical Journal* 474.  
<https://doi.org/10.1042/BCJ20160849>
- Huang, B., Perroud, T.D., Zare, R.N., 2004. Photon Counting Histogram: One-Photon Excitation. *ChemPhysChem* 5, 1523–1531.  
<https://doi.org/10.1002/cphc.200400176>
- Huang, S., Xu, P., Shen, D.-D., Simon, I.A., Mao, C., Tan, Y., Zhang, H., Harpsøe, K., Li, H., Zhang, Yumu, You, C., Yu, X., Jiang, Y., Zhang, Yan, Gloriam, D.E., Xu, H.E., 2022. GPCRs steer Gi and Gs selectivity via TM5-TM6 switches as revealed by structures of serotonin receptors. *Mol Cell* 82, 2681-2695.e6. <https://doi.org/10.1016/j.molcel.2022.05.031>
- Huber, M.E., Toy, L., Schmidt, M.F., Vogt, H., Budzinski, J., Wiefhoff, M.F.J., Merten, N., Kostenis, E., Weikert, D., Schiedel, M., 2022. A Chemical Biology Toolbox Targeting the Intracellular Binding Site of CCR9: Fluorescent Ligands, New Drug Leads and PROTACs. *Angewandte Chemie International Edition* 61.  
<https://doi.org/10.1002/anie.202116782>
- Huber, M.E., Wurnig, S., Toy, L., Weiler, C., Merten, N., Kostenis, E., Hansen, F.K., Schiedel, M., 2023. Fluorescent Ligands Enable Target Engagement Studies for the Intracellular Allosteric Binding Site of the Chemokine Receptor CXCR2. *J Med Chem*.  
<https://doi.org/10.1021/ACS.JMEDCHEM.3C00769>
- Hubner, H., Schellhorn, T., Gienger, M., Schaab, C., Kaindl, J., Leeb, L., Clark, T., Moller, D., Gmeiner, P., 2016. Structure-guided development of heterodimer-selective GPCR ligands. *Nat Commun* 7.  
<https://doi.org/10.1038/ncomms12298>

- Hulme, E.C., Trevethick, M.A., 2010. Ligand binding assays at equilibrium: validation and interpretation. *Br J Pharmacol* 161, 1219.  
<https://doi.org/10.1111/J.1476-5381.2009.00604.X>
- Ilien, B., Glasser, N., Clamme, J.P., Didier, P., Piemont, E., Chinnappan, R., Daval, S.B., Galzi, J.L., Mely, Y., 2009. Pirenzepine Promotes the Dimerization of Muscarinic M1 Receptors through a Three-step Binding Process. *Journal of Biological Chemistry* 284, 19533–19543.  
<https://doi.org/10.1074/JBC.M109.017145>
- Inoue, A., Raimondi, F., Kadji, F.M.N., Singh, G., Kishi, T., Uwamizu, A., Ono, Y., Shinjo, Y., Ishida, S., Arang, N., Kawakami, K., Gutkind, J.S., Aoki, J., Russell, R.B., 2019. Illuminating G-Protein-Coupling Selectivity of GPCRs. *Cell* 177. <https://doi.org/10.1016/j.cell.2019.04.044>
- Irannejad, R., Tomshine, J.C., Tomshine, J.R., Chevalier, M., Mahoney, J.P., Steyaert, J., Rasmussen, S.G.F., Sunahara, R.K., El-Samad, H., Huang, B., Von Zastrow, M., 2013. Conformational biosensors reveal adrenoceptor signalling from endosomes. *Nature* 495, 534–538.  
<https://doi.org/10.1038/NATURE12000>
- J Olsen, R.H., English, J.G., Reid J Olsen, C.H., Pharmacology, G., 2022. Advancements in G protein-coupled receptor biosensors to study GPCR-G protein coupling. *Br J Pharmacol*. <https://doi.org/10.1111/BPH.15962>
- Jiang, C., Amaradhi, R., Ganesh, T., Dingledine, R., 2020. An Agonist Dependent Allosteric Antagonist of Prostaglandin EP2 Receptors. *ACS Chem Neurosci* 11, 1436–1446.  
[https://doi.org/10.1021/ACSCHEMNEURO.0C00078/SUPPL\\_FILE/CNO00078\\_SI\\_001.PDF](https://doi.org/10.1021/ACSCHEMNEURO.0C00078/SUPPL_FILE/CNO00078_SI_001.PDF)
- Johnstone, E.K.M., Ayoub, M.A., Hertzman, R.J., See, H.B., Abhayawardana, R.S., Seeber, R.M., Pflieger, K.D.G., 2022. Novel Pharmacology Following Heteromerization of the Angiotensin II Type 2 Receptor and the Bradykinin Type 2 Receptor. *Front Endocrinol (Lausanne)* 13.  
<https://doi.org/10.3389/fendo.2022.848816>

- Kammermeier, P.J., 2012. Functional and pharmacological characteristics of metabotropic glutamate receptors 2/4 heterodimers. *Mol Pharmacol* 82. <https://doi.org/10.1124/mol.112.078501>
- Katritch, V., Cherezov, V., Stevens, R.C., 2013. Structure-function of the G protein-coupled receptor superfamily. *Annu Rev Pharmacol Toxicol*. <https://doi.org/10.1146/annurev-pharmtox-032112-135923>
- Katritch, V., Fenalti, G., Abola, E.E., Roth, B.L., Cherezov, V., Stevens, R.C., 2014. Allosteric sodium in class A GPCR signaling. *Trends Biochem Sci* 39, 233–244. <https://doi.org/10.1016/J.TIBS.2014.03.002>
- Kawakami, K., Yanagawa, M., Hiratsuka, S., Yoshida, M., Ono, Y., Hiroshima, M., Ueda, M., Aoki, J., Sako, Y., Inoue, A., 2022. Heterotrimeric Gq proteins act as a switch for GRK5/6 selectivity underlying  $\beta$ -arrestin transducer bias. *Nature Communications* 2022 13:13, 1–16. <https://doi.org/10.1038/s41467-022-28056-7>
- Keatings, V.M., Collins, P.D., Scott, D.M., Barnes, P.J., 1996. Differences in interleukin-8 and tumor necrosis factor-alpha in induced sputum from patients with chronic obstructive pulmonary disease or asthma. *Am J Respir Crit Care Med* 153, 530–534. <https://doi.org/10.1164/AJRCCM.153.2.8564092>
- Keller, M., Schindler, L., Bernhardt, G., Buschauer, A., 2015. Toward labeled argininamide-type NPY Y1 receptor antagonists: Identification of a favorable propionylation site in BIBO3304. *Arch Pharm (Weinheim)* 348. <https://doi.org/10.1002/ardp.201400427>
- Kenakin, T., 2010. G protein coupled receptors as allosteric proteins and the role of allosteric modulators. *Journal of Receptors and Signal Transduction* 30, 313–321. <https://doi.org/10.3109/10799893.2010.503964>
- Kenakin, T., Christopoulos, A., 2013. Signalling bias in new drug discovery: Detection, quantification and therapeutic impact. *Nat Rev Drug Discov*. <https://doi.org/10.1038/nrd3954>

- Kent, R.S., De Lean, A., Lefkowitz, R.J., 1980. A quantitative analysis of beta-adrenergic receptor interactions: resolution of high and low affinity states of the receptor by computer modeling of ligand binding data. *Mol Pharmacol* 17.
- Keppler, A., Pick, H., Arrivoli, C., Vogel, H., Johnsson, K., 2004. Labeling of fusion proteins with synthetic fluorophores in live cells. *Proc Natl Acad Sci U S A* 101, 9955. <https://doi.org/10.1073/PNAS.0401923101>
- Khan, S.M., Sleno, R., Gora, S., Zylbergold, P., Laverdure, J.P., Labbé, J.C., Miller, G.J., Hébert, T.E., 2013. The expanding roles of G $\beta\gamma$  subunits in G protein-coupled receptor signaling and drug action. *Pharmacol Rev.* <https://doi.org/10.1124/pr.111.005603>
- Kilpatrick, L.E., Hill, S.J., 2016. The use of fluorescence correlation spectroscopy to characterize the molecular mobility of fluorescently labelled G protein-coupled receptors. *Biochem Soc Trans* 44, 624–629. <https://doi.org/10.1042/BST20150285>
- Kilpatrick, L.E., Humphrys, L.J., Holliday, N.D., 2015. A G Protein–Coupled Receptor Dimer Imaging Assay Reveals Selectively Modified Pharmacology of Neuropeptide Y Y1/Y5 Receptor Heterodimers. *Mol Pharmacol* 87, 718–732. <https://doi.org/10.1124/mol.114.095356>
- Kim, K., Paulekas, S., Sadler, F., Gupte, T.M., Ritt, M., Dysthe, M., Vaidehi, N., Sivaramakrishnan, S., 2021.  $\beta$ 2-adrenoceptor ligand efficacy is tuned by a two-stage interaction with the G $\alpha$ s C terminus. *Proceedings of the National Academy of Sciences* 118, e2017201118. <https://doi.org/10.1073/pnas.2017201118>
- Kinney, G.G., O’Brien, J.A., Lemaire, W., Burno, M., Bickel, D.J., Clements, M.K., Chen, T.B., Wisnoski, D.D., Lindsley, C.W., Tiller, P.R., Smith, S., Jacobson, M.A., Sur, C., Duggan, M.E., Pettibone, D.J., Conn, P.J., Williams, D.L., 2005. A novel selective positive allosteric modulator of metabotropic glutamate receptor subtype 5 has in vivo activity and antipsychotic-like effects in rat behavioral models. *Journal of*

Pharmacology and Experimental Therapeutics 313.

<https://doi.org/10.1124/jpet.104.079244>

Knowles, T.J., Finka, R., Smith, C., Lin, Y.P., Dafforn, T., Overduin, M., 2009. Membrane proteins solubilized intact in lipid containing nanoparticles bounded by styrene maleic acid copolymer. *J Am Chem Soc* 131. <https://doi.org/10.1021/ja810046q>

Koehl, A., Hu, H., Maeda, S., Zhang, Y., Qu, Q., Paggi, J.M., Latorraca, N.R., Hilger, D., Dawson, R., Matile, H., Schertler, G.F.X., Granier, S., Weis, W.I., Dror, R.O., Manglik, A., Skiniotis, G., Kobilka, B.K., 2018. Structure of the  $\mu$ -opioid receptor-Gi protein complex. *Nature*. <https://doi.org/10.1038/s41586-018-0219-7>

Koelink, P.J., Overbeek, S.A., Braber, S., De Kruijf, P., Folkerts, G., Smit, M.J., Kraneveld, A.D., 2012. Targeting chemokine receptors in chronic inflammatory diseases: an extensive review. *Pharmacol Ther* 133, 1–18. <https://doi.org/10.1016/J.PHARMTHERA.2011.06.008>

Kok, Z.Y., Stoddart, L.A., Mistry, S.J., Mocking, T.A.M., Vischer, H.F., Leurs, R., Hill, S.J., Mistry, S.N., Kellam, B., 2022. Optimization of Peptide Linker-Based Fluorescent Ligands for the Histamine H1 Receptor. *J Med Chem* 65. <https://doi.org/10.1021/acs.jmedchem.2c00125>

Kolb, H.C., Finn, M.G., Sharpless, K.B., 2001. Click Chemistry: Diverse Chemical Function from a Few Good Reactions. *Angewandte Chemie - International Edition*. [https://doi.org/10.1002/1521-3773\(20010601\)40:11<2004::AID-ANIE2004>3.0.CO;2-5](https://doi.org/10.1002/1521-3773(20010601)40:11<2004::AID-ANIE2004>3.0.CO;2-5)

Kossoń, P., Dyniewicz, J., Lipiński, P.F.J., Matalińska, J., Misicka, A., Bojarski, A.J., Mordalski, S., 2023. Gai-derived peptide binds the  $\mu$ -opioid receptor. *Pharmacological Reports* 75. <https://doi.org/10.1007/s43440-023-00457-5>

Kozak, M., 1987. At least six nucleotides preceding the AUG initiator codon enhance translation in mammalian cells. *J Mol Biol* 196, 947–950. [https://doi.org/10.1016/0022-2836\(87\)90418-9](https://doi.org/10.1016/0022-2836(87)90418-9)

- Krause, J., Eva, C., Seeburg, P.H., Sprengel, R., 1992. Neuropeptide Y1 subtype pharmacology of a recombinantly expressed neuropeptide receptor. *Mol Pharmacol* 41.
- Kroeze, W.K., 2003. G-protein-coupled receptors at a glance. *J Cell Sci* 116, 4867–4869. <https://doi.org/10.1242/jcs.00902>
- Kruse, A.C., Ring, A.M., Manglik, A., Hu, J., Hu, K., Eitel, K., Hübner, H., Pardon, E., Valant, C., Sexton, P.M., Christopoulos, A., Felder, C.C., Gmeiner, P., Steyaert, J., Weis, W.I., Garcia, K.C., Wess, J., Kobilka, B.K., 2013. Activation and allosteric modulation of a muscarinic acetylcholine receptor. *Nature* 504. <https://doi.org/10.1038/nature12735>
- Kufareva, I., Stephens, B.S., Holden, L.G., Qin, L., Zhao, C., Kawamura, T., Abagyan, R., Handel, T.M., 2014. Stoichiometry and geometry of the CXC chemokine receptor 4 complex with CXC ligand 12: molecular modeling and experimental validation. *Proc Natl Acad Sci U S A* 111, E5363–E5372. <https://doi.org/10.1073/PNAS.1417037111>
- Latorraca, N.R., Venkatakrishnan, A.J., Dror, R.O., 2017. GPCR dynamics: Structures in motion. *Chem Rev*. <https://doi.org/10.1021/acs.chemrev.6b00177>
- Lay, C.S., Bridges, A., Goulding, J., Briddon, S.J., Soloviev, Z., Craggs, P.D., Hill, S.J., 2022. Probing the binding of interleukin-23 to individual receptor components and the IL-23 heteromeric receptor complex in living cells using NanoBRET. *Cell Chem Biol* 29. <https://doi.org/10.1016/j.chembiol.2021.05.002>
- Leach, K., Sexton, P.M., Christopoulos, A., 2007. Allosteric GPCR modulators: taking advantage of permissive receptor pharmacology. *Trends Pharmacol Sci* 28. <https://doi.org/10.1016/j.tips.2007.06.004>
- Lee, A.G., 2011. Lipid-protein interactions, in: *Biochemical Society Transactions*. <https://doi.org/10.1042/BST0390761>
- Lee, K.B., Pals-Rylaarsdam, R., Benovic, J.L., Hosey, M.M., 1998. Arrestin-independent internalization of the m1, m3, and m4 subtypes of muscarinic

cholinergic receptors. *Journal of Biological Chemistry*.

<https://doi.org/10.1074/jbc.273.21.12967>

Lefkowitz, R.J., Shenoy, S.K., 2005. Transduction of Receptor Signals by  $\beta$ -Arrestins. *Science* (1979) 308, 512–517.

<https://doi.org/10.1126/science.1109237>

Lefkowitz, R.J., Williams, L.T., 1977. Catecholamine binding to the beta-adrenergic receptor. *Proc Natl Acad Sci U S A* 74, 515.

<https://doi.org/10.1073/PNAS.74.2.515>

Leitz, A.J., Bayburt, T.H., Barnakov, A.N., Springer, B.A., Sligar, S.G., 2006. Functional reconstitution of  $\beta$ 2-adrenergic receptors utilizing self-assembling Nanodisc technology. *Biotechniques* 40.

<https://doi.org/10.2144/000112169>

Li, S.H., Abd-Elrahman, K.S., Ferguson, S.S.G., 2022. Targeting mGluR2/3 for treatment of neurodegenerative and neuropsychiatric diseases.

*Pharmacol Ther.* <https://doi.org/10.1016/j.pharmthera.2022.108275>

Liao, Y.Y., Zhang, H., Shen, Q., Cai, C., Ding, Y., Shen, D.D., Guo, J., Qin, J., Dong, Y., Zhang, Y., Li, X.M., 2023. Snapshot of the cannabinoid receptor 1-arrestin complex unravels the biased signaling mechanism.

*Cell* 186, 5784-5797.e17. <https://doi.org/10.1016/J.CELL.2023.11.017>

Liau, B.W.-H., Foroutan, A., Schamber, M.R., Lu, W., Samareh Afsari, H., Vafabakhsh, R., 2022. Conformational fingerprinting of allosteric modulators in metabotropic glutamate receptor 2. *Elife* 11.

<https://doi.org/10.7554/eLife.78982>

Liu, K., Shen, L., Wu, M., Liu, Z., Hua, T., 2022. Structural insights into the activation of chemokine receptor CXCR2. *FEBS J* 289, 386–393.

<https://doi.org/10.1111/febs.15865>

Liu, M., Richardson, R.R., Mountford, S.J., Zhang, L., Tempone, M.H., Herzog, H., Holliday, N.D., Thompson, P.E., 2016. Identification of a Cyanine-Dye Labeled Peptidic Ligand for Y1R and Y4R, Based upon the

Neuropeptide Y C-Terminal Analogue, BVD-15. *Bioconjug Chem* 27, 2166–2175. <https://doi.org/10.1021/ACS.BIOCONJCHEM.6B00376>

Liu, X., Ahn, S., Kahsai, A.W., Meng, K.-C., Latorraca, N.R., Pani, B., Venkatakrisnan, A.J., Masoudi, A., Weis, W.I., Dror, R.O., Chen, X., Lefkowitz, R.J., Kobilka, B.K., 2017a. Mechanism of intracellular allosteric  $\beta$ 2AR antagonist revealed by X-ray crystal structure. *Nature* 548, 480–484. <https://doi.org/10.1038/nature23652>

Liu, X., Ahn, S., Kahsai, A.W., Meng, K.-C., Latorraca, N.R., Pani, B., Venkatakrisnan, A.J., Masoudi, A., Weis, W.I., Dror, R.O., Chen, X., Lefkowitz, R.J., Kobilka, B.K., 2017b. Mechanism of intracellular allosteric  $\beta$ 2AR antagonist revealed by X-ray crystal structure. *Nature* 548, 480–484. <https://doi.org/10.1038/nature23652>

Lu, H., Yang, T., Xu, Z., Lin, X., Ding, Q., Zhang, Y., Cai, X., Dong, K., Gong, S., Zhang, W., Patel, M., Copley, R.C.B., Xiang, J., Guan, X., Wren, P., Ren, F., 2018. Discovery of Novel 1-Cyclopentenyl-3-phenylureas as Selective, Brain Penetrant, and Orally Bioavailable CXCR2 Antagonists. *J Med Chem*. <https://doi.org/10.1021/acs.jmedchem.7b01854>

Lulich, K.M., Goldie, R.G., Ryan, G., Paterson, J.W., 1986. Adverse Reactions to  $\beta$ 2-Agonist Bronchodilators. *Med Toxicol*. <https://doi.org/10.1007/BF03259844>

Ma, X., Aoki, T., Tsuruyama, T., Narumiya, S., 2015. Definition of prostaglandin E2-EP2 signals in the colon tumor microenvironment that amplify inflammation and tumor growth. *Cancer Res* 75, 2822–2832. <https://doi.org/10.1158/0008-5472.CAN-15-0125/651871/AM/DEFINITION-OF-PROSTAGLANDIN-E2-EP2-SIGNALS-IN-THE>

Maeda, S., Qu, Q., Robertson, M.J., Skiniotis, G., Kobilka, B.K., 2019. Structures of the M1 and M2 muscarinic acetylcholine receptor/G-protein complexes. *Science* (1979). <https://doi.org/10.1126/science.aaw5188>

- Maehle, A.H., Prüll, C.R., Halliwell, R.F., 2002. The emergence of the drug receptor theory. *Nat Rev Drug Discov* 1, 637–641.  
<https://doi.org/10.1038/NRD875>
- Mafi, A., Kim, S.-K., Iii, W.A.G., 2023. The dynamics of agonist- $\beta$ 2-adrenergic receptor activation induced by binding of GDP-bound Gs protein. *Nature Chemistry* 2023 1–11. <https://doi.org/10.1038/s41557-023-01238-6>
- Magde, D., Elson, E., Webb, W.W., 1972. Thermodynamic fluctuations in a reacting system measurement by fluorescence correlation spectroscopy. *Phys Rev Lett* 29. <https://doi.org/10.1103/PhysRevLett.29.705>
- Makrides, S.C., 1999. Components of Vectors for Gene Transfer and Expression in Mammalian Cells. *Protein Expr Purif* 17, 183–202.  
<https://doi.org/10.1006/PREP.1999.1137>
- Mannes, M., Martin, C., Triest, S., Dimmito, M.P., Mollica, A., Laeremans, T., Menet, C.J., Ballet, S., 2021. Development of Generic G Protein Peptidomimetics Able to Stabilize Active State Gs Protein-Coupled Receptors for Application in Drug Discovery. *Angewandte Chemie International Edition* anie.202100180.  
<https://doi.org/10.1002/anie.202100180>
- Mant, C.T., Chen, Y., Yan, Z., Popa, T. V., Kovacs, J.M., Mills, J.B., Tripet, B.P., Hodges, R.S., 2007. HPLC Analysis and Purification of Peptides. *Peptide Characterization and Application Protocols* 386, 3.  
[https://doi.org/10.1007/978-1-59745-430-8\\_1](https://doi.org/10.1007/978-1-59745-430-8_1)
- May, L., 2003. Allosteric modulators of G-protein-coupled receptors. *Curr Opin Pharmacol* 3, 551–556. [https://doi.org/10.1016/S1471-4892\(03\)00107-3](https://doi.org/10.1016/S1471-4892(03)00107-3)
- Mazzoni, M.R., Taddei, S., Giusti, L., Rovero, P., Galoppini, C., D’Ursi, A., Albrizio, S., Triolo, A., Novellino, E., Greco, G., Lucacchini, A., Hamm, H.E., 2000. A G $\alpha$ (s) carboxyl-terminal peptide prevents G(s) activation by the A(2A) adenosine receptor. *Mol Pharmacol* 58, 226–236.  
<https://doi.org/10.1124/mol.58.1.226>

- McCullough, L., Wu, L., Haughey, N., Liang, X., Hand, T., Wang, Q., Breyer, R.M., Andreasson, K., 2004. Neuroprotective Function of the PGE2 EP2 Receptor in Cerebral Ischemia. *Journal of Neuroscience* 24. <https://doi.org/10.1523/JNEUROSCI.4485-03.2004>
- Medepalli, K., Alphenaar, B.W., Keynton, R.S., Sethu, P., 2013. A new technique for reversible permeabilization of live cells for intracellular delivery of quantum dots. *Nanotechnology* 24, 205101. <https://doi.org/10.1088/0957-4484/24/20/205101>
- Merrifield, R.B., 1963. Solid Phase Peptide Synthesis. I. The Synthesis of a Tetrapeptide. *J Am Chem Soc* 85. <https://doi.org/10.1021/ja00897a025>
- Meyrath, M., Szpakowska, M., Plessier, J.M., Domingues, O., Langlet, J., Weber, B., Krüger, R., Ollert, M., Chevigné, A., 2022. Nanoluciferase-based cell fusion assay for rapid and high-throughput assessment of SARS-CoV-2-neutralizing antibodies in patient samples. *Methods Enzymol* 675, 351–381. <https://doi.org/10.1016/BS.MIE.2022.07.015>
- Middleton, R.J., Briddon, S.J., Cordeaux, Y., Yates, A.S., Dale, C.L., George, M.W., Baker, J.G., Hill, S.J., Kellam, B., 2007. New fluorescent adenosine A1-receptor agonists that allow quantification of ligand-receptor interactions in microdomains of single living cells. *J Med Chem* 50, 782–793. <https://doi.org/10.1021/jm061279i>
- Miller, M.C., Mayo, K.H., 2017. Chemokines from a Structural Perspective. *Int J Mol Sci* 18. <https://doi.org/10.3390/IJMS18102088>
- Miller, R.T., Masters, S.B., Sullivan, K.A., Beiderman, B., Bourne, H.R., 1988. A mutation that prevents GTP-dependent activation of the  $\alpha$  chain of Gs. *Nature*. <https://doi.org/10.1038/334712a0>
- Mohammad Nezhady, M.A., Rivera, J.C., Chemtob, S., 2020. Location Bias as Emerging Paradigm in GPCR Biology and Drug Discovery. *iScience*. <https://doi.org/10.1016/j.isci.2020.101643>
- Mohanty, S.K., Mittal, A., Gaur, A., Solanki, S., Kumar, S., Duari, S., Arora, S., Gautam, V., Dixit, N.K., Ghosh, T.S., Sengupta, D., Gupta, S.K.,

Murugan, N.A., Ahuja, G., 2023. Artificial Intelligence uncovers Evolutionarily Conserved Intracellular Allosteric Modulators of GPCR- $G\alpha$  interface. *bioRxiv*.

Mosslehy, W., Voskoboynikova, N., Colbasevici, A., Ricke, A., Klose, D., Klare, J.P., Mulkidjanian, A.Y., Steinhoff, H.J., 2019. Conformational Dynamics of Sensory Rhodopsin II in Nanolipoprotein and Styrene–Maleic Acid Lipid Particles. *Photochem Photobiol* 95. <https://doi.org/10.1111/php.13096>

Motulsky, H.J., Mahan, L.C., 1984. The kinetics of competitive radioligand binding predicted by the law of mass action. *Mol Pharmacol* 25, 1–9.

Mountford, S.J., Liu, M., Zhang, L., Groenen, M., Herzog, H., Holliday, N.D., Thompson, P.E., 2014. Organic & Biomolecular Chemistry Synthetic routes to the Neuropeptide Y Y1 receptor antagonist 1229U91 and related analogues for SAR studies and cell-based imaging †. *Org. Biomol. Chem* 12, 3271. <https://doi.org/10.1039/c4ob00176a>

Navarro, G., Varani, K., Reyes-Resina, I., de Medina, V.S., Rivas-Santisteban, R., Callado, C.S.C., Vincenzi, F., Casano, S., Ferreiro-Vera, C., Canela, E.I., Borea, P.A., Nadal, X., Franco, R., 2018. Cannabigerol Action at Cannabinoid CB1 and CB2 Receptors and at CB1-CB2 Heteroreceptor Complexes. *Front Pharmacol* 9. <https://doi.org/10.3389/FPHAR.2018.00632>

Nguyen, A.D., Mitchell, N.F., Lin, S., Macia, L., Yulyaningsih, E., Baldock, P.A., Enriquez, R.F., Zhang, L., Shi, Y.C., Zolotukhin, S., Herzog, H., Sainsbury, A., 2012. Y1 and Y5 receptors are both required for the regulation of food intake and energy homeostasis in mice. *PLoS One* 7. <https://doi.org/10.1371/journal.pone.0040191>

Nicholls, D.J., Tomkinson, N.P., Wiley, K.E., Brammall, A., Bowers, L., Grahames, C., Gaw, A., Meghani, P., Shelton, P., Wright, T.J., Mallinder, P.R., 2008. Identification of a putative intracellular allosteric antagonist binding-site in the CXC chemokine receptors 1 and 2. *Mol Pharmacol* 74, 1193–1202. <https://doi.org/10.1124/mol.107.044610>

- Nobles, K.N., Xiao, K., Ahn, S., Shukla, A.K., Lam, C.M., Rajagopal, S., Strachan, R.T., Huang, T.Y., Bressler, E.A., Hara, M.R., Shenoy, S.K., Gygi, S.P., Lefkowitz, R.J., 2011. Distinct phosphorylation sites on the  $\beta(2)$ -adrenergic receptor establish a barcode that encodes differential functions of  $\beta$ -arrestin. *Sci Signal* 4.  
<https://doi.org/10.1126/SCISIGNAL.2001707>
- Norman, P., 2013. Evidence on the identity of the CXCR2 antagonist AZD-5069. *Expert Opin Ther Pat* 23, 113–117.  
<https://doi.org/10.1517/13543776.2012.725724>
- Oates, J., Watts, A., 2011. Uncovering the intimate relationship between lipids, cholesterol and GPCR activation. *Curr Opin Struct Biol*.  
<https://doi.org/10.1016/j.sbi.2011.09.007>
- Oluwole, A.O., Klingler, J., Danielczak, B., Babalola, J.O., Vargas, C., Pabst, G., Keller, S., 2017. Formation of Lipid-Bilayer Nanodiscs by Diisobutylene/Maleic Acid (DIBMA) Copolymer. *Langmuir* 33.  
<https://doi.org/10.1021/acs.langmuir.7b03742>
- Ortiz Zacarías, N. V., Lenselink, E.B., IJzerman, A.P., Handel, T.M., Heitman, L.H., 2018. Intracellular Receptor Modulation: Novel Approach to Target GPCRs. *Trends Pharmacol Sci*. <https://doi.org/10.1016/j.tips.2018.03.002>
- Ostrom, R.S., Gregorian, C., Drenan, R.M., Xiang, Y., Regan, J.W., Insel, P.A., 2001. Receptor Number and Caveolar Co-localization Determine Receptor Coupling Efficiency to Adenylyl Cyclase. *Journal of Biological Chemistry* 276, 42063–42069. <https://doi.org/10.1074/jbc.M105348200>
- Oswald, C., Rappas, M., Kean, J., Doré, A.S., Errey, J.C., Bennett, K., Deflorian, F., Christopher, J.A., Jazayeri, A., Mason, J.S., Congreve, M., Cooke, R.M., Marshall, F.H., 2016a. Intracellular allosteric antagonism of the CCR9 receptor. *Nature* 540, 462–465.  
<https://doi.org/10.1038/nature20606>
- Oswald, C., Rappas, M., Kean, J., Doré, A.S., Errey, J.C., Bennett, K., Deflorian, F., Christopher, J.A., Jazayeri, A., Mason, J.S., Congreve, M.,

- Cooke, R.M., Marshall, F.H., 2016b. Intracellular allosteric antagonism of the CCR9 receptor. *Nature* 540. <https://doi.org/10.1038/nature20606>
- Palm, D., Münch, G., Malek, D., Dees, C., Hekman, M., 1990. Identification of a G s-protein coupling domain to the  $\beta$ -adrenoceptor using site-specific synthetic peptides. *FEBS Lett* 261, 294–298. [https://doi.org/10.1016/0014-5793\(90\)80575-4](https://doi.org/10.1016/0014-5793(90)80575-4)
- Park, C., Kim, J., Ko, S.B., Choi, Y.K., Jeong, H., Woo, H., Kang, H., Bang, I., Kim, S.A., Yoon, T.Y., Seok, C., Im, W., Choi, H.J., 2022. Structural basis of neuropeptide Y signaling through Y1 receptor. *Nat Commun* 13. <https://doi.org/10.1038/s41467-022-28510-6>
- Parmar, V.K., Grinde, E., Mazurkiewicz, J.E., Herrick-Davis, K., 2017. Beta2-adrenergic receptor homodimers: Role of transmembrane domain 1 and helix 8 in dimerization and cell surface expression. *Biochimica et Biophysica Acta (BBA) - Biomembranes* 1859, 1445–1455. <https://doi.org/10.1016/J.BBAMEM.2016.12.007>
- Paton, W.D., Rang, H.P., 1965. THE UPTAKE OF ATROPINE AND RELATED DRUGS BY INTESTINAL SMOOTH MUSCLE OF THE GUINEA-PIG IN RELATION TO ACETYLCHOLINE RECEPTORS. *Proc R Soc Lond B Biol Sci* 163, 1–44. <https://doi.org/10.1098/RSPB.1965.0058>
- Pfleger, K.D.G., Eidne, K.A., 2006. Illuminating insights into protein-protein interactions using bioluminescence resonance energy transfer (BRET). *Nature Methods* 2006 3:3 3, 165–174. <https://doi.org/10.1038/nmeth841>
- Philip, F., Sengupta, P., Scarlata, S., 2007. Signaling through a G Protein-coupled Receptor and Its Corresponding G Protein Follows a Stoichiometrically Limited Model. *Journal of Biological Chemistry* 282, 19203–19216. <https://doi.org/10.1074/jbc.M701558200>
- Piekielna-Ciesielska, J., Ferrari, F., Calo', G., Janecka, A., 2018. Cyclopeptide Dmt-[D-Lys-p-CF3-Phe-Phe-Asp]NH<sub>2</sub>, a novel G protein-biased agonist of the mu opioid receptor. *Peptides (N.Y.)* 101, 227–233. <https://doi.org/10.1016/J.PEPTIDES.2017.11.020>

- Planells-Cases, R., Lerma, J., Ferrer-Montiel, A., 2006. Pharmacological Intervention at Ionotropic Glutamate Receptor Complexes. *Curr Pharm Des* 12, 3583–3596. <https://doi.org/10.2174/138161206778522092>
- Popot, J.L., 2010. Amphipols, nanodiscs, and fluorinated surfactants: Three nonconventional approaches to studying membrane proteins in aqueous solutions. *Annu Rev Biochem*.  
<https://doi.org/10.1146/annurev.biochem.052208.114057>
- Postis, V., Rawson, S., Mitchell, J.K., Lee, S.C., Parslow, R.A., Dafforn, T.R., Baldwin, S.A., Muench, S.P., 2015. The use of SMALPs as a novel membrane protein scaffold for structure study by negative stain electron microscopy. *Biochim Biophys Acta* 1848, 496.  
<https://doi.org/10.1016/J.BBAMEM.2014.10.018>
- Prasanna, G., Carreiro, S., Anderson, S., Gukasyan, H., Sartnurak, S., Younis, H., Gale, D., Xiang, C., Wells, P., Dinh, D., Almaden, C., Fortner, J., Toris, C., Niesman, M., Lafontaine, J., Krauss, A., 2011. Effect of PF-04217329 a prodrug of a selective prostaglandin EP 2 agonist on intraocular pressure in preclinical models of glaucoma. *Exp Eye Res* 93.  
<https://doi.org/10.1016/j.exer.2011.02.015>
- Qin, Q., Chen, P., Cui, Z., Wang, J., Xie, B., Zhang, S., Mei, X., Duan, X., Zhang, J., Wang, S., 2019. Neuropeptide Y knockdown in the dorsomedial hypothalamus improved basal and obesity-induced decrease in bone mass density. *Neuroendocrinology Letters* 40.
- Qu, C., Mao, C., Xiao, P., Shen, Q., Zhong, Y.N., Yang, F., Shen, D.D., Tao, X., Zhang, H., Yan, X., Zhao, R.J., He, J., Guan, Y., Zhang, C., Hou, Guihua, Zhang, P.J., Hou, Guige, Li, Z., Yu, X., Chai, R.J., Guan, Y.F., Sun, J.P., Zhang, Y., 2021. Ligand recognition, unconventional activation, and G protein coupling of the prostaglandin E2 receptor EP2 subtype. *Sci Adv* 7.  
[https://doi.org/10.1126/SCIADV.ABF1268/SUPPL\\_FILE/ABF1268\\_SM.PDF](https://doi.org/10.1126/SCIADV.ABF1268/SUPPL_FILE/ABF1268_SM.PDF)

- Quirke, V., 2006. Putting theory into practice: James Black, receptor theory and the development of the beta-blockers at ICI, 1958-1978. *Med Hist* 50, 69–92. <https://doi.org/10.1017/S0025727300009455>
- Rasenick, M.M., Watanabe, M., Lazarevic, M.B., Hatta, S., Hamm, H.E., 1994. Synthetic peptides as probes for G protein function. Carboxyl-terminal G alpha s peptides mimic Gs and evoke high affinity agonist binding to beta-adrenergic receptors. *Journal of Biological Chemistry* 269, 21519–21525. [https://doi.org/10.1016/S0021-9258\(17\)31835-5](https://doi.org/10.1016/S0021-9258(17)31835-5)
- Rasmussen, S.G.F., Devree, B.T., Zou, Y., Kruse, A.C., Chung, K.Y., Kobilka, T.S., Thian, F.S., Chae, P.S., Pardon, E., Calinski, D., Mathiesen, J.M., Shah, S.T.A., Lyons, J.A., Caffrey, M., Gellman, S.H., Steyaert, J., Skiniotis, G., Weis, W.I., Sunahara, R.K., Kobilka, B.K., 2011. Crystal structure of the  $\beta$  2 adrenergic receptor-Gs protein complex. *Nature*. <https://doi.org/10.1038/nature10361>
- Rasmussen, S.G.F., Jensen, A.D., Liapakis, G., Ghanouni, P., Javitch, J.A., Gether, U., 1999. Mutation of a highly conserved aspartic acid in the  $\beta$ 2 adrenergic receptor: Constitutive activation, structural instability, and conformational rearrangement of transmembrane segment 6. *Mol Pharmacol* 56. <https://doi.org/10.1124/mol.56.1.175>
- Ratkeviciute, G., Cooper, B.F., Knowles, T.J., 2021. Methods for the solubilisation of membrane proteins: The micelle-aneous world of membrane protein solubilisation. *Biochem Soc Trans*. <https://doi.org/10.1042/BST20210181>
- Reiter, E., Ahn, S., Shukla, A.K., Lefkowitz, R.J., 2012. Molecular mechanism of  $\beta$ -arrestin-biased agonism at seven-transmembrane receptors. *Annu Rev Pharmacol Toxicol*. <https://doi.org/10.1146/annurev.pharmtox.010909.105800>
- Rens-Domiano, S., Hamm, H.E., 1995. Structural and functional relationships of heterotrimeric G-proteins. *The FASEB Journal* 9, 1059–1066. <https://doi.org/10.1096/FASEBJ.9.11.7649405>

- Reutershan, J., Morris, M.A., Burcin, T.L., Smith, D.F., Chang, D., Saprito, M.S., Ley, K., 2006. Critical role of endothelial CXCR2 in LPS-induced neutrophil migration into the lung. *J Clin Invest* 116, 695–702.  
<https://doi.org/10.1172/JCI27009>
- Rigler, R., Mets, U., Widengren, J., Kask, P., 1993. Fluorescence correlation spectroscopy with high count rate and low background: analysis of translational diffusion. *European Biophysics Journal* 22.  
<https://doi.org/10.1007/BF00185777>
- Robers, M.B., Friedman-Ohana, R., Huber, K.V.M., Huber, K.V.M., Kilpatrick, L., Kilpatrick, L., Vasta, J.D., Berger, B.T., Chaudhry, C., Hill, S., Hill, S., Müller, S., Müller, S., Knapp, S., Knapp, S., Knapp, S., Knapp, S., Wood, K. V., Wood, K. V., 2020. Quantifying Target Occupancy of Small Molecules Within Living Cells. *Annu Rev Biochem* 89, 557–581. <https://doi.org/10.1146/ANNUREV-BIOCHEM-011420-092302>
- Robertson, M.J., Papasergi-Scott, M.M., He, F., Seven, A.B., Meyerowitz, J.G., Panova, O., Peroto, M.C., Che, T., Skiniotis, G., 2022. Structure determination of inactive-state GPCRs with a universal nanobody. *Nature Structural & Molecular Biology* 2022 29:12 29, 1188–1195.  
<https://doi.org/10.1038/s41594-022-00859-8>
- Roccatano, D., Colombo, G., Fioroni, M., Mark, A.E., 2002. Mechanism by which 2,2,2-trifluoroethanol/water mixtures stabilize secondary-structure formation in peptides: A molecular dynamics study. *Proc Natl Acad Sci U S A* 99, 12179–12184.  
<https://doi.org/10.1073/PNAS.182199699/ASSET/1ECA2570-C95C-49F3-88B8-DFD884331418/ASSETS/GRAPHIC/PQ1821996005.JPEG>
- Rosenbaum, D.M., Cherezov, V., Hanson, M.A., Rasmussen, S.G.F., Foon, S.T., Kobilka, T.S., Choi, H.J., Yao, X.J., Weis, W.I., Stevens, R.C., Kobilka, B.K., 2007. GPCR engineering yields high-resolution structural insights into  $\beta$ 2-adrenergic receptor function. *Science* (1979) 318.  
<https://doi.org/10.1126/science.1150609>

- Rosenbaum, D.M., Rasmussen, S.G.F., Kobilka, B.K., 2009. The structure and function of G-protein-coupled receptors. *Nature* 2009 459:7245 459, 356–363. <https://doi.org/10.1038/nature08144>
- Rostovtsev, V. V., Green, L.G., Fokin, V. V., Sharpless, K.B., 2002. A stepwise Huisgen cycloaddition process: Copper(I)-catalyzed regioselective “ligation” of azides and terminal alkynes. *Angewandte Chemie - International Edition* 41. [https://doi.org/10.1002/1521-3773\(20020715\)41:14<2596::AID-ANIE2596>3.0.CO;2-4](https://doi.org/10.1002/1521-3773(20020715)41:14<2596::AID-ANIE2596>3.0.CO;2-4)
- Routledge, S.J., Jamshad, M., Little, H.A., Lin, Y.P., Simms, J., Thakker, A., Spickett, C.M., Bill, R.M., Dafforn, T.R., Poyner, D.R., Wheatley, M., 2020. Ligand-induced conformational changes in a SMALP-encapsulated GPCR. *Biochim Biophys Acta Biomembr* 1862. <https://doi.org/10.1016/j.bbamem.2020.183235>
- Rouzer, C.A., Marnett, L.J., 2009. Cyclooxygenases: structural and functional insights. *J Lipid Res* 50, S29. <https://doi.org/10.1194/JLR.R800042-JLR200>
- Sachpatzidis, A., Benton, B.K., Manfredi, J.P., Wang, H., Hamilton, A., Dohlman, H.G., Lolis, E., 2003. Identification of allosteric peptide agonists of CXCR4. *Journal of Biological Chemistry*. <https://doi.org/10.1074/jbc.M204667200>
- Sadana, R., Dessauer, C.W., 2009. Physiological roles for G protein-regulated adenylyl cyclase isoforms: Insights from knockout and overexpression studies. *Neurosignals*. <https://doi.org/10.1159/000166277>
- Sadler, F., Ma, N., Ritt, M., Sharma, Y., Vaidehi, N., Sivaramakrishnan, S., 2023. Autoregulation of GPCR signalling through the third intracellular loop. *Nature* 2023 615:7953 615, 734–741. <https://doi.org/10.1038/s41586-023-05789-z>
- Saha, S., Shukla, A.K., 2020. The Inside Story: Crystal Structure of the Chemokine Receptor CCR7 with an Intracellular Allosteric Antagonist. *Biochemistry* 59, 12–14. <https://doi.org/10.1021/acs.biochem.9b00893>

- Salchow, K., Bond, M., Evans, S., Press, N., Charlton, S., Hunt, P., Bradley, M., 2010. A common intracellular allosteric binding site for antagonists of the CXCR2 receptor. *Br J Pharmacol* 159, 1429–1439. <https://doi.org/10.1111/j.1476-5381.2009.00623.x>
- Salpeter, S.R., Ormiston, T.M., Salpeter, E.E., 2004. Cardiovascular effects of beta-agonists in patients with asthma and COPD: a meta-analysis. *Chest* 125, 2309–2321. <https://doi.org/10.1378/CHEST.125.6.2309>
- Samama, P., Cotecchia, S., Costa, T., Lefkowitz, R.J., 1993. A mutation-induced activated state of the beta 2-adrenergic receptor. Extending the ternary complex model. *Journal of Biological Chemistry* 268, 4625–4636. [https://doi.org/10.1016/S0021-9258\(18\)53442-6](https://doi.org/10.1016/S0021-9258(18)53442-6)
- Sandhu, M., Touma, A.M., Dysthe, M., Sadler, F., Sivaramakrishnan, S., Vaidehi, N., 2019. Conformational plasticity of the intracellular cavity of GPCR–G-protein complexes leads to G-protein promiscuity and selectivity. *Proc Natl Acad Sci U S A* 116, 11956–11965. [https://doi.org/10.1073/PNAS.1820944116/SUPPL\\_FILE/PNAS.1820944116.SM01.MPG](https://doi.org/10.1073/PNAS.1820944116/SUPPL_FILE/PNAS.1820944116.SM01.MPG)
- Schild, H.O., 1947. pA, a new scale for the measurement of drug antagonism. *Br J Pharmacol Chemother.* <https://doi.org/10.1111/j.1476-5381.1947.tb00336.x>
- Schiöth, H.B., Lagerström, M.C., 2008. Structural diversity of G-protein-coupled receptors and significance for drug discovery. *Nat Rev Drug Discov.* <https://doi.org/10.1038/nrd2518>
- Schjerning, A.M., McGettigan, P., Gislason, G., 2020. Cardiovascular effects and safety of (non-aspirin) NSAIDs. *Nat Rev Cardiol.* <https://doi.org/10.1038/s41569-020-0366-z>
- Schmid, C.L., Lovell, K.M., Bohn, L.M., Yue, Z., Cameron, M.D., Kennedy, N.M., Bannister, T.D., Ross, N.C., Morgenweck, J., 2017. Bias Factor and Therapeutic Window Correlate to Predict Safer Opioid Analgesics. *Cell.* <https://doi.org/10.1016/j.cell.2017.10.035>

- Schneider, E., Keller, M., Brennauer, A., Hoefelschweiger, B.K., Gross, D., Wolfbeis, O.S., Bernhardt, G., Buschauer, A., 2007. Synthesis and characterization of the first fluorescent nonpeptide NPY Y1 receptor antagonist. *ChemBioChem* 8, 1981–1988.  
<https://doi.org/10.1002/cbic.200700302>
- Scholten, D., Canals, M., Maussang, D., Roumen, L., Smit, M., Wijtmans, M., de Graaf, C., Vischer, H., Leurs, R., 2012. Pharmacological modulation of chemokine receptor function. *Br J Pharmacol* 165, 1617–1643.  
<https://doi.org/10.1111/j.1476-5381.2011.01551.x>
- Scholten, D.J., Canals, M., Wijtmans, M., De Munnik, S., Nguyen, P., Verzijl, D., De Esch, I.J.P., Vischer, H.F., Smit, M.J., Leurs, R., 2012. Pharmacological characterization of a small-molecule agonist for the chemokine receptor CXCR3. *Br J Pharmacol* 166, 898–911.  
<https://doi.org/10.1111/J.1476-5381.2011.01648.X>
- Schwencke, C., Okumura, S., Yamamoto, M., Geng, Y.J., Ishikawa, Y., 1999. Colocalization of  $\beta$ -adrenergic receptors and caveolin within the plasma membrane. *J Cell Biochem* 75. [https://doi.org/10.1002/\(SICI\)1097-4644\(19991001\)75:1<64::AID-JCB7>3.0.CO;2-L](https://doi.org/10.1002/(SICI)1097-4644(19991001)75:1<64::AID-JCB7>3.0.CO;2-L)
- Seddon, A.M., Curnow, P., Booth, P.J., 2004. Membrane proteins, lipids and detergents: Not just a soap opera. *Biochim Biophys Acta Biomembr.*  
<https://doi.org/10.1016/j.bbamem.2004.04.011>
- Seifert, R., Wenzel-Seifert, K., 2002. Constitutive activity of G-proteins-coupled receptors: Cause of disease and common property of wild-type receptors. *Naunyn Schmiedeberg's Arch Pharmacol.*  
<https://doi.org/10.1007/s00210-002-0588-0>
- Selent, J., Sanz, F., Pastor, M., de Fabritiis, G., 2010. Induced effects of sodium ions on dopaminergic G-protein coupled receptors. *PLoS Comput Biol* 6. <https://doi.org/10.1371/journal.pcbi.1000884>
- Sengmany, K., Singh, J., Stewart, G.D., Conn, P.J., Christopoulos, A., Gregory, K.J., 2017. Biased allosteric agonism and modulation of metabotropic glutamate receptor 5: Implications for optimizing preclinical

neuroscience drug discovery. *Neuropharmacology* 115.

<https://doi.org/10.1016/j.neuropharm.2016.07.001>

Seven, A.B., Barros-Álvarez, X., de Lapeyrière, M., Papasergi-Scott, M.M., Robertson, M.J., Zhang, C., Nwokonko, R.M., Gao, Y., Meyerowitz, J.G., Rocher, J.P., Schelshorn, D., Kobilka, B.K., Mathiesen, J.M., Skiniotis, G., 2021. G-protein activation by a metabotropic glutamate receptor. *Nature* 2021 595:7867–7872, 450–454. <https://doi.org/10.1038/s41586-021-03680-3>

Shamri, R., Grabovsky, V., Feigelson, S.W., Dwir, O., Van Kooyk, Y., Alon, R., 2002. Chemokine stimulation of lymphocyte alpha 4 integrin avidity but not of leukocyte function-associated antigen-1 avidity to endothelial ligands under shear flow requires cholesterol membrane rafts. *J Biol Chem* 277, 40027–40035. <https://doi.org/10.1074/JBC.M206806200>

Sheikh, S.P., Williams, J.A., 1990. Structural characterization of Y1 and Y2 receptors for neuropeptide Y and peptide YY by affinity cross-linking. *Journal of Biological Chemistry* 265. [https://doi.org/10.1016/s0021-9258\(19\)39072-6](https://doi.org/10.1016/s0021-9258(19)39072-6)

Shenoy, S.K., Lefkowitz, R.J., 2011.  $\beta$ -arrestin-mediated receptor trafficking and signal transduction. *Trends Pharmacol Sci* 32, 521. <https://doi.org/10.1016/J.TIPS.2011.05.002>

Shukla, A.K., Dwivedi-Agnihotri, H., 2020. Structure and function of  $\beta$ -arrestins, their emerging role in breast cancer, and potential opportunities for therapeutic manipulation. *Adv Cancer Res* 145, 139. <https://doi.org/10.1016/BS.ACR.2020.01.001>

Sivertsen, B., Holliday, N., Madsen, A.N., Holst, B., 2013. Functionally biased signalling properties of 7TM receptors - opportunities for drug development for the ghrelin receptor. *Br J Pharmacol* 170, 1349–1362. <https://doi.org/10.1111/bph.12361>

Sluter, M.N., Hou, R., Li, L., Yasmen, N., Yu, Y., Liu, J., Jiang, J., 2021. EP2 Antagonists (2011-2021): A Decade's Journey from Discovery to

Therapeutics HHS Public Access. *J Med Chem* 64, 11816–11836.

<https://doi.org/10.1021/acs.jmedchem.1c00816>

Soave, M., Briddon, S.J., Hill, S.J., Stoddart, L.A., 2020a. Fluorescent ligands:

Bringing light to emerging GPCR paradigms. *Br J Pharmacol* 177, 978–

991. <https://doi.org/10.1111/bph.14953>

Soave, M., Briddon, S.J., Hill, S.J., Stoddart, L.A., 2020b. Fluorescent ligands:

Bringing light to emerging GPCR paradigms. *Br J Pharmacol*.

<https://doi.org/10.1111/bph.14953>

Soave, M., Briddon, S.J., Hill, S.J., Stoddart, L.A., 2020c. Fluorescent ligands:

Bringing light to emerging GPCR paradigms. *Br J Pharmacol*.

<https://doi.org/10.1111/bph.14953>

Soave, M., Heukers, R., Kellam, B., Woolard, J., Smit, M.J., Briddon, S.J.,

Hill, S.J., 2020d. Monitoring Allosteric Interactions with CXCR4 Using

NanoBiT Conjugated Nanobodies. *Cell Chem Biol* 27, 1250-1261.e5.

<https://doi.org/10.1016/J.CHEMBIOL.2020.06.006>

Stahl, E.L., Schmid, C.L., Acevedo-Canabal, A., Read, C., Grim, T.W.,

Kennedy, N.M., Bannister, T.D., Bohn, L.M., 2021. G protein signaling–

biased mu opioid receptor agonists that produce sustained G protein

activation are noncompetitive agonists. *Proceedings of the National*

*Academy of Sciences* 118. <https://doi.org/10.1073/pnas.2102178118>

Stephenson, R.P., 1956. A modification of receptor theory. *Br J Pharmacol*

*Chemother* 11, 379–393. <https://doi.org/10.1111/J.1476->

5381.1956.TB00006.X

Stiller, C.O., Hjemdahl, P., 2022. Lessons from 20 years with COX-2

inhibitors: Importance of dose–response considerations and fair play in

comparative trials. *J Intern Med* 292, 557–574.

<https://doi.org/10.1111/JOIM.13505>

Stoddart, L.A., Johnstone, E.K.M., Wheal, A.J., Goulding, J., Robers, M.B.,

MacHleidt, T., Wood, K. V., Hill, S.J., Pflieger, K.D.G., 2015.

Application of BRET to monitor ligand binding to GPCRs. *Nat Methods* 12, 661–663. <https://doi.org/10.1038/NMETH.3398>

Stoddart, L.A., Kilpatrick, L.E., Hill, S.J., 2018. NanoBRET Approaches to Study Ligand Binding to GPCRs and RTKs. *Trends Pharmacol Sci.* <https://doi.org/10.1016/j.tips.2017.10.006>

Stoddart, L.A., White, C.W., Nguyen, K., Hill, S.J., Pflieger, K.D.G., 2016. Fluorescence- and bioluminescence-based approaches to study GPCR ligand binding. *Br J Pharmacol* 173, 3028–3037. <https://doi.org/10.1111/bph.13316>

Stott, L.A., Hall, D.A., Holliday, N.D., 2016. Unravelling intrinsic efficacy and ligand bias at G protein coupled receptors: A practical guide to assessing functional data. *Biochem Pharmacol* 101, 1–12. <https://doi.org/10.1016/J.BCP.2015.10.011>

Strader, C.D., Candelore, M.R., Hill, W.S., Sigal, I.S., Dixon, R.A.F., 1989. Identification of two serine residues involved in agonist activation of the  $\beta$ -adrenergic receptor. *Journal of Biological Chemistry* 264. [https://doi.org/10.1016/s0021-9258\(18\)80035-7](https://doi.org/10.1016/s0021-9258(18)80035-7)

Strader, C.D., Sigal, I.S., Register, R.B., Candelore, M.R., Rands, E., Dixon, R.A., 1987. Identification of residues required for ligand binding to the beta-adrenergic receptor. *Proc Natl Acad Sci U S A* 84, 4384. <https://doi.org/10.1073/PNAS.84.13.4384>

Sykes, D.A., Bradley, M.E., Riddy, D.M., Willard, E., Reilly, J., Miah, A., Bauer, C., Watson, S.J., Sandham, D.A., Dubois, G., Charlton, S.J., 2016. Fevipiprant (QAW039), a slowly dissociating CRTh2 antagonist with the potential for improved clinical efficacy. *Mol Pharmacol* 89, 593–605. <https://doi.org/10.1124/MOL.115.101832/-/DC1>

Sykes, D.A., Charlton, S.J., 2018. Single Step Determination of Unlabeled Compound Kinetics Using a Competition Association Binding Method Employing Time-Resolved FRET, in: *Methods in Molecular Biology*. pp. 177–194. [https://doi.org/10.1007/978-1-4939-8630-9\\_10](https://doi.org/10.1007/978-1-4939-8630-9_10)

- Sykes, D.A., Moore, H., Stott, L., Holliday, N., Javitch, J.A., Lane, J.R., Charlton, S.J., 2017. Extrapyramidal side effects of antipsychotics are linked to their association kinetics at dopamine D2 receptors. *Nat Commun* 8, 763. <https://doi.org/10.1038/s41467-017-00716-z>
- Sykes, D.A., Stoddart, L.A., Kilpatrick, L.E., Hill, S.J., 2019. Binding kinetics of ligands acting at GPCRs. *Mol Cell Endocrinol*. <https://doi.org/10.1016/j.mce.2019.01.018>
- Syrovatkina, V., Alegre, K.O., Dey, R., Huang, X.Y., 2016. Regulation, Signaling, and Physiological Functions of G-Proteins. *J Mol Biol*. <https://doi.org/10.1016/j.jmb.2016.08.002>
- Tani, K., Naganawa, A., Ishida, A., Egashira, H., Sagawa, K., Harada, H., Ogawa, M., Maruyama, T., Ohuchida, S., Nakai, H., Kondo, K., Toda, M., 2001. Design and synthesis of a highly selective EP2-receptor agonist. *Bioorg Med Chem Lett* 11. [https://doi.org/10.1016/S0960-894X\(01\)00359-6](https://doi.org/10.1016/S0960-894X(01)00359-6)
- Taylor, S.S., Ilouz, R., Zhang, P., Kornev, A.P., 2012. Assembly of allosteric macromolecular switches: Lessons from PKA. *Nat Rev Mol Cell Biol*. <https://doi.org/10.1038/nrm3432>
- Thaker, T.M., Sarwar, M., Preininger, A.M., Hamm, H.E., Iverson, T.M., 2014. A Transient Interaction between the Phosphate Binding Loop and Switch I Contributes to the Allosteric Network between Receptor and Nucleotide in G $\alpha$ i1. *Journal of Biological Chemistry* 289, 11331–11341. <https://doi.org/10.1074/jbc.M113.539064>
- Thal, D.M., Glukhova, A., Sexton, P.M., Christopoulos, A., 2018. Structural insights into G-protein-coupled receptor allostery. *Nature* 559, 45–53. <https://doi.org/10.1038/s41586-018-0259-z>
- Thal, D.M., Sun, B., Feng, D., Nawaratne, V., Leach, K., Felder, C.C., Bures, M.G., Evans, D.A., Weis, W.I., Bachhawat, P., Kobilka, T.S., Sexton, P.M., Kobilka, B.K., Christopoulos, A., 2016. Crystal structures of the M1 and M4 muscarinic acetylcholine receptors. *Nature* 531, 335–340. <https://doi.org/10.1038/nature17188>

- Thomsen, A.R.B., Plouffe, B., Cahill, T.J., Shukla, A.K., Tarrasch, J.T., Dosey, A.M., Kahsai, A.W., Strachan, R.T., Pani, B., Mahoney, J.P., Huang, L., Breton, B., Heydenreich, F.M., Sunahara, R.K., Skiniotis, G., Bouvier, M., Lefkowitz, R.J., 2016. GPCR-G Protein- $\beta$ -Arrestin Super-Complex Mediates Sustained G Protein Signaling. *Cell* 166, 907. <https://doi.org/10.1016/J.CELL.2016.07.004>
- Tornøe, C.W., Christensen, C., Meldal, M., 2002. Peptidotriazoles on solid phase: [1,2,3]-Triazoles by regioselective copper(I)-catalyzed 1,3-dipolar cycloadditions of terminal alkynes to azides. *Journal of Organic Chemistry* 67, 3057–3064. [https://doi.org/10.1021/JO011148J/SUPPL\\_FILE/JO011148J\\_S.PDF](https://doi.org/10.1021/JO011148J/SUPPL_FILE/JO011148J_S.PDF)
- Touma, A.M., Malik, R.U., Gupte, T., Sivaramakrishnan, S., 2020. Allosteric modulation of adenosine A1 and cannabinoid 1 receptor signaling by G-peptides. *Pharmacol Res Perspect* 8. <https://doi.org/10.1002/prp2.673>
- Toy, L., Huber, M.E., Schmidt, M.F., Weikert, D., Schiedel, M., 2022. Fluorescent Ligands Targeting the Intracellular Allosteric Binding Site of the Chemokine Receptor CCR2. *ACS Chem Biol* 17. <https://doi.org/10.1021/acscchembio.2c00263>
- Toyoda, Y., Zhu, A., Kong, F., Shan, S., Zhao, J., Wang, N., Sun, X., Zhang, L., Yan, C., Kobilka, B.K., Liu, X., 2023. Structural basis of  $\alpha$ 1A-adrenergic receptor activation and recognition by an extracellular nanobody. *Nat Commun* 14. <https://doi.org/10.1038/S41467-023-39310-X>
- Tsukihara, T., Aoyama, H., Yamashita, E., Tomizaki, T., Yamaguchi, H., Shinzawa-Itoh, K., Nakashima, R., Yaono, R., Yoshikawa, S., 1995. Structures of metal sites of oxidized bovine heart cytochrome c oxidase at 2.8 Å. *Science* (1979) 269. <https://doi.org/10.1126/science.7652554>
- Tsvetanova, N.G., von Zastrow, M., 2014. Spatial encoding of cyclic AMP signaling specificity by GPCR endocytosis. *Nat Chem Biol* 10, 1061–1065. <https://doi.org/10.1038/nchembio.1665>

- Tummino, P.J., Copeland, R.A., 2008. Residence time of receptor-ligand complexes and its effect on biological function. *Biochemistry* 47, 5481–5492. <https://doi.org/10.1021/BI8002023>
- Vasta, J.D., Corona, C.R., Robers, M.B., 2021. A High-Throughput Method to Prioritize PROTAC Intracellular Target Engagement and Cell Permeability Using NanoBRET. *Methods Mol Biol* 2365, 265–282. [https://doi.org/10.1007/978-1-0716-1665-9\\_14](https://doi.org/10.1007/978-1-0716-1665-9_14)
- Vasta, J.D., Corona, C.R., Wilkinson, J., Zimprich, C.A., Hartnett, J.R., Ingold, M.R., Zimmerman, K., Machleidt, T., Kirkland, T.A., Huwiler, K.G., Ohana, R.F., Slater, M., Otto, P., Cong, M., Wells, C.I., Berger, B.T., Hanke, T., Glas, C., Ding, K., Drewry, D.H., Huber, K.V.M., Willson, T.M., Knapp, S., Müller, S., Meisenheimer, P.L., Fan, F., Wood, K. V., Robers, M.B., 2018. Quantitative, Wide-Spectrum Kinase Profiling in Live Cells for Assessing the Effect of Cellular ATP on Target Engagement. *Cell Chem Biol* 25, 206-214.e11. <https://doi.org/10.1016/J.CHEMBIOL.2017.10.010>
- Vauquelin, G., Van Liefde, I., 2006. Slow antagonist dissociation and long-lasting in vivo receptor protection. *Trends Pharmacol Sci* 27, 355–359. <https://doi.org/10.1016/J.TIPS.2006.05.001>
- Viola, A., Luster, A.D., 2008. Chemokines and Their Receptors: Drug Targets in Immunity and Inflammation. *Annu Rev Pharmacol Toxicol*. <https://doi.org/10.1146/annurev.pharmtox.48.121806.154841>
- Wacker, D., Fenalti, G., Brown, M.A., Katritch, V., Abagyan, R., Cherezov, V., Stevens, R.C., 2010. Conserved binding mode of human  $\beta$ 2 adrenergic receptor inverse agonists and antagonist revealed by X-ray crystallography. *J Am Chem Soc* 132, 11443. <https://doi.org/10.1021/JA105108Q>
- Walker, J., Penn, R., Hanania, N., Dickey, B., Bond, R., 2011. New perspectives regarding  $\beta$ 2-adrenoceptor ligands in the treatment of asthma. *Br J Pharmacol* 163, 18–28. <https://doi.org/10.1111/j.1476-5381.2010.01178.x>

- Walters, M.J., Wang, Y., Lai, N., Baumgart, T., Zhao, B.N., Dairaghi, D.J., Bekker, P., Ertl, L.S., Penfold, M.E.T., Jaen, J.C., Keshav, S., Wendt, E., Pennell, A., Ungashe, S., Wei, Z., Wright, J.J.K., Schall, T.J., 2010. Characterization of CCX282-B, an orally bioavailable antagonist of the CCR9 chemokine receptor, for treatment of inflammatory bowel disease. *Journal of Pharmacology and Experimental Therapeutics* 335. <https://doi.org/10.1124/jpet.110.169714>
- Wan, Q., Okashah, N., Inoue, A., Nehme, R., Carpenter, B., Tate, C.G., Lambert, N.A., 2018. Mini G protein probes for active G protein-coupled receptors (GPCRs) in live cells. *J Biol Chem* 293, 7466. <https://doi.org/10.1074/JBC.RA118.001975>
- Warne, T., Edwards, P.C., Dorfe, A.S., Leslie, A.G.W., Tate, C.G., 2019. Molecular basis for high-affinity agonist binding in GPCRs. *Science* (1979). <https://doi.org/10.1126/science.aau5595>
- Wassler, M., Jonasson, I., Persson, R., Fries, E., 1987. Differential permeabilization of membranes by saponin treatment of isolated rat hepatocytes. Release of secretory proteins. *Biochemical Journal* 247. <https://doi.org/10.1042/bj2470407>
- Weis, W.I., Kobilka, B.K., 2008. Structural insights into G-protein-coupled receptor activation. *Curr Opin Struct Biol*. <https://doi.org/10.1016/j.sbi.2008.09.010>
- Weiss, J.M., Morgan, P.H., Lutz, M.W., Kenakin, T.P., 1996. The cubic ternary complex receptor-occupancy model. III. Resurrecting efficacy. *J Theor Biol* 181. <https://doi.org/10.1006/jtbi.1996.0139>
- Wendell, S.G., Fan, H., Zhang, C., 2020. G protein-coupled receptors in asthma therapy: Pharmacology and drug actions. *Pharmacol Rev* 72, 1–49. <https://doi.org/10.1124/pr.118.016899>
- White, C.W., Caspar, B., Vanyai, H.K., Pflieger, K.D.G., Hill, S.J., 2020a. CRISPR-Mediated Protein Tagging with Nanoluciferase to Investigate Native Chemokine Receptor Function and Conformational Changes. *Cell*

Chem Biol 27, 499-510.e7.  
<https://doi.org/10.1016/j.chembiol.2020.01.010>

White, C.W., Caspar, B., Vanyai, H.K., Pflieger, K.D.G., Hill, S.J., 2020b. CRISPR-Mediated Protein Tagging with Nanoluciferase to Investigate Native Chemokine Receptor Function and Conformational Changes. *Cell Chem Biol* 27, 499-510.e7.  
<https://doi.org/10.1016/J.CHEMBIOL.2020.01.010>

White, C.W., Vanyai, H.K., See, H.B., Johnstone, E.K.M., Pflieger, K.D.G., 2017. Using nanoBRET and CRISPR/Cas9 to monitor proximity to a genome-edited protein in real-time. *Sci Rep* 7.  
<https://doi.org/10.1038/s41598-017-03486-2>

Wieland, H. A., Engel, W., Eberlein, W., Rudolf, K., Doods, H.N., 1998. Subtype selectivity of the novel nonpeptide neuropeptide Y Y1 receptor antagonist BIBO 3304 and its effect on feeding in rodents. *Br J Pharmacol* 125, 549–555. <https://doi.org/10.1038/SJ.BJP.0702084>

Wieland, Heike A., Willim, K., Doods, H.N., 1998. Divalent cations influencing neuropeptide Y receptor subtype binding in rat hippocampus and cortex membranes as well as in recombinant cells. *Regul Pept* 75–76, 263–269. [https://doi.org/10.1016/S0167-0115\(98\)00077-9](https://doi.org/10.1016/S0167-0115(98)00077-9)

Williams, J.T., Egan, T.M., North, R.A., 1982. Enkephalin opens potassium channels on mammalian central neurones. *Nature* 1982 299:5878 299, 74–77. <https://doi.org/10.1038/299074a0>

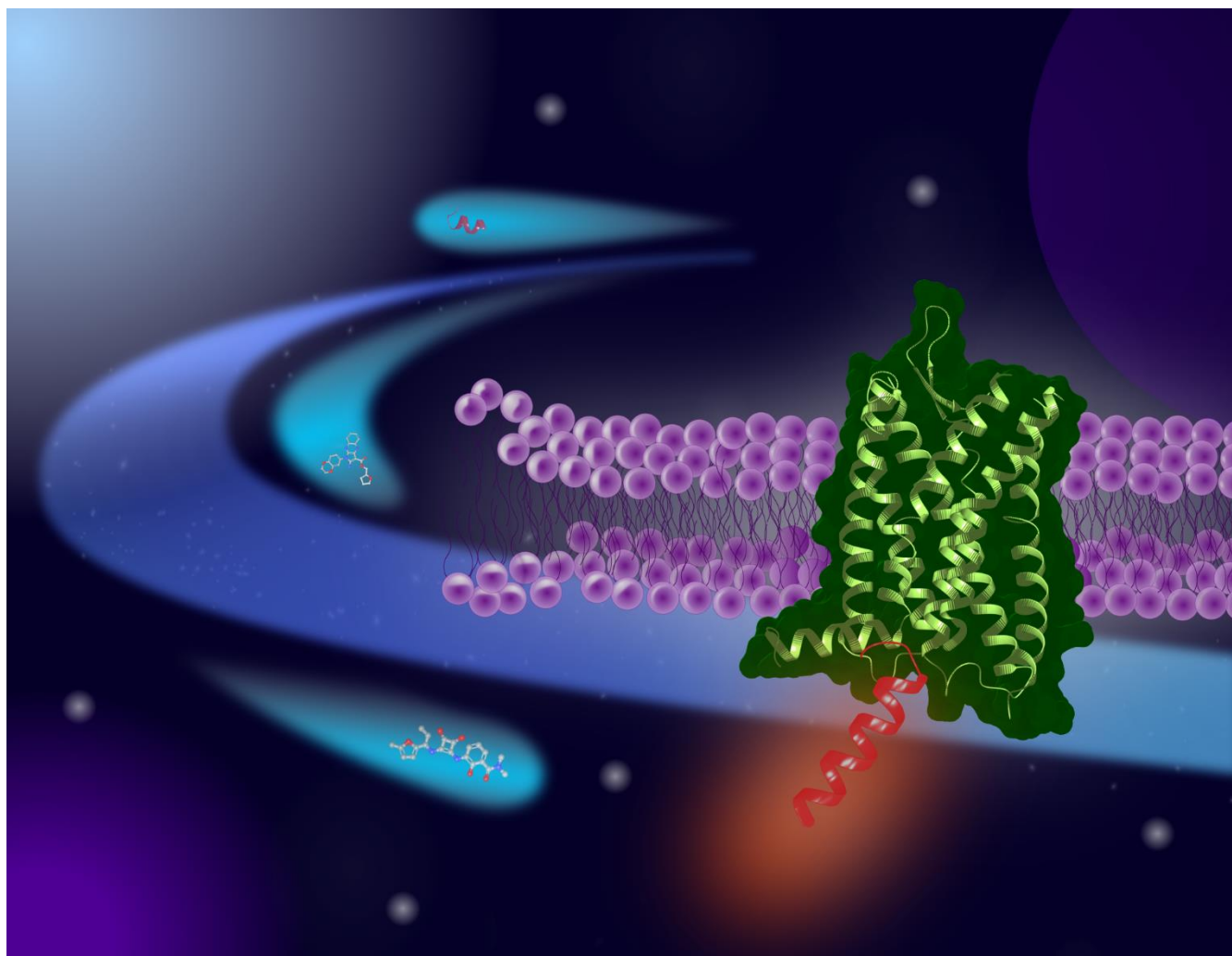
Wingert, B., Doruker, P., Bahar, I., 2022. Activation and Speciation Mechanisms in Class A GPCRs. *J Mol Biol* 434, 167690.  
<https://doi.org/10.1016/j.jmb.2022.167690>

Xu, J., Wang, Q., Hübner, H., Hu, Y., Niu, X., Wang, H., Maeda, S., Inoue, A., Tao, Y., Gmeiner, P., Du, Y., Jin, C., Kobilka, B.K., 2023. Structural and dynamic insights into supra-physiological activation and allosteric modulation of a muscarinic acetylcholine receptor. *Nat Commun* 14, 376.  
<https://doi.org/10.1038/s41467-022-35726-z>

- Xu, X., Kaindl, J., Clark, M.J., Hübner, H., Hirata, K., Sunahara, R.K., Gmeiner, P., Kobilka, B.K., Liu, X., 2021. Binding pathway determines norepinephrine selectivity for the human  $\beta$ 1AR over  $\beta$ 2AR. *Cell Res* 31. <https://doi.org/10.1038/s41422-020-00424-2>
- Yan, M., Du, J., Gu, Z., Liang, M., Hu, Y., Zhang, W., Priceman, S., Wu, L., Zhou, Z.H., Liu, Z., Segura, T., Tang, Y., Lu, Y., 2010. A novel intracellular protein delivery platform based on single-protein nanocapsules. *Nat Nanotechnol* 5. <https://doi.org/10.1038/nnano.2009.341>
- Yang, D., Zhou, Q., Labroska, V., Qin, S., Darbalaei, S., Wu, Y., Yuliantie, E., Xie, L., Tao, H., Cheng, J., Liu, Q., Zhao, S., Shui, W., Jiang, Y., Wang, M.W., 2021a. G protein-coupled receptors: structure- and function-based drug discovery. *Signal Transduction and Targeted Therapy* 2020 6:1 6, 1–27. <https://doi.org/10.1038/s41392-020-00435-w>
- Yang, D., Zhou, Q., Labroska, V., Qin, S., Darbalaei, S., Wu, Y., Yuliantie, E., Xie, L., Tao, H., Cheng, J., Liu, Q., Zhao, S., Shui, W., Jiang, Y., Wang, M.-W., 2021b. G protein-coupled receptors: structure- and function-based drug discovery. *Signal Transduct Target Ther* 6, 7. <https://doi.org/10.1038/s41392-020-00435-w>
- Yang, F., Ling, S., Zhou, Y., Zhang, Y., Lv, P., Liu, S., Fang, W., Sun, W., Hu, L.A., Zhang, L., Shi, P., Tian, C., 2021. Different conformational responses of the  $\beta$ 2-adrenergic receptor-Gs complex upon binding of the partial agonist salbutamol or the full agonist isoprenaline. *Natl Sci Rev* 8. <https://doi.org/10.1093/NSR/NWAA284>
- Yang, F., Ling, S., Zhou, Y., Zhang, Y., Lv, P., Liu, S., Fang, W., Sun, W., Hu, L.A., Zhang, L., Shi, P., Tian, C., 2020. Different conformational responses of the  $\beta$ 2-adrenergic receptor-Gs complex upon binding of the partial agonist salbutamol or the full agonist isoprenaline. *Natl Sci Rev*. <https://doi.org/10.1093/nsr/nwaa284>
- Yang, Z., Han, S., Keller, M., Kaiser, A., Bender, B.J., Bosse, M., Burkert, K., Kögler, L.M., Wifling, D., Bernhardt, G., Plank, N., Littmann, T., Schmidt, P., Yi, C., Li, B., Ye, S., Zhang, R., Xu, B., Larhammar, D.,

- Stevens, R.C., Huster, D., Meiler, J., Zhao, Q., Beck-Sickinger, A.G., Buschauer, A., Wu, B., 2018. Structural basis of ligand binding modes at the neuropeptide Y Y1 receptor. *Nature* 2018 556:7702 556, 520–524. <https://doi.org/10.1038/s41586-018-0046-x>
- Yi, M., Li, H., Wu, Z., Yan, J., Liu, Q., Ou, C., Chen, M., 2018. A Promising Therapeutic Target for Metabolic Diseases: Neuropeptide Y Receptors in Humans. *Cellular Physiology and Biochemistry* 45, 88–107. <https://doi.org/10.1159/000486225>
- Zerbe, O., Fossa, P., Vu, O., Bender, B.J., Pankewitz, L., Huster, D., Beck-Sickinger, A.G., Meiler, J., 2021. The Structural Basis of Peptide Binding at Class A G Protein-Coupled Receptors. *Molecules* 2022, Vol. 27, Page 210 27, 210. <https://doi.org/10.3390/MOLECULES27010210>
- Zhang, L., Bijker, M.S., Herzog, H., 2011. The neuropeptide y system: Pathophysiological and therapeutic implications in obesity and cancer. *Pharmacol Ther.* <https://doi.org/10.1016/j.pharmthera.2011.03.011>
- Zhao, M., Wimmer, A., Trieu, K., Discipio, R.G., Schraufstatter, I.U., 2004. Arrestin regulates MAPK activation and prevents NADPH oxidase-dependent death of cells expressing CXCR2. *Journal of Biological Chemistry.* <https://doi.org/10.1074/jbc.M405118200>
- Zheng, Y., Han, G.W., Abagyan, R., Wu, B., Stevens, R.C., Cherezov, V., Kufareva, I., Handel, T.M., 2017. Structure of CC Chemokine Receptor 5 with a Potent Chemokine Antagonist Reveals Mechanisms of Chemokine Recognition and Molecular Mimicry by HIV. *Immunity* 46, 1005-1017.e5. <https://doi.org/10.1016/J.IMMUNI.2017.05.002>
- Zheng, Y., Qin, L., Zacarías, N.V.O., De Vries, H., Han, G.W., Gustavsson, M., Dabros, M., Zhao, C., Cherney, R.J., Carter, P., Stamos, D., Abagyan, R., Cherezov, V., Stevens, R.C., Ijzerman, A.P., Heitman, L.H., Tebben, A., Kufareva, I., Handel, T.M., 2016. Structure of CC chemokine receptor 2 with orthosteric and allosteric antagonists. *Nature.* <https://doi.org/10.1038/nature20605>

- Zhou, Q., Yang, D., Wu, M., Guo, Y., Guo, W., Zhong, L., Cai, X., Dai, A., Jang, W., Shakhnovich, E., Liu, Z.J., Stevens, R.C., Lambert, N.A., Babu, M.M., Wang, M.W., Zhao, S., 2019. Common activation mechanism of class a GPCRs. *Elife* 8. <https://doi.org/10.7554/eLife.50279>
- Zou, L., Peng, Q., Wang, P., Zhou, B., 2017. Progress in Research and Application of HIV-1 TAT-Derived Cell-Penetrating Peptide. *Journal of Membrane Biology*. <https://doi.org/10.1007/s00232-016-9940-z>
- Zu, Z., McKendry, R., Chavez, C.L., 2000. Signaling in Copper Ion Homeostasis. *Cell and Molecular Response to Stress* 1, 293–300. [https://doi.org/10.1016/S1568-1254\(00\)80022-4](https://doi.org/10.1016/S1568-1254(00)80022-4)
- Zukowska-Grojec, Z., Shen, G.H., Capraro, P.A., Vaz, C.A., 1991. Cardiovascular, neuropeptide Y, and adrenergic responses in stress are sexually differentiated. *Physiol Behav* 49. [https://doi.org/10.1016/0031-9384\(91\)90317-H](https://doi.org/10.1016/0031-9384(91)90317-H)
- Zweemer, A.J.M., Bunnik, J., Veenhuizen, M., Miraglia, F., Lenselink, E.B., Vilums, M., De Vries, H., Gibert, A., Thiele, S., Rosenkilde, M.M., IJzerman, A.P., Heitman, L.H., 2014. Discovery and mapping of an intracellular antagonist binding site at the chemokine receptor CCR2. *Mol Pharmacol*. <https://doi.org/10.1124/mol.114.093328>
- Zweemer, A.J.M., Nederpelt, I., Vrieling, H., Hafith, S., Doornbos, M.L.J., De Vries, H., Abt, J., Gross, R., Stamos, D., Saunders, J., Smit, M.J., IJzerman, A.P., Heitman, L.H., 2013. Multiple binding sites for small-molecule antagonists at the CC chemokine receptor 2. *Mol Pharmacol* 84. <https://doi.org/10.1124/mol.113.086850>



*Edited Front cover art designed by J.Farmer from Journal of Medicinal Chemistry official front cover for Casella, B. M., Farmer, J., Nesheva, D. et al 2023.*